The RabGAP TBC1D14 Regulates Autophagosome Formation via Recycling Endosomes and Rab11

Andrea Dora Longatti

University College London

and

Cancer Research UK London Research Institute

PhD Supervisor: Sharon A. Tooze

A thesis submitted for the degree of

Doctor of Philosophy

University College London

September 2010

Declaration

I Andrea Dora Longatti confirm that the work presented in this thesis is my own. Where information has been derived from other sources, I confirm that this has been indicated in the thesis.

Abstract

Autophagy is a bulk degradation process characterised by the formation of double membrane vesicles called autophagosomes. Autophagosomes derive from a small precursor structure called phagophore, which is expanded to enclose a portion of cytoplasm or organelle, and finally fuses with the endo-lysosomal system to acquire degradative capacity. Autophagy is often studied as a response to starvation, since the degraded components can be re-used for biosynthetic pathways. However, in multicellular organisms, it has many additional functions in tissue homeostasis, during development, in infection and immunity, and in programmed cell death. Regarding autophagy many questions remain such as the origin of the autophagosomal membrane, the mechanism of phagophore extension and many of the signalling pathways that lead to autophagosome assembly. To better understand the membrane trafficking events involved in autophagosome formation I did an over-expression screen for Rab GTPase activating proteins (RabGAPs) inhibiting this process. RabGAPs act inhibitory on Rab GTPases, which are major regulators of intracellular membrane traffic. I have identified 11 RabGAPs that inhibit autophagosome formation, one of which is TBC1D14, which binds to ULK1, an important kinase for initiation of autophagy. TBC1D14 also binds to Rab11 and tubulates recycling endosomes when over-expressed. I found that both ULK1 and another essential autophagy protein mAtg9 localise to recycling endosomes under normal conditions. I propose that recycling endosomes can signal through both ULK1 and mAtg9 to initiate autophagosome formation upon starvation and may be important in monitory cellular nutrient status, and/or provide membrane to autophagosomes.

Investigating the role of ULK1 *in vivo*, I found that ULK1 knock-out mice are able to undergo basal autophagy as assessed by LC3 lipidation in various tissues. However, ULK1 knock-out mice have less CD4 and CD8-positive mature T cells and their response to TCR stimulation is impaired compared to T cells from wild type animals.

Graphical abstract

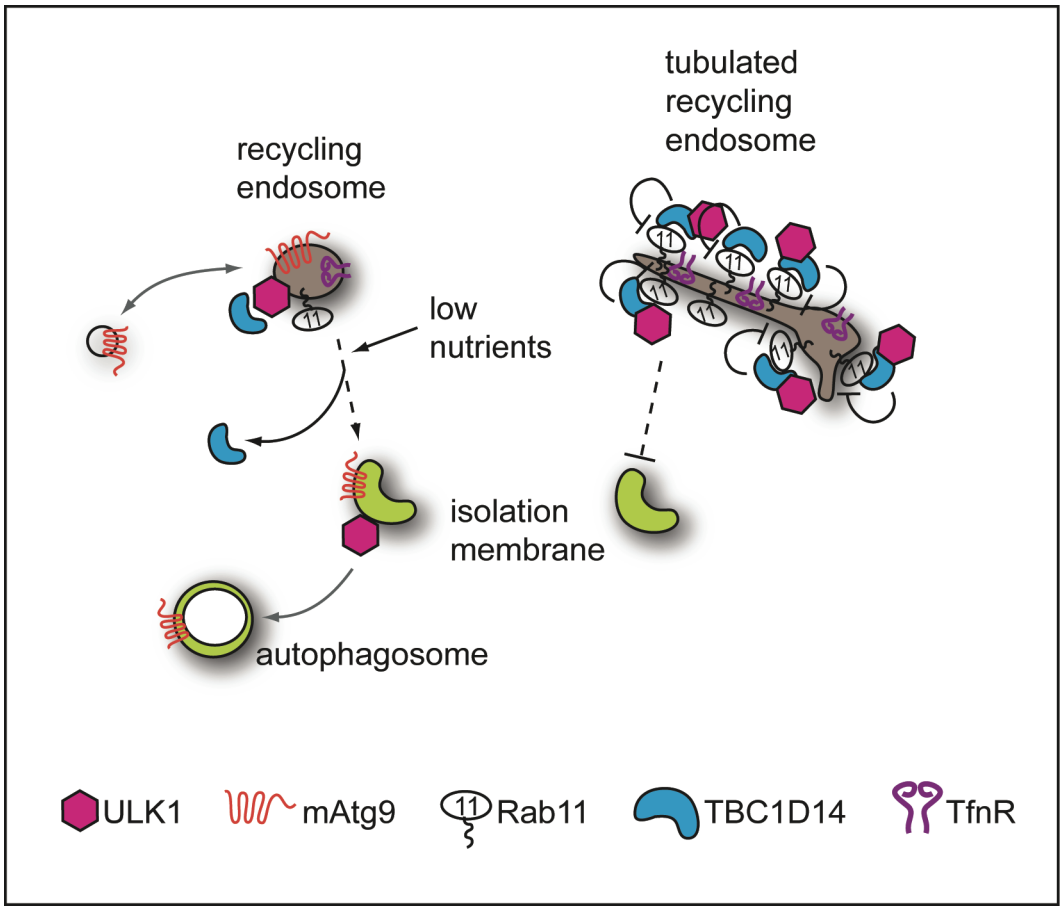

Acknowledgements

First and foremost I would like to thank my supervisor Sharon Tooze for giving me the opportunity to work in her lab, for her continuous support and enthusiasm for my project, for encouraging me to go to conferences, and for putting in the late night sessions to finish the paper. I would like to thank my thesis committee members Giampietro Schiavo and David Ish-Horowicz for their input and fruitful discussions. Thanks to Gipi in particular for his enthusiasm in my work, suggestions in joint lab meetings, and critical reading of the paper.

I would like to thank our collaborator Francis Barr for sending constructs, useful discussions and suggestions, and for letting me perform experiments in his lab. Thank you also to all members of the Barr lab in particular Alex Haas and Shin-Ichiro Yoshimura for teaching me yeast-2-hybrid and *in vitro* GAP assays. I would also like to thank Caetano Reis e Sousa for letting me use reagents and lab space to do the mouse cell experiments, and for his helpful suggestions and discussions. A big thank you to Fabiola Osorio Olivares and Diego Mourao-Sa in the Reis e Sousa lab for patiently teaching me immunology.

Many thanks to the staff in the biological resource unit at LRI: Clare, Scott, and Ian for teaching me mouse handling and looking after the mice brilliantly; and also the Clare Hall staff: Helen, Antony, and Samantha for looking after the mouse colony. Thank you to everyone at the equipment park at LRI, especially Vicky, Graham, and Lakshmi for helping out with using the equipment and often accepting my miniprep samples late. Thank you to Lucy at the EM unit and especially Ken for processing the thymi and taking the beautiful EM pictures. Thank you to the histopathology unit, especially Emma, for showing me how to find pancreas and lymph nodes in a mouse. Thank you to everyone at the confocal microscopy unit for their help. Thank you also to Paul and Ismael for making the best coffee and putting a smile on my face on even the grumpiest of mornings. A big thank you to all the lab aides without whom this place wouldn't be running as well as it does, especially Nicky and Ian for all their help and friendly football banter.

Thank you to Clare Futter for giving us gold-anti-EFR antibody and to Jeremy Henley for sending the HA-Syntenin1 construct.

A big thank you to everyone in the SPW lab past and present for creating the best work environment ever: Ed, who showed me how do cloning in 2 days (and it works!), for patiently helping me out whenever I needed it, and for critically reading parts of my thesis; Grant, master of cell biology, who taught me a lot and made me laugh and shout many times; Joelle, for being the nicest desk neighbour ever and coping with all my moods; Minoo, for help with EM and Tfn uptake and for kicking my bum to go running; Harold (I can't hear you), for getting all my ordering done perfectly; Nicole and Jemma, my fellow PhD students for great company and moral support; Hannah for helping me with Prism and hiding from Minoo (erm I can't go running today because…); Eyal, for finding the funniest you tube clips; Orsi, for having crazy ideas (Monopoly…) and always believing in Atg9 and REs (not); Fiona, for being best pub buddy ever. Also thank you to everyone in the MNP lab (keep calm and carry on). Thank you to my fellow PhDs Viduth (very best pub buddy ever), Dan (my travel buddy and flat mate), Diego, Fabiola, Devanshi, Marco, and Guillermo for having many a great time together.

Last but definitely not least I would like to thank my parents, who have supported, loved, and encouraged me all my life and without whom I would not be where I am today. Thank you to Alex for all his support and encouragement, for putting up with my crazy work hours, and for travelling the world with me (you are my rock).

Table of Contents

Table of Figures

List of tables

Abbreviations

APC	Antigen presenting cell
Atg	**Aut**opha**g**y gene/protein
AV	Autophagosome
CI-MPR	Cation-independent mannose-6-phosphate receptor
C-terminal	Carboxy-terminal
CRUK	Cancer research UK
DMEM	Dulbecco's modified eagle medium
EBSS	Earle's buffered saline solution
EEA1	Early endosomal autoantigen 1
EGF	Epidermal growth factor
EGFR	Epidermal growth factor receptor
EM	Electron microscopy
ER	Endoplasmic reticulum
ERGIC	ER Golgi intermediate compartment
FACS	Fluorescence activated cell sorting
FBS	Foetal bovine serum
FCS	Foetal calf serum
FIP200	Focal adhesion kinase family interacting protein of 200kDa

GABARAP	γ-aminobutyric acid type A receptor associated protein
GAP	GTPase activating protein
GATE-16	Golgi-associated ATPase enhancer of 16kDa
GEF	Guanine nucleotide exchange factor
GFP	Green fluorescent protein
GST	Glutathion S-transferase
GTP	Guanosine-5'-triphosphate
h	hour(s)
HA	haemagglutinin
HEK293A	Human embryonic kidney 293 A cells
HET	Heterozygous
IF	immunofluorescence
IM	Isolation membrane
IP	Immunoprecipitation
kDa	kilo Dalton
KO	Knock-out
LAMP2	Lysosome-associated membrane protein 2A
Leu	Leupeptin
MAP-LC3/LC3	Microtubule-associated protein 1 light chain 3
mAtg9	Mammalian Atg9

min	Minute(s)
MW	Molecular weight
N-terminus	Amino-terminus
PAS	Phagophore assembly site
PBS	Phosphate buffered saline solution
PCR	Polymerase chain reaction
PE	Phosphatidylethanolamine
PFA	Paraformaldehyde
PNS	Post-nuclear supernatant
PI	Phosphatidylinositol
PI3P	Phosphatidylinositol-3-phosphate
PI3K	Phosphatidylinositol-3 kinase
Rab	Ras-related found in brain
RE	Recycling endosome
RFP	Red fluorescent protein
RPM	Revolutions per minute
RPMI	Roswell Park Memorial Institute medium
SDS-PAGE	Sodium dodecyl sulfate-polyacrylamide gel electrophoresis
SEM	Standard error of the mean
siRNA	small inhibitory RNA

TCA	Trichloroacetic acid
Tfn	Transferrin
TfnR	Transferrin receptor
TGN	Trans-Golgi network
mTOR	Mammalian target of rapamycin
TX-100	Triton-X-100
ULK1	Unc-51 like kinase 1
UVRAG	UV irradiation resistance-associated gene 1
Vps	Vacuolar protein involved in sorting
WB	Western blot
WT	Wild type

Publications

Longatti A, Yoshimura S, Barr FA, Tooze SA.

TBC1D14 regulates autophagosome formation via ULK1 and Rab11-positive recycling endosomes.

Manuscript in preparation.

Longatti A, Orsi A, Tooze SA.

Autophagosome formation: Not necessarily an inside job.

Cell Research. Epub 2010 Sep 14. Research Highlight.

PMID: 20838417

Longatti A, Tooze SA.

Vesicular trafficking and autophagosome formation.

Cell Death Differ. 2009 Jul;16(7):956-65. Epub 2009 Apr 17. Review.

PMID: 19373247

Chan EY, Longatti A, McKnight NC, Tooze SA.

Kinase-inactivated ULK proteins inhibit autophagy via their conserved C-terminal domains using an Atg13-independent mechanism.

Mol Cell Biol. 2009 Jan;29(1):157-71. Epub 2008 Oct 20.

PMID: 18936157

Chapter 1. Introduction

1.1 Autophagy

Autophagy is a degradative process characterised by the formation of double membrane vesicles called autophagosomes. It is highly conserved throughout all eukaryotes and genetic studies in yeast first revealed the major protein machinery involved. These proteins were called the Atg proteins and many of them are conserved in higher eukaryotes [1]. Autophagosomes start out as small membrane structures called phagophores or isolation membranes (IMs), which are expanded through an unknown mechanism to autophagosomes of various sizes but usually with a diameter of about 300-900 nm [2]. Note that the terms phagophore and IM will be used interchangeably. Autophagosomes fuse with endosomes and lysosomes to form autolysosomes leading to the degradation of the inner autophagosomal membrane along with all its contents by lysosomal hydrolases (Fig. 1-1). Unlike the proteasome, which degrades single proteins one at a time autophagosomes can enclose an entire portion of cytoplasm containing organelles or parts of organelles, protein aggregates, invading pathogens, etc. leading to their degradation. The resulting broken down components such as amino and fatty acids are then released into the cytosol and can be reused for biosynthetic pathways, which is why it is often studied as a starvation response (Fig. 1-1). However, in multicellular organisms autophagy has many additional roles in development, immunity, ageing, and tissue homeostasis. Because autophagy has such diverse functions and because it happens in almost every nucleated cell in the body, tight control is necessary and malfunctions in the process can lead to a plethora of diseases such as

neurodegeneration, myopathies, autoimmune disease, and cancer depending on which tissue is affected [3].

The aim of this study was to further elucidate the molecular mechanisms of mammalian autophagy in particular the membrane trafficking events involved in autophagosome formation.

Three major forms of autophagy exist: Macroautophagy, which I refer to as autophagy throughout; microautophagy, which describes the uptake of cytoplasmic material by invagination of the lysosomal or vacuolar membrane directly; chaperone mediated autophagy (CMA), which is the delivery of cytoplasmic material to the lysosome (and probably vacuole [4]) surface directly via protein channels and chaperones; and the cytosol to vacuole (Cvt) targeting pathway, which only exists in yeast and serves to deliver the yeast proteins aminopeptidase1 and α-mannosidase to the vacuolar lumen.

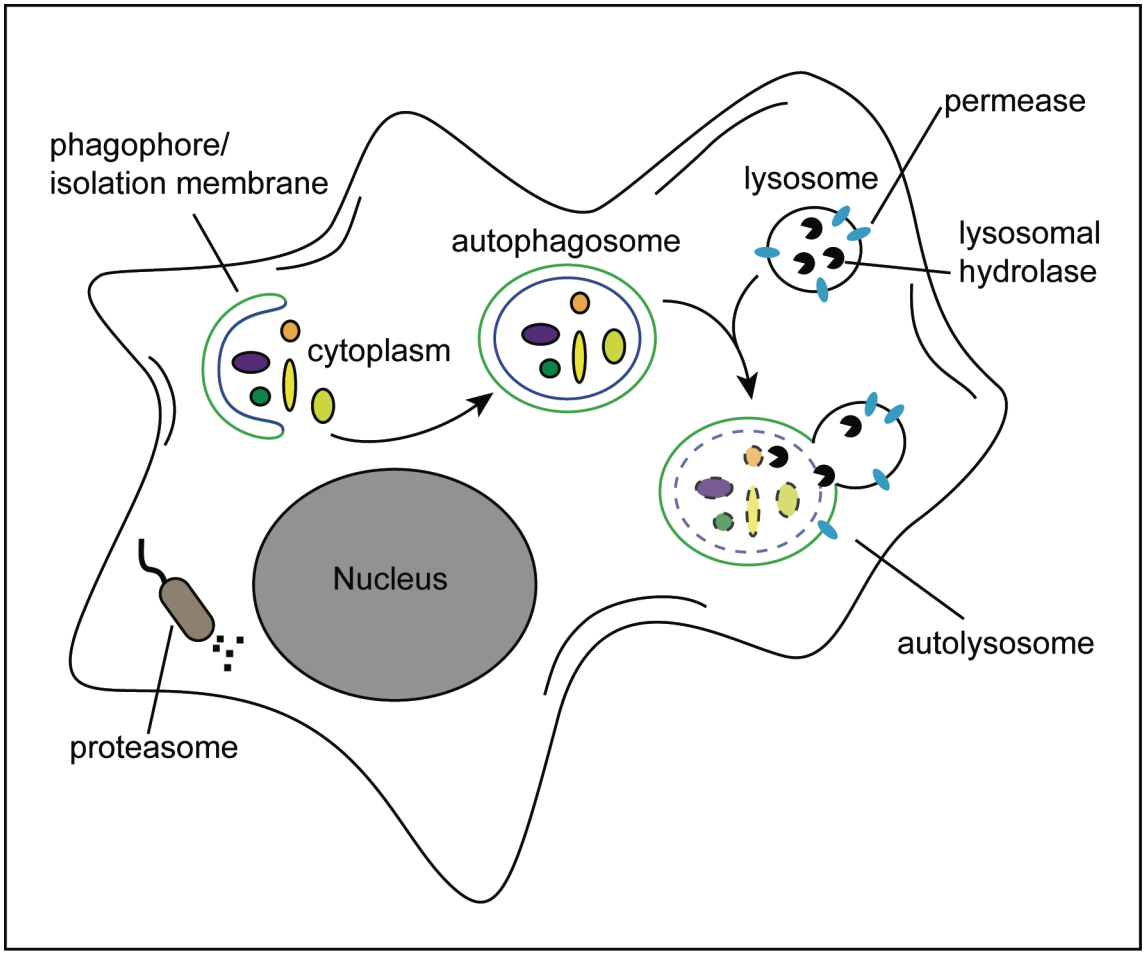

Figure 1-1 Autophagy overview
Autophagy is a degradative process characterised by the formation of double membrane vesicles called autophagosomes. These vesicles start out as small membrane structures called phagophores or isolation membranes (IMs), which are expanded through an unknown mechanism to autophagosomes of various sizes with a diameter normally ranging from 300-900 nm. Autophagosomes fuse with endosomes (not depicted) and lysosomes to form autolysosomes leading to the degradation of the inner autophagosomal membrane along with all its contents by lysosomal hydrolases. The resulting broken down components such as amino and fatty acids are then released into the cytosol through permeases and can be reused for biosynthetic pathways. Unlike the proteasome, which degrades single proteins one at a time, autophagosomes can enclose an entire portion of cytoplasm containing organelles, protein aggregates, invading pathogens, etc. Figure drawn with reference to Mizushima et al., 2008 [3].

Autophagosomes were first noted by S. Clark in 1957 when he examined the kidneys of newborn mice by electron microscopy (EM), but it was Christian De Duve and others

who discovered the degradative capacity of these organelles (Fig. 1-2). Interestingly, Clarke notes that most of these structures, which he describes as vacuoles or large round bodies containing an amorphous material, are abundant in the kidney just after birth but mostly disappear in the following weeks [5]. A plethora of biochemical studies over the next two decades revealed the connection between autophagy and energy/nutrient status, for example, reports showing induction of autophagy by glucagon or amino acid deprivation in the liver [6, 7]. More recently, confirming Clark's observations, it was indeed found that there is a burst in autophagic activity just after birth to overcome the nutrient deprivation experienced by the foetus after separation from the maternal trans-placental supply. It was found that autophagy is immediately up-regulated after birth returning to basal levels after 1-2 days. Atg7 and Atg5 knock-out mice who cannot undergo this autophagy burst do not survive this period and die within 24 hours after birth even when force fed [8, 9].

It was not until the 1990'ies when yeast genetic screens were designed to study autophagy that significant progress in understanding the molecular machinery of this process was made. Autophagy screens in *Saccharomyces cerevisiae* revealed essential genes involved in starvation induced autophagy in yeast [10-16], and for many of these the mammalian homologues have been identified [17], advancing the field enormously in the last 15 years. However, in 1967 De Duve noted that "very little is known concerning the mechanisms whereby these [autophagosomes] are formed and their contents degraded" and this is still largely true today.

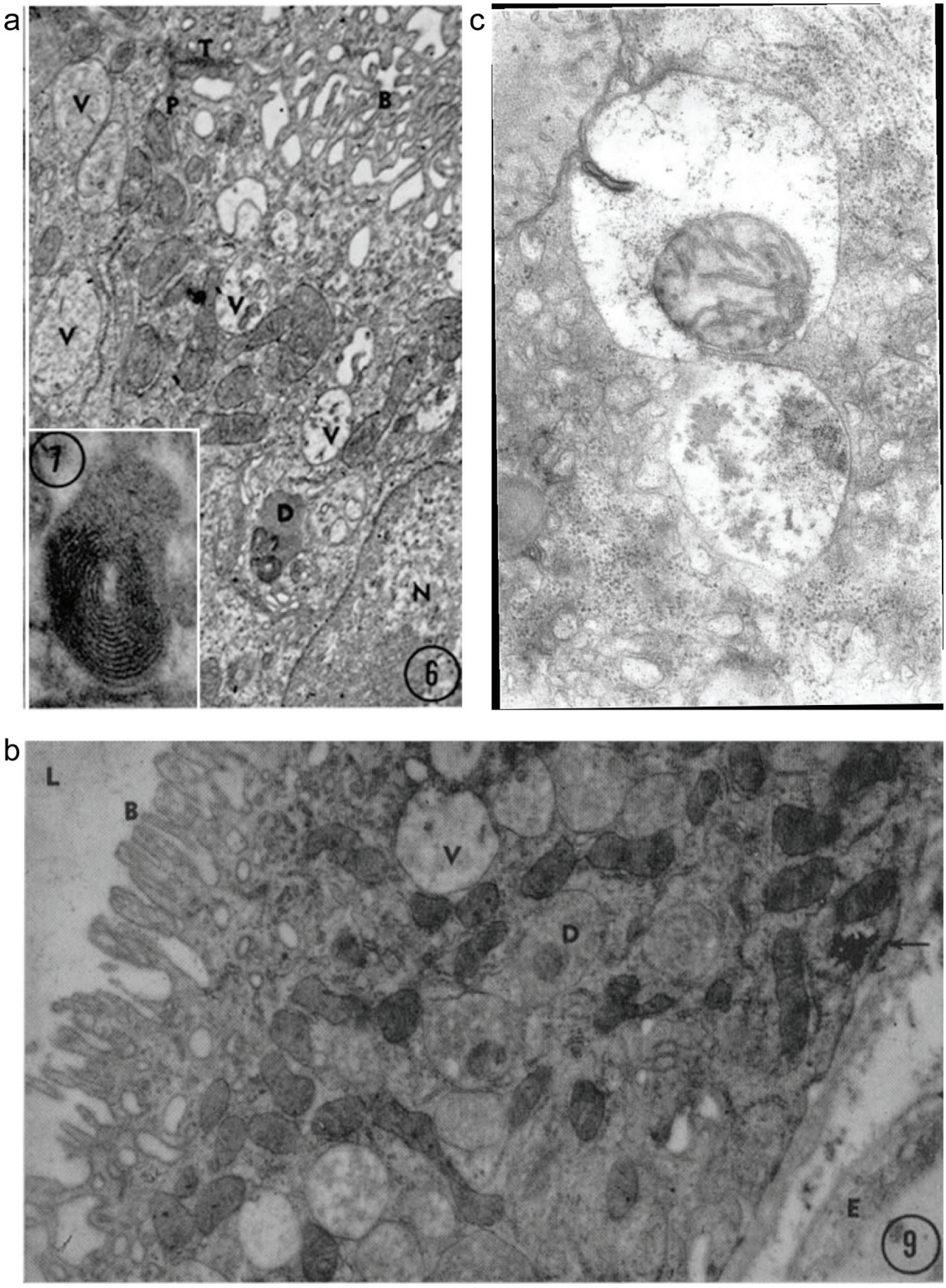

Figure 1-2 Autophagosomes were first observed in the 1950'ies by EM
(a,b) First observation of autophagosomes by Sam L. Clark in EM micrographs of proximal tubules of mouse kidneys. Pictures taken from [5] **(a)** He notes that the three vacuoles (V) on the left contain an amorphous material. **(b)** Large round bodies (D) containing varying concentrations of an amorphous

material are present throughout the cytoplasm and disappear from the proximal tubules of infant mice during the first week after birth. **(c)** Autophagosomes containing a mitochondrion and other material taken from De Duve and Wattiaux, 1965 [18].

1.1.1 Autophagy proteins and complexes

The exact nature of the IM, called pre-autophagosomal structure (PAS) in yeast, is unclear and it is not known whether these structures are pre-existing or form upon induction of autophagy. The IM is expanded through an unknown mechanism to form immature autophagosomes (AVi), which are closed and can fuse with endosomes and lysosomes to become a degradative compartment (AVd) also called autolysosome (Fig. 1-3). Several proteins and protein complexes localise to the IM and autophagosomes successively and although they do not seem to act in a strictly linear order at all times a hierarchy of Atg proteins has been established in yeast, which seems to be very similar or identical in mammals (Fig. 1-4 and see section 1.1.3).

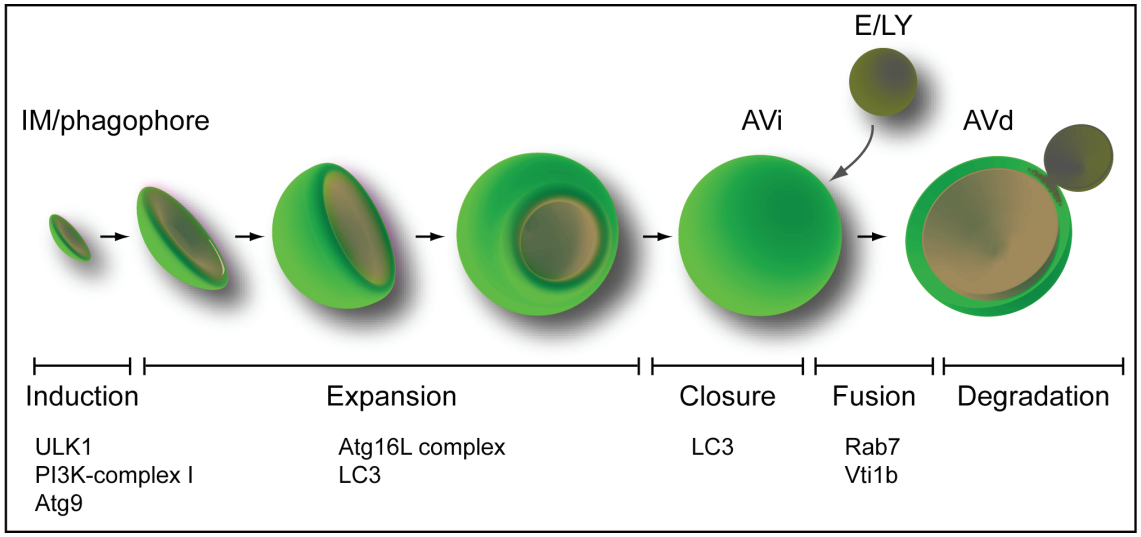

Figure 1-3 Autophagosome formation
Autophagosome formation is a multi-step process starting with the expansion of a small crescent shaped vesicle called isolation membrane (IM) or phagophore. It is unclear whether the IM is pre-existing or forms upon induction of autophagy and the mechanism of membrane expansion is not known. Once the immature autophagosome (AVi) is closed it can fuse with endosomes (E) and lysosomes (LY) and acquired degradative capacity (AVd). AVds are also called autolysosomes. Listed underneath are some of the important proteins involved in each step, which can also be used as markers to distinguish IMs from AVis or AVds. Figure modified from Longatti and Tooze, 2009 [19].

In yeast 33 Atg proteins have been identified so far, 18 of which are involved in autophagosomes formation (Atg1-10, Atg12-14, Atg16-18, Atg29, and Atg31). The most important proteins involved in mammalian autophagy are listed in Table 1-1.

Table 1-1 Important proteins in mammalian autophagy
The nomenclature of autophagy proteins in yeast has been unified to Atg (formerly Apg, Aut, Cvt, and Gsa) [1], however, many mammalian proteins have been assigned different names due to their involvement in other processes, or if they lack sequence homology with yeast Atg proteins.

Protein with alternative names	Description
Atg1 (*S. cerevisiae. D. melanogaster, D. discoideum*) ULK1 (*H. sapiens, M. musculus*) Unc51 (*C. elegans*)	Serine/threonine kinase important in induction of autophagy. There are five homologues in mammals ULK1, ULK2, ULK3, ULK4, STK36/fused. [20-27]
Atg2	Involved in Atg9 trafficking. The mammalian homologue has not been studied well. [28, 29]
Atg3	E2-like enzyme conjugating Atg8/LC3 to PE. [16, 30]
Atg4	Cysteine protease cleaves the ultimate C-terminus of Atg8/LC3 to expose a glycine. Can also de-conjugate Atg8/LC3 from PE. In mammalian cells there are at least four homologues Atg4A, B, C, and D. [31-33]
Atg5	A protein that is part of the Atg16L complex upon autophagy induction. Atg12 is constitutively conjugated to Atg5 shortly after synthesis. [34, 35]
Atg6/Vps30 (yeast) Beclin1 (mammals)	Component of the PI3K complex. Interacts with Bcl-2. [36, 37]
Atg7	E1-like enzyme that activates both Atg8/LC3 and Atg12 in an ATP dependent manner to be conjugated to their targets. [38]
Atg8 (yeast) LC3 (mammals)	Ubiquitin-like protein, which is conjugated to PE upon induction of autophagy. Localises to autophagosomes and is partly degraded in them. LC3A has two splice variants B and C. There are four other mammalian Atg8 homologues GABARAP, GABARAPL1, GAPARAPL2/GATE16, and GABARAPL3 [33, 39, 40]
Atg9 (yeast) mAtg9 (mammals)	Transmembrane protein. There are two mammalian homologues Atg9A and

	Atg9B. Atg9A is ubiquitous whereas Atg9B is only expressed in the placenta and pituitary gland. Mammalian Atg9 has 6 transmembrane domains and cycles between the TGN and endosomes. [13, 41-43]
Atg10	An E2-like enzyme that conjugates Atg12 to Atg5. [34, 44]
Atg12	Protein conjugated to Atg5 constitutively. Part of the Atg16L complex. [34]
Atg13	Component of the Atg1/ULK1 kinase complex [21, 45-48]
Atg14 (yeast) Atg14L/Barkor (mammals)	Component of the PI3K complex necessary for function in autophagy. [37, 49, 50]
Atg16 (yeast) Atg16L (mammals)	Component of the Atg16L complex. There are two mammalian homologues Atg16L1 and Atg16L2. Atg16L associates with the Atg5-12 complex upon autophagy induction and localises to the phagophore. [51, 52]
Atg17 (yeast) FIP200 (mammals)	Component of the Atg1/ULK1 kinase complex. FIP200 is functionally homologous to Atg17 but shares no sequence homology with it. [53-55]
Atg18 (yeast) WIPI2 (mammals)	PI3P binding protein. Localises to IMs and may prevent LC3 de-conjugation by Atg4. Involved in Atg9 traffic. There are four mammalian homologues WIPI1-4. [11, 56-58]
Atg21	PI3P binding protein homologous to Atg18 but more specific for the Cvt pathway in yeast. [59]
Atg24/Cvt13 (yeast) SNX4 (mammals)	PI3P binding protein. In yeast Atg24 is part of the ULK1 kinase complex but may be specific to the Cvt pathway and/or pexophagy. In mammals SNX4 regulates TfnR sorting to the ERC but has not been linked to autophagy. [60-62]
Atg101	Atg13 binding protein therefore part of the ULK1 kinase complex. Conserved in various eukaryotes but not in yeast. [63, 64]

Alfy	Targets proteins aggregates in the cytosol for autophagic degradation. [65, 66]
Ambra1	Positive regulator of autophagy. Binds Beclin1 and modulates its activity. [67]
Bif-1/Endophilin B1	Interacts with the Beclin1 complex and is required for autophagy. Has a BAR domain. [68]
DFCP1	PI3P binding protein. Localises to omegasomes, which may act as cradles for autophagosome formation. [69]
FYCO1	Protein that binds LC3, Rab7 and PI3P to move autophagosomes to lysosomes. [70]
TOR (yeast) mTOR (mammalian)	Serine/threonine kinase that forms two complexes called TORC1 and TORC2. Autophagy is negatively regulated by TORC1. [71]
Rheb	Small GTPase that activates mTOR when GTP bound. [25]
Rubicon	Beclin1 interactor. Part of the PI3K complex. Negative regulator of autophagy. [72, 73]
TRAPPIII	Multimeric GEF that activates the GTPase Ypt1p. Functions in autophagy in yeast. [74]
TSC1/2 complex	May act as a GAP for Rheb thus inhibiting mTOR. [75]
UVRAG	Can be part of the Beclin1/PI3K complex positively regulating autophagy. [76]
Vps34	The class III PI3K in the autophagic PI3K complex. There are 3 complexes in mammalian cells containing Vps34/Vps15/Atg14L/Beclin1 and a combination of UVRAG, Ambra1 and/or Rubicon. [77]
p62/Sequestosome1 (SQSTM1)	Adaptor protein binding ubiquitinated protein aggregates and LC3 leading to incorporation of aggregated proteins into autophagosomes. [78]
Jumpy	PI3-phosphatase that negatively regulates initiation of autophagy. [79]

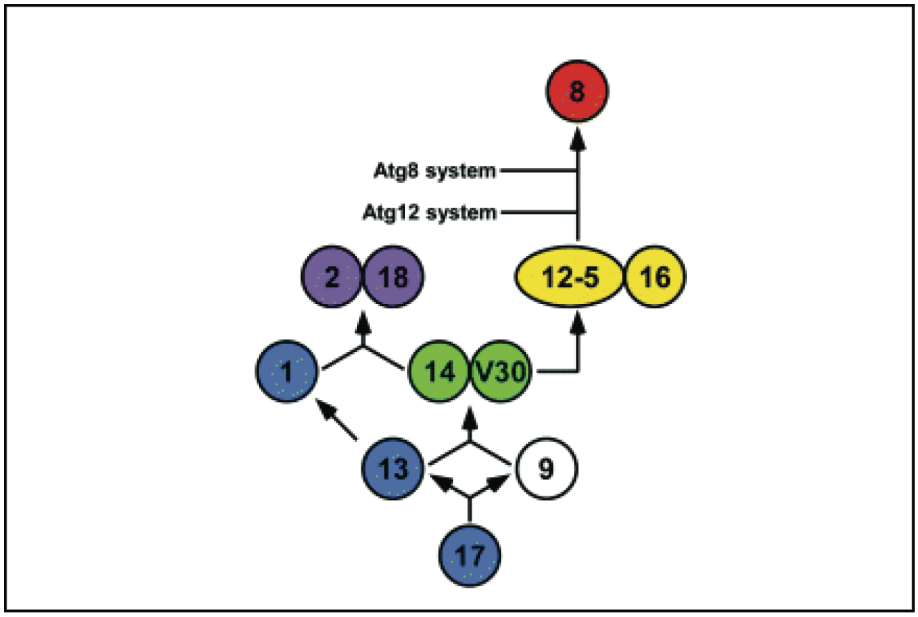

Figure 1-4 Hierarchy of Atg proteins in yeast
A hierarchy of Atg proteins was established by examining their localisation to the PAS in various yeast mutants. The Atg1 kinase complex and the PI3K complex act in parallel and are some of the first proteins to be recruited to the PAS, followed by Atg18, Atg5-12-16, and finally Atg8. Numbers indicate Atg proteins; V30 is Vps30/Atg6. Figure taken from Suzuki et al., 2007 [80].

1.1.2 The ULK1 kinase complex

The most upstream event in autophagosome formation is probably activation of the ULK1 kinase complex. ULK1 has an N-terminal kinase domain, a serine/proline rich middle domain and a C-terminal domain, which interacts with Atg13 and FIP200. The kinase domain of ULK2 shares about 78% homology with the kinase domain of ULK1 (about 50% overall) and the two proteins may be functionally partly redundant. Interestingly, ULK1 is essential for autophagy in HEK293A cells whereas ULK2 is not but ULK1 knock-out mice are healthy (see Chapter 5 and [81]). ULK3, ULK4, and STK36 show high similarity to ULK1 in their kinase domain but the serine/proline rich regions and the C-terminus are not conserved. Since it is the C-terminus that interacts

with Atg13 and FIP200 the role of the other ULK1 orthologues in autophagy remains unclear although ULK3 has been shown to induce autophagy when over-expressed [82].

ULK1, Atg13, FIP200 and Atg101 together form the ULK1 kinase complex, a stable complex in both fed and starved conditions. All four proteins are essential for autophagosome formation and associate with the isolation membrane (IM) upon autophagy initiation [83]. Activity of the ULK1 kinase complex is directly regulated by the mammalian target of rapamycin (mTOR) and autophagy can be induced by inhibition of the mTOR complex 1 (mTORC1) by either rapamycin or torin. mTORC1 binds the ULK1 kinase complex in fed conditions and phosphorylates ULK1 inhibiting its kinase activity and preventing Atg protein recruitment to the phagophore. In starvation mTORC1 releases ULK1 leading to its dephosphorylation, kinase activation, subsequent auto-phosphorylation, and phosphorylation of FIP200, and Atg13. The ULK1 complex can then associate with the IM and recruit other Atg proteins (Fig. 1-5). The activity of the mTORC1 complex itself is regulated by the small monomeric GTPase Rheb and other upstream signals linked to nutrient sensing but the exact mechanism of how the cell measures its nutrient status is not known. Rheb activates mTORC1 when it is GTP-bound and the activity of Rheb in turn is regulated by the tuberous sclerosis complex (TSC) consisting of two proteins TSC1 and TSC2, the latter of which contains a GAP domain that acts on Rheb [84-86]. The former is necessary for stability of TSC2, which is otherwise degraded by the proteasome and mutation in either of those genes leads to the cancerous tuberous sclerosis syndrome [87-89].

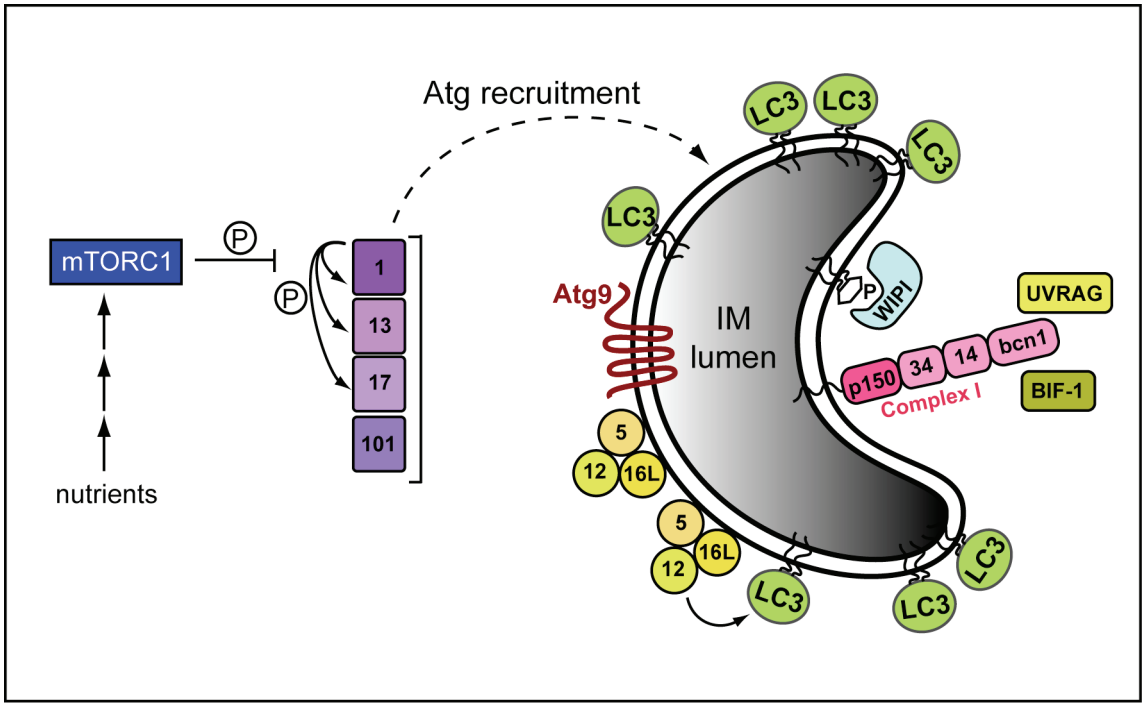

Figure 1-5 Proteins localising to the isolation membrane
The most upstream event in autophagosome formation is activation of the ULK1 kinase complex, which consists of ULK1, Atg13, FIP200/Atg17, and Atg101 and is constitutively assembled in both fed and starved conditions. In nutrient rich conditions ULK1 is directly phosphorylated by the mTORC1 complex, inhibiting its kinase activity, and Atg protein recruitment to the IM. mTORC1 activity in turn is regulated by cellular nutrient status through the action of various proteins (not depicted for simplicity). Upon starvation mTORC1 releases its inhibition on ULK1 whose kinase activity becomes active to phosphorylate itself, Atg13, and FIP200 subsequently leading to recruitment of other Atg proteins to the IM. The contents of the IM lumen would depend on the origin of the membrane. The Atg16L complex seems to localise pre-dominantly to the convex side of the IM whereas the PI3K complex is more on the concave side. Numbers indicate Atg proteins except 34, which is vps34; bcn1 is Beclin1; FIP200 is represented as Atg17. Figure modified from Longatti and Tooze, 2009 [19].

Although ULK1 clearly has an important function in autophagy it is also involved in vesicular trafficking processes not linked to autophagosome formation. It was shown to be essential for neurite extension in the developing mouse brain by regulating the GAP activity of SynGAP, which can inhibit Rab5 and Ras activity [90] (Fig. 1-6a). Rab5 and Ras can subsequently coordinate vesicular traffic necessary for axon extension.

Additionally, ULK1 can regulate motor-cargo assembly to transport synaptic vesicles to the axon tip in *Drosophila* [91]. By phosphorylating the kinesin-1 adaptor protein Unc76 ULK1 increases Unc76 affinity for Synaptotagmin-1 (Syt-1), which is found on synaptic vesicles. This links synaptic vesicles to the kinesin-1 motor protein via Unc76 leading to anterograde transport of the cargo to the axon tip (Fig. 1-6b). At the axon tip of mouse neurons ULK1 was also shown to regulate endocytosis of TrkA, the receptor for nerve growth factor (NGF) [92, 93]. It remains to be elucidated whether ULK1 has specialised roles in neurons where autophagy rates are low or whether it is a general feature of the ULK1 kinase that it can regulate so many different processes. Depending on nutrient status and developmental signals ULK1 may be able to form different complexes to perform various functions. In spite of this plethora of functions controlled by ULK1, mice lacking the protein show no obvious neurological phenotypes and only mild impairments of the hematopoietic system suggesting that ULK2 can compensate for most functions [81] (see also Chapter 5).

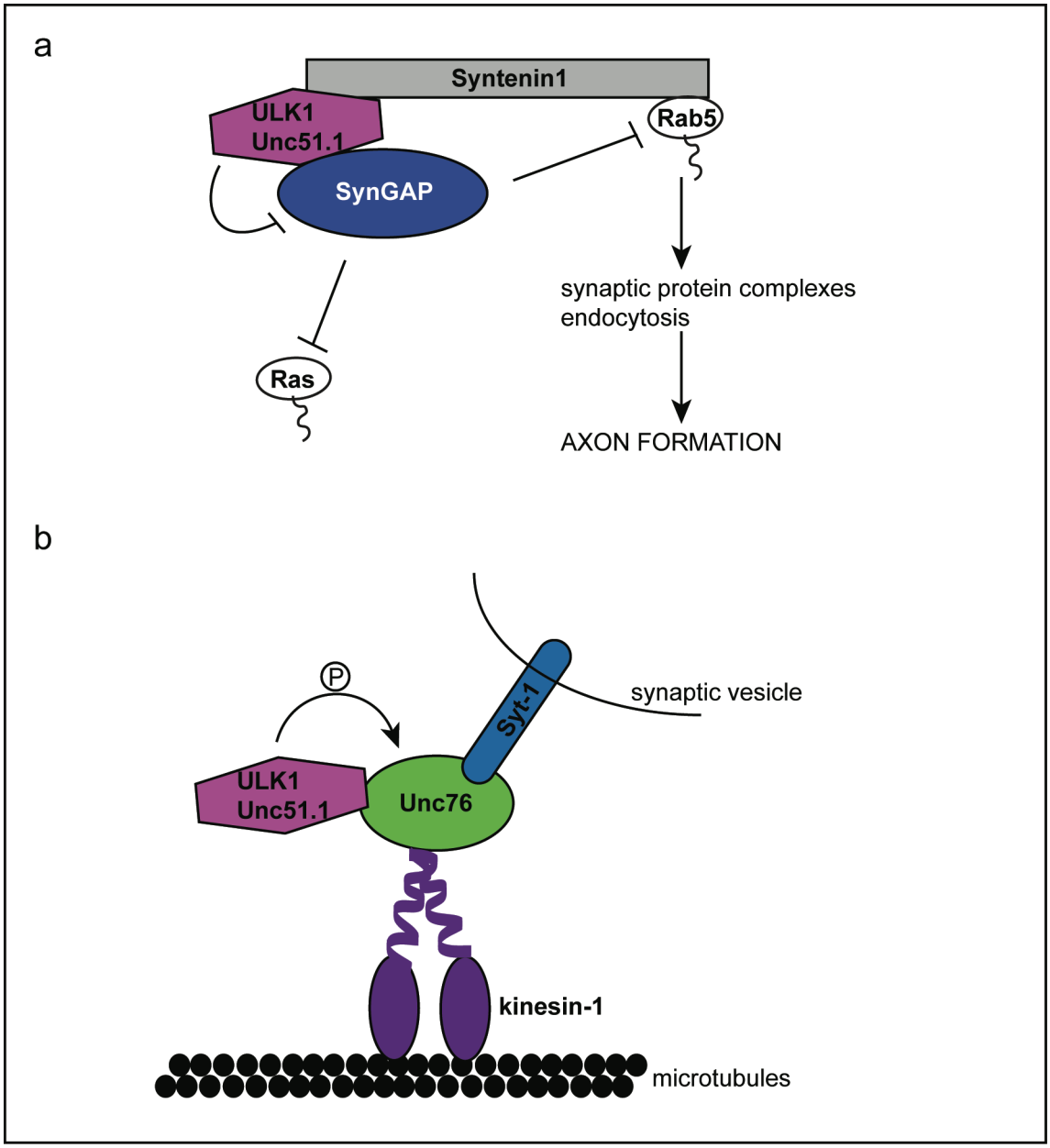

Figure 1-6 ULK1 is involved in axonal vesicular traffic
(a) ULK1 binds to the adaptor protein Syntenin-1 and SynGAP. ULK1 can down-regulate the GAP activity of SynGAP, which can act on Rab5 and Ras. This leads to activation of Rab5 and Ras who can then regulate axonal vesicular traffic leading to axon extension. **(b)** In *Drosophila* Atg1 can phosphorylate Unc76, which is a kinesin-1 adaptor protein. Unc76 also binds Synaptotagmin-1 (Syt-1) linking the kinesin-1 motor to synaptic vesicles and anterograde transport of the cargo.

1.1.3 The phosphatidylinositol-3-phosphate kinase complex

There are two class III phosphatidylinositol-3-phosphate (PI3P) kinase (PI3K) complexes in mammalian cells. Complex I (hereafter just referred to as PI3K complex) is essential for autophagy and consists of the PI3K Vps34, p150, Beclin1, and Barkor/Atg14. Complex II is involved in endocytic trafficking and autophagy and consist of Vps34, p150, Beclin1, and ultraviolet irradiation resistance-associated gene (UVRAG). Interestingly, UVRAG binds Bif1 which is a BAR domain containing protein required for autophagy [68]. BAR domains cause membrane curvature [94] and it is tempting to speculate that Bif-1 is needed to regulate autophagosome shape. The production of PI3P is essential for autophagy as treatment with the PI3K inhibitor Wortmannin completely inhibits autophagosome formation.

Production of PI3P on IMs and autophagosomes leads to recruitment of the PI3P binding protein WIPI2 [57]. Interestingly, PI3P seems to be produced preferentially on the inner autophagosomal membrane at least in yeast [95, 96]. The function of WIPI2 remains elusive but it may prevent premature LC3 de-lipidation by Atg4 before the autophagosome is closed [56]. Another PI3P binding protein is double FYVE domain containing protein 1 (DFCP1) but it is not clear whether it binds to PI3P on the isolation membrane directly or to PI3P on the ER, which forms a fold termed omegasome around nascent IMs possibly providing structural support or even membrane to the autophagosomes [69]. Recently, a PI3-phosphatase called Jumpy or MTMR14 has been identified that negatively regulates autophagy by antagonising the action of the PI3K

complex [79]. Jumpy controls the localisation of LC3 and mAtg9 and also recruits WIPI1, which is a negative regulator of autophagy in some cells [57].

Recent studies have established a hierarchy among mammalian Atg proteins [97, 98]. They showed that ULK1 is the most upstream Atg protein necessary for recruitment of Atg14 independently of PI3K activity. Both ULK1 and Atg14 associate with the ER and lead to recruitment of PI3K, followed by recruitment of the PI3P binding proteins WIPI1 and DFCP1, followed by Atg16L and LC3 localisation to the IM. Interestingly, ULK1, Atg14, WIPI1, Atg16L, and LC3 localised to the same structure but DFCP1 was found adjacent.

1.1.4 The ubiquitin-like conjugation systems

1.1.4.1 Atg5-12 conjugation

Two ubiquitin-like conjugation systems are involved in autophagosome formation. The first one results in the conjugation of Atg12 to Atg5. The second one leads to the conjugation of LC3 (or one of its paralogues) to the lipid phosphatidylethanolamine (PE) (Fig. 1-7). The conjugation of Atg12 to Atg5 is essentially constitutive and independent of autophagy. It happens shortly after translation of the proteins by the action of Atg7 (E1-like activating enzyme) and Atg10 (E2-like conjugating enzyme). The C-terminal glycine of the small 140 amino acid protein Atg12 is covalently linked to an internal lysine of Atg5. The Atg5-12 complex associates with Atg16L upon induction of autophagy and through Atg16L homo-dimerisation forms a complex of

800kDa [34, 52, 99]. This complex associates with the IM through an unknown recognition mechanism, but subsequently it may act as an E3-like enzyme to determine the site of LC3 conjugation to PE [100] and it has been shown that the Atg16L complex is required for elongation of the IM [101]. Furthermore, Atg5 as well as Atg7 knock-out mice die within 24 hours after birth even though they are normal at birth. They cannot undergo autophagy and therefore cannot overcome the period of nutrient deprivation encountered after separation from the maternal supply. Interestingly, it was found that autophagy is essential for pre-implantation development of mouse embryos as oocytes derived from oocyte-specific Atg5 knock-out mice failed to develop past the four and eight cells stage when fertilised with Atg5 knock-out sperm [102]. It is thought that homozygous Atg5 knock-out mice develop normally due to the presence of maternal Atg5 mRNA and protein in the oocyte.

1.1.4.2 LC3-PE conjugation

The second conjugation system involves the covalent linkage of LC3 orthologues to the lipid PE. PE is an abundant lipid but LC3 is specifically conjugated to PE on autophagosomes because of the E3-like action of the Atg16L complex, which localises to the IM before LC3. Unlike Atg12 where the terminal glycine is exposed, LC3 needs to be cleaved by the cysteine protease Atg4, which removes C-terminal amino acids of LC3 to expose a terminal glycine. This cleavage is constitutive and happens immediately after translation. Upon induction of autophagy LC3 is conjugated to PE in the IM via the action of Atg7 and Atg3 (E2-like conjugating enzyme). This lipidated form of LC3 is called LC3-II and the unlipidated form is called LC3-I, which runs slightly slower on SDS-PAGE. Atg4 can also cleave LC3-II to release it from

autophagosomes. Interestingly, over-expression of a catalytically inactive mutant of Atg4B, which seems to be the pre-dominant Atg4 homologue, led to a larger percentage of open autophagosomes and those that were closed were smaller compared to those in control cells [103]. This and recent data investigating siRNA mediated knock downs of LC3 homologues suggests that LC3 may have a role in phagophore extension and determining autophagosomes size [40]. This is supported by the finding that LC3 has fusogenic properties *in vitro,* which may catalyse the elongation process [104]. Interestingly, the study by Weidberg et al. also found that while LC3 acts early during expansion of autophagosomes the GATE-16 and GABARAP homologues are essential at later stages possibly in sealing the membrane. On the other hand it has been shown that mammalian Atg8 family members recognise specific cargo adaptor proteins. Nix, for example, binds specifically to GABARAP-L1 recruiting mitochondria into autophagosomes [105-107].

LC3 lipidation or LC3 puncta formation are some of the most reliable assays to measure autophagy [108]. It is important to keep in mind, however, that LC3 itself is degraded in the autolysosome. Therefore, a reduction in LC3-II or LC3 spots could be due to either decreased autophagosome formation or enhanced autophagic turnover or flux leading to more LC3-II degradation. To distinguish the two possibilities protease inhibitors such as leupeptin or other lysosomal inhibitors such as Bafilomycin1A, which inhibits the H^+-ATPase (V-ATPase) preventing lysosomal acidification should be tested for each condition. This will prevent LC3-II degradation and lead to an accumulation of lipidated LC3 or LC3 spots if flux is enhanced or reveal if autophagosome formation is impaired, in which case a reduction will be observed. Another caveat is that GFP

fluorescence is quenched in an acidic environment such as the lysosome and autolysosome and therefore these late stage autophagic organelles cannot be observed using GFP-tagged LC3. Note that leupeptin and other protease inhibitors cannot prevent GFP-LC3 quenching whereas Bafilomycin1A can. Using a tandem fluorescent RFP-GFP-LC3 (tfLC3) both immature (red+green=yellow) and mature (red) autophagosomes can be observed because RFP fluorescence can withstand the acidic autolysosomal environment [109].

Until recently it was believed that Atg5 and Atg7 are absolutely essential for mammalian autophagy. However, in a recent study using mostly EM and protein degradation assays to measure autophagy it was found that there might be Atg5 and Atg7 independent autophagy termed alternative autophagy [110]. Vesicles appearing to be autophagosomes could be readily induced by etoposide, a topoisomerase II inhibitor, staurosporin, an inhibitor of various kinases including PKC and PKA, and starvation but not by rapamycin. However, as of yet there are no markers for these alternative autophagosomes available and their exact nature remains unclear. Alternative autophagy is dependent on ULK1, FIP200, Beclin1, and Vps34 but not Atg7, Atg5, Atg12, Atg16, or mAtg9.

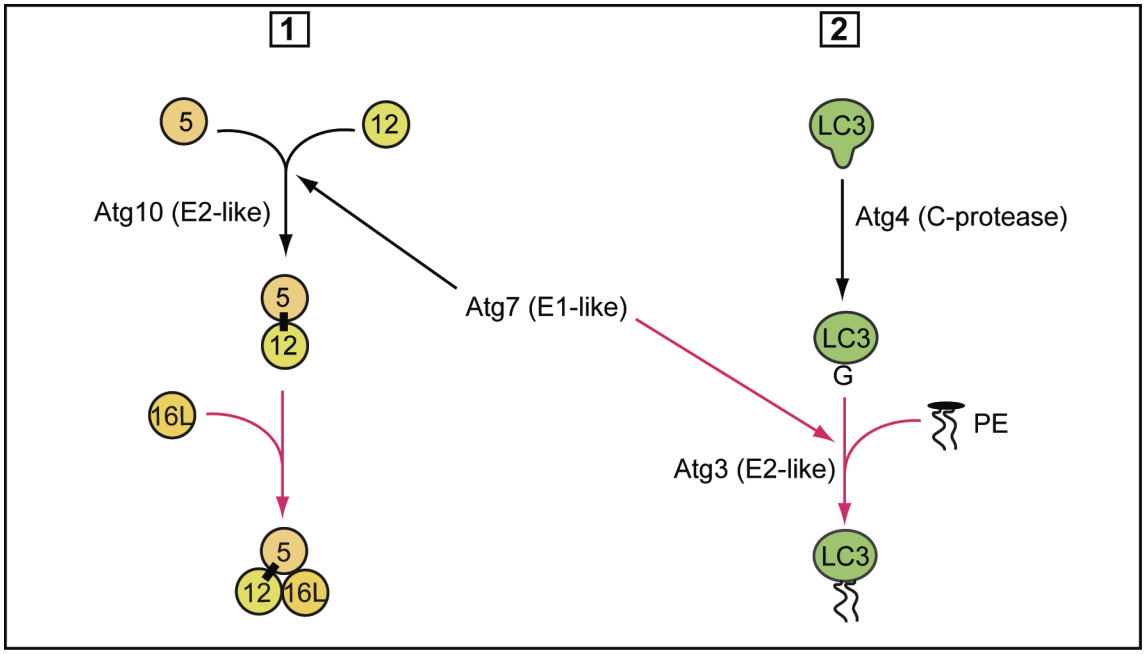

Figure 1-7 Two ubiquitin-like conjugation systems are essential for autophagosome formation

[1] In the first ubiquitin-like conjugation system the C-terminal glycine of Atg12 is covalently conjugated to lysine 130 of Atg5 via the action of Atg7 (E1-like activating enzyme) and Atg10 (E2 like conjugating enzyme) [111]. The Atg5-12 complex is formed constitutively just after protein translation. Upon activation of autophagy Atg5-12 associates with Atg16L, which can homo-oligomerise all together forming an 800kDa complex called the Atg16L complex, which localises to the IM. **[2]** In the second conjugation system LC3 is conjugated to the lipid phosphatidylethanolamine (PE). However, unlike Atg12 LC3 first has to be cleaved by the cysteine protease Atg4 to expose a C-terminal glycine, which is conjugated by the action of Atg7 and Atg3 (E2 like conjugating enzyme) to PE. It has been suggested that the Atg16L complex has E3-like activity determining the site of LC3 conjugation [100]. Autophagy induction dependent steps are indicated by red arrows.

1.1.5 mAtg9 and VMP1 transmembrane proteins

1.1.5.1 mAtg9

The only transmembrane protein found to be essential for autophagy in yeast is Atg9. Its function is thought to be the delivery of membrane to the phagophore but definitive proof for this is still missing [13, 42]. In mammalian cells there are two homologues

mAtg9A and mAtg9B but the latter is only expressed in the placenta and pituitary gland [112]. Therefore, I will refer to mAtg9A simply as mAtg9. In mammalian cells mAtg9 is found on the TGN and a peripheral endosomal pool, which consists to about 30% of Rab7 positive late endosomes but a lot of mAtg9 is also found on CI-MPR positive and other endosomes [41]. mAtg9 has 6 transmembrane domains with both N, and C-termini in the cytosol and one of the luminal loops is Asn-glycosylated in the ER and modified in the Golgi. Upon starvation mAtg9 disperses to the periphery as the TGN pool is significantly reduced (Fig. 1-8). This dispersal is dependent on the ULK1 kinase since knock down of ULK1 leads to an accumulation of mAtg9 on the TGN. However, the mechanism through which ULK1 controls mAtg9 traffic is poorly understood and it is unclear whether ULK1 is essential for anterograde traffic or prevents retrograde movement of mAtg9 to the TGN. It is tempting to speculate that this starvation induced dispersal of mAtg9 leads to delivery of TGN membranes to the phagophore or that endosomal mAtg9 can recruit other Atg proteins to induce phagophore formation and expansion. Recent evidence from yeast suggests that mAtg9 is found on vesiculo-tubular membranes and moves towards the vacuole upon induction of autophagy to assemble into the PAS [113]. Data from mammalian cells suggests that mAtg9-positive vesicles transiently interact with phagophores (unpublished observations A. Orsi).

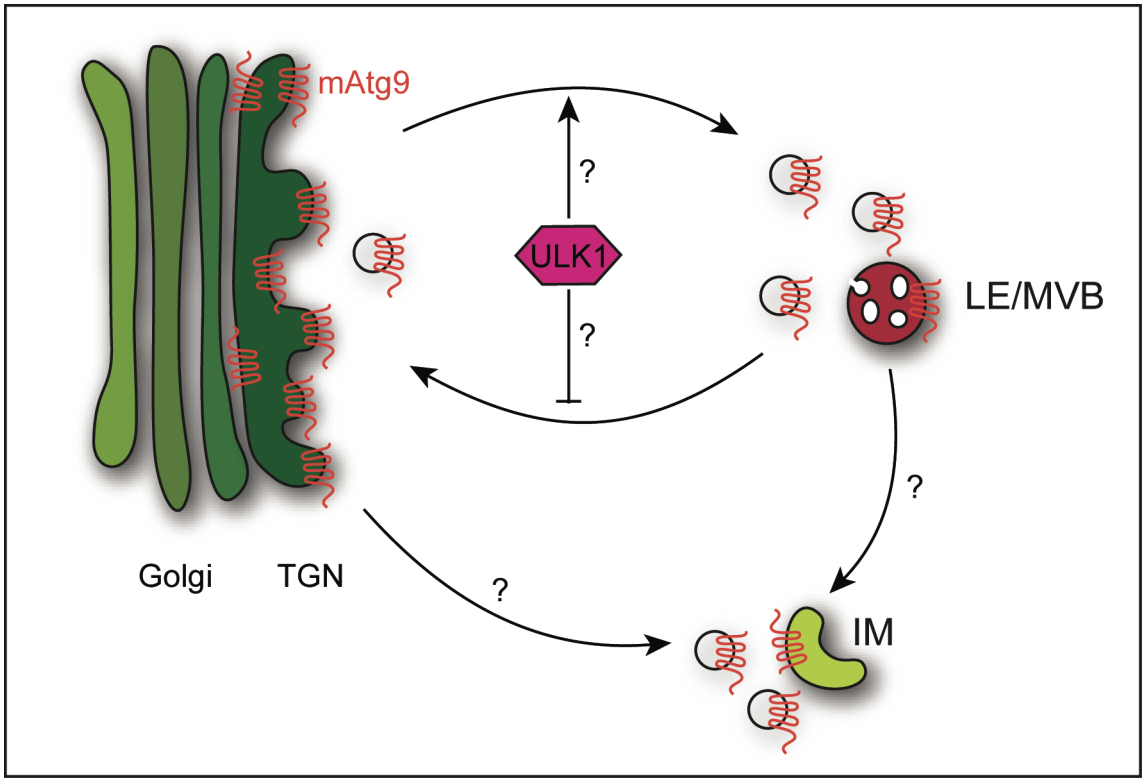

Figure 1-8 mAtg9 traffics between the TGN and a peripheral pool
In basal conditions mAtg9 is found on the TGN and a peripheral pool, which at least in some part seem to be late endosomes (LEs) or multivesicular bodies (MVBs). Upon starvation mAtg9 disperses to the periphery partly co-localising with IMs. However, evidence in mammalian cells suggests that mAtg9 may be on vesicles close to autophagosomes and endosomes (indicated as small transparent vesicles) but not actually share the same membrane or at least only localise transiently to subdomains of said membranes (unpublished observation A. Orsi, LRI). ULK1 is involved in trafficking of mAtg9 but the exact mechanism is poorly understood. Upon knock down of ULK1 mAtg9 re-localises to the TGN and can no longer undergo starvation induced dispersal to the periphery. However, whether this is due to reduced transport away from the TGN or enhanced retrograde traffic remains to be elucidated. Also, it is not clear whether mAtg9 can move from the TGN to IMs directly or via endosomes or whether indeed mAtg9 is able to turn endosomes themselves into IMs by recruitment of other Atg proteins (indicated by question marks).

1.1.5.2 VMP1

The only other transmembrane protein implicated in mammalian autophagy is vacuolar membrane protein 1 (VMP1), which has no homologues in yeast [114]. VMP1 is highly expressed in acute pancreatitis, a disease, which is associated with morphological

changes resembling autophagosome formation but it is debatable whether autophagy in this case is beneficial to the patient or not. Like mAtg9 VMP1 is also predicted to have 6 transmembrane domains and is essential for mammalian autophagy as siRNA mediated knock down leads to an inhibition of autophagosome formation [115]. The homologue of VMP1 in *D. discoideum* functions in organelle biogenesis, the secretory pathway, and potentially, autophagy as well [116]. Although the topology of VMP1 has not been determined, its C-terminus binds Beclin1 suggesting that it is cytosolic. VMP1 expression is induced by induction of autophagy via rapamycin or starvation and over-expression of the protein leads to induction of autophagosome formation. Intriguingly, unlike mAtg9, VMP1 localises predominantly to the ER raising the possibility of multiple membrane sources for autophagosomes if that is the function of these transmembrane proteins.

1.1.6 Origins of the autophagosomal membrane

A typical autophagosome of 400nm in diameter has a surface area (SA) of about 500μm^2 ($SA=4\pi r^2$), which has to be multiplied by two for the outer and inner membranes. In comparison, an average endocytic vesicle has a diameter of around 100nm and therefore a surface area of around 30μm^2 illustrating the large amount of membrane that has to be re-directed to autophagosome formation within just a few minutes upon induction. Luckily, cellular membranes are not static but highly dynamic structures as exemplified by the plasma membrane of a macrophage, which is a specialised cell that can ingest 25% of its own volume of fluid an hour. This means that 3% of its plasma membrane per minute or 100% per half an hour is endocytosed [117].

Other cells like fibroblasts may endocytose more slowly at about 1% per minute but this is still a remarkable feat. Intracellular membranes may be similarly dynamic concerning vesicle budding and fusion providing fast and abundant membrane sources for autophagosome formation. Indeed, many origins for the autophagosomal membranes have been suggested including the plasma membrane, ER, Golgi and mitochondria, which will be introduced briefly below.

A striking feature of autophagosomal membranes is their lack of intramembrane particles, which clearly distinguishes them from other intracellular organelles. Freeze-fracture EM of autophagosomes revealed that the inner membrane is essentially free of any intramembrane particles and the outer membrane contained only very few [118]. This led to the hypothesis that autophagosomal membranes may be formed de novo and are not derived from any pre-existing organelles, which has gained some support [19, 119](Fig. 1-9). However, to my knowledge there has not been found any evidence for this theory such as specific lipid transport or synthesis machinery involved uniquely during autophagy.

Smooth ER was suggested to be the source of autophagic membranes by investigation of EM pictures of rat livers, which contain numerous autophagosomes or cytolysomes as they were also called then [120]. Ribosome depleted rough ER has also been suggested based on later studies [121]. This hypothesis has recently gained support by electron tomography studies showing close association of the ER around IMs with

interconnections between them [122-124]. Furthermore, it was shown that the small GTPases Rab1 and Sar1 that control ER to Golgi traffic are needed for autophagy [125].

The plasma membrane was originally suggested to be the origin of autophagosomal membranes based on EM studies during human corpus luteum involution, which is accompanied by formation of autophagic vacuoles [126]. Another recent study [127] supports this hypothesis as they show that Atg16L co-immunoprecipitates clathrin heavy chain (CHC) and AP-2, which are involved in vesicle budding from the plasma membrane and early tubular sorting endosomes in a dynamin-II dependent manner. Formation of IMs, or even precursors of IMs, was proposed to require scission of the Atg16L/clathrin/AP-2 vesicles. Furthermore, IM formation was AP-2 but not AP-1 dependent suggesting that these clathrin coated vesicles do not originate from the Golgi complex. This is an intriguing possibility for IM formation but leaves open the question where the membranes for IM extension come from.

Mitochondria were first hypothesised to provide autophagosomal membrane based on the observation that Atg9 was often co-localised with mitochondrial markers by immunofluorescence in yeast [128]. Even though closer investigation by EM revealed that Atg9 is not actually localised on the mitochondrial membrane but in close proximity to it [129], another recent study suggests that autophagosomes arise from the outer mitochondrial membrane [130].

Finally the Golgi/TGN complex has also been suggested as a membrane source for autophagosomes in an EM study where it was found that osmium staining, which predominantly labels the Golgi also labelled IMs [131]. Recent studies in yeast cells support this showing that post Golgi secretory proteins are essential for autophagosome formation and may redirect membrane from the Golgi/TGN to the PAS [132-134]. In mammalian cells it remains to be determined whether homologous secretory proteins are involved and whether mAtg9 delivers membrane to the phagophore.

Four models for phagophore extension are presented in Figure 1-9. The IM expansion model as presented in 4) would be supported by ER, mitochondria, and plasma membrane origins but other sources such as the Golgi and TGN would favour the vesicular transport model 2). However, it is very possible that a mixture of two or more models occurs and accumulating evidence suggests that autophagosomes may form using several membrane sources. This may depend on the autophagic stimulus, the cargo, the cell type, or the organism but it may also be a more general principle applying to all autophagosomes, after all, autophagy is mainly a stress response and it makes sense for the cell to exploit all possible resources under cytotoxic conditions.

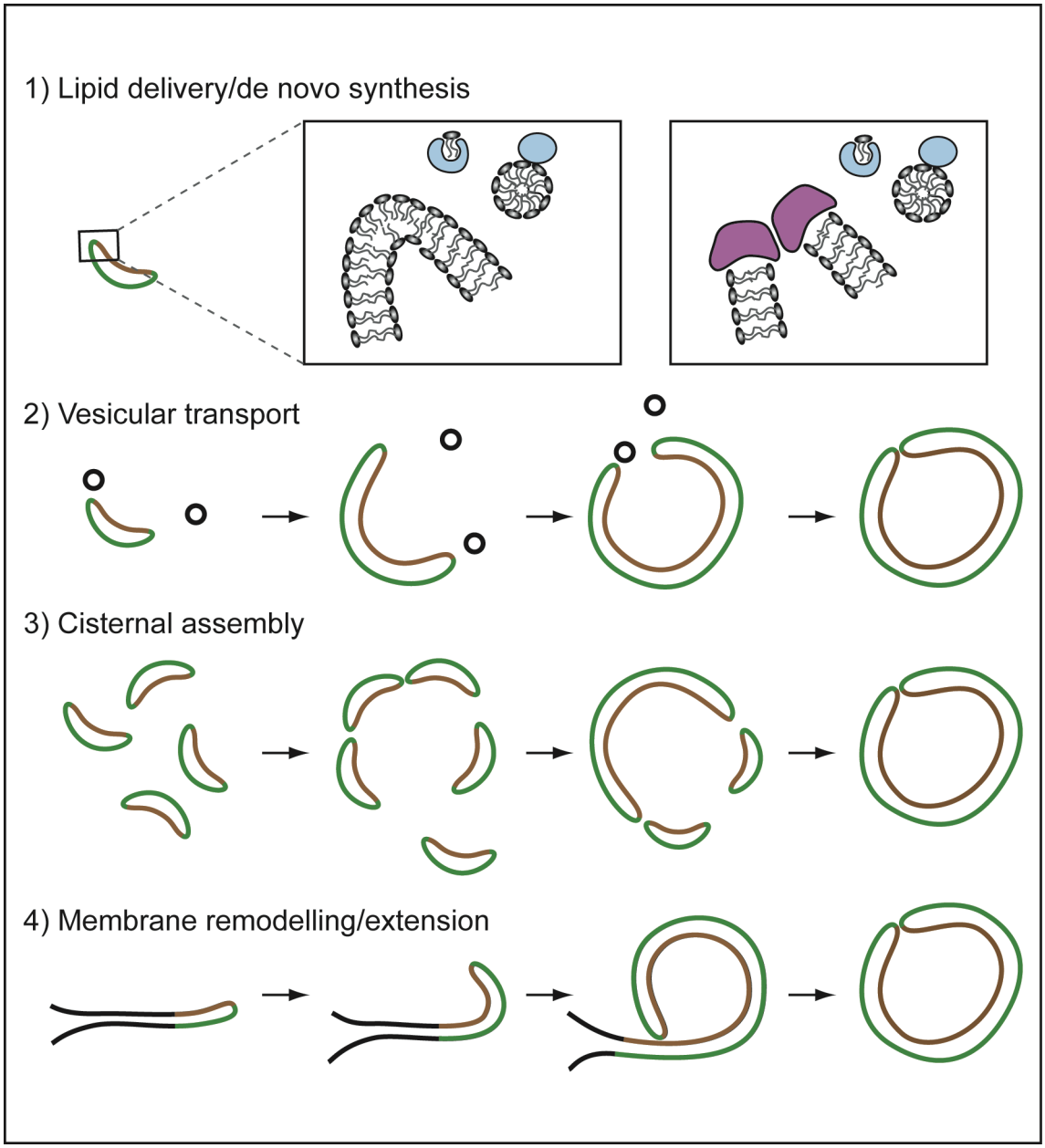

Figure 1-9 Models for autophagosome extension
1) Lipids may be delivered to IMs by lipid binding proteins as single lipids, lipid droplets or micelles. This would necessitate the presence of proteins that catalyse lipid insertion into bilayers and flipping, and possibly capping proteins for the expanding membrane sheets. Alternatively, close association with the lipid synthesis machinery in the ER could provide lipids to autophagosomes. 2) Membrane expansion by fusion of small vesicles from one or many different donor membranes. 3) Fusion of multiple pre-existing IM-like structures. 4) Membrane remodelling whereby sheets of pre-existing membrane sources are sequestered in their entirety to form autophagosomes. Finally, a combination of two or more models may be used for phagophore expansion. Figure taken from Longatti and Tooze, 2009 [19].

1.1.7 Autophagy in health and disease

Because autophagy is such an important housekeeping mechanism and stress response occurring in practically all nucleated cells it can lead to, or exacerbate a variety of diseases when not properly regulated or dysfunctional.

1.1.7.1 Autophagy and cancer

The role of autophagy in cancer is often described as a double edged sword as it has both tumour suppressive and tumour promoting properties. Beclin1 is a haplo-insufficient tumour suppressor, which is mutated in 40-75% of human breast, ovarian, and prostate cancers [135, 136]. Beclin1 null mice die early during embryogenesis due to severe developmental defects probably due to abnormal visceral endoderm formation, which provides an exchange system responsible for nutrition and waste product detoxification in the developing embryo. Heterozygous mice develop normally and are fertile [137, 138] but suffer from a high incidence of spontaneous tumours, which still express the remaining Beclin1 allele. Other proteins binding to the PI3K complex such as Ambra1 (activating molecule in Beclin1-regulated autophagy), UVRAG, and Bif1 were also shown to have tumour suppressive properties [67, 68, 76]. This seems to be true also for Atg proteins not binding to Beclin1, for instance, mice lacking Atg4C show increased susceptibility to develop fibrosarcomas induced by chemical carcinogens but only mild defects in autophagy under starvation conditions and are otherwise viable and fertile [139].

Induction of autophagy usually leads to down-regulation of cell growth and proliferation and through this interrelation may exert tumour suppressive properties. In turn, many commonly known tumour suppressor genes such as PTEN, p53, and TSC1/2 stimulate autophagy [3]. Other functions of autophagy including removal of damaged mitochondria, reactive oxygen species (ROS), peroxisomes, and other cytotoxic agents may ensure genomic stability by preventing DNA damage. However, it seems autophagy may have additional, poorly understood, roles in maintaining genomic stability such as preventing aneuploidy.

Autophagy has also been described as a non-apoptotic type of programmed cell death. Although it is now thought that this only applies to cells unable to undergo apoptosis [140] this raises intriguing possibilities for the treatment of cancer, where most cells are deficient in apoptosis. Furthermore, it has been shown that blocking autophagy increased sensitivity of tumours to chemotherapeutic agents probably either preventing direct degradation of chemotherapeutics in autophagosomes or preventing degradation of mitochondria and other inducers of caspase mediated apoptosis such as active caspase 8 protein [141-143].

Paradoxically, in normal cells autophagy is mostly a cell survival mechanism, which can help cells to overcome periods of nutrient and growth factor deprivation, hypoxia, and other stresses often encountered in primary tumours and also during metastasis. There are two popular possibilities to explain this paradox. Firstly, autophagy could prevent necrosis, which leads to inflammation thereby increasing tumour growth rate.

Secondly, it may be that the effects of autophagy are cancer-stage specific: Early on it could act mainly as a tumour suppressor preventing formation and early tumour progression by prevention of genotoxicity but at later stages it may be advantageous to the cancer promoting cell survival and metastasis. Therefore, autophagy should be targeted accordingly for therapeutic intervention.

1.1.7.2 Neurodegenerative disease

Because neurons are post-mitotic basal autophagy is especially important in these cells for the removal of damaged mitochondria, protein aggregates, and other cytotoxic components. Indeed, many neurodegenerative diseases associated with protein aggregates have been linked to autophagy including Huntington's (HD), Alzheimer's, and Parkinson's disease. However, studies in mice with neuron specific deletions of Atg5 or Atg7 show that even in the absence of disease causing mutant proteins, which may aggregate, impaired autophagy can lead to neurodegeneration [144, 145]. Interestingly, as shown in Atg5 knock-out neurons it seems that the primary target of autophagy are diffuse cytosolic abnormal proteins that form aggregates and not the aggregates themselves.

Many neurodegenerative diseases are characterised by the aggregation of mutant proteins. In Huntington's disease an expanded polyglutamine tract in the N terminus of the huntingtin protein causes its aggregation accompanied by cell death and induction of autophagy [146]. Induction of autophagy by treatment with rapamycin enhances autophagic clearance of huntingtin aggregates and reduces neuronal cell death [147]. This may be similar in other diseases characterised by aggregation of proteins with a

polyglutamine extension such as spinocerebellar ataxia, amyotrophic lateral sclerosis, and familial Parkinson's disease where autophagy has a beneficial effect protecting against neurodegeneration [3, 148].

However, the situation is not always that simple as generation of aggregates may be a cytoprotective mechanism [149]. Alzheimer's disease is characterised by aggregation of tau protein and deposition of amyloid-β (Aβ) peptide. Aβ is generated predominantly by cleavage of the Aβ precursor protein (APP) by γ-secretase. Autophagosomes accumulate in dystrophic neurites of Alzheimer's disease patients probably due to a maturation defect. Interestingly, the toxic product Aβ is produced within these autophagosomes because both APP and γ-secretase are present in the ER sequestered by the phagophores [150]. Treatment with rapamycin in this case enhanced Aβ production suggesting that autophagy can be disease promoting under these circumstances. Therefore, it may be therapeutically advantageous for some neurodegenerative diseases to block autophagy whereas activation would be beneficial others.

1.1.7.3 Crohn's disease

A polymorphism in the Atg16L1 gene (T300A) was found in patients with Crohn's disease an inflammatory bowel disorder of the small intestine. Over 30 loci have been identified controlling susceptibility to this autoimmune disease and the Atg16L1 gene is one of them [151]. Interestingly, the Atg16L1T300A variant had little effect on canonical autophagy when expressed in MEFs lacking wild type Atg16L1 as LC3 and Atg16L1T300A puncta formed normally upon starvation [152]. However, Crohn's disease can be induced experimentally in mice with hypomorphic Atg16L1 expression

[153]. This may be due to a specialised function of Atg16L1, and maybe autophagy, in intestinal paneth cells, which function in the secretion of antimicrobial peptides and other proteins that alter the intestinal environment.

1.1.7.4 Myopathies, pancreatitis, diabetes, liver and heart disease

Although neurodegeneration and cancer are probably the best studied diseases with an involvement of autophagy, the process has been shown to be involved in many other pathologies. But like in the previous two examples, it is often unclear whether autophagy plays mainly a protective or disease causing role.

In myopathies, autophagy can have a general protective role but also contribute to muscle wasting and interfere with cellular function. Cardiac-specific Atg5-deficient mice develop cardiomyopathy and die earlier than wild type animals [154]. In autophagic vacuolar myopathy an accumulation of autophagosomes is seen, which may contribute to disease [155]. In many diseases that affect a specific organ such as the kidney, liver, or lung it is unclear whether excess autophagy can contribute to organ damage or is a sign of failed repair as is well illustrated in cardiovascular heart disease with damage caused after ischemia and reperfusion accompanied by autophagy [156]. Similar questions remain about the role of autophagy in pancreatic beta-cell dysfunction, which is the main cause of diabetes type 2 [157].

In conclusion, there clearly is great interest in understanding the molecular mechanisms of autophagy in order to be able to target it therapeutically at different stages or in different ways depending on the disease or the disease stage.

1.2 Membrane trafficking

Eukaryotic cells are highly compartmentalised with many different membrane bound organelles. Transport between organelles and delivery of specific cargo has to be directed and tightly regulated because, for example, mistargeting of growth factors or other molecules can lead to a variety of diseases including cancer. Transport between compartments is achieved by vesicular trafficking and a plethora of regulatory proteins and lipids that coordinate it. It is important to understand how the different trafficking routes are intertwined and where autophagy is to be placed in this context and this study aimed at further elucidating these questions.

1.2.1 Intracellular trafficking pathways

Small vesicles transport material in between organelles in a controlled and directed fashion as was first described by George Palade in the 1960'ies and 1970'ies [158]. Some cells such as melanocytes, which secrete melanin in the skin or polarised epithelial cells exhibit highly specialised protein trafficking to fulfil their function. However, here I will describe some of the best studied major trafficking routes that apply to most nucleated cells and are relevant to the cell lines I used as models.

Proteins are synthesised in the cytosol or on the ER membrane and are subsequently targeted to their site of function. This location may be the cytoplasm itself in which case no special sorting may be necessary but most often proteins are targeted to a very specific organelle. For instance, lysosomal hydrolases, which function in protein degradation, are targeted to the lysosome. Missorting of proteins can lead to a variety of diseases as illustrated by various forms of lysosomal storage disease [159]. Generally, proteins that are secreted or targeted to intracellular organelles and the plasma membrane co-translationally enter the ER where they are folded and delivered to the Golgi apparatus for further processing. Transport to the Golgi is mainly regulated by vesicles coated with coat protein II (COPII) and coat protein I (COPI) two multimeric coatomer complexes. Assembly and trafficking of COPII vesicles is regulated among others by the small GTPases Rab1 and Sar1 and goes to the ER Golgi intermediate compartment (ERGIC) from where COPI vesicles regulate traffic to the Golgi complex [160-163]. Interestingly, Rab1 and Sar1 have recently been shown to be essential for autophagosome formation whereas COPI subunits are important for autophagosome maturation [125, 164].

Retrograde traffic from the Golgi to the ER and intra Golgi trafficking is mediated by vesicles coated by the COPI coatomer regulated by the Arf GTPase [165]. Furthermore, COPI vesicles have also been shown to regulate endosomal trafficking and autophagosome maturation [164, 166-168]. From the Golgi complex and the trans-Golgi network (TGN) proteins can be sorted to endosomes or the plasma membrane via clathrin coated vesicles. Clathrin coated vesicles are another form of coated carriers and

can mediate endocytosis from the plasma membrane to early endosomes but one important difference is that while clathrin coated vesicle transport between the TGN and endosomes requires the adaptor protein AP-1, endocytosis requires AP-2 [169]. Two related adaptors AP-3 and AP-4 have also been found to localise to the TGN and endosomes but are not necessarily enriched in clathrin coated vesicles suggesting that they can regulate assembly of other vesicles [170]. AP-3-coated vesicles deliver their cargo to lysosomes or late endosomes and may be important in lysosome biogenesis. AP-4 is the least well studies adaptor complex but a recent study has found that it regulates transport of amyloid precursor protein from the TGN to endosomes thereby reducing amyloidogenic processing, which contributes to Alzheimer's disease [171].

An astonishing number of different endocytic pathways have been described (Fig. 1-10) and most of them deliver their cargo to early endosomes.

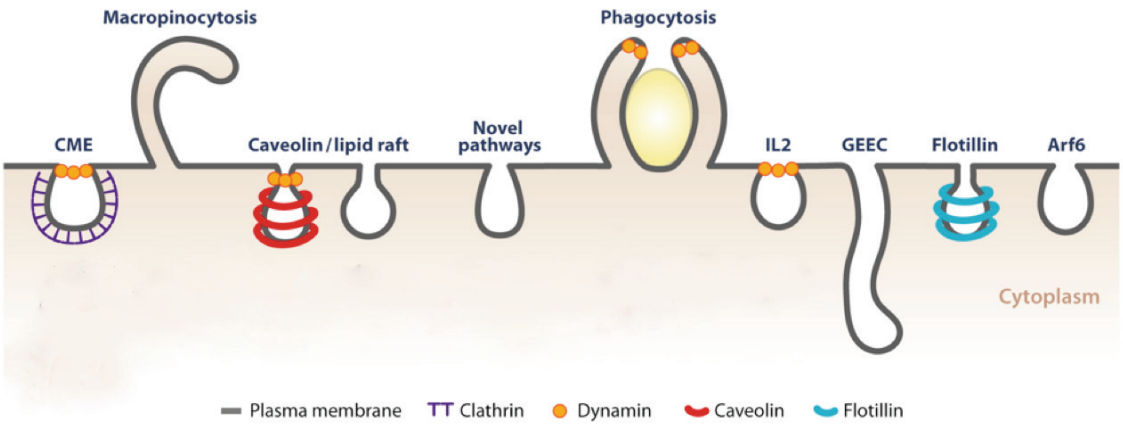

Figure 1-10 Endocytic pathways
A plethora of endocytic pathways have been described so far. Some share common machinery such as the GTPase Dynamin, which mediates pinching or popping off of vesicles. Others use unknown machinery. Figure modified from Mercer et al., 2010 [172].

The best studied mechanism of uptake is receptor mediated endocytosis through clathrin coated pits/vesicles (CCPs/CCVs). CCPs are small, invaginated membrane structures intracellularly coated by a regular lattice formed by the clathrin protein complex [173]. First discovered in electron micrographs because of their distinct regular appearance seen as spikes emanating from membrane invaginations [174] and even more impressively visualised in freeze fracture electron micrographs done by John Heuser [175] (Fig. 1-11), there are now countless studies that have helped to elucidate the molecular mechanisms of CCP mediated endocytosis [176]. CCPs can be pre-existing on the plasma membrane or assemble upon receptor activation. Two important proteins in CCV formation are the adaptor protein AP-2 and the GTPase Rab5. AP-2 is important for cargo selection through specific recognition signals whereas Rab5 recruits necessary effectors for vesicle targeting and transport [177]. Interestingly, both proteins have been shown to be involved in autophagosome formation and AP-2 and/or clathrin seem to bind Atg16L [127]. Once endocytosed the clathrin coat is disassembled and the vesicle can fuse with early endosomes where further sorting takes place.

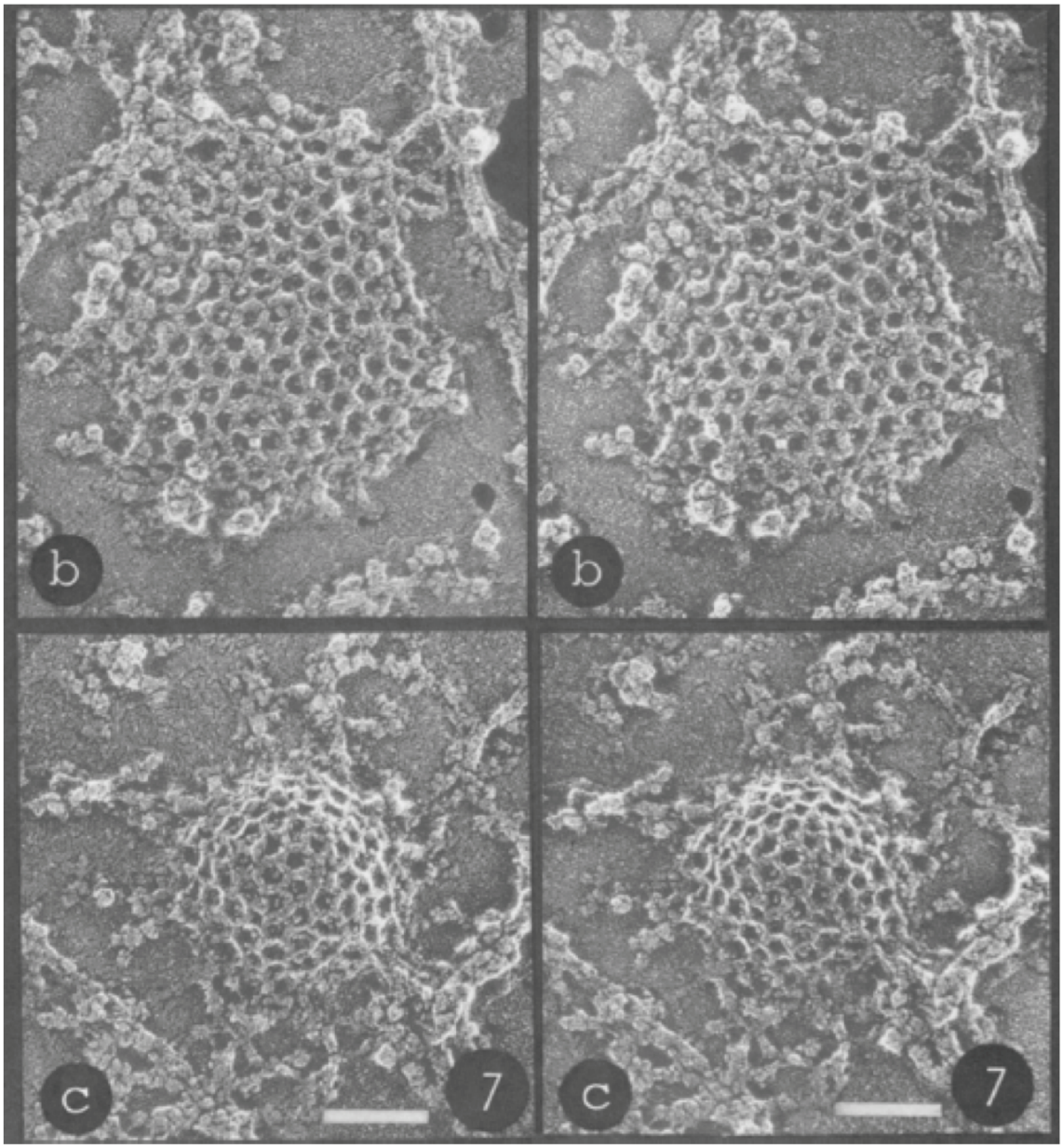

Figure 1-11 Internalisation of a CCP
Clathrin lattices can be flat or bulging inward forming CCPs. CCPs eventually form round vesicles that pinch off the plasma membrane. The clathrin coat is then removed and the vesicle can fuse with an early/sorting endosome. Image taken form Heuser, 1980 [175].

Once the cargo has reached the early endosome, also called sorting endosome, it can follow various intracellular routes. The best studied proteins and most relevant to this thesis are the cation-independent mannose-6-phosphate receptor (CI-MPR), the

epidermal growth factor receptor (EGFR) and ligand (EGF), and the transferrin receptor (TfnR) with its ligand transferrin (Tfn). CI-MPR is responsible for the delivery of lysosomal enzymes from the Golgi/TGN and cycles rapidly between late endosomes and the TGN [178] (Fig. 1-12). Lysosomal enzymes are tagged with a mannose-6-phosphate (M6P) in the Golgi that is recognised by CI-MPR to deliver them to the lysosome. mAtg9 co-localises with CI-MPR both on the TGN and late endosomes but the functional significance of this is not known [41].

EGF on the other hand is taken up from the extracellular space via its receptor EGFR. Both EGF and EGFR are thought to stay associated with early endosomal membranes as they acidify and mature into late endosomes. Invagination of the endosomal membrane mediated by the endosomal sorting complex required for transport (ESCRT) machinery leads to multivesicular body (MVB) formation and eventually lysosomal degradation of EGF and EGFR [179, 180]. Interestingly, the ESCRT complexes have been shown to be essential for autophagosome maturation but it is unclear what their exact role in this process is [181, 182]. The two likely possibilities are that a block in MVB formation leads to impaired fusion of autophagosomes with endosomes or that the ESCRT complexes themselves are responsible for autophagosome closure or a combination of the two [19, 181]. There are four ESCRT complexes in mammalian cells ESCRT-0, ESCRT-I, ESCRT-II, and ESCRT-III, which are multi-protein complexes themselves. They are thought to coordinate membrane invagination, closure and pinching off of the internal vesicles [179]. Topologically this is very similar to the closure of an autophagosome and it is easy to imagine that the ESCRT complexes could

act on both vesicles. Rab7 is essential for early to late endosome maturation and also for autophagosome endosome fusion [183, 184].

Unlike EGFR, which stays associated with endosomal membranes as they mature to MVBs and lysosomes, Tfn and its receptor TfnR are actively sorted away from the early endosomes through the action of the BAR domain containing protein SNX4 and the GTPase Rab11. TfnR is sequestered into SNX4 coated tubules from where vesicles bud off and are transported in a dynein dependent manner to the pericentriolar endocytic recycling compartment (ERC). The ERC is a cluster of vesicles and tubules close to the Golgi apparatus involved in protein recycling to the plasma membrane [60]. Tfn remains bound to its receptor TfnR at all times but the iron bound by Tfn is released in the slightly acidic environment of the early endosome. From the ERC Tfn is recycled back to the plasma membrane where it can bind fresh iron. TfnR can also be sorted back to the plasma membrane from the early endosome directly in a Rab4 dependent manner.

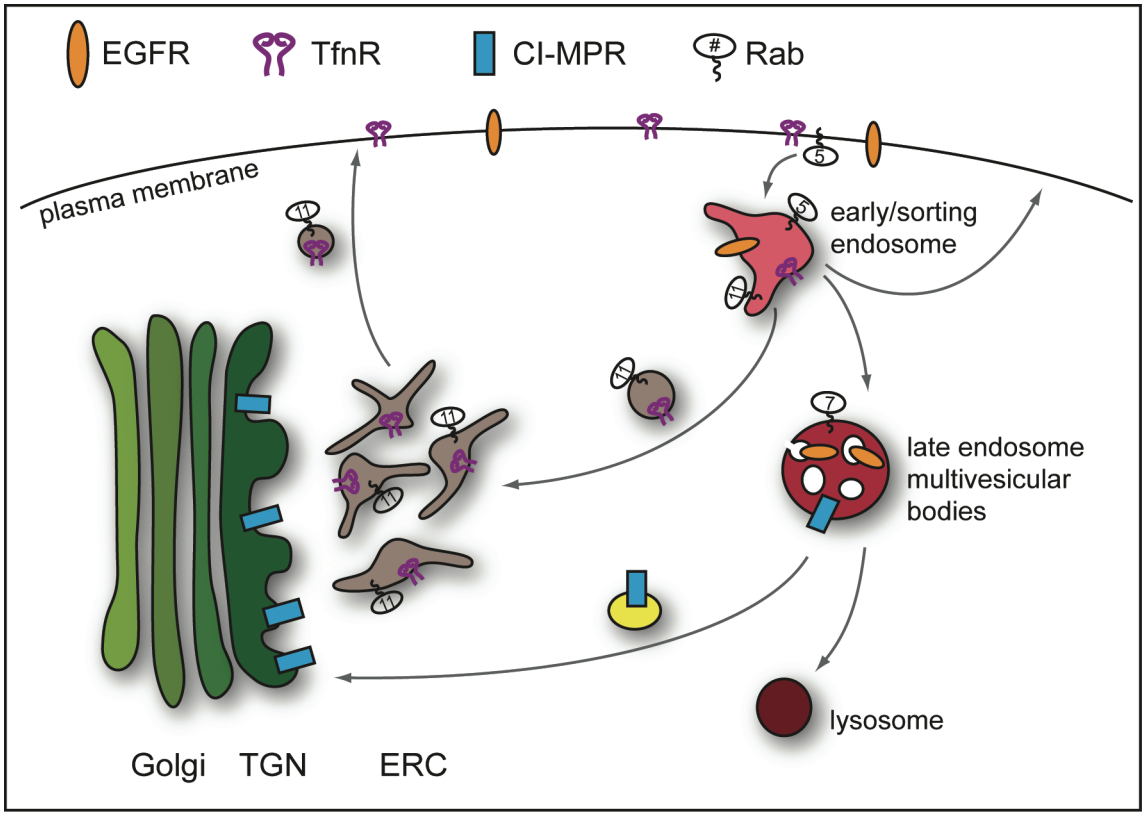

Figure 1-12 Intracellular vesicular trafficking
Depicted are the vesicular trafficking routes of CI-MPR, EGFR, and TfnR with their ligands M6P, EGF, and Tfn respectively. CI-MPR shuttles between the TGN and late endosomes/MVBs to deliver lysosomal proteins tagged with M6P. EGFR is internalised from the plasma membrane upon EGF binding. MVB formation leads to internalisation of EGFR in vesicles inside the endosome and ultimately to lysosomal degradation of the ligand and receptor. Tfn is internalised and delivered to the early endosome from where it is sorted in a Rab11 dependent manner to the ERC. From the ERC TfnR can be returned to the plasma membrane. TfnR can also be sorted back to the plasma membrane from the early endosome directly in a Rab4 dependent manner.

1.2.2 Rab GTPases, RabGAPs, and GEFs

1.2.2.1 Rab GTPases

Rab GTPases are small monomeric GTP binding proteins related to Ras GTPase. There are about 60 Rabs encoded in the human genome and each one is thought to regulate a different membrane trafficking step (Fig. 1-13). Rab GTPases are synthesised as

cytosolic proteins but are quickly bound by Rab escort protein (REP), which presents them to the geranylgeranyl transferase [185]. The geranylgeranyl transferase attaches one or in most cases two hydrophobic geranylgeranyl groups to cysteines in the C-terminus of Rabs. This allows reversible membrane anchoring of the Rab protein. Major conformational changes occur between the GDP and GTP bound forms of Rab proteins mainly in two regions termed switch I and switch II [186]. In their GDP bound form Rabs are cytosolic and can be regarded as inactive. GDP dissociation inhibitor (GDI) binds GDP bound Rab GTPases and chaperones them in the cytosol masking the hydrophobic lipid tail [187-189]. GDI also ensures that GDP remains bound [190] and shuttles Rabs to their cognate membrane and back to the cytosol. How the distinct membrane localisation of each Rab is achieved is poorly understood [191]. However, there is evidence that membrane-bound GDI displacement factors (GDFs) can target Rabs to the correct membrane by recognising specific Rab-GDI complexes and displacing the GDI, which will lead to membrane insertion of the Rab [192]. Conserved residues in the Rab GTPases are responsible for nucleotide binding. Mutation of the conserved glutamine to alanine (QA) leads to preferential binding of GTP rendering the Rab constitutively active. Mutation of the conserved asparagine to isoleucine (NI) leads to inability of the Rab to bind any nucleotide at all, whereas mutation of the conserved serine/threonine to asparagine (S/TN) leads to preferential GDP binding in each case leaving the Rab constitutively inactive.

In their active GTP bound state Rabs are on their cognate membrane and recruit various effectors to mediate vesicular traffic including motor proteins such as dynein, SNARES (soluble N-ethylmaleimide-sensitive factor attachment protein receptor), which catalyse

membrane fusion, tethering proteins, and regulators such as PI kinases. In this manner, each Rab is thought to direct a specific trafficking step in the cell and localises to those membranes accordingly (Fig. 1-13). As depicted in Figure 1-13 many Rab proteins can form distinct subdomains on a single organelle. For example recycling endosomes contain both Rab11 and Rab4 positive subdomains whereas early endosomes contain Rab4 and Rab5 subdomains within the same continuous membrane [193]. This compartmentalisation is important for proper protein sorting since different cargo in the same organelle has to be transported to different destinations.

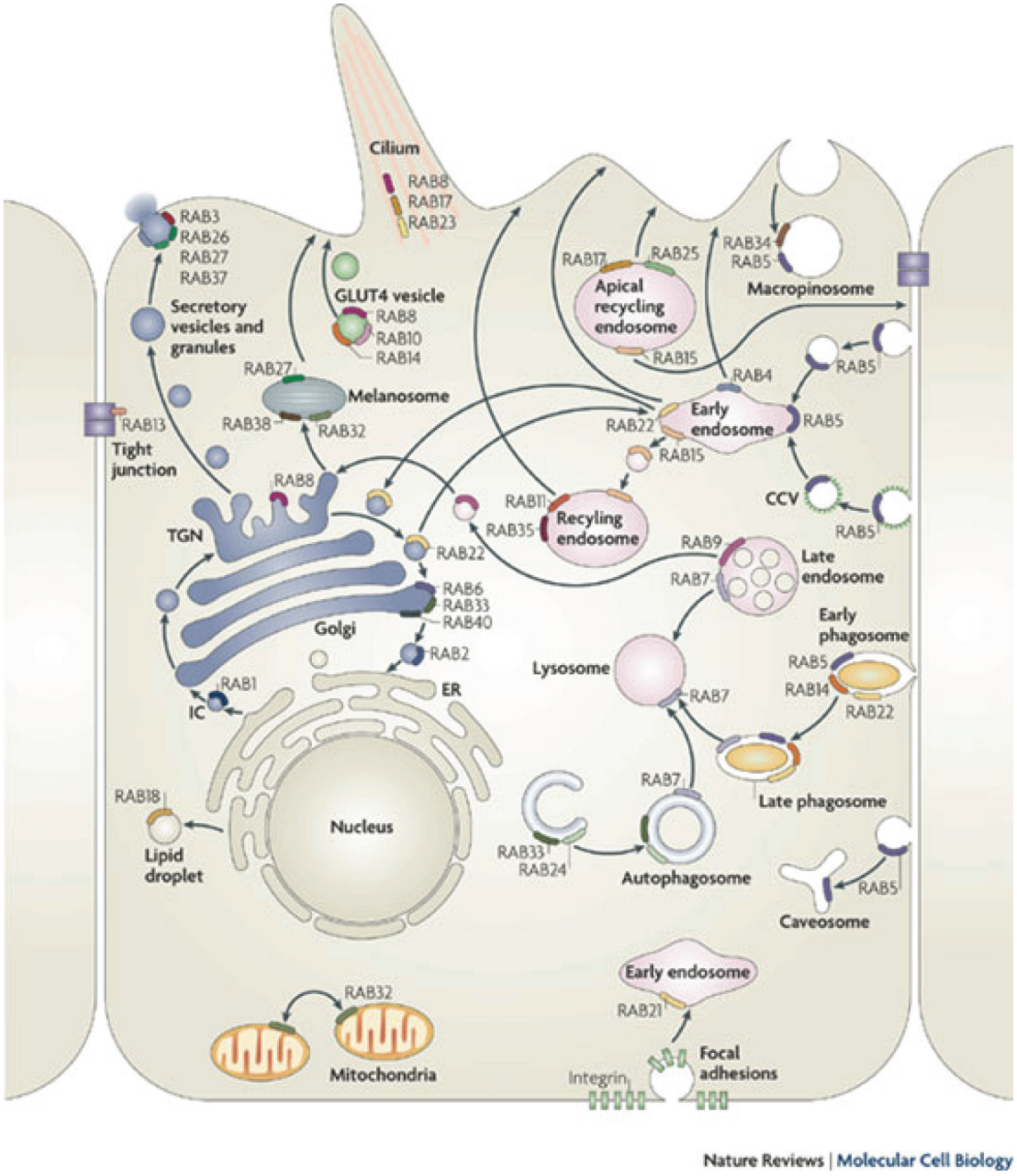

Figure 1-13 Overview of Rab GTPases in membrane traffic
Illustrated are the major cellular trafficking routes and the Rab GTPases that regulate them. Figure taken from Stenmark, 2009 [194].

1.2.2.2 RabGAPs

Rab GTPases generally have very low intrinsic GTPase activity. Their activity is controlled by a family of proteins termed Rab GTPase activating proteins (RabGAPs),

which is a misleading name since they catalyse GTP hydrolysis in the Rab thereby inactivating it (Fig. 1-14). The crystal structure of a yeast RabGAP Gyp1p together with Rab33 revealed that RabGAPs contribute two catalytic residues an arginine and a glutamine *in trans* that mediate GTP hydrolysis [195]. These two residues also called arginine finger and glutamine thumb extend into the GTP binding pocket of the Rab and lead to GTP hydrolysis. These residues are highly conserved in all 38 putative human RabGAPs and it is thought that this mechanism applies to all GAPs. The GAP domain is also called Tre-2/Bub2/Cdc16 (TBC) domain, which was used to identify the 38 putative human RabGAPs [196, 197]. The TBC domains consist mostly of alpha helical folds and seem to be structurally similar between different TBC proteins even though there is relatively little sequence homology between them with only the arginine and glutamine residues conserved.

This is supported by the crystal structure of two human RabGAPs TBC1D22A and TBC1D14 [198]. The structures of the GAP domains were modelled on the Gyp1p (similar to TBC1D22) crystal structure. Interestingly, the two catalytic residues of TBC1D22A align closely with those of Gyp1p but the conserved arginine and glutamine of TBC1D14 do not. Binding of the target Rab, which is not known, to TBC1D14 may induce the conformational changes necessary for the residues to align in order to catalyse GTP hydrolysis. However, this is not supported by the Rab-bound and unbound structures of Gyp1p, which are very similar. Otherwise the alignment could be done differently so that the catalytic A and Q and immediately adjacent residues of TBC1D14 are aligned with the catalytic residues of Gyp1p while allowing significant distortions to the rest of the TBC domain.

It is thought that each RabGAP acts on a specific Rab family since there are about 40 of those and there is good evidence that supports this hypothesis [196, 197, 199-204].

1.2.2.3 GEFs and GEF/GAP-cascades

The antagonists of RabGAPs are the guanine nucleotide exchange factors (GEFs), which facilitate the exchange of GDP for GTP. The high cytosolic GTP concentration (~1mM) ensures that as soon as the GDP in the Rabs is removed it is replaced by GTP leading to Rab activation and effector recruitment. GAPs and GEFs act in cascades and can also be recruited by a Rab that is not their target but is immediately upstream or downstream, respectively, of their target Rab to regulate Rab conversion of a compartment. A well studied Rab conversion is the transition from early to late endosomes from a Rab5 to a Rab7 positive compartment [205]. These conversions are regulated by GEF cascades and counter-current GAP cascades. For example, Rab5 recruits the GEF for Rab7 during early to late endosome maturation [206]. Conversely GAP cascades exist such as the one described for the yeast GAP Gyp1p, which is recruited by Ypt32p (similar to Rab11) and acts on Ypt1p (similar to Rab1) to ensure conversion of the compartment from Ypt1p to Ypt32p positive vesicles [207].

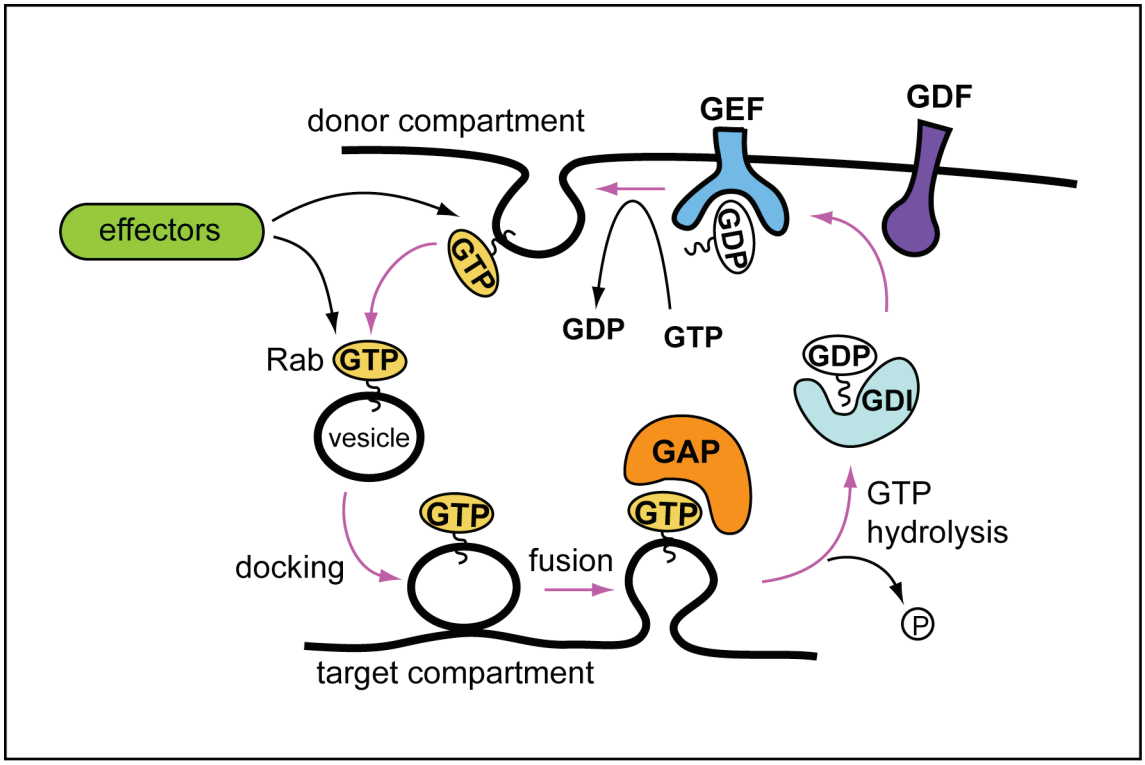

Figure 1-14 The Rab cycle
Rab GTPases cycle between an active GTP bound and an inactive GDP bound state and act like molecular switches. In the on state they are membrane bound and can recruit various effector proteins to guide and facilitate vesicular trafficking. In the off state they are cytosolic and bound to GDP dissociation inhibitor (GDI). Two families of enzymes regulate the activation state of their corresponding Rab proteins: the Rab GTPase activating proteins (RabGAPs), which catalyse GTP hydrolysis rendering the Rab inactive and the guanine nucleotide exchange factors (GEFs), which facilitate exchange of GDP for GTP thereby activating the Rab. GDI displacement factors (GDFs) may facilitate targeting of Rabs to their cognate membrane compartment.

Another striking feature of intracellular compartmentalisation is the localisation of different lipids and in particular phosphoinositides (PIs) to different membranes (Fig. 15). This is an important feature contributing to membrane identity as proteins can bind specifically to certain PIs. This PI distribution is maintained by the PI kinases (PIKs) and PI phosphatases, whose activation is often regulated by Rab GTPases. For example, the class III PI3K on endosomes is an effector of Rab5 and Rab7 [208, 209]. However,

it is unclear whether a specific Rab protein recruits the autophagic class III PI3K complex to IMs.

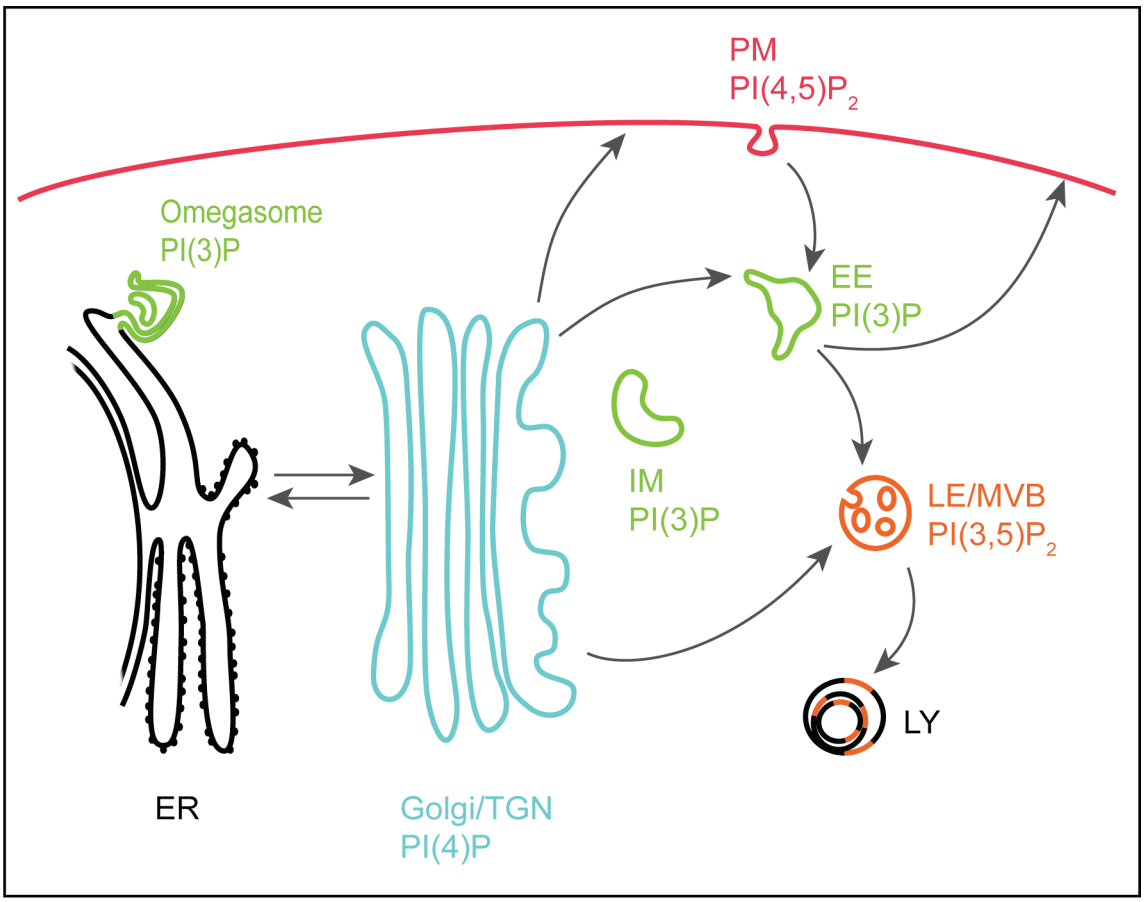

Figure 1-15 Distribution of major PI species
Different intracellular compartments maintain different PI lipid species, which is important for the integrity of each organelle. Autophagosomes and/or omegasomes are enriched in PI(3)P but it is not clear how IM localised Atg proteins can distinguish between early endosomes (EE) and the phagophore (IM). LE/MVB=late endosome/multi-vesicular body; LY=lysosome; PM=plasma membrane.

1.2.3 Rab GTPases in autophagy

Rab GTPases are important regulators of membrane traffic and it is reasonable to assume that one or more are involved in autophagosome formation, which involves major membrane shaping and/or trafficking events. Some Rab GTPases have already been shown to be involved in autophagy and will be introduced here (Fig. 1-16).

Rab1 was recently shown to be involved in autophagy but its exact role remains unclear [125]. Rab1 is found on ER exit sites (ERES) and the cis and medial-Golgi cisternae where it is thought to regulate ER to Golgi traffic [161]. Over-expressed Rab1b co-localises with LC3 positive autophagosomes and staining with lyso-tracker revealed that Rab1b associates with acidic compartments, which presumably are autolysosomes since there is no co-localisation with lyso-tracker in fed conditions. Furthermore, they could show that the small GTPase Sar1, which is also involved in ER to Golgi traffic is essential for autophagy.

Rab32 is another ER localised GTPase that was shown to be essential for autophagosome formation [210]. Interestingly, Rab32 does not seem to be essential for starvation induced autophagy but specifically basal autophagosome formation. Inactivation of Rab32 by over-expressing the dominant negative mutants of Rab32 or by siRNA mediated knock down led to protein aggregate formation and a block in autophagosome formation. This finding may be particularly important in neurodegenerative pathologies where a block in basal autophagy seems to contribute to

disease. Rab32 is also involved in melanosome formation and transport, which is specific to melanocytes [211, 212].

Rab24 is an atypical Rab GTPase, which is inefficiently geranylgeranylated and therefore mostly cytosolic but also localises to the ER, ERGIC and Golgi compartment [213]. Rab24 redistributes to autophagic vacuoles upon starvation but seems to be associated mainly with degradative autophagosomes suggesting it is involved in maturation and not formation [214].

Rab7 is another GTPase that is involved in autophagosome maturation most likely by mediating fusion of autophagosomes with late endosomes and lysosomes [183, 184]. The SNARE protein Vti1b seems to catalyse this fusion process since mice deficient in it accumulate autophagosomes [215]. Note that fusion of autophagosomes with early endosomes is also essential since loss of COPI function which causes disruption of early endosomes also led to autophagosome maturation defects [164]. Likewise, Rab11, which usually regulates RE traffic was found to be on MVBs in K562 cells and may mediate fusion of MVBs with autophagosomes in those cells [216].

The only Rabs that have been shown to act at early stages of autophagosome formation are Rab5 and Rab33. Previous extensive research has shown that Rab5 is found on early endosomes and the plasma membrane regulating traffic between those compartments. With regard to autophagosome formation it was found to regulate Atg5-12 conjugation and to act in a macromolecular complex with Beclin1 and Vps34 [217]. Interestingly,

this autophagic function of Rab5 is independent of its role in endocytosis since blocking endocytosis leads to inhibition of autophagosome maturation whereas Rab5 inactivation hampers autophagosome formation and leads to impaired clearance of mutant huntingtin. In a more recent paper, the same group found that blocking clathrin-mediated endocytosis leads to impaired IM formation [127] but the exact relation between Rab5, clathrin-mediated endocytosis and autophagosomes remains to be elucidated.

Rab33b on the other hand is a Golgi located protein involved in retrograde traffic to the ER, intra-Golgi traffic, and Golgi homeostasis [218]. Isoform Rab33a is expressed in the brain, lymphocytes, and normal melanocytes whereas Rab33b is ubiquitous [219-221]. Both isoforms of Rab33 were shown to bind Atg16L in a GTP dependent manner and when over-expressed are able to recruit the Atg16L complex to the Golgi [222]. Expression of a constitutively active Rab33 induces LC3 lipidation even under fed conditions but leads to an overall block in autophagy presumably because phagophore expansion cannot progress. Their data suggests that Rab33 is responsible for Atg16L complex trafficking but additional factors are needed to complete autophagosome formation.

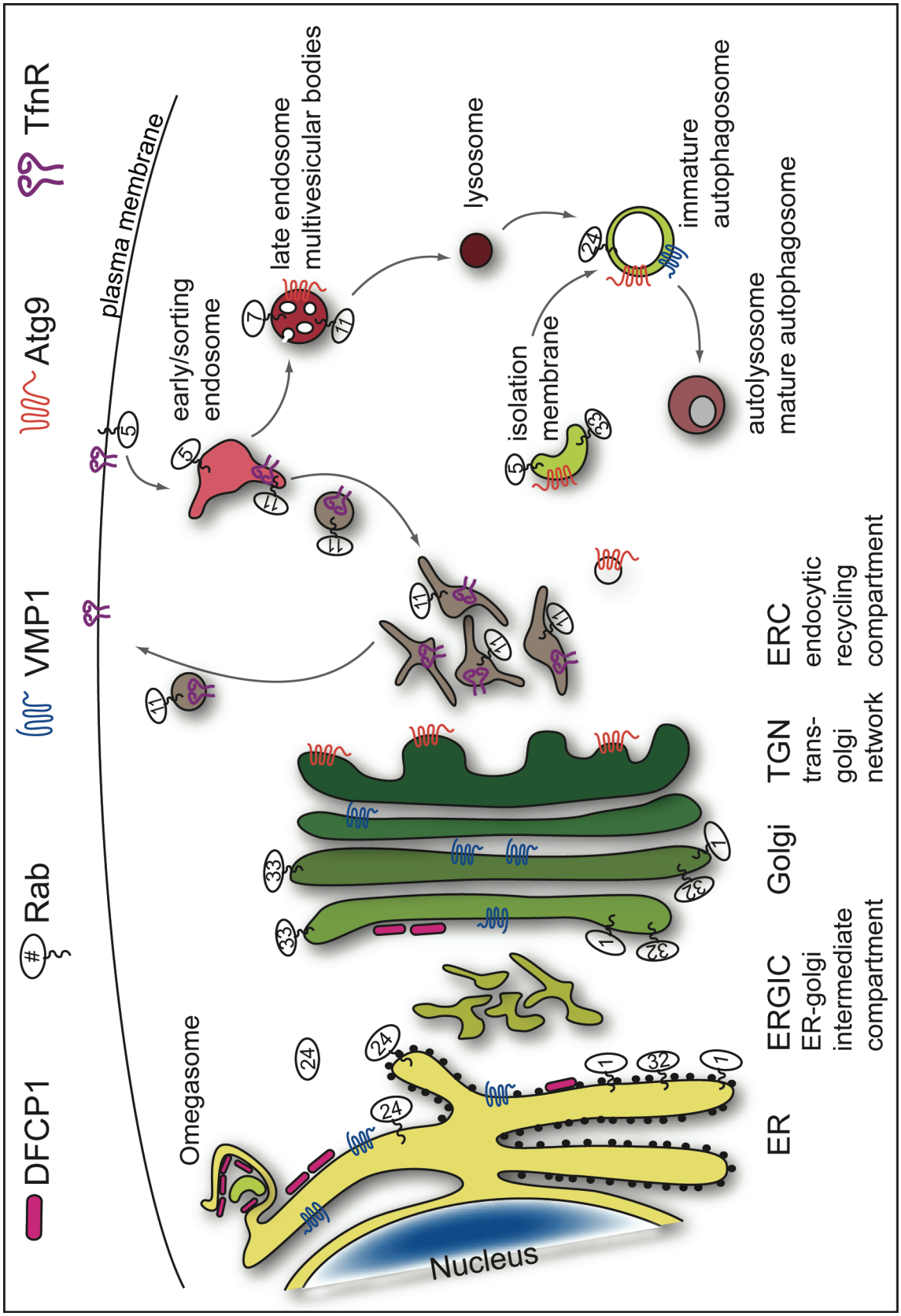

Figure 1-16 Rab GTPases involved in autophagy

Depicted are the Rab GTPases that have been shown to be involved in autophagy and their subcellular localisation. Rab33 and Rab5 act at early stages of autophagosome formation whereas Rab1, Rab24, Rab11, and Rab7 are involved in autophagosome maturation. Interestingly, Rab32 seems to be involved in basal but not starvation induced autophagy.

1.3 Autophagy and the immune system

The vertebrate immune system can mount both an innate and adaptive immune response. The innate response is the first line of defence against pathogens and acts early recognising conserved patterns of invading organisms. The adaptive immune response happens later but is much more specific and dependent on the innate responses. The adaptive immune response becomes more and more accurate over the course of an infection and is able to retain memory cells that can be activated much more quickly in case of re-infection with the same pathogen. The adaptive immune response depends on B and T lymphocytes, which recognise specific antigens via their B and T cell receptor (TCR), respectively. Whereas B cell receptors can recognise soluble antigens TCRs only recognise antigens presented on MHC complexes on the plasma membrane of antigen-presenting cells (APCs) [223]. The TCR itself cannot transmit intracellular signal and relies on the TCR associated transmembrane protein CD3, which activates the TCR responses (Fig. 1-17). In addition to that TCR/CD3 stimulation is not enough to trigger T cell activation but a co-stimulatory receptor CD28 has to be bound by its ligand, which can also be provided by APCs. Intracellular pathways include PKC activation and Ca^{2+} signalling leading to proliferation, survival, and activation of gene transcription in T cells. Another co-stimulatory signal is provided by CD4, which recognises MHC class II molecules, or CD8, which recognises MHC

class I molecules. Immature T cells in the thymus initially express both CD4 and CD8 but if their TCR recognises a peptide presented by MHC class II complexes CD8 expression is down-regulated and vice versa. After activation, CD4 positive T cells will act as helper T cells, whereas CD8 positive T cells will act as cytotoxic or killer T cells.

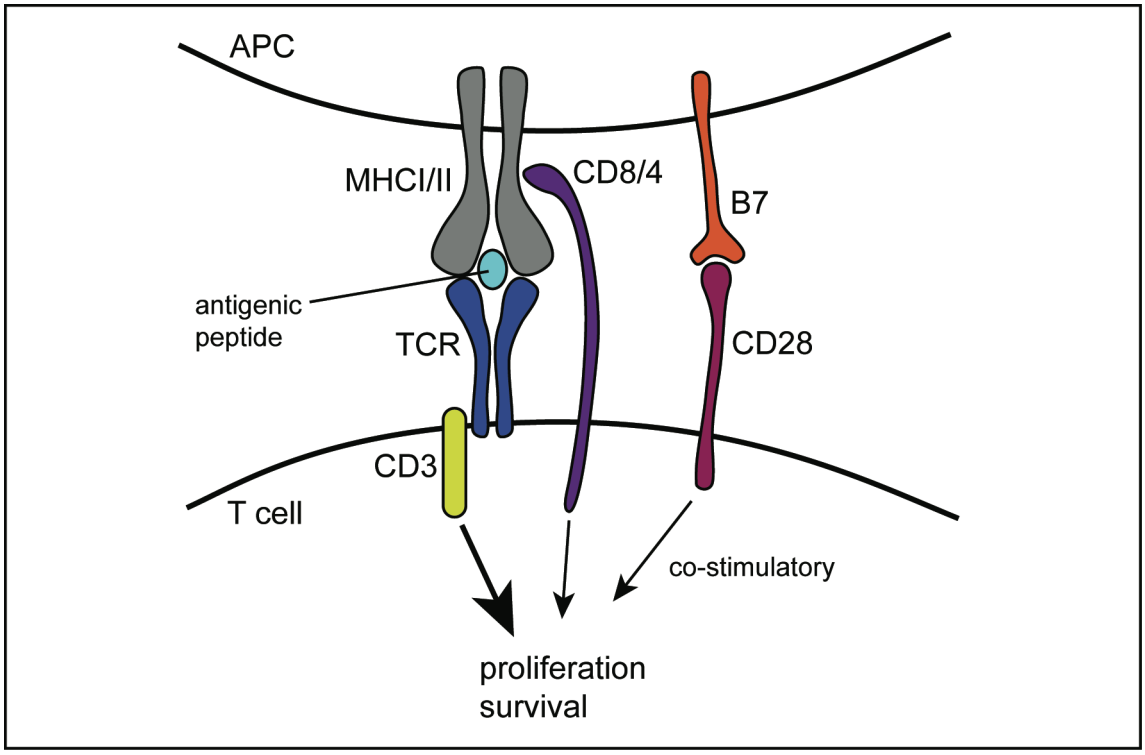

Figure 1-17 The TCR recognises antigenic peptides bound to MHC molecules
A specific peptide bound to an MHC complex is recognised by the TCR leading to downstream signalling via CD3. CD8 or CD4 provide co-stimulatory signals for MHC class I or MHC class II complexes, respectively. CD28 also provides co-stimulatory signals when bound by its ligand B7. This leads to activation of transcription, T cell survival, and proliferation.

Autophagy genes have been shown to be involved in both branches of the immune system although it is not always clear whether classical autophagy as described above is involved in fighting disease or whether autophagy proteins can have other independent functions in the immune system [224]. Figure 1-18 gives an overview of the functions

of autophagy or autophagy genes involved in the immune system, which will be introduced in more detail below.

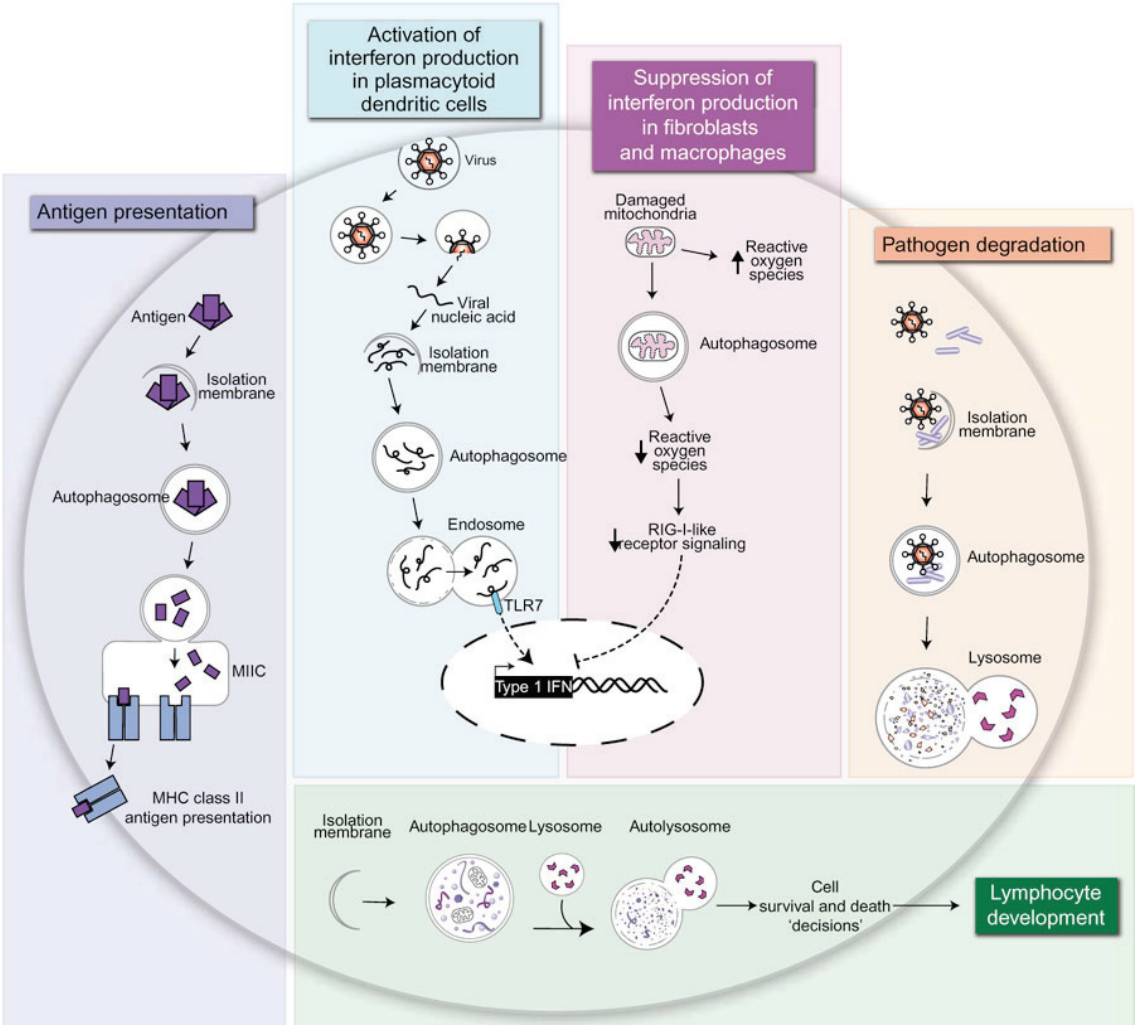

Figure 1-18 Autophagy in the immune system
Overview of the major functions of autophagy in the immune system. Clockwise from left: Autophagy can deliver endogenously expressed antigens to MHC class II complexes in endosomes. Autophagosomes can capture cytosolic antigens and deliver them to endosomes for Toll-like receptor (TLR) activation. Mitophagy can reduce production or reactive oxygen species (ROS) to prevent excess production of type I interferons (IFNs) in fibroblasts and macrophages. Autophagy can engulf invading pathogens and deliver them to the lysosome for degradation. Autophagy is important for lymphocyte development and homeostasis. Figure taken from Virgin and Levine, 2009 [224].

1.3.1 Innate immunity

Innate immunity is the first line of defence against infectious agents. Pattern recognition receptors (PRRs) such as the Toll-like receptors (TLRs) detect microbial components and can activate immune responses. However, these have to be closely controlled since excessive activation of the innate immune system can lead to massive inflammation and autoimmune disease [225].

The most straightforward autophagy related innate immune response is direct engulfment of invading pathogens by autophagosomes leading to lysosomal degradation. Autophagic clearance has been shown for many different infectious agents such as *Listeria monocytogenes* [226], group A *Streptococcus* [227, 228], and *Coxiella burnetii* [229, 230]. However, other functions of autophagy in the innate immune system are more complex and Atg genes may exert immuno-modulatory functions not related to classical autophagosome formation. For example, during *Toxoplasma gondii* infection Atg5 is critical for the recruitment of immunity related GTPases but does not lead to engulfment of the pathogen by an autophagosome [231, 232]. Furthermore, autophagy proteins may be recruited to enhance phagolysosomal maturation, for example LC3 and Beclin1 can be recruited to phagosomes without the involvement of classical autophagosome formation [233, 234]. Some pathogens have evolved mechanisms to avoid autophagic elimination for example *Shigella flexneri* expresses a protein that inhibits Atg5 function [235]. Others have even found ways to exploit autophagy as is the case with some RNA viruses such as hepatitis C virus (HCV), which depends on at least parts of the autophagic machinery to replicate [236, 237].

Another important aspect of autophagy in innate immunity is the delivery of microbial components to TLRs. Because some TLRs reside in endosomes cytoplasmic infectious agents have to be delivered to them via autophagy. One example is the engulfment of cytosolic viral nucleic acid by autophagosomes in plasmacytoid dendritic cells (pDCs), which leads to induction of anti-viral type I interferon (IFN) via TLRs signalling [238]. Interestingly, in some cases TLR activation in turn leads to induction of autophagy [239, 240]. However, it is not clear whether this is a mechanism to increase autophagic degradation of pathogens, to enhance delivery of microbial components to TLRs and other innate immune receptors, or to enhance autophagic delivery of peptides to MHC class II complexes to aid activation of the adaptive immune response.

In pDCs, induction of autophagy leads to the delivery of viral nucleic acid to endosomes and subsequent TLR signalling induces activation of type I IFN. Somewhat paradoxically, in macrophages and fibroblasts autophagy seems to prevent the activation of type I IFN and other inflammatory cytokines [241]. It seems that in these cells mitophagy prevents the production of reactive oxygen species (ROS) by damaged mitochondria. This, in turn leads to reduced activation of another cytosolic PRR called RIG-I-like leading to down-regulation of type I IFN and inflammatory cytokines [242, 243]. This may be of importance in the pathobiology of Crohn's disease, which is an inflammatory bowel disorder that can be experimentally induced in mice with hypomorphic Atg16L1 expression [153]. Enhanced secretion of type I IFN and cytokines in these mice may lead to or exacerbate inflammation, which is a hallmark of the disease. A polymorphism in the Atg16L1 gene (Atg16L1T300A) was found

associated with Crohn's disease in humans but further studies are necessary to elucidate whether similar changes relating to Atg16L activity occur in patients carrying the T300A polymorphism [151]. However, it has been shown that canonical autophagy is not affected in fibroblasts expressing mutant Atg16L1T300A [152].

1.3.2 Adaptive immunity

In the adaptive immune system autophagy was shown to play an important role in T cell selection in the thymus [244]. T cells mature in the thymus where they undergo positive and negative selection. The latter ensures that no autoreactive T cells escape into the periphery and the former ensures that T cells do not mature if their TCR does not recognise any peptides presented by the MHC complexes. This selection is supervised by APCs such as thymic epithelial cells (TECs) present in the thymus, which constantly display MHC loaded antigens to immature T cells. If a T cell strongly recognises an auto-antigen they are induced to undergo apoptosis to prevent autoimmune reactions. Growing evidence suggests that endogenous antigen presentation by MHC class II molecules depends on autophagy [245]. The MHC class II complex is loaded with antigenic peptides in an endosomal compartment and it seems that TECs use autophagy to deliver endogenous antigens there. Indeed, when embryonic thymi from Atg5 knock-out or wild type mice were transplanted into athymic nude mice these started to show signs of autoimmune disease in several organs including the gut [244]. This was shown to be due to the inability of Atg5-/- TECs to undergo autophagy, which leads to reduced or absent presentation of auto-antigens and maturation of autoreactive T cells. These T cells can then escape to the peripheral blood stream and are activated upon auto-antigen

encounter in the spleen. In a healthy immuno-competent mouse there are other mechanisms to prevent autoimmune disease such as regulatory T cells, which can cause apoptosis or anergy in self-reactive T cells but nude mice lack these responses. Impaired positive selection of T cells might explain susceptibility to Crohn's disease in patients with an Atg16L1 polymorphism [224] but it remains to be shown whether this polymorphism causes any specific autophagy defects as it does not affect canonical autophagy [152]. While the physiological role of autophagy during T cell selection is clear it remains to be elucidated whether this is a major pathway for it MHC class II antigen loading *in vivo* and the role of autophagy in MHC class I antigen presentation remains speculative [246, 247].

Another important function of autophagy is in lymphocyte homeostasis and activation. Upon antigen encounter lymphocytes undergo clonal expansion and massive rearrangement of the cytoplasm and organelles in order to become effector B and T cells. Furthermore, T and B cells regularly encounter lowered growth factor and nutrient environment in the blood stream upon leaving the lymphoid organs (spleen, thymus, bone marrow, and lymph nodes). Indeed loss of Atg5 or Atg7 has been shown to impair survival and proliferation of mature T cells and Atg5 is necessary for B cell development and survival [248]. One explanation for this may be impaired clearance of damaged mitochondria and accumulation of ROS [249, 250]. However, the question remains as to why this would affect lymphocyte survival and proliferation so specifically and whether these effects are truly through autophagy or through separate functions of the Atg5 and Atg7 proteins.

1.4 Aim of study /objective

The core components of the autophagic machinery have been well defined, which has opened up countless possibilities to manipulate the autophagy system as a whole in order to study its role in various biological processes. However, key questions regarding the origin of the autophagosomal membrane and the mechanism of phagophore extension remain. Answers to these questions will doubtlessly allow us to not only manipulate the autophagic system more precisely but also offer more possibilities to target autophagy therapeutically. Autophagosome formation is a complex, multi-step process, involving the re-arrangement of large amounts of membrane and/or lipids in a short period of time but in a closely controlled fashion. Since Rab GTPases are major regulators of membrane traffic I aimed to identify novel Rab GTPases and their corresponding RabGAPs involved in autophagosome formation.

Chapter 2. Materials and Methods

2.1 Molecular biology

All chemicals and oligonucleotides were purchased from Sigma unless otherwise indicated. Cell culture dishes were from Corning. dH_2O, PBS, Loria Broth (LB), SOC medium, sterile glycerol, and EBSS (123.2mM NaCl, 5.366mM KCl, 2.388mM $CaCl_2$,1.662mM $MgSO_4$, 5.551mM D-glucose, 13.094mM $NaHCO_3$) were provided by LRI services.

2.1.1 PCR

Polymerase chain reactions (PCRs) were performed using for each reaction (1X):

0.4µl Accuprime Pfx DNA polymerase (Invitrogen)

5µl Accuprime buffer (10X; Invitrogen)

1.5µl forward primer [10µM]

1.5µl reverse primer [10µM]

50ng template DNA

ad 50µl dH_2O

Cycling parameters were done in a thermal cycler and are outlined in Table 2-1. PCR reactions were purified using a QIAquick PCR purification kit (QIAGEN).

Table 2-1 PCR parameters

Segment	Cycles	Temperature (ºC)	Time (min)
1	1	94	3
2	30	94	0.5
		55	0.5
		68	1/kb of plasmid length

2.1.2 Sequencing

Plasmids were sequence verified using the following sequencing reaction (1X):

8µl big dye terminator (BDT, LRI)

0.32µl primer [10µM]

500ng DNA

ad 20µl dH_2O

The cycling parameters used for the sequencing reaction are outlined in Table 2-2. Sequencing reactions were purified using a DyeEx 2.0 spin kit (QIAGEN) according to the manufacturer's instructions, followed by drying in a vacuum centrifuge for 20min at 45ºC. Samples were loaded onto the ABI Prism 377 DNA sequencer (Applied

biosystems) by LRI sequencing services. Sequencing analysis and alignments were carried out using Lasergene (DNASTAR) software.

Table 2-2 Sequencing PCR parameters

Segment	Cycles	Temperature (ºC)	Time (min)
1	1	96	2
2	24	96	0.5
		60	4

2.1.3 Restriction enzyme digest

DNA plasmids and PCR products were digested using the following reaction (1X) for 1h at 37ºC:

10µl/2µg PCR product/vector, respectively

4µl BSA in dH_2O

4µl restriction enzyme buffer (10X, NEB)

1µl restriction enzyme 1 (NEB)

1µl restriction enzyme 2 (NEB)

ad 40µl dH_2O

2.1.4 Ligation

DNA constructs were fused using the following ligation reaction (1X) for ≥5h but usually over night at 16ºC:

1/2µl vector

9/8µl PCR product

2µl T4 DNA ligase buffer (10X, NEB)

1µl T4 DNA ligase (NEB)

ad 20µl dH_2O

2.1.5 Bacterial transformation

For bacterial transformations to amplify plasmid constructs, 50µl of chemically competent DH5α bacteria stored at -80ºC were thawed for 20min on ice. Then, 5µl of the ligation reaction or 0.1µl of plasmid were added to the bacteria, which were put first for 10min back on ice, then for 40sec at 37ºC followed by 30sec on ice and finally addition of 1ml SOC growth medium (0.5% yeast extract, 2% tryptone, 10mM NaCl, 2.5mM KCl, 10mM $MgCl_2$, 10mM $MgSO_4$, 20mM glucose; LRI). Bacteria in SOC medium were allowed to reconstitute for 1h at 37ºC on a shaker before they were plated on LB-agar plates (0.5% yeast extract, 2% tryptone, 1.5% agar; LRI) containing the appropriate antibiotic (50µg/ml) followed by over night incubation at 37ºC.

If ligation reactions were transformed, cells were spun down at 5000rpm for 2min after reconstitution and 750µl of supernatant medium was removed to concentrate bacteria before plating on agar.

Transformed bacteria were stored at -80ºC in 15% glycerol for re-plating.

2.1.6 DNA agarose gel electrophoresis

Typically 0.8% agarose (Invitrogen) was dissolved in 1X TAE buffer (40mM Tris, 20mM acetic acid, 1mM EDTA) by heating for 7-9min at ~700W in a microwave (Panasonic) with occasional swirling and one drop of ethidiumbromide (0.625mg/ml; Amresco) was added per 100ml of TAE/agarose. Liquid agarose was added to the gel holder and left to cool down until solid. DNA was resuspended in 5X sample buffer (Bioline) and run at a constant 100V in 1X TAE buffer together with a DNA ladder (Hyperladder I, Bioline). DNA was visualised by placing the gel on a UV irradiator. If applicable, the DNA band was cut out with a sterile scalpel and purified using a QIAquick gel extraction kit (QIAGEN), according to the manufacturer's instructions. DNA bound to the QIAquick column was eluted with sterile deionised water (dH_2O).

2.1.7 Preparation of plasmid DNA

For initial testing and verification of constructs DNA minipreps were done by the LRI equipment park miniprep service. To obtain larger amounts and transfection quality plasmids DNA was purified using an Endo-free Plasmid DNA maxi kit (QIAGEN)

following the manufacturer's instructions. DH5α bacteria containing the plasmid of interest were grown in 2.5ml (miniprep) or 200ml (maxiprep) LB medium (0.5% yeast extract, 2% tryptone, 10mM NaCl; LRI) containing the appropriate selective antibiotic (50μg/ml). From maxipreps DNA was eluted with endotoxin free dH_2O (QIAGEN) and the concentration was measured using a NanoDrop spectrophotometer (Thermo scientific). DNA stocks were stored as 1mg/ml aliquots at -20ºC.

2.1.8 Constructs

Expression plasmids for myc-ULK1ΔC, myc-ULK1ΔVYA, and myc-ULK1K46I were cloned by E. Chan (Strathclyde University and LRI) and have been described [21].

All 3x-myc-tagged RabGAP constructs were kindly provided by F. Barr (University of Liverpool, UK) and have been described previously [197, 199, 251].

GFP-tagged constructs, including GFP-TBC1D14 and its truncation mutants, as well as all GFP-tagged Rab constructs and their mutants, were also provided by F. Barr and were made in pEGFP-C2 vector (CLONTECH Laboratories, Inc.).

Point mutations were introduced using the QuikChange method (Stratagene) as described [197, 199, 251].

HA-Sytnenin1 was kindly provided by J. Henley (University of Bristol) and has been described [252].

2.1.8.1 HA-ULK1

HA-tagged ULK1 was generated amplifying human ULK1 wild type protein by PCR from a full length IMAGE clone (IMAGE40080552) containing human ULK1 as template using the following primers:

5'-

GGCCAAGCTTGCCACCATGGAGTACCCATACGACGTACCAGATTACGCTG

GCGCCATGGAGCCCGGCCGCGGCGGC-3'

and

5'-GGCCGAATTCTCAGGCACAGATGCCAGTCAGC-3'

The forward primer contains the sequence for the HA-tag (underlined), which was added to the N-terminus of ULK1. The PCR product was fused into pcDNA3.1+ vector (Invitrogen) using HindIII and EcoRI restriction enzymes (New England Biolabs, NEB) and T4 DNA ligase (NEB).

2.1.8.2 ULK1 in pFBT9

For yeast-2-hybrid assays human ULK1 was cloned into pFBT9 vector, which is a modified version of pGBT9 (CLONTECH Laboratories, Inc.) carrying kanamycin resistance. myc-ULK1 was used as the PCR template with the following primers:

5'-GCAAGAATTCATGGAGCCGGGCCGCGGCGGCGTC-3'

and

5'-GCTT GTC GAC TCA GGC ATA GAC ACC ACT CAG-3'

The PCR product was fused into pFBT9 vector using EcoRI and SalI restriction enzymes and T4 DNA ligase (both NEB).

2.1.8.3 HA-ULK2

HA-tagged ULK2 was generated amplifying human ULK2 wild type protein by PCR from a full length IMAGE clone (IMAGE5268025) containing human ULK2 as template using the following primers:

5'-GGCCAAGCTTGCCACCATGGAGTACCCATACGACGTACCAGATTAC GCTGGCGCCATGGAGGTGGTGGGTGACTTCG-3'

and

5'-GGCCTCTAGATCACACGGTTGCGGTGCTATGG-3'

The forward primer contains the sequence for the HA-tag (underlined), which was added to the N-terminus of ULK2. The PCR product was fused into pcDNA3.1+ vector (Invitrogen) using HindIII and XbaI restriction enzymes and T4 DNA ligase (both NEB).

2.1.8.4 FLAG-Syntenin1

FLAG-tagged Syntenin1 was generated amplifying human Syntenin1 wild type protein by PCR from a full length IMAGE clone (IMAGE6979797) containing human Syntenin1 as template using the following primers:

5'-GGCCGCGGCCGCATGTCTCTCTATCCATCTCTC-3'

and

5'-GGCCGGATCCTTAAACCTCAGGAATGGTGTG-3'

The PCR product was fused into pFLAG-CMV-6c vector (Sigma) using NotI and BamHI restriction enzymes and T4 DNA ligase (both NEB).

2.1.8.5 Syntenin1 in pACT2

For yeast-2-hybrid assays Syntenin1 was cloned into pACT2 (CLONTECH Laboratories, Inc.) using HA-Syntenin1 as a PCR template with the following primers:

5'-GCAAGGATCCTGATGTCTCTCTATCCATCTCTC-3'

and

5'-GCTTCTCGAGTTAAACCTCAGGAATGGTGTG-3'

The PCR product was fused into pACT2 (CLONTECH Laboratories, Inc.) using BamHI and XhoI restriction enzymes and T4 DNA ligase (both NEB).

2.1.8.6 GST-TBC1D14

For expression in insect cells using the baculovirus system GST-TBC1D14 was cloned into pBacPAKGST (LRI) using myc-TBC1D14 as a PCR template with the following primers

5'-ACAAGCTTTATGACTGATGGAAAACTCTCC-3'

and

5'-GCGATTGAATTCTCATCAGTGTCGGAGGGACGGACTTCC-3'

The PCR product was fused into pBacPAKGST using HindIII and EcoRI restriction enzymes and T4 DNA ligase (both NEB). pBacPAKGST encodes GST followed by a 3C protease cleavage site, which is added N-terminally of TBC1D14.

2.1.8.7 Myc-TBC1D14RA/QA mutagenesis

Mutant myc-TBC1D14QA and myc-TBC1D14RAQA constructs were generated with a QuikChange multi site-directed mutagenesis kit (Stratagene) using either the wild type or RA-mutant vector DNA as template with the following primer:

5'-CCAGATGTGGGTTATGTCGCGGGCATGTCCTTCATAGCAGC-3'

All steps were carried out according to the manufacturer's instructions. Briefly, the primer was designed mutating the first two base pairs of the glutamine (CAG) codon to an alanine (GCG; underlined). Cycling parameters are outlined in Table 2-3. The cycling reaction creates a single stranded DNA plasmid. The double stranded parent (methylated) DNA plasmid was digested by the addition of 10U DpnI and incubation at 37ºC for 1h. The single stranded unmethylated DNA strand was then transformed into XL10-Gold Ultracompetent bacteria (Stratagene).

Table 2-3 PCR parameters for site-directed mutagenesis

Segment	Cycles	Temperature (ºC)	Time (min)
1	1	95	1
2	30	95	1
		55	1
		65	16 (2min/kb)

2.2 Cell biology and biochemistry

2.2.1 Cell culture and maintenance

Human embryonic kidney 293A (HEK293A) cells were provided by LRI services. Their derivative cell line stably expressing EGFP-rat-LC3 (2GL9) were created by E. Chan and have been described [20]. HEK293A cells stably expressing GPF-DFCP1 (201 cells) were kindly given by N. Ktistakis and have been described [69]. Cells were

cultured in DMEM (Gibco and LRI) supplemented with 10% FBS (Sigma), 4.8mM L-Glutamine (LRI), and 1% penicillin/streptomycin (pen/strep; LRI) under humidified conditions at 37ºC in 10% CO_2. 201 cells were grown under selection in the presence of geneticin (400µg/ml; Gibco). Where cells are indicated as fed they were grown in this medium. Starvation medium consisted of Earle's balanced saline solution (EBSS; LRI) containing 0.25 mg/ml (0.5mM) leupeptin (Roche) where indicated. All cells were used for experiments between passage 1 and 30 and split for maintenance when 80-100% confluent (every 3-4 days) to plate at 1:15 in 20ml medium in 75cm^2 flasks. To passage cells they were washed once with versene (0.02% EDTA (w/v), 1% phenol red in PBS), washed once with 0.05% trypsin in versene and incubated in the remaining trypsin for 5min until they detached. Cells were resuspended in 10ml growth medium initially and further diluted to plate according to the experiment (see below).

Cells were stored frozen in liquid nitrogen. To freeze down, 80% confluent cells from a 10cm dish were trypsinised and centrifuged for 5min at 1000rpm. Cell pellets were resuspended in 1ml ice cold DMEM with 20% FBS and 5% DMSO. Aliquots were frozen at -80ºC in a styrofoam rack for one week and then transferred to liquid N_2. To thaw cells aliquots were warmed to 37ºC rapidly (water bath) and diluted into fresh warm growth medium in a 10cm dish. To ensure even distribution of cells plates were mixes performing figures of 8.

For autophagy assays cells were starved by washing once with EBSS (LRI) followed by incubation in EBSS±leupeptin (0.5mM) for 2h. Cells indicated as fed were left in normal growth medium (not replaced) unless otherwise indicated.

2.2.2 Transfections

For biochemical analyses, cells were transfected using Lipofectamine2000 (Invitrogen), for immunofluorescence imaging cells were transfected using FuGene6 (Roche), for siRNA transfection Oligofectamine (Invitrogen) was used, all according to the manufacturers instructions.

2.2.2.1 Lipofectamine2000

All values described here are for 12-well plate format but were adjusted accordingly for 6cm, and 10cm dishes, or 24, and 6-well plates.

Plates were coated for ≥15min with poly-D-lysine (1mg/ml; Sigma), washed once with 3ml PBS and 80'000 cells in 1ml medium without pen/strep were added to each well. To ensure even distribution of cells plates were mixes performing figures of 8. Cells were left to settle over night and the next day the medium was replaced by 500µl transfection mix. 1ml transfection mix was prepared as follows: 160µl optiMEM (Gibco) were mixed with 3.2µl Lipofectamine2000 reagent by gentle tapping and left at room temperature (RT) for 5min. During those 5min 0.5µg DNA construct (0.8µg myc-TBC construct for the GAP screen) was added to 200µl optiMEM. The Lipofectamine2000 solution was then added to the DNA solution and mixed by gentle

tapping 8 times. This transfection mix was incubated for ≥20min (but no longer than an hour) at RT. After this 640µl of optiMEM were added to obtain 1ml transfection mix. Transfection mix was left on cells for 3h (exactly) and then replaced by full medium. Cells were harvested for biochemical analyses the next day.

Note that cells have to be 80% confluent when transfection mix is added otherwise Lipofectamine2000 is toxic.

2.2.2.2 FuGene6

For immunofluorescence experiments round coverslips were placed in 12-well plates and coated with poly-D-lysine for ≥15min. 80'000 cells in pen/strep-free growth medium were added to each well, mixed performing figures of 8, and left over night to settle. Next morning for each well the following transfection mix was prepared: 50ml optiMEM, with 1.5µl FuGene6 reagent, and 0.5µg DNA construct. This was mixed by gentle tapping 8 times and incubated at RT for 20min. During this incubation the growth medium on the cells was replaced by 450µl optiMEM. The transfection mix was added to cells in optiMEM by drop-wise slow pipetting and left for >5h before it was replaced by pen/strep-free growth medium.

2.2.2.3 Oligofectamine

For siRNA mediated knock down 40'000 cells in pen/strep-free medium were plated per well of a 6-well plate. Note that plates should not be coated with poly-D-lysine as this reduces transfection efficiency. Transfection mix was prepared as follows: 40µl of optiMEM was mixed with 3µl Oligofectamine by gentle tapping 8 times and incubated

at RT for 5min. Meanwhile, 25nM (for Rab11) or 50nM (for TBC1D14, and ULK1) siRNA duplexes were added to 140µl optiMEM. DNA and Oligofectamine mixes were joined, mixed by gentle tapping 8 times and incubated at RT for 20min. The medium of cells was replaced by 815µl optiMEM and then the transfection mix was added drop-wise. After ≥5h 1ml of growth medium containing 20% FBS was added carefully to the cells. The next day this procedure was repeated exactly the same way. On the 3rd day the transfection medium was replaced by fresh growth medium and cells were harvested on day 4 after 72h of knock down.

2.2.3 RNA interference

All siRNAs were purchased from Dharmacon and cells were transfected using Oligofectamine as described above.

TBC1D14 silencing was performed using a siRNA duplex (J-014032-1230010) targeting the following sequence: 5'-UCACAGAAAUGAACCGUUU-3'.

ULK1 was silenced with a siRNA duplex (D-005049-04-0010) targeting the following sequence: 5'-UGUAGGUGUUUAAGAAUUG-3'.

Rab11a was targeted with a siRNA duplex (D-004726-01) with the following sequence: 5'-GUAGGUGCCUUAUUGGUUU-3'.

Rab11b was targeted with a siRNA duplex (D-004727-03-0005) with the following sequence: 5'-GACAGAAGCCCAACAAGCU-3'.

2.2.4 Antibodies

Anti-TBC1D14 antibody was generated by LRI polyclonal antisera services injecting rabbits with a C-terminal peptide consisting of the amino acids 671-691 of TBC1D14 with the sequence: CLTALQKDSREMEKGSPSLR

Rabbit sera were tested by western blot for specificity. Serum from rabbit STO291 was affinity purified using a SulfoLink kit (Pierce) with the original peptide used for STO291. All other antibodies used are listed in Table 2-4. Secondary antibodies are listed in Table 2-5.

Table 2-4 Primary antibodies

Antibody	Antigen	Species	Application, dilution and blocking solution	Supplier
anti-mAtg9	mAtg9	Hamster	IF 1:1000 (PFA)	LRI [253]
STO219	mAtg9	Rabbit	WB 1:500 (milk), IF 1:1000 (PFA), IP	LRI
9E10	myc	Mouse	WB 1:500 (LI-COR), IF 1:500 (PFA), IP	LRI
anti-LC3	LC3	Rabbit	1:2000	Abcam (UK)
5F10	LC3	Mouse	WB 1:250 (LI-COR), IF 1:100 (MeOH)	NanoTools (Germany)
Anti-β-actin	actin	Rabbit	WB 1:1000 (LI-COR)	Abcam (UK)
AC40	actin	Mouse	WB 1:1000 (LI-COR)	Sigma (USA)
12CA5	haemagglutinin	Mouse	WB 1:500 (LI-COR), IP	LRI

anti-HA	HA-tag	Rat	IF 1:1000 (PFA)	Roche (UK)
anti-HA	HA-tag	Mouse	WB 1:500 (LI-COR), IP	Covance (UK)
4E12/8	GFP	Mouse	IP	LRI (T. Hunt)
SGE5/6	GFP	Rabbit	WB 1:500 (LI-COR)	LRI
STO291	TBC1D14	Rabbit	WB 1:250 (Milk), IF 1:250 (PFA)	LRI
STO289	TBC1D14	Rabbit	WB 1:100 (Milk)	LRI
STO255	mouse ULK1	Rabbit	WB 1:250 (milk), IP	LRI
anti-ULK1	human ULK1	Rabbit	WB 1:250 (milk), IF 1:250 (PFA)	Santa Cruz (USA)
anti-ULK2	ULK2	Goat	WB 1:250 (milk)	Santa Cruz (USA)
STO280	WIPI2	Rabbit	IF 1:500 (PFA)	LRI [57]
anti-WIPI2	WIPI2	Mouse	IF 1:50 (PFA)	LRI [57]
anti-GM130	GM130	Mouse	IF 1:500 (PFA)	BD Transduction Labs (USA)
anti-TGN46	TGN46	Sheep	IF 1:500 (PFA)	AbD Serotec (UK)
anti-Rab11	Rab11	Mouse	IF 1:500 (PFA)	BD Transduction Labs (USA)
anti-Rab11a (121-1)	Rab11a	Rabbit	IF 1:500 (PFA) with saponin	M. Zerial
anti-Rab11b	Rab11b	Rabbit	IF 1:500 (PFA) with saponin	Cell Signalling (USA)
13E4	TfnR	Mouse	IF 1:500 (PFA)	Abcam (UK)
STO52	CI-MPR	Rabbit	IF 1:500 (PFA)	LRI [254]

anti-EEA1	EEA1	Mouse	IF 1:500 (PFA)	BD Transduction Labs (USA)
anti-LAMP2	LAMP2	Mouse	IF 1:500 (PFA)	BD PharMingen (USA)
anti-calreticulin	calreticulin	Rabbit	IF 1:500 (PFA)	Stressgen (UK)
108	EGFR	Mouse		C. Futter
anti-Rab7	Rab7	Rabbit	IF 1:500 (PFA)	Cell Signalling (USA)
M2	FLAG-tag	Mouse	WB 1:2000 (LI-COR), IF 1:4000 (PFA), IP	Sigma (USA)
anti-p62	p62	Guinea pig	IF 1:500 (PFA)	Progen (UK)
anti-p62/lck-ligand	p62	Mouse	WB 1:500 (LI-COR)IF 1:500 (PFA)	BD Transduction Labs (USA)
anti-CD4 (RM4-5)	CD4	Rat	FACS 1:100 Fluorescently labelled	BD PharMingen (USA)
anti-CD8 (53-6.7)	CD8α	Rat	FACS 1:100 Fluorescently labelled	BD PharMingen (USA)
anti-CD19	CD19	Rat	FACS 1:100 Fluorescently labelled	BD PharMingen (USA)
anti-CD3ε (145-2C11)	CD3ε	Hamster	T cell activation, plate bound in PBS	BD PharMingen (USA)
anti-CD28	CD28	Hamster	T cell activation, plate bound in PBS	BD PharMingen (USA)

Table 2-5 Secondary antibodies

Antibody tag	Antigen	Species	Application and dilution	Supplier
Alexa Fluor 488	Mouse, Rat or Rabbit IgG	Goat	IF 1:1000	Molecular Probes, Invitrogen (USA)
Alexa Fluor 555	Mouse, Rat or Rabbit IgG	Goat	IF 1:1000	Molecular Probes, Invitrogen (USA)
Alexa Fluor 647	Mouse, Rat or Rabbit IgG	Goat	IF 1:1000	Molecular Probes, Invitrogen (USA)
Alexa Fluor 647	Sheep IgG	Donkey	IF 1:1000	Molecular Probes, Invitrogen (USA)
Cy3	Armenian hamster IgG	Goat	IF 1:1000	Jackson Immunoresearch (USA)
IRdye680	Mouse IgG	Goat	WB 1:4000	Invitrogen (USA)
IRdye800	Rabbit IgG	Goat	WB 1:4000	Rockland (USA)
HRP	Goat IgG	Chicken	WB 1:2000	Amersham (UK)
HRP	Mouse or Rabbit IgG	Sheep	WB 1:2000	Amersham (UK)

2.2.5 Bradford assay

Protein concentration was determined by Bradford assay using serial dilutions of an IgG standard (Biorad). Protein was added to 800µl of dH_2O and mixed with 200µl of Biorad

dye solution. Samples were vortexed, incubated for 15-60min at RT and the absorbance at 595nm was measured using a spectrophotometer.

2.2.6 SDS-PAGE and protein transfer

2.2.6.1 Standard SDS-PAGE

For all experiments except GFP-LC3-blotting (see section 1.2.6.3) SDS-PAGE was performed using precast NuPAGE 4-12% Bis-Tris mini or midi gels (Invitrogen). Gels were run at 200V for ~1h in MOPS SDS running buffer (20X stock: 50mM MOPS, 50mM Tris base, 0.1% SDS, 1mM EDTA, pH7.7; Invitrogen) to resolve big proteins or MES SDS running buffer (20X stock: 50mM MES, 50mM Tris base, 0.1% SDS, 1mM EDTA, pH7.3; Invitrogen) to resolve small proteins such as LC3.

HEK293A cells were lysed in ice cold TNTE (20mM Tris pH7.5, 150mM NaCl, 0.3% v/v Triton-X-100, 5mM EDTA) containing Complete EDTA-free protease inhibitor cocktail (dilution was 1 tablet in 25ml of TNTE) and PhosStop phosphatase inhibitors (dilution was one tablet in 10ml of TNTE; both Roche) on ice. Immediately after TNTE addition, lysates were transferred to 1.5ml eppendorf tubes on ice by pipetting up and down 3-4 times to maximise cell lysis. Cell debris and nuclei were pelleted at 2500g (5000rpm in a conventional bench top centrifuge) for 5 min at 4ºC. Lysates were resuspended in 5xSDS sample buffer (15% SDS (w/v), 312.5mM Tris-HCL (v/v) pH6.8, 50% glycerol (w/v), 16% β-mercaptoethanol (v/v), some bromophenol blue; all

Sigma), heated to 65ºC for 15 min and then loaded onto 4-12% Bis-Tris NuPAGE gels (Invitrogen) together with Rainbow marker (Amersham GE healthcare).

2.2.6.2 Protein transfer

Proteins were transferred onto Immobilon-P polyvinylidene (PVDF) or PVDF-FL membrane (Millipore), which was previously wetted in Methanol (MeOH; analytical grade; Fisher scientific) for 30sec, and soaked in NuPAGE transfer buffer (20X; Invitrogen diluted in 20% MeOH and water) for ≥5min. Extra thick blot paper (Biorad) was also soaked in transfer buffer and proteins were transferred onto membrane at 6V constant for 9.5h at 4ºC in a trans blot SD semi-dry transfer cell (Biorad). Next the membrane was again wetted in MeOH for 30sec and left to dry at RT for ≥15min to fix proteins. For ponceau staining the membranes were re-wetted in MeOH for 30sec and directly transferred into ponceau solution (Sigma) for ≥5min on a shaker. To remove excess staining membranes were washed twice with dH_2O for 5 to 10min. To completely remove ponceau staining, membranes were washed twice with PBS for 10min before being transferred into blocking solution.

2.2.6.3 SDS-PAGE for GFP-LC3 blotting

2GL9 cells on ice were lysed in (150µl per well of a 24-well plate) RT 1xSDS Laemmli sample buffer (3% SDS (w/v), 62.5mM Tris-HCl (v/v) pH6.8, 10% glycerol (w/v), 3.33% β-mercaptoethanol (v/v), some bromophenol blue), immediately transferred to 1.5ml eppendorf tubes on ice, and then heated to 65ºC for 10 min. To reduce viscosity samples were passed through a 27G needle 8 times before analysis on 10% Laemmli SDS-PAGE. The gel composition is listed in Table 2-6. The separating gel was covered

with isopropanol to even out the surface until polymerisation was complete and the stacking gel could be poured on top. Gels were electrophoresed at 120V constant for approximately 1h in running buffer (10X stock: 1.9M glycine, 250mM Tris-HCl, 1% SDS, pH8.8) and transferred onto PVDF membrane as described above.

Table 2-6 Separating and stacking gel composition
Acrylamide, upper, and lower gel buffers were purchased from National Diagnostics. TEMED (*N*,*N*,*N*′,*N*′-Tetramethylethylenediamine) and APS (ammoniumpersulfate) were purchased from Sigma. The indicated volumes are enough for two large 1mm thick gels.

Separating gel	7.5%	**10%**	12%	**Stacking gel**	**4%**
Lower gel buffer (ml)	8.75	**8.75**	8.75	**Upper gel buffer (ml)**	**3.75**
30% acrylamide (ml)	8.75	**11.7**	14	**30% acrylamide (ml)**	**2**
dH_2O (ml)	17.5	**14.6**	12.25	**dH_2O (ml)**	**9.25**
TEMED (µl)	40	**40**	40	**TEMED (µl)**	**15**
APS (µl)	120	**120**	120	**APS (µl)**	**150**

2.2.7 Immunoblotting/western blotting and detection

2.2.7.1 ECL

Membranes were blocked in 5% milk made from powder (Marvel) in PBS with 0.05% tween20 (PBS/tween) for ≥1h. Next, membranes were incubated with primary antibody in PBS or 5% milk made in PBS/tween for ≥2h at RT but usually over night at 4ºC. Membranes were washed 3 times for 5min in 5% milk made in PBS/tween and then incubated with secondary HRP-conjugated antibody in 5% milk made in PBS/tween for

≥1h. Finally, membranes were washed for 15min twice in 5% milk in PBS/tween, once in PBS/tween, and once in PBS before adding ECL reagent (Amersham GE healthcare) for 1min to detect HRP activity. Lastly, Membranes were exposed to film for various time points. To re-probe the same membrane, it was washed in PBS and incubated in Restore western blot stripping buffer (Thermo scientific) for 15min prior to restarting the blotting procedure.

2.2.7.2 LI-COR

Membranes were incubated in Odyssey blocking buffer (LI-COR infrared imaging system) for ≥1h directly followed (no wash) by incubation with one or two primary antibody(-ies) in PBS for ≥2h at RT but usually over night at 4ºC. Note that antibodies in PBS can be stored at 4ºC to reuse, and that if two antibodies are used one has to have been raised in mouse and the other one in rabbit. Next, membranes were washed 3 times for 5min in PBS with PBS/tween before incubating with secondary antibody(-ies) coupled to infrared chromophores with different excitation/emission wavelengths for ≥1h. Membranes were washed 3 times in PBS/tween and once in PBS for 15min before scanning using a 2-channel scanner (LI-COR Odyssey). Protein levels revealed by LI-COR scanning were quantified using Metamorph software by drawing narrow boxes around each band and recording the average pixel intensity.

2.2.8 Immunofluorescence labelling and confocal microscopy

All steps were performed at room temperature and solutions are room temperature unless otherwise indicated. Cells on glass coverslips were washed with PBS warmed to 37ºC once, if applicable incubated in saponin/pipes (0.05% saponin, 80mM pipes pH7, 1mM $MgCl_2$, 5mM EGTA in dH_2O prepared freshly) for 5min, washed with 37ºC PBS once, fixed in 4% paraformaldehyde (agar scientific) in PBS warmed to 37ºC for 20 min, washed with PBS 2 times, quenched with 50nM NH_4Cl/PBS for 10 min, washed with PBS 2 times, permeabilised with 0.2% Triton-X-100 in PBS for 3 min, washed with PBS 3 times, and blocked with 0.2% gelatin in PBS (PBS-G) for 20 min.

Alternatively, cells were washed with 37ºC PBS once, treated with saponin/pipes for 5min or not, fixed with -20ºC MeOH for 20min at RT, washed with PBS once, permeabilised with 0.2% Triton-X-100 in PBS for 3 min, washed with PBS once, fixed again with -20ºC MeOH for 5min at RT, washed with PBS once, quenched with 50nM NH_4Cl/PBS for 10 min, washed 3 times with PBS, and blocked with PBS-G for 20 min. After fixation and blocking, cells were incubated with primary antibodies diluted in PBS-G for 20 min, washed 3 times with PBS-G, incubated with secondary antibodies diluted in PBS-G for 20 min, washed 3 times with PBS-G, washed 3 times with PBS, washed once with sterile water and mounted on microscope slides with Moviol 4-88 (Calbiochem) mounting medium.

Confocal images with a slice thickness of 0.7µm were obtained with a Zeiss Axioplan 2 LSM510 or LSM710 laser scanning microscope equipped with a 63x, 1.4 NA, oil-

immersion objective (Carl Zeiss MicroImaging, Inc.) and images were processed using LSM510/LSM710 software.

2.2.9 Immunoprecipitation

HEK293A cells were grown to ~80% confluency in 6cm dishes and lysed in 1ml ice cold TNTE supplemented with Complete Protease inhibitor cocktail and PhosStop on ice. Cells were scraped and transferred to eppendorf tubes on ice and spun down at 2500g for 5 min to clear the lysates. 25µl Protein-G sepharose beads (Sigma) were washed twice in TNTE and once in TNTE with protease and phosphatase inhibitors. 2µl of appropriate antibody was added to the beads and left for 10min to allow binding to the protein G followed by addition of 450µl of cell extracts but first removing a small aliquot of total cleared lysate. This mix was incubated at 4ºC for ≥4h but usually over night on a spinning wheel. Beads were spun down at 5000rpm for 2min, an aliquot of unbound supernatant was removed, and beads were washed 3 times in 500ml TNTE with protease and phosphatase inhibitors. Finally, beads were resuspended in 25µl 3X SDS sample buffer (9% SDS (w/v), 187.5mM Tris-HCl (v/v) pH6.8, 30% glycerol (w/v), 10% β-mercaptoethanol (v/v), some bromophenol blue; all Sigma) as were the total lysate and supernatant aliquots. Samples were heated to 65ºC for 15 min, and analysed on 4-12% Bis-Tris NuPAGE gels (Invitrogen) as described above.

2.2.10 Long-lived protein degradation

Transfected HEK293A cells were incubated with growth medium containing 65µM valine and 0.2µCi/ml [^{14}C]valine (GE healthcare) over night. Cells were chased with full medium containing 2mM valine for 24h and then either incubated with EBSS or full medium with 2mM valine for 2h. Next, medium was removed and cells were harvested in ice cold PBS containing 1% triton-X-100 (TX100). Proteins from the medium and cell lysates were precipitated with trichloroacetic acid (TCA) over-night at 4ºC. TCA soluble medium fraction and the TCA insoluble cell lysate fractions were added to scintillation fluid and the radioactivity present was counted using a Beckman LS 6500 multipurpose scintillation counter. The extent of long-lived protein degradation was expressed as the percentage of the TCA-soluble counts in the medium compared to the total TCA-soluble counts in the medium plus TCA-insoluble counts from the cells.

2.2.11 Yeast-two-hybrid

The yeast-two-hybrid assay has been described before [197]. All TBC and Rab constructs were provided by F. Barr (currently University of Liverpool, UK) and experiments were performed at the Max Planck Institute of Biochemistry, Martinsried, Germany. Briefly, competent PJ694A yeast cells were transfected with ULK1 (in pFBT9 vector) and a TBC construct (in pACT2 vector), or Syntenin1 (in pACT2 vector) and a Rab GTPase (in pFBT9 vector) and grown on plates lacking leucine and tryptophan (DDO) to select for double transfected cells (pFBT9 contains the leucine, pACT2 the tryptophan cassette). After 3 to 5 days growing at 30ºC medium sized

colonies were re-streaked on DDO plates and plates lacking leucine, tryptophan, histidine, and adenine (QDO). A medium sized colony was picked with a pipette tip and streaked first on the DDO plate and then on the QDO plate and this was done for five different colonies from each plate. Plates were then put back at 30ºC to grow for 3 to 5 days after which plates were analysed for interactions and scanned.

2.2.12 *In vitro* GAP assay

The in vitro GAP assay has been described [251]. Briefly, recombinant TBC1D14 was purified from Sf9 and High5 insect cells (pooled to enhance yield) by the protein purification facility at LRI. The GST moiety was cleaved off by 3C protease thanks to the presence of a cleavage site between the GST and TBC1D14. TBC1D14 was eluted and stored frozen in glycerol containing buffer (50mM Tris pH 7.5, 150mM NaCl, 1mM EDTA, 1% (v/v) Triton-X-100, 5% (v/v) glycerol, 1mM DTT or TCEP, 10mM Benzamidine, 1mM NaF, 10mM b-glycerophosphate) until thawed for the GAP assay. 5µg (100pmol) of each Rab GTPase was incubated with 10µl of 10X assay buffer (10X: 500mM Hepes-NaOH pH6.8, 10mM DTT, 2mg/ml bovine serum albumin), 10µl of 10mM EDTA pH8, 5µl of 1mM Mg^{2+}-GTP and 1µl of [γ^{32}P]GTP (GE healthcare 10mCi/ml; 5mCi/mmol) for 15min at 30ºC. This was then split in half and to one half buffer was added, to the other 200ng of TBC1D14 was added followed by 1h incubation at 30ºC. 2.5µl of the assay mix was scintillation counted to allow calculation of the specific activity. Next 5µl in duplicates were added to 800µl of ice-cold activated charcoal slurry in 50mM NaH_2PO_4 and incubated on ice for 1h. Then samples were centrifuged at 16000g for 5min to pellet the charcoal. The supernatant was carefully

removed with a pipette and 400µl aliquots are scintillation counted in 4ml of Ultima Gold scintillation liquid (Perkin-Elmer).

To calculate the amount of GTP in the reaction mix the activity measured in 2.5µl of assay mix was multiplied by 40 since the total volume was 100µl. This value was then divided by the total of 5000pmol GTP that was in the reaction mix (5µl(1mM)GTP/100µl => 0.05mM GTP in the reaction mix, which for 100µl is 5000pmol) to obtain the specific activity in [cpm/pmol]. The duplicate values [cpm] of the 5µl aliquot from each reaction were averaged and multiplied by two because only 400µl out of the 800µl charcoal mix were counted. Because 5µl out of the 100µl reaction mix was counted, these values were multiplied by 20. Finally to calculate the amount of GTP hydrolysed these values are divided by the specific activity. The formulae are indicated below:

$$(\frac{100\mu l}{5\mu l}) \times (\frac{CPM^{reaction} \times 2}{spec[\frac{CPM}{pmol}]}) = GTP^{hydrolysed}[pmol]$$

with *spec* indicating the specific activity calculated as follows:

$$\frac{CPM^{mix} \times \frac{100\mu l}{2.5\mu l}}{5000\,pmol} = spec[\frac{CPM}{pmol}]$$

2.2.13 Tfn and EGF trafficking

Transfected HEK293 cells plated on Poly-D-Lysine coated coverslips were serum starved for 2 hours and then incubated in 37ºC warm serum-free DMEM containing alexa-fluor-647 (AF647)-labelled Tfn (5mg/ml stock used 1:500; Invitrogen) and AF555-labelled EGF (200µg/ml stock used 1:500; Invitrogen) for 15 min at 37ºC, washed once with 37ºC warm PBS and then chased for the indicated time in serum free medium in cell culture conditions. Cells were then fixed by transferring the coverslip into wells containing 4% paraformaldehyde warmed to 37ºC for 20 min. Coverslips were washed 3 times with PBS, mounted on microscope slides in Moviol 4-88, and analysed by confocal microscopy.

2.2.14 [^{125}I]Tfn uptake assay

Transfected HEK293 cells plated in Poly-D-Lysine coated wells were serum starved for 2 hours and then incubated with [^{125}I]Tfn (0.3µg/ml; Perkin Elmer) in binding medium (0.05% BSA in serum free culture medium) for 10 minutes at 37°C. [^{125}I]Tfn was washed off and cells were surface stripped using 0.1M glycine, 0.9% NaCl pH 3.0 at 4°C and washed with binding medium. Next cells were incubated in fresh pre-warmed binding medium. After each time point the medium was collected and replaced by fresh medium for the subsequent time point. Cells were lysed in PBS containing 1% Triton-X-100 and the amount of radioactivity in the chase medium and the cell lysates was

counted using a Beckman LS 6500 multipurpose scintillation counter. Data presented includes the stimulation period. The percent recycled [^{125}I]Tfn was determined by dividing the CPM in the medium (adding all counts from previous time points if applicable) by the total CPM (lysate+medium). The formula for the 60min time point is indicated below as an example:

$$\frac{(CPM^{t\,0\,\mathrm{min}} + CPM^{t\,30\,\mathrm{min}} + CPM^{t\,60\,\mathrm{min}})^{MEDIUM}}{(CPM^{t\,0\,\mathrm{min}} + CPM^{t\,30\,\mathrm{min}} + CPM^{t\,60\,\mathrm{min}})^{MEDIUM} + (CPM^{t\,0\,\mathrm{min}} + CPM^{t\,30\,\mathrm{min}} + CPM^{t\,60\,\mathrm{min}})^{LYSATES}}$$

2.3 *In vivo* and primary mouse cell analyses

2.3.1 Animal maintenance and back-crossing

All mice were maintained and bred at the animal unit at CRUK Clare Hall laboratories. Back-crossings for ULK1 gene trapped mice (clone AC0566) were done mating heterozygous females with wild type C57BL/6J males obtained from the animal unit. Post-mortem analysis was done by Dr. Geza Hrivnak at the Clare Hall animal unit. For experiments mice were transferred to the LRI animal unit. Ear snips were sent to LRI for genotyping.

2.3.1.1 Genotyping

Ear snips were incubated over night in 150µl DirectPCR lysis reagent (Viagen Biotech) with 0.1mg/ml proteinase K at 55ºC on a shaker. Next day the samples were heated to 85ºC for 45min. Then samples were spun down briefly and 2µl were used for PCR. For

PCR 2.5nM of forward and 2.5nM of reverse primer were added to 15µl of MegaMix blue (Microzone limited) with 2µl of the ear snip DNA extract. To identify animals that carry the gene trap mutation (KO or HET) the following primers were used (EN80: the reverse primer lies within the gene trap cassette) and the PCR parameters are indicated in Table 2-7:

5'-ACTCGTGAGATCTCATGGCCAT-3'

and

5'-GCATAAATAGGACCAAGTGGGCACGC-3'

To identify animals carrying the wild type gene (WT and HET) the following primers were used (W4340: the two primers lie on each side of the gene trap insertion site so in mutant animals they are too far apart to produce a PCR product) and the PCR parameters are indicated in Table 2-8:

5'-ACAACCAGGTCCCAGGTCCCG-3'

5'-TTCAGGCTGCGCAACTGTTGG-3'

After the PCR programme has finished the MegaMix blue solution containing the PCR product, if amplified, can be directly loaded onto a 0.8% agarose gel.

Table 2-7 PCR parameters for genotyping EN80

Segment	Cycles	Temperature (ºC)	Time (min)
1	1	94	3
2	35	94	0.5
		60	0.5
		72	$\frac{2}{3}$

Table 2-8 PCR parameters for genotyping W4340

Segment	Cycles	Temperature (ºC)	Time (min)
1	1	94	3
2	35	94	0.5
		60	0.5
		72	0.5

2.3.2 Primary T cell preparation and culture

Animals were sacrificed to harvest organs between 1 and 6 months of age. Primary splenocytes and thymocytes were cultured in Roswell Park Memorial Institute (RPMI) 1640 medium supplemented with 10%FBS (Autogen Bioclear), 0.3µg/ml L-Glutamine (GIBCO), 100U/ml (each) pen/strep, 1mM sodium pyruvate (GIBCO), 0.1mM non-essential amino acids (NEAAs; GIBCO), 10mM HEPES (GIBCO), and 50µM β-mercaptoethanol (GIBCO) (=R10*). Cells and organs were kept on ice in between all

steps. Organs and tissues for western blot analysis were shock-frozen in liquid nitrogen and stored at -80ºC until lysis and homogenisation in TNTE containing protease and phosphatase inhibitors using a polytronic homogeniser.

To obtain primary splenocyte cultures whole spleen was passed through a 70µm mesh using a plunger of a 1ml syringe and washing the mesh with medium frequently. Cells were centrifuged at 1700rpm for 5min and incubated in red blood cell (RBC) lysis buffer (Sigma; or make up: 155mM NH_4Cl, 10mM $KHCO_3$, 0.1mM EDTA, pH7-7.2) for 5min at RT, if applicable. Cells were washed with fresh medium once and then counted in a Neubaur haemocytometer not counting RBCs (exclusion by size and shape) if no RBC lysis buffer was used. Cells were cultured at 37ºC under humified conditions and 5% CO_2 in R10*. The same procedures and conditions apply for thymocytes from whole thymi. For FACS sorting the cell suspension was filtered through a 40µm mesh to avoid clumps in the sorter. FACS sorting was done by the FACS laboratory at LRI.

2.3.3 Flow cytometry

2.3.3.1 Cell surface staining and FACS analysis

For cell surface staining of primary splenocytes and thymocytes cell suspensions were washed once in ice-cold FACS buffer (5mM EDTA, 1% FCS (Autogen bioclear), 0.02% NaN_3 in PBS) and stained with surface staining antibodies (1:100) for 20 min at 4ºC in the dark. Data were acquired on a FACSCalibur (BD Biosciences) or LSRII (BD

Biosciences) and analyzed using FlowJo software (Treestar). An example of cell gates (Fig. 2-1a, excluding debris) is shown in Figure 2-1. Cell clusters were excluded by (Fig. 2-1b, gating on single cells). To determine total cell number a known number of beads was added as a reference (Fig. 2-1c; to calculate number of cells: (#beads added to sample divided by #beads acquired in FACS profile)x(#CD4 acquired)=total CD4+) or, alternatively, for cells diluted to equal amounts the FACS profile was acquired for the same amount of time.

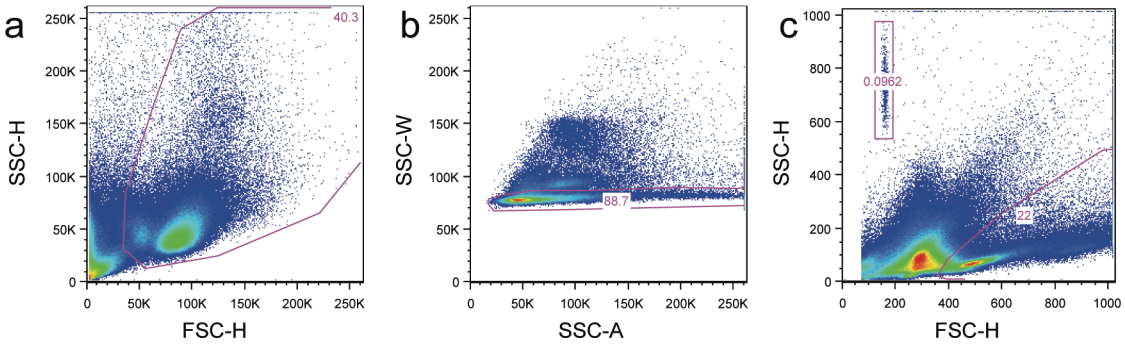

Figure 2-1 Typical FACS analysis
(a) Forward (~size) and side (~granularity) scatter (FSC and SSC, respectively) heights (H) are used to exclude debris, **(b)** SSC width (W) and area (A) are used to exclude cell clusters, and **(c)** beads can be added and counted to calculate total cell number.

2.3.3.2 AnnexinV, TO-PRO3, and DAPI staining

For AnnexinV (PharMingen) staining cell suspensions were spun down and resuspended in Annexin binding buffer (PharMingen; alternatively to the commercial buffer use: 1mM Hepes-NaOH pH7.4, 140mM NaCl, 2.5mM $CaCl_2$). 3µl of AnnexinV-FITC were added and cells were incubated for 20min at RT in the dark. 1nM TO-PRO3 or 1µM DAPI were added to cells shortly before FACS profile acquisition.

2.3.4 Cell viability assays

2.3.4.1 Anti-CD3ε titration

For anti-CD3ε titration assays, 96-well plates were coated with serial dilutions of anti-CD3ε in PBS over night in a moisture chamber at 4ºC. Splenocytes were processed as described above not using RBC lysis buffer. Per well 500'000 splenocytes (not counting RBCs) in 100µl R10* were added using a multi-well pipette and cultured for 3 days at 37ºC. Each condition was done in quadruplicates (4 wells). After 3 days in culture plates and CellTitre-Glo reagent were equilibrated to RT for 30min. 100µl of CellTitre-Glo reagent was added to each well using a multi-well pipette and plates were incubated on an orbital shaker for 2min. Plates were further incubated on the bench at RT for 10min and luminescence was recorded using an Envision multilabel reader (Perkin Elmer).

2.3.4.2 CFSE proliferation assay

For the CFSE proliferation assay splenocytes were labelled with 5µM CFSE (Molecular Probes) for 5min at RT in R10* in the dark. Cells were washed once and 10^6 cells per well were added to a 96-well plate. Cells were stimulated by plate-bound anti-CD3ε (5µg/ml) with or without plate-bound anti-CD28 (1µg/ml), or recombinant IL-2 (100U/ml; RnD Systems), or 10ng/ml PMA with 300mg/ml ionomycin. Cells were stained with anti-CD4 and proliferation was assayed by flow cytometry after 4 days in culture.

2.4 Statistical analysis

Statistical analysis was done using Prism (GraphPad software). Two-tailed student's t-tests were performed unpaired or paired as indicated. Two-way ANOVA test was performed two-tailed followed by Bonferroni posttest analysis. Asterisk(s) indicate significance, * $p \leq 0.05$, ** $p \leq 0.01$, *** $p \leq 0.001$. Data represent mean of indicated number of independent experiments. Error bars indicate standard error of the mean.

Chapter 3. Identification of RabGAPs and Rabs involved in autophagosome formation

3.1 Aim

Many questions remain concerning autophagosome formation as it is still unclear what the exact mechanism of autophagosome expansion is and where the donor membrane comes from [19]. Upon induction of autophagy large amounts of membrane are sequestered very quickly to form multiple autophagosomes throughout the cytoplasm. To better understand the mechanisms and the molecular machinery involved in phagophore extension I wanted to do a comprehensive analysis of the membrane trafficking events involved in autophagosome formation. With Rab GTPases being major regulators of membrane traffic in the cell [194], I hypothesised that one or more Rabs are involved in autophagosome formation. The activity of Rab GTPases in the cell is controlled by a family of enzymes called RabGAPs, which when over-expressed inactivate their target Rab. Therefore, my main approach was to do an over-expression screen testing all putative human RabGAP proteins for their ability to inhibit autophagosome formation.

3.2 A RabGAP over-expression screen to identify negative regulators of autophagosome formation

I screened a library of 38 human Tre-2/Bub2/Cdc16 (TBC)-domain containing proteins, putative RabGAPs, for their ability to inhibit autophagosome formation when over-expressed in HEK293A cells stably expressing GFP-LC3 (2GL9 cells). All TBC constructs were kindly provided by Prof. F. Barr (University of Liverpool, UK). To measure autophagosome formation I assayed lipidation of GFP-LC3 during a two-hour starvation period (Fig. 3-1). I added the lysosomal protease inhibitor leupeptin to the starvation medium to prevent lysosomal degradation of GFP-LC3-II. This allowed me to assess total accumulation of GFP-LC3-II during the two hour starvation period as a measurement of the number of autophagosomes formed. The screen will only identify RabGAPs that inhibit autophagosome formation and not maturation or turnover for two reasons: 1) Autophagosome maturation is affected by disruption of lysosome function, which cannot be distinguished from the effect of leupeptin. 2) RabGAPs that increase and those that accelerate autophagosome formation would cause enhanced GFP-LC3-II degradation in the absence of leupeptin seemingly inhibiting autophagy. However, in the presence of leupeptin they will lead to accumulation of GFP-LC3-II ensuring that any inhibition of GFP-LC3-II accumulation seen is due to decreased lipidation and not enhanced turnover.

2GL9 cells were transfected with one of the 38 myc-tagged RabGAP constructs and GFP-LC3 lipidation was assessed by western blot. To avoid gel to gel variations the renilla vector control was loaded onto each gel for normalisation. A truncation mutant

of ULK1, which is known to inhibit autophagy, was used as a positive control. The renilla vector rather than empty vector was used because protein over-expression mildly enhances basal autophagy. All conditions were done in duplicates with two wells for fed and two for starved with leupeptin. Membranes were probed using the LI-COR system, which uses special Odyssey blocking buffer and secondary antibodies tagged with infrared fluorophores with an excitation wave length of 700nm or 800nm. Both secondaries can be applied at the same time to the membrane and scanned so that there is no bleed through from one channel to another. This allowed me to reveal the levels of actin (polyclonal 800nm) and LC3 (monoclonal 700nm) simultaneously even though GFP-LC3 and actin migrate similarly on SDS-PAGE. Antibodies against LC3 and actin were used to quantify protein levels first, followed by anti-myc to detect over-expressed myc-tagged TBC proteins. Membranes were scanned using the Odyssey infrared imaging system and all quantification was done with Metamorph software by drawing individual boxes around each actin and LC3-II band.

A 40% or more reduction in GFP-LC3-II production was detected after expression of 11 RabGAPs. To test whether GAP activity, and therefore Rab inactivation, was necessary for inhibition of autophagosome formation I investigated whether mutation of the catalytic arginine residue within the TBC domain (RA mutant, see Introduction section 1.2.2.2), would rescue this inhibition. The RA mutant was only available for 8 out of the 11 candidates and I found that seven out of these eight mutant proteins were no longer able to inhibit autophagy when over-expressed (Fig. 3-1).

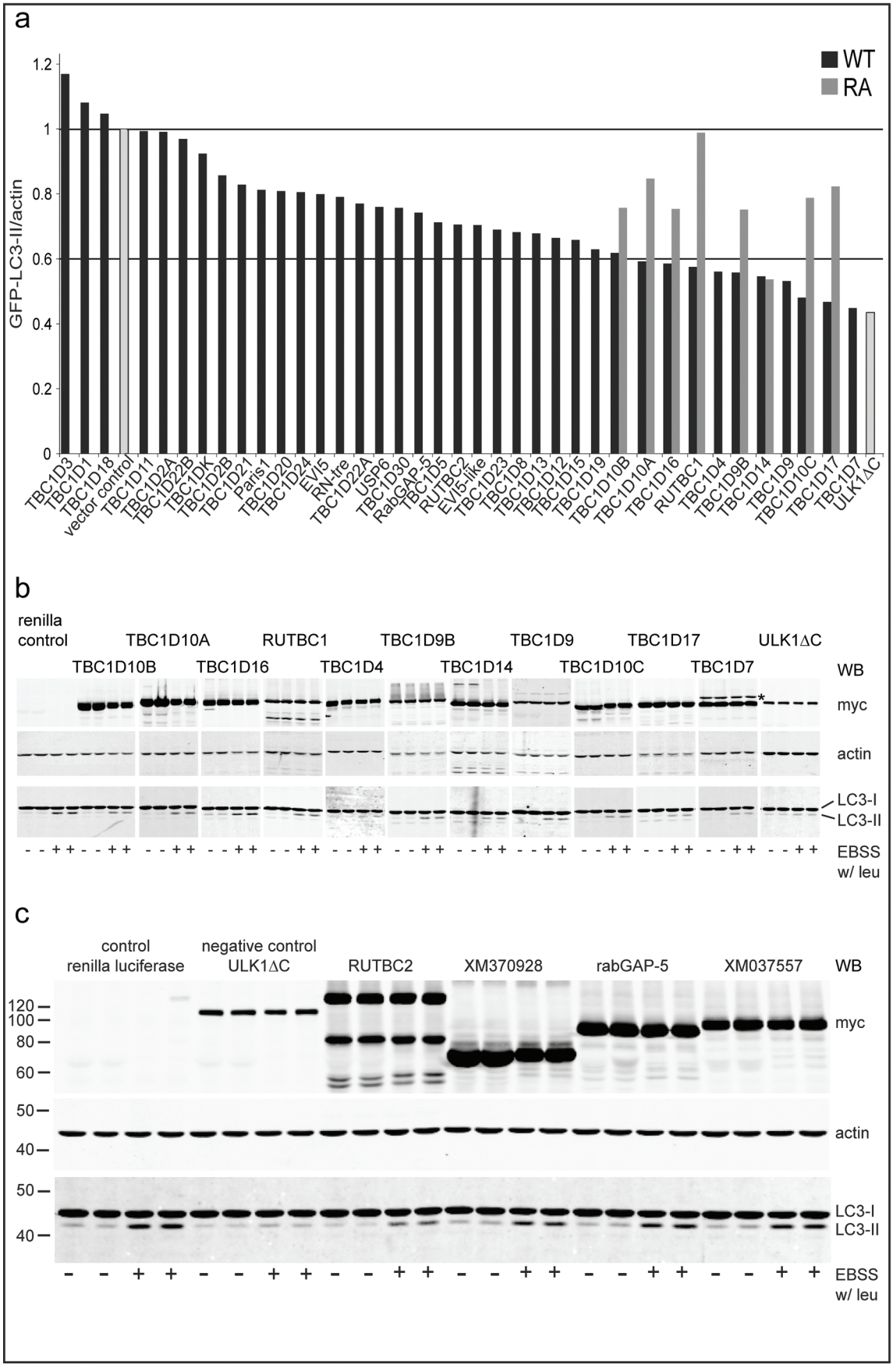
a
WT
RA
GFP-LC3-II/actin
1.2
1
0.8
0.6
0.4
0.2
0
TBC1D3
TBC1D1
TBC1D18
vector control
TBC1D11
TBC1D2A
TBC1D22B
TBC1DK
TBC1D2B
TBC1D21
Paris1
TBC1D20
TBC1D24
EVI5
RN-tre
TBC1D22A
USP6
TBC1D30
RabGAP-5
TBC1D5
RUTBC2
EVI5-like
TBC1D23
TBC1D8
TBC1D13
TBC1D12
TBC1D15
TBC1D19
TBC1D10B
TBC1D10A
TBC1D16
RUTBC1
TBC1D4
TBC1D9B
TBC1D14
TBC1D9
TBC1D10C
TBC1D17
TBC1D7
ULK1ΔC
b
renilla control
TBC1D10A
RUTBC1
TBC1D9B
TBC1D9
TBC1D17
ULK1ΔC
TBC1D10B
TBC1D16
TBC1D4
TBC1D14
TBC1D10C
TBC1D7
WB
myc
actin
LC3-I
LC3-II
EBSS
w/ leu
c
control renilla luciferase
negative control ULK1ΔC
RUTBC2
XM370928
rabGAP-5
XM037557
WB
120
100
80
60
50
40
50
40
myc
actin
LC3-I
LC3-II
EBSS
w/ leu

Figure 3-1 11 RabGAPs inhibit autophagosome formation
(a) 38 N-terminally myc-tagged TBC-domain containing proteins were over-expressed in HEK293A cells stably expressing GFP-LC3 (2GL9 cells) and accumulation of GFP-LC3-II was measured as a read out for autophagic activity. Cells were seeded in 24-well plates and 24 h after transfection cells were starved in Earle's buffered saline solution (EBSS) with 0.25 mg/ml leupeptin (leu) for 2 h or not. In each experiment, TBC proteins were done in duplicate for each condition (4 wells per TBC protein in total). Membranes were probed using the LI-COR system with antibodies against LC3 and actin for quantification, followed by the anti-myc antibody. Black bars show levels of GFP-LC3-II after starvation normalised to the renilla vector control, which was present on each gel. In fed conditions no significant differences were seen and data is not shown. Each myc-TBC was repeated at least twice (n=2) and if inhibition was seen, then three or more times (n≥3). ULK1ΔC, a C-terminal truncation mutant that is known to inhibit autophagy [21] was included in each experiment. **(b)** Representative western blots for TBC proteins that inhibited autophagy by 40% or more are shown. Of the 11 hits, eight GAP-activity deficient mutants (RA), TBC1D17R381A, TBC1D10CR141A, TBC1D14R472A, TBC1D9BR559A, RUTBC1R848A, TBC1D16R494A, TBC1D10AR160A, TBC1D10BR134A, were tested for rescue of the inhibition of autophagy (grey bars). Partial rescue can be seen for 7 of the 8 mutants tested. **(c)** Shown is a representative gel from the screen. All gels contained the renilla vector control, which the other samples were normalised to. Triple myc-tagged TBC constructs in pcDNA3.1 vector were kindly provided by F. Barr (University of Liverpool, UK).

3.3 Analysis of 11 RabGAP candidates that inhibit autophagosome formation

To further characterise the role of the 11 RabGAP hits from the over-expression screen, I first investigated whether any of these localise to intermediate and late stage autophagosomes marked by GFP-LC3 (Fig. 3-2). 2GL9 cells were transfected with one of the hits, starved for 2 hours, fixed, and labelled with anti-myc antibody followed by Alexa Fluor 555 tagged anti-mouse secondary antibody. As expected, cells over-expressing TBC-constructs have generally less autophagosomes, however, only partial co-localisation with GFP-LC3 puncta can be observed for some of the GAPs in starved 2GL9 cells. The size and distribution of the remaining GFP-LC3 spots appears normal

in transfected cells, excluding the possibility that one of the TBC-proteins may induce ectopic GFP-LC3-II formation or that any of them severely disrupt autophagosome transport. TBC1D7 and TBC1D14 vesicles show some degree of juxta-position with GFP-LC3 and TBC1D17, TBC1D9B, TBC1D4, and RUTBC1 show partial co-localisation with GFP-LC3 positive autophagosomes, however, in some cases this may be due to engulfment of the over-expressed protein by the autophagosome.

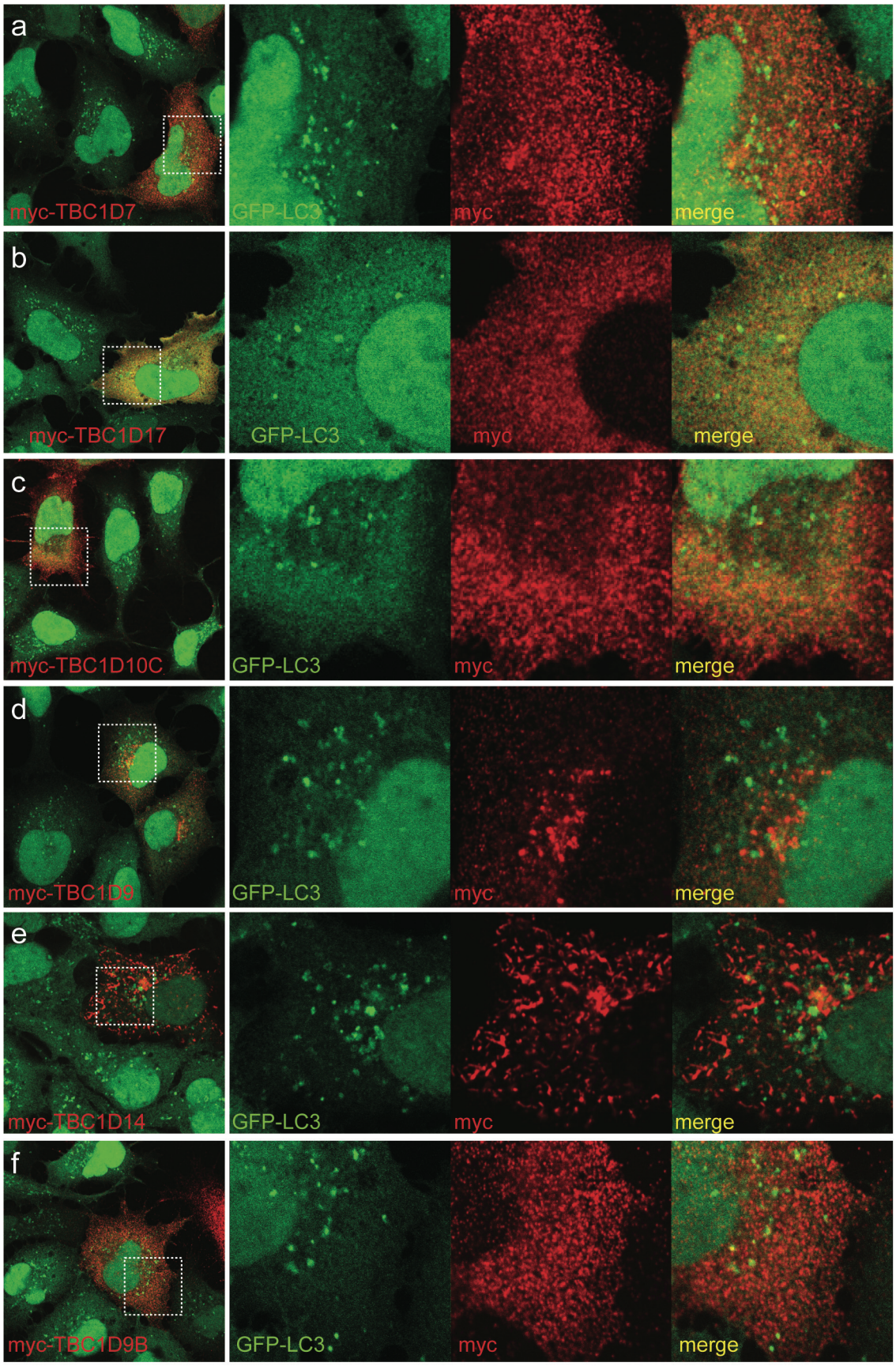
a
myc-TBC1D7
GFP-LC3
myc
merge
b
myc-TBC1D17
GFP-LC3
myc
merge
c
myc-TBC1D10C
GFP-LC3
myc
merge
d
myc-TBC1D9
GFP-LC3
myc
merge
e
myc-TBC1D14
GFP-LC3
myc
merge
f
myc-TBC1D9B
GFP-LC3
myc
merge

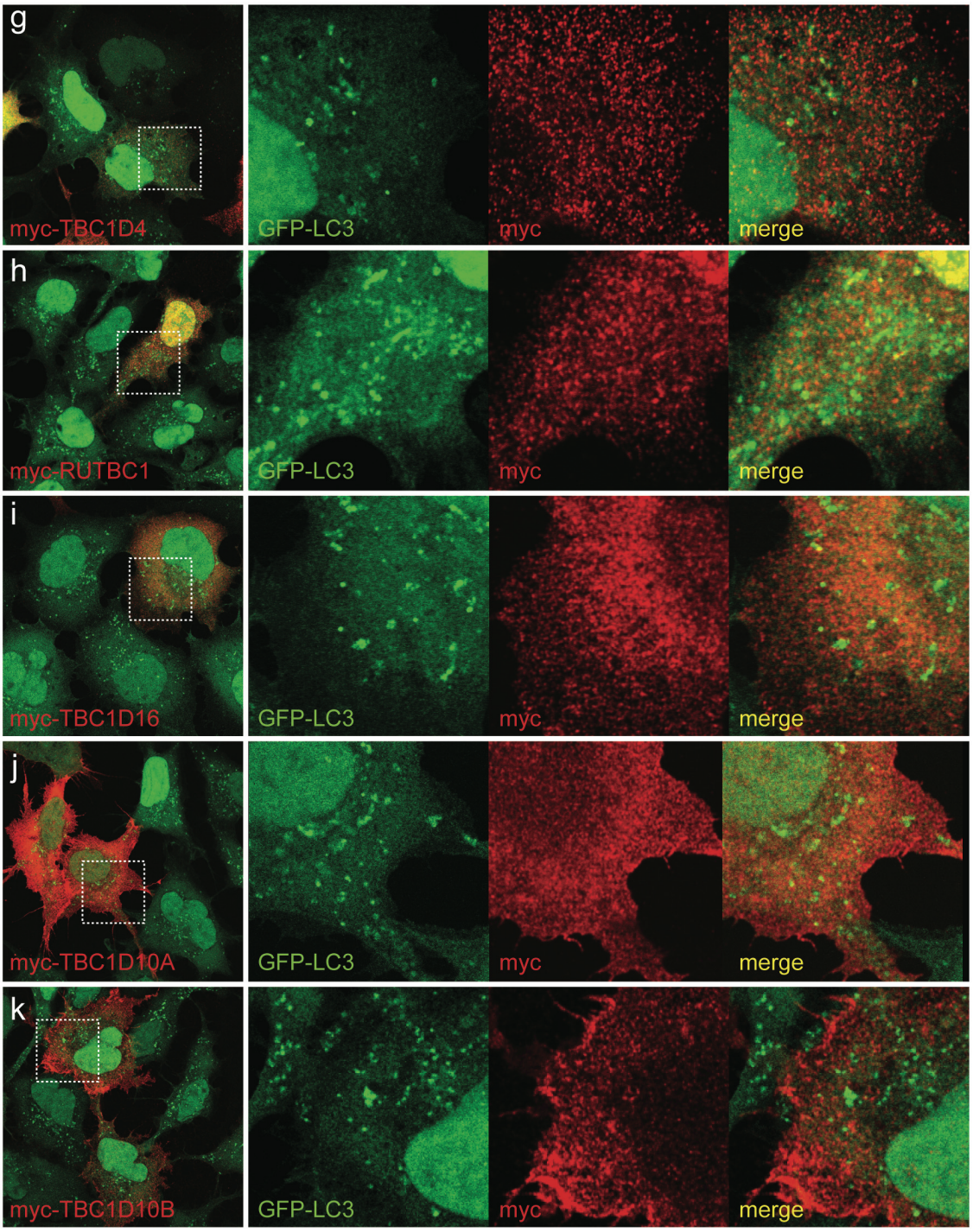

Figure 3-2 Screening candidates from the RabGAP screen for co-localisation with GFP-LC3-positive autophagosomes

(a - k) 2GL9 cells were transfected with the indicated TBC-protein. After 24h expression cells were labelled with anti-myc antibody and specific fluorescently tagged secondary antibody. Boxes shown in merge are enlarged in right panels with GFP-LC3 in green and myc in red. **(a)** myc-TBC1D7, **(b)** myc-TBC1D17, **(c)** myc-TBC1D10C, **(d)** myc-TBC1D9 **(e)** myc-TBC1D14 **(f)** myc-TBC1D9B, **(g)** myc-TBC1D4, **(h)** myc-RUTBC1, **(i)** myc-TBC1D16, **(j)** myc-TBC1D10A, **(k)** myc-TBC1D10B.

Next I wanted to investigate whether any of the 11 candidate TBC proteins co-localise with very early phagophores labelled by ULK1 (Fig. 3-3). Catalytically inactive RA mutant TBC-constructs were over-expressed where available to allow autophagosomes to form. HEK293A cells were starved for 2 hours and cells were fixed and labelled with anti-myc and anti-ULK1 antibodies followed by specific fluorescently tagged secondary antibodies.

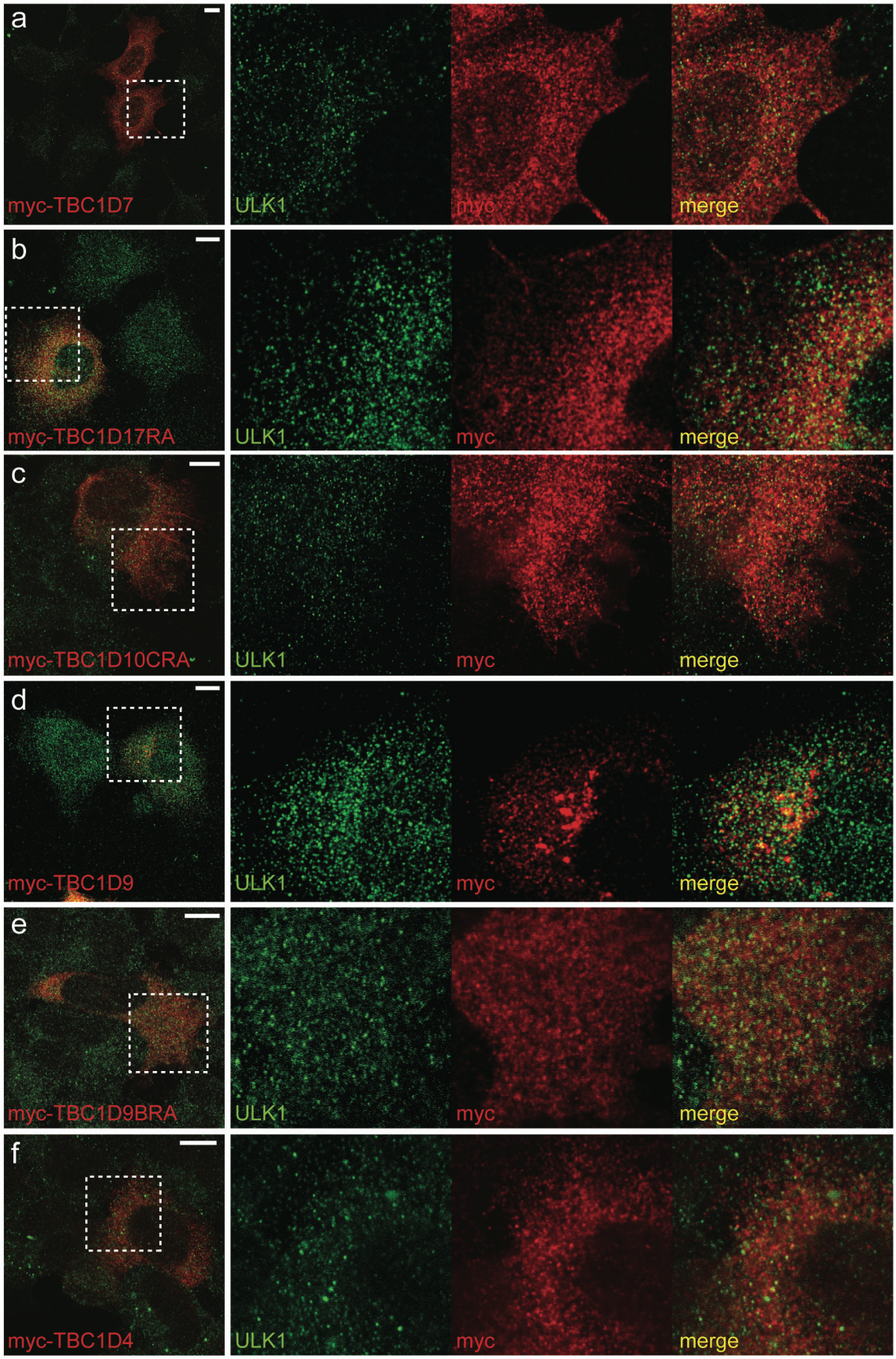
a
myc-TBC1D7
ULK1
myc
merge
b
myc-TBC1D17RA
ULK1
myc
merge
c
myc-TBC1D10CRA
ULK1
myc
merge
d
myc-TBC1D9
ULK1
myc
merge
e
myc-TBC1D9BRA
ULK1
myc
merge
f
myc-TBC1D4
ULK1
myc
merge

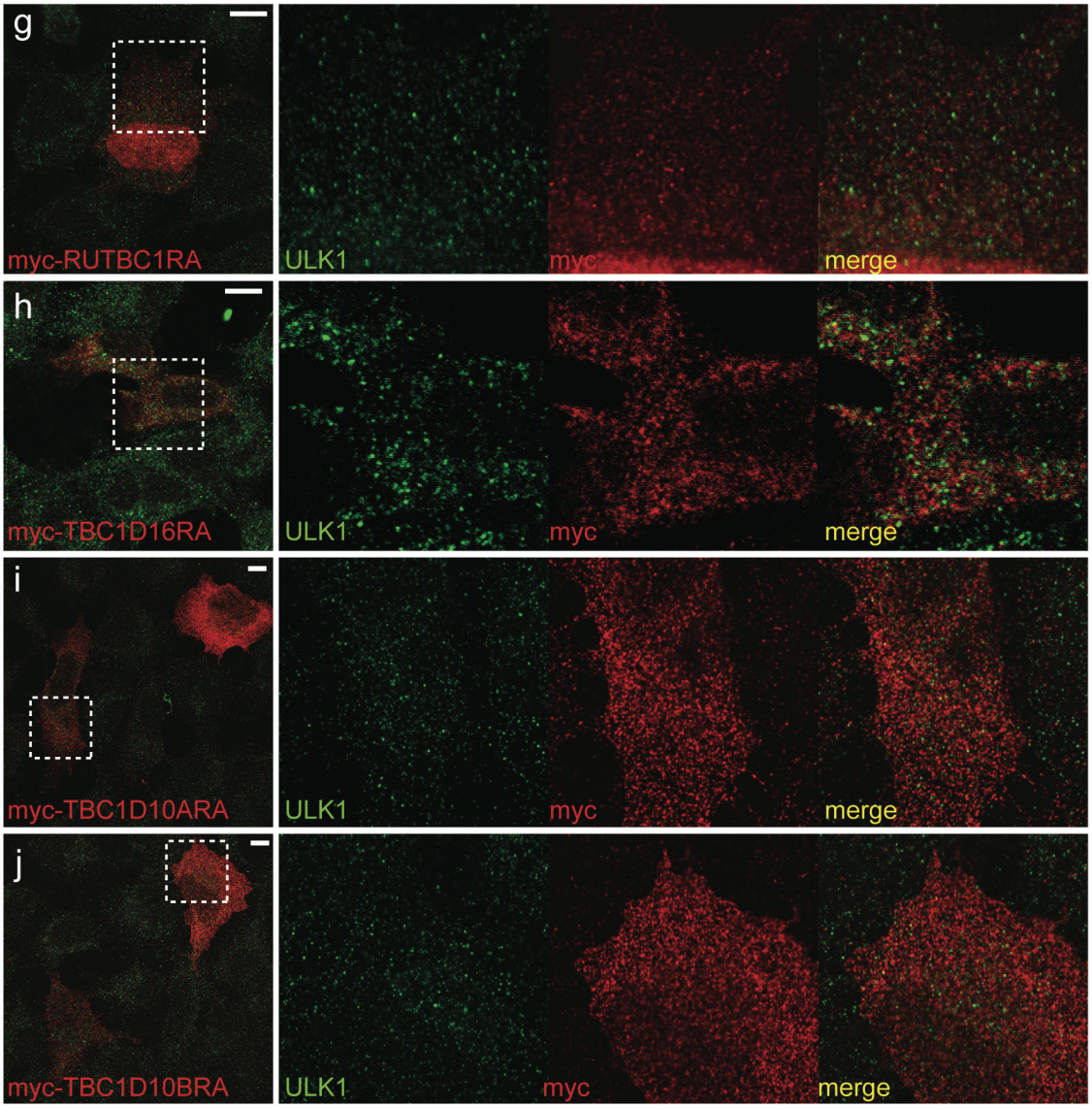

Figure 3-3 Screening candidates from the RabGAP screen for co-localisation with ULK1

(a - j) HEK293A cells were transfected with the indicated TBC-protein, wild type or RA mutant as indicated. After 24h expression cells were stained with anti-myc and anti-ULK1 antibodies and specific fluorescently tagged secondary antibodies. Inserts shown in merge panel on left are shown in right panels. **(a)** myc-TBC1D7, **(b)** myc-TBC1D17R381A, **(c)** myc-TBC1D10CR141A, **(d)** myc-TBC1D9 **(e)** myc-TBC1D9BR559A, **(f)** myc-TBC1D4, **(g)** RUTBC1R848A, **(h)** TBC1D16R494A, **(i)** TBC1D10AR160A, **(j)** TBC1D10BR134A. Scale bars are equal to 10µm.

Out of the 11 candidate proteins only TBC1D14 showed substantial co-localisation with ULK1 (Fig. 3-4a). In transfected HEK293A cells myc-TBC1D14 forms tubular

structures throughout the cytosol and ULK1 is found concentrated on subdomains of these tubules. In some cases tubular structures are observed in a juxta-nuclear position (Fig. 3-4b). The length of the TBC1D14 tubules varies and may depend on the level of over-expression (Fig. 3-4c). Shown in Figure 3-4c is a starved 2GL9 cell expressing high levels of myc-TBC1D14 demonstrating that the tubules can get very long.

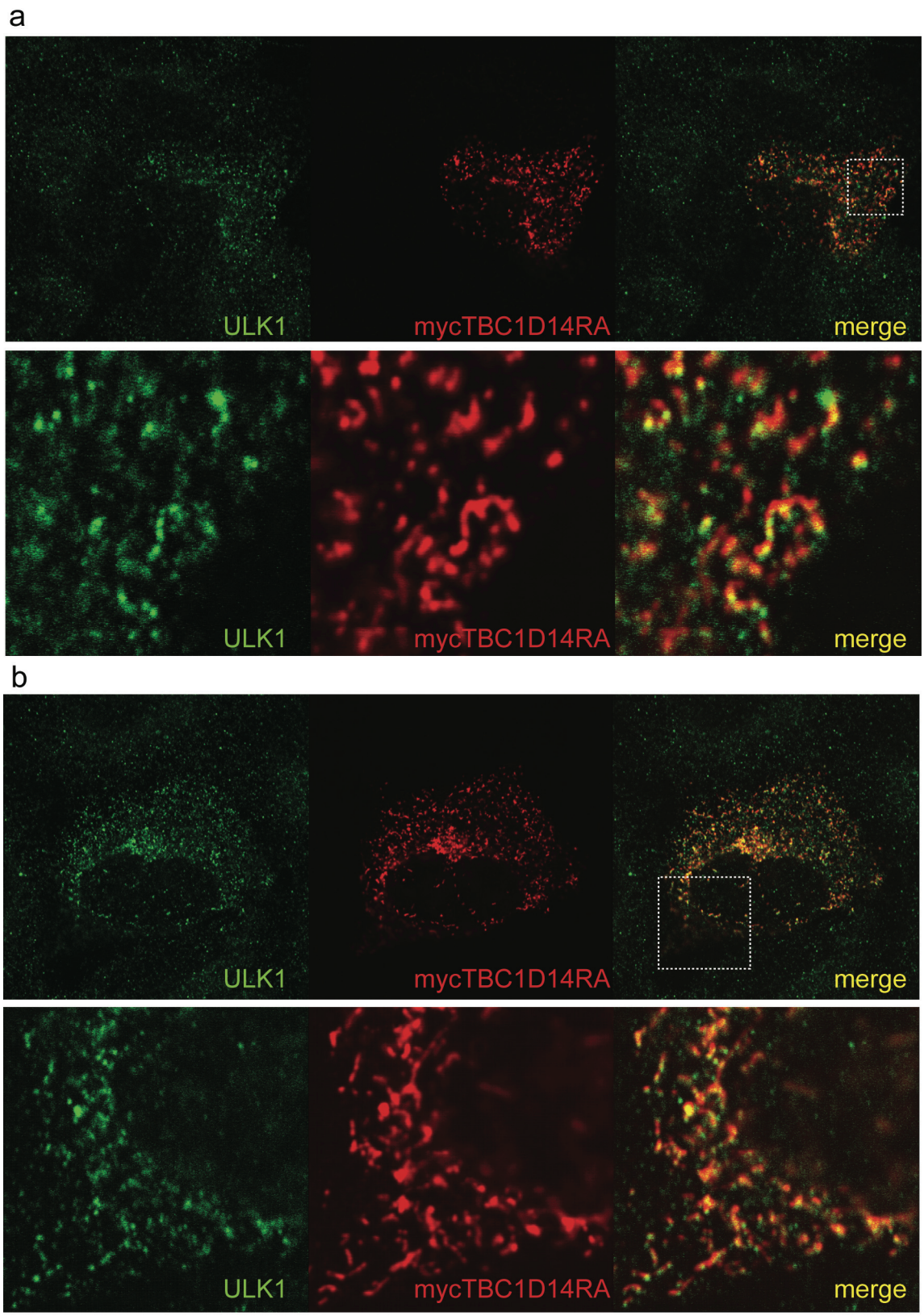
a
ULK1
mycTBC1D14RA
merge
ULK1
mycTBC1D14RA
merge
b
ULK1
mycTBC1D14RA
merge
ULK1
mycTBC1D14RA
merge

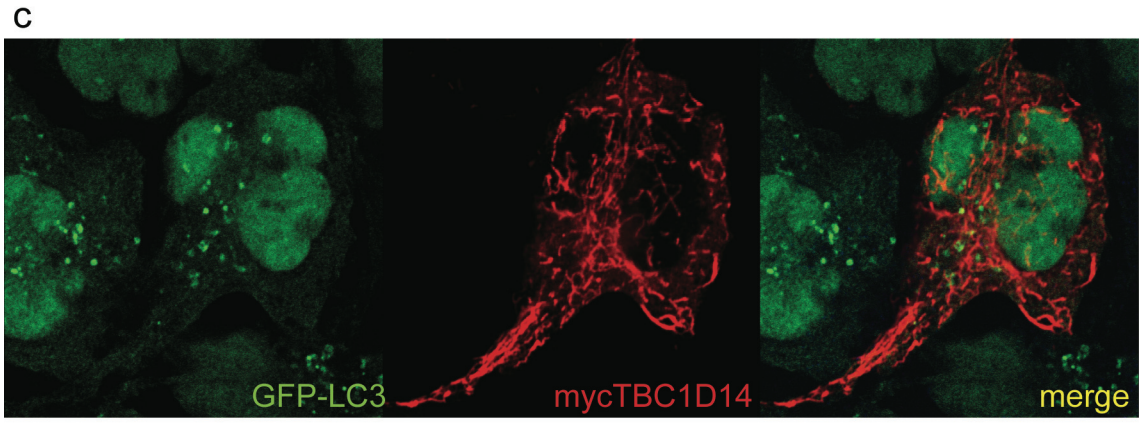

Figure 3-4 Over-expressed TBC1D14 forms tubules in the cytosol and sequesters ULK1
(a,b) HEK293A cells were transfected with myc-TBC1D14R472A (myc-TBC1D14RA), fixed, and stained 24h later with antibodies against myc (red) and ULK1 (green) followed by specific fluorescently tagged secondary antibodies. **(a)** A representative cell with tubules throughout the cytosol. **(b)** A representative cells with tubules concentrated in a juxta-nuclear position and throughout the cytosol. **(c)** A 2GL9 cell transfected with myc-TBC1D14 and starved for 2h in EBSS showing long tubules.

3.4 RabGAPs interacting with ULK1

ULK1 was shown to form a complex with Rab5, the adaptor protein Syntenin1 and SynGAP, a GAP for Rab5 [90]. This complex seems to be neuronal specific and regulates vesicular traffic during axon extension. However, I hypothesised that ULK1 could form a similar complex to regulate autophagosome formation since I could confirm that Syntenin1 binds ULK1 in HEK293A cells via a co-immunoprecipitation assay (Fig. 3-5). Syntenin1 is a PDZ-domain containing protein and ULK1 has a classical PDZ binding motif consisting of the last three C-terminal amino acids valine/tyrosine/alanine (VYA) in mouse and isoleucine/cysteine/alanine (ICA) in human ULK1 [255]. Consistent with the notion that ULK1 and Syntenin1 interact via these two domains, deletion of these last three amino acids in ULK1 abolishes binding

to Syntenin1. For the co-immunoprecipitation experiment HEK293A cells were transfected with HA-Syntenin1 and myc-ULK1 or myc-ULK1ΔVYA or with either construct alone. Cell lysates were then immunoprecipitated using anti-HA or anti-myc antibodies.

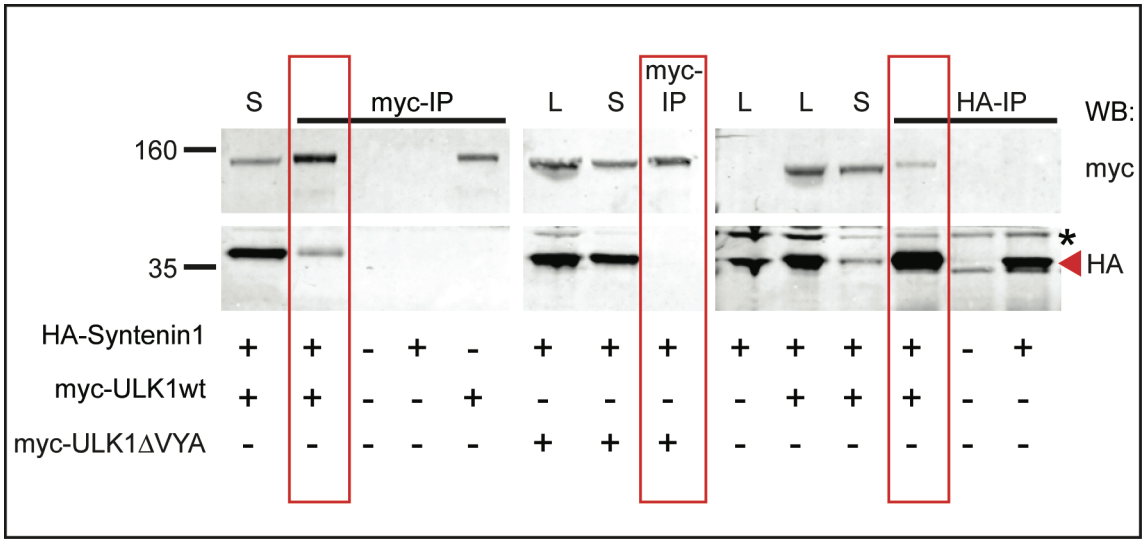

Figure 3-5 ULK1 binds Syntenin1 in HEK293A cells via its PDZ binding motif
HEK293A cells were transfected with the indicated construct(s) and allowed to express the proteins for 24 hours. Cell lysates were then incubated with protein-G-sepharose bound anti-HA or anti-myc over-night at 4ºC on a spinning wheel. Membranes were cut and the top part was labelled with anti-myc to detect myc-ULK1; the bottom part was labelled with anti-HA to detect HA-Syntenin1 using the LI-COR system. Red box left: HA-Syntenin1 co-immunoprecipitates with myc-ULK1. Red box middle: HA-Syntenin1 does not co-immunoprecipitate with myc-ULK1ΔVYA. Red box right: myc-ULK1 co-immunoprecipitates with HA-Syntenin1. S indicates 5% unbound supernatant; L indicates 5% lysate; IP indicates immunoprecipitated proteins. Asterisk indicates a non-specific band, red arrowhead indicates HA-Syntenin1.

Next, I undertook a yeast-2-hybrid screen to find RabGAPs interacting with ULK1 (Fig. 3-6) using full length wild type ULK1 as bait against the GAP library using RA mutants where available. A truncation mutant of ULK1 containing only the C-terminus from

amino acids 653 to the end (1051) was also tested as this region was reported to contain the GAP binding domain of ULK1 but this construct was auto-activating and could not be used. RabGAP constructs for yeast-2-hybrid analysis were provided by Prof. F. Barr (Max Planck Institute of Biochemistry, Martinsried, Germany and currently University of Liverpool, UK). Competent PJ694A yeast cells were transfected with ULK1 and one of the RabGAPs. Double transfected cells were selected on plates lacking leucine and tryptophan. Five colonies were taken from each plate and re-streaked on both selective plates. Protein interaction allows growth of yeast on quadruple drop out (QDO) plates lacking leucine, tryptophan, histidine, and adenine. Some constructs are toxic to the yeast cells such as EVI5-like, where only one colony grew but this colony is probably untransfected and has coincidentally acquired mutations that allow it to grow on selective plates. Surprisingly, ULK1 interacts with 17 out of 35 GAPs tested.

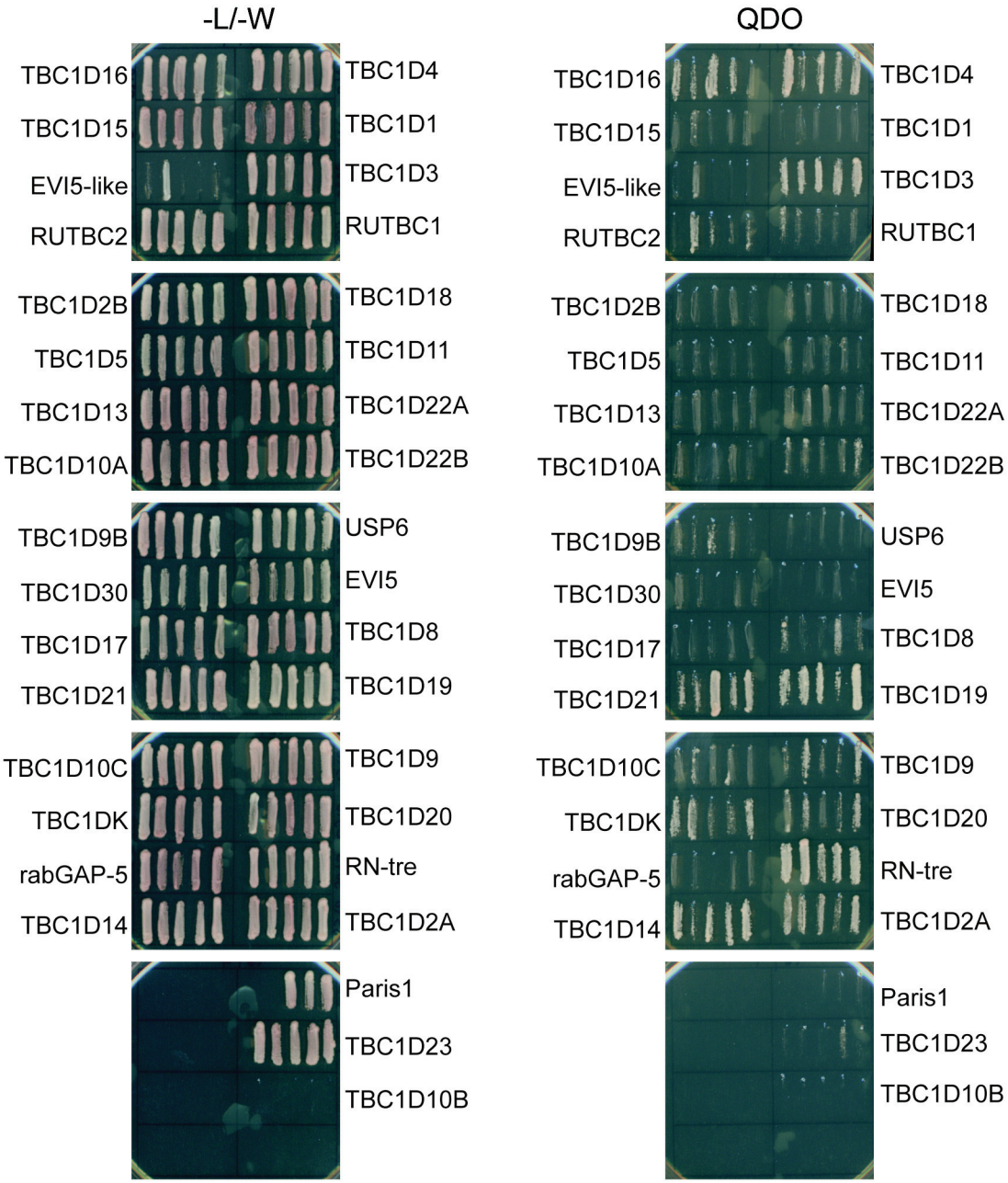

Figure 3-6 Yeast-2-hybrid screen to identify RabGAP binding partners of ULK1
Cells were transfected with the indicated inactive (RA) RabGAP constructs (prey, in pACT2 vector) where available, and ULK1 (bait, in pFBT9 vector) and selected for double transfected cells on plates lacking leucine and tryptophan (-L/-W left). Cells were allowed to grow at 30ºC for 72h. Each box shows five colonies with each colony having been streaked on both selective media. Binding of ULK1 to the RabGAP allows growth on quadruple drop out medium (QDO) lacking leucine, tryptophan, histidine and adenine (right panel). TBC constructs in pACT2 vector were kindly provided by F. Barr (University of Liverpool, UK).

ULK1 does not bind to a specific branch of TBC-proteins when the full length proteins were aligned in a phylogenetic tree (Fig. 3-7a) nor when only the TBC-domains were aligned [196] but this could be explained by the fact that TBC domains share little amino acid sequence homology but high structural homology so the ULK1 binding fold may still look similar even if the amino acid sequence does not.

Furthermore, RabGAPs that inhibit autophagy as found in my screen, do not group into a particular family or branch, and ULK1 sequestration alone cannot explain their inhibitory effect when over-expressed, since many ULK1 binding partners show no reduction of GFP-LC3-II formation (Fig. 3-7b).

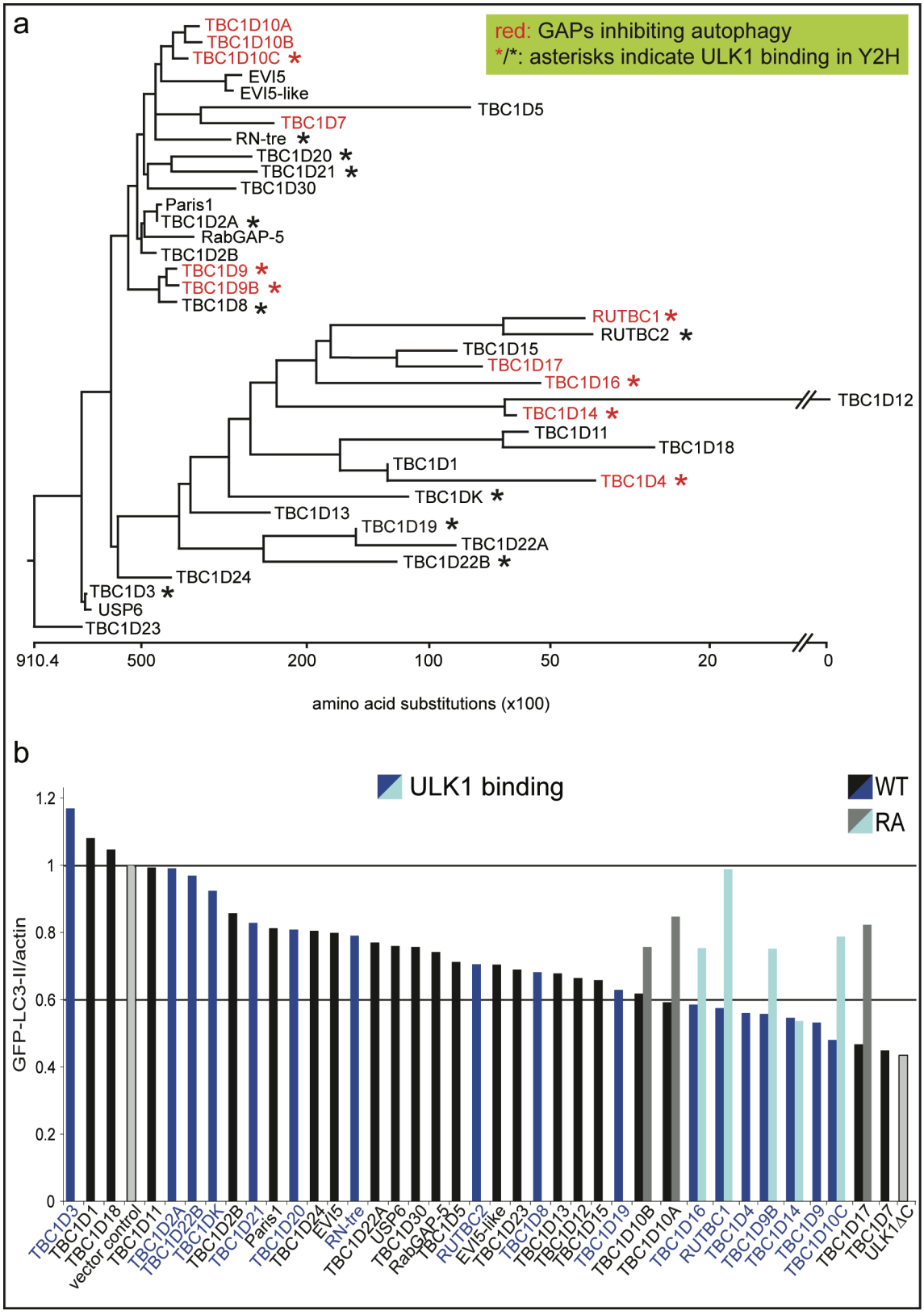

Figure 3-7 A phylogenetic tree of full length human RabGAPs

(a) Full length human TBC-domain proteins were aligned using the ClustalW method. The 11 RabGAPs inhibiting autophagy are coloured red and asterisks indicate binding to ULK1 in a yeast-2-hybrid assay. **(b)** Same as in (a) with RabGAPs binding to ULK1 indicated by blue bars.

3.5 A yeast-2-hybrid screen to identify Rab GTPases binding to Syntenin1.

Lastly, since I hypothesised that ULK1 can regulate autophagosome formation in a complex with a Rab-RabGAP pair bridged by the adaptor protein Syntenin1, I investigated which Rabs, if any, Syntenin1 can bind to. Therefore, I undertook a yeast-2-hybrid screen using full length Syntenin1 as bait against a library of Rab GTPases (the Rabome; Fig. 3-8). The yeast-2-hybrid screen was done exactly as described above but using Syntenin1 as bait (in pFBT9 vector) and GTP-locked active Rab GTPases as prey (in pACT2 vector). All Rab constructs were kindly provided by Prof. F. Barr (University of Liverpool, UK). As previously shown by Tomoda et al., Syntenin1 binds Rab5a, b, and c but not its most closely related homologues Rab21 or Rab22. It also binds Rab37, which is found on secretory granules in mast cells [256], and Rab33a and b. Importantly, Rab33b was shown to control localisation of the Atg16L complex [222] involved in autophagosome formation, and over-expression of a dominant active mutant of Rab33b (Rab33bQ92L) induced autophagy. However, the GAP for Rab33 is thought to be TBC1D22B (personal communication F. Barr; University of Liverpool, UK) and had no inhibitory effect on GFP-LC3 lipidation (Fig. 3-1). Over-expression of a dominant negative mutant Rab33a/bT50N also did not inhibit autophagosome formation in my hands (Fig. 3-9). The Rab45-pACT2 construct is auto-activating and does not need to interact with a pFBT9 construct to activate transcription. However, it was

included as an internal control even though no conclusion can be drawn as to whether Rab45 interacts with Syntenin1 or not.

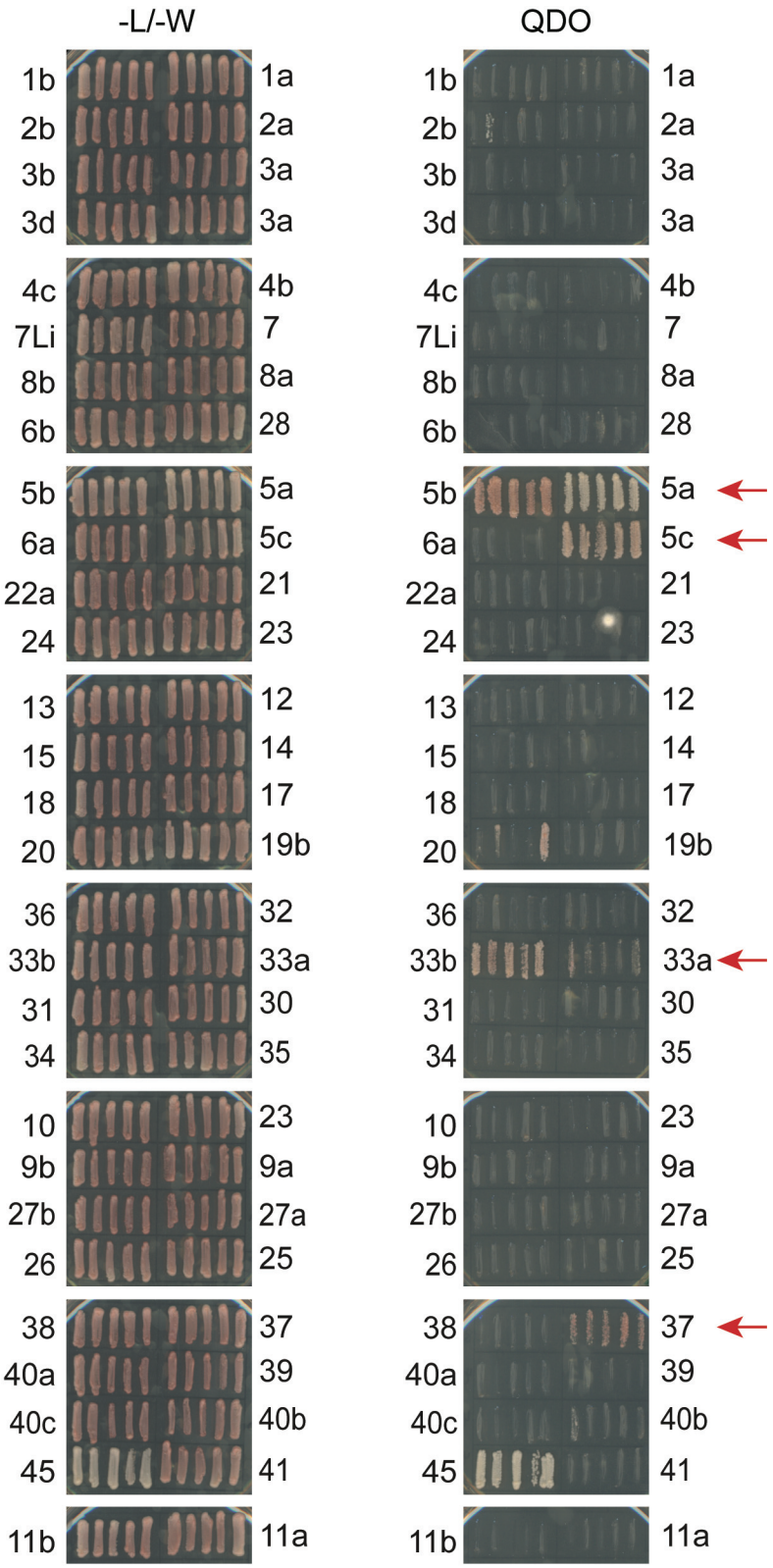

Figure 3-8 Syntenin1 binds Rab5, Rab33, and Rab37
Cells were transfected with the indicated active GTP-locked (QA) Rab construct (prey, in pFBT9 vector) and full length Syntenin1 (bait, in pACT2 vector) and selected for double transfected cells on plates lacking leucine and tryptophan (-L/-W left). Cells were allowed to grow at 30ºC for 72h. Each box shows five colonies with each colony having been streaked on both selective media. Binding of Syntenin1 to the Rab GTPase allows growth on quadruple drop out medium (QDO) lacking leucine, tryptophan, histidine and adenine (right panel). Syntenin1 binds all 3 isoforms of Rab5 (a, b, and c), Rab37, and Rab33a and 33b (indicated by red arrows). The Rab45 construct is auto-activating. Rab GTPase constructs in pFBT9 vector were provided by F. Barr (University of Liverpool, UK).

3.6 Screening putative target Rab GTPases of RabGAPs that inhibit autophagy

It is thought that each RabGAP targets a specific family of Rab GTPases and ongoing research is aiming to identify such Rab-RabGAP pairs and their role in membrane traffic. Of the RabGAPs I have found to inhibit autophagy some target Rabs have been discovered and their functions in cellular transport have been described (summarised in Table 3-1). These RabGAP targets were tested using mutant Rabs available through a collaboration with Francis Barr (University of Liverpool, UK) and the results are summarised below. Endogenous LC3 lipidation was chosen as a readout for autophagic activity looking at fed, starved, and starved with leupeptin conditions to be able to distinguish between defects in autophagosome formation and autophagosome maturation (see Introduction section 1.1.4.2).

Rab17 was shown to be the target of TBC1D7 and they are involved in cilia formation [251]. Importantly however, TBC1D7 binds and inhibits TSC1 [75], which is upstream

of mTOR. It would seem that Rab17 is also involved in this pathway since inactive Rab17N132I over-expression inhibits autophagosome formation (Fig. 3-9).

Rab35 is the target of the TBC1D10 family [199, 257] and has been shown to be involved in various processes, including Tfn recycling. However, over-expression of Rab35N120I did not inhibit LC3 lipidation but slightly activated it. This is unexpected since over-expressing the inactive Rab should pheno-copy the effect of over-expression of its GAP.

Rab36 may be the target of TBC1D16 and regulate the spatial distribution of late endosomes and lysosomes [258]. The constitutively active mutant Rab36Q182A led to a slight increase in LC3 lipidation as expected. This could be due to fewer lysosomes being available for autophagosomes to fuse with due to aberrant distribution of lysosomes. However, as inactivating Rab36 by over-expressing TBC1D16 did not lead to a maturation defect leading to accumulation of GFP-LC3-II but to decreased LC3 lipidation this is unlikely to be the case here and there must be an additional effect affecting autophagosome formation.

Rab37 was tested because a yeast-2-hybrid screen revealed that it binds the ULK1 interactor Syntenin1 (Fig. 3-5). Again the constitutively active mutant Rab37Q82A was over-expressed but it had no effect on autophagy.

Rab5 was shown to bind TBC1D17 [196] and has been shown to be involved in the removal of aggregated mutant huntingtin (htt) by selective autophagy [217]. However, when I tested the ability of inactive mutant Rab5N133I to inhibit LC3 lipidation in response to starvation it had no effect although there may be slightly less total LC3 in Rab5N133I over-expressing cells. This was apparently not due to enhanced degradation during the two hour starvation period since addition of leupeptin does not prevent the reduction in LC3 observed. Further investigation by RT-PCR or investigating proteasomal protein turnover would be necessary to explain this effect.

Lastly, I tested the effect of inactive Rab22aS19N on autophagosome formation because it is the target Rab of TBC1D9B and was found by N. McKnight (LRI) in a siRNA screen to be involved in autophagy (unpublished). Over-expression of this GDP-locked mutant had no effect on LC3 lipidation, but it might be worth investigating a different mutant, which cannot bind nucleotides.

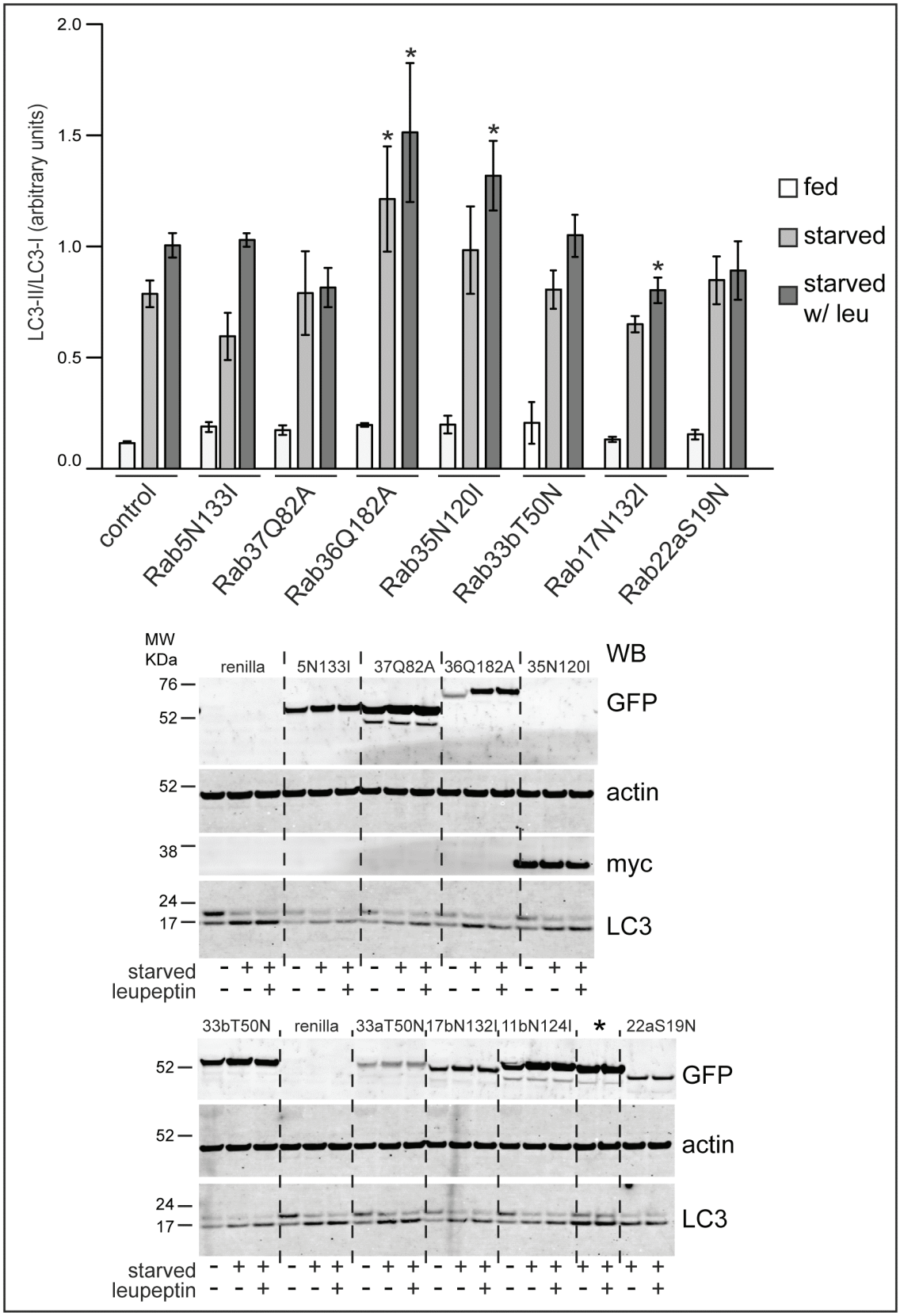

Figure 3-9 Mutant Rab targets tested in HEK293A cells

HEK293A cells were transfected with the indicated Rab constructs: GFP-Rab17N132I (nucleotide empty), myc-Rab35N120I (nucleotide empty), GFP-Rab36Q182A (GTP-bound), GFP-Rab37Q82A (GTP-bound), GFP-Rab5N133I (nucleotide empty), GFP-Rab22aS19N (GDP-bound), or renilla vector control. Cells were starved 24h later in EBSS with (dark grey) or without (light grey) leupeptin (leu). Endogenous LC3 conversion was measured by western blot using anti-LC3 antibody. The mean of 3 independent experiments is shown with the starved and starved with leupeptin samples done in duplicates. Asterisks indicate results of unpaired Student's t-test comparing to the vector control (fed vs. fed; starved vs. starved; etc.). Rab17N132I starved with leupeptin p=0.0207; Rab35N120I starved with leupeptin p=0.0339; Rab36Q182A starved p=0.0433; Rab36Q182A starved with leupeptin p=0.0429. Error bars indicate SEM. A representative western blot done with the LI-COR system is shown using anti-GFP and anti-myc antibodies to detect transfected Rab proteins, anti-actin, and anti-LC3 antibodies to detect the respective endogenous proteins. Asterisk in western blot indicates irrelevant samples. Only Rab33b is shown in the quantification because of space constraints but Rab33a has a very similar effect. Note that the effect of Rab11 on autophagy will be described in more detail below.

3.7 Conclusion

In an over-expression screen with all putative human RabGAPs 11 TBC-proteins were found to inhibit autophagosome formation when over-expressed in 2GL9 cells (listed in Table 3-1). Out of these 11 RabGAPs, TBC1D7 and TBC1D14-positive vesicles show some juxta position with GFP-LC3 positive autophagosomes and TBC1D17, TBC1D9B, TBC1D4, and RUTBC1 show a partial co-localisation. Only TBC1D14 shows substantial overlap with early ULK1-positive autophagosomes. A screen for RabGAP binding partners of ULK1 revealed 17 RabGAPs that interact with ULK1 and TBC1D14 was one of them. The ULK1 complex may transiently form a bigger multi-protein complex with TBC1D22B, Syntenin1, and Rab33b. Out of these proteins Rab33b has already been shown to be involved in autophagy. However, over-expression of TBC1D22B does not inhibit autophagosome formation. ULK1 may be able to form different Rab-RabGAP complexes in different cells, at different stages of development,

or at different nutrient levels since it has been shown to form a complex with Syntenin1, Rab5, and SynGAP in developing neurons to regulate neurite extension [90]. SynGAP is a neuronal specific GAP with a RasGAP rather than a TBC domain but it seems to be able to act as a Rab5 GAP in these cells. Interestingly, Rab5 has been shown to be essential for autophagosome formation to remove mutant huntingtin aggregates and it would be interesting to investigate whether it does so in a complex with ULK1 as well [217]. Investigating target Rab GTPases of RabGAP that inhibit autophagy using mutant Rab constructs I found that over-expression of inactive Rab17N132I decreased and constitutively active Rab36Q182A increased autophagosome formation**.**

Table 3-1 Summary of RabGAPs found to inhibit autophagy
Table 3-1 shows a summary of the RabGAPs found to inhibit autophagy indicating their putative target Rab and demonstrated function(s).

Rab-GAP and alternative names	Possible target Rab	Demonstrated function(s)
TBC1D7 PIG51	Rab17	Inhibits TSC1, which in turn inhibits mTOR [75] Cilia formation [251] Expressed in a majority of lung cancers [259]
TBC1D17	Rab21 Rab5a/b/c	Shiga toxin uptake [199] Binds Rab5 [196]
TBC1D10C Carabin EPI64C	Rab35	Inhibits Ras and Calcineurin [260] Shiga toxin uptake [199] Tfn recycling and immunological synapse formation [202] Exosome secretion [261] Regulates Ca^{2+}-activated K^{+} channel KCa2.3 recycling involved in endothelial function [202, 257]
TBC1D9 KIAA0882		Contains two GRAM domains, which are similar to plekstrin homology (PH) domains involved in PI lipid binding.
TBC1D14 KIAA1322		Yeast homologue Sbe22p binds Atg18p [262] 3D crystal structure of the TBC domain solved [198]
TBC1D9B	Rab22a	Binds Rab22a (personal communication F. Barr; University of Liverpool, UK) siRNA mediated knock down of Rab22a inhibits autophagy in 2GL9 cells (unpublished N. McKnight et al.) Contains a single span transmembrane and two GRAM domains, which are similar to plekstrin homology (PH) domains involved in PI lipid binding [263]

TBC1D4 AS160	Rab2a, Rab8a, Rab10, Rab14	Akt substrate, GLUT4 translocation [264] Rab8a, 10, and 14 are involved in endocytic recycling [194, 265, 266]
RUTBC1 KIAA0397 SGSM2	Rab4, 11	Interacts with Rab and Rap [267]
TBC1D16	Rab36	Rab36 may regulate the spatial distribution of late endosomes and lysosomes and is found in the Golgi and TGN [258]
TBC1D10A EPI64	Rab27a	Shiga toxin uptake [199] Microvillar structure [268] Exosome secretion [261]
TBC1D10B		Shiga toxin uptake [199] Exosome secretion [199, 261]

Over-expression of TBC1D14 inhibits autophagosome formation and leads to tubulation of a membrane compartment, which sequesters ULK1. It is able to bind directly to ULK1 as shown by a yeast-2-hybrid assay but this interaction may not be exclusive and ULK1 can bind other GAPs as well. A PSI blast revealed distant homology to the yeast protein Sbe22p, which binds Atg18, another essential autophagy protein. For all these reasons and since I was particularly interested in early events of autophagosome formation, which involve ULK1, I chose to investigate this TBC1D14 further.

Chapter 4. Characterisation of TBC1D14

4.1 Aim

TBC1D14 is a 693 amino acid long protein with a C-terminal TBC domain and an N-terminus containing no known motifs (Fig. 4-1). A structure of the TBC domain of TBC1D14 has been published by Tempel et al. [198] encompassing amino acids 357-672, however, the entire TBC domain is predicted to be longer stretching from amino acids 223 to 669. The crystal structure revealed that a significant realignment of the two catalytic arginine and glutamine residues is necessary for TBC1D14 to act as a GAP. This is probably achieved by interaction with its target Rab causing conformational changes in the GAP domain so the catalytic residues can be aligned leading to GTP hydrolysis. However, the target Rab GTPase of TBC1D14 has not been reported, and the role of TBC1D14 in membrane traffic is not known. Therefore, I investigated the role of TBC1D14 in intracellular traffic and autophagy.

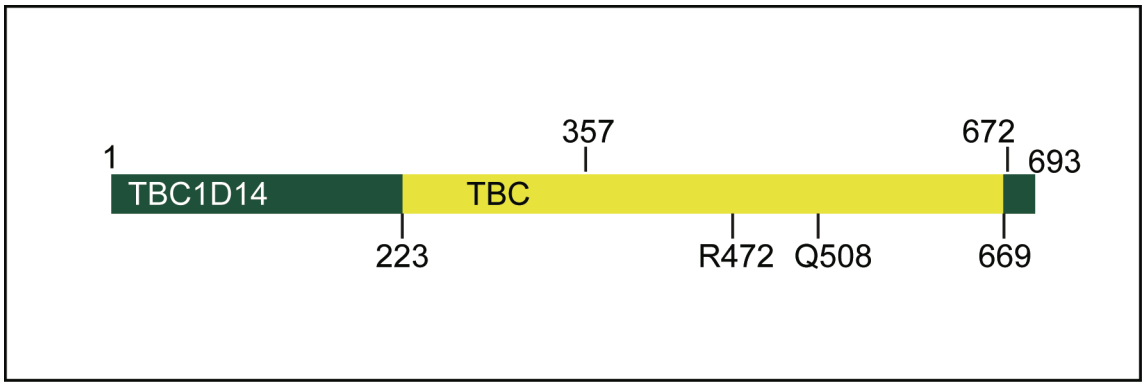

Figure 4-1 Domain structure of TBC1D14

TBC1D14 is a 693 amino acid protein containing a C-terminal TBC domain and an N-terminus with no known motifs. The predicted molecular weight is around 80 kDa. The crystal structure of the TBC domain from amino acid 357 to 672 has been solved [198] but the functional TBC domain is predicted to stretch from amino acid 223 to 669 (yellow). The two catalytic residues necessary for GAP activity arginine R472 and glutamine Q508 are indicated.

4.2 TBC1D14 inhibits long-lived protein degradation and endogenous LC3 lipidation in a GAP activity dependent manner

To confirm that the effect of TBC1D14 over-expression on autophagy is not limited to the inhibition of LC3 lipidation, I performed a long-lived protein degradation assay [269, 270]. Whereas short-lived proteins are mostly degraded by the proteasome, more stable long-lived proteins are usually removed by autophagy. HEK293A cells were labelled with radioactive [^{14}C]valine over-night to allow its incorporation into newly synthesised proteins. To allow degradation of radioactively labelled short-lived proteins, cells were then chased in cold medium for 24h. Autophagy was induced by starvation for 2h, during which degradation of labelled proteins leads to release of [^{14}C]valine into the medium. Trichloroacetic acid (TCA)-soluble ^{14}C counts were then measured from the medium of TBC1D14 transfected and renilla vector control transfected cells. Over-expression of TBC1D14 and the TBC1D14R472A mutant inhibit long-lived protein degradation to a similar extent as a kinase deficient mutant of ULK1, ULK1K46I, which is known to inhibit autophagy [21] (Fig. 4-2).

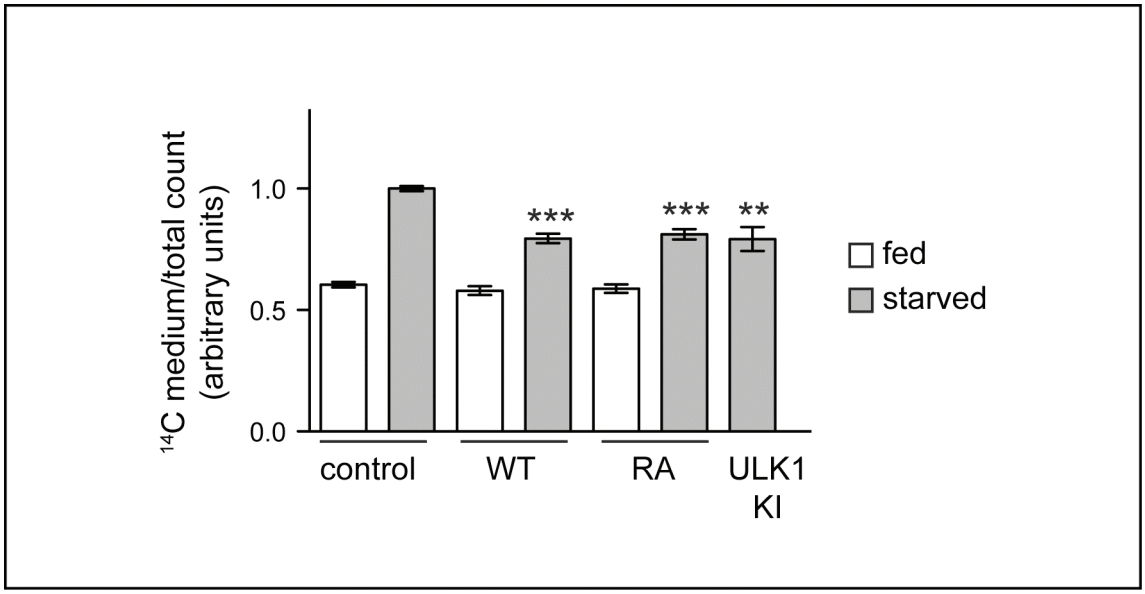

Figure 4-2 TBC1D14 over-expression inhibits long-lived protein degradation
HEK293A cells were transfected with either renilla vector control, TBC1D14WT (WT), TBC1D14R472A (RA) or, kinase inactive ULK1K46I (ULK1 KI), which is known to inhibit autophagy. Cells were labelled with [^{14}C]valine overnight and chased in cold medium for 24h to allow degradation of short-lived proteins. Cells were then starved for 2h in EBSS, and the acid-soluble ^{14}C released into the medium was counted, the cells were harvested and the acid insoluble ^{14}C from the cells was counted. Each condition was done in triplicate and the experiment was repeated twice. Long-lived protein degradation was calculated from the ^{14}C cpm medium/^{14}C cpm total (medium and cells), normalized to control starved samples, and presented as arbitrary units. Asterisks indicate results from unpaired Student's t-test compared to starved control values. WT, $p<0.0001$; RA, $p<0.0001$; ULK1 KI, $p=0.0021$.

As described above the crystal structure of TBC1D14 shows that its catalytic arginine and glutamine residues have an atypical conformation compared to the TBC domains of Gyp1p and TBC1D22A, which have also been crystallised. This may explain why the single mutant TBC1D14R472A fails to rescue the inhibition of autophagy when over-expressed. Therefore, I tested a double mutant TBC1D14R472A/Q508A (TBC1D14RA/QA) protein and monitored endogenous LC3 lipidation as a read-out for autophagy. I also tested the other single mutant lacking the catalytic glutamine TBC1D14Q508A (TBC1D14QA). The RA/QA and QA mutant constructs were cloned

using a QuickChange Multi Site-directed mutagenesis kit using the myc-TBC1D14 wild type or RA mutant constructs as a template. Over-expression of TBC1D14RA/QA fails to inhibit LC3 lipidation in HEK293A cells suggesting that the double mutant protein lacks GAP activity (Fig. 4-3). The single mutant TBC1D14QA inhibits autophagy to a similar extent as TBC1D14RA and TBC1D14WT.

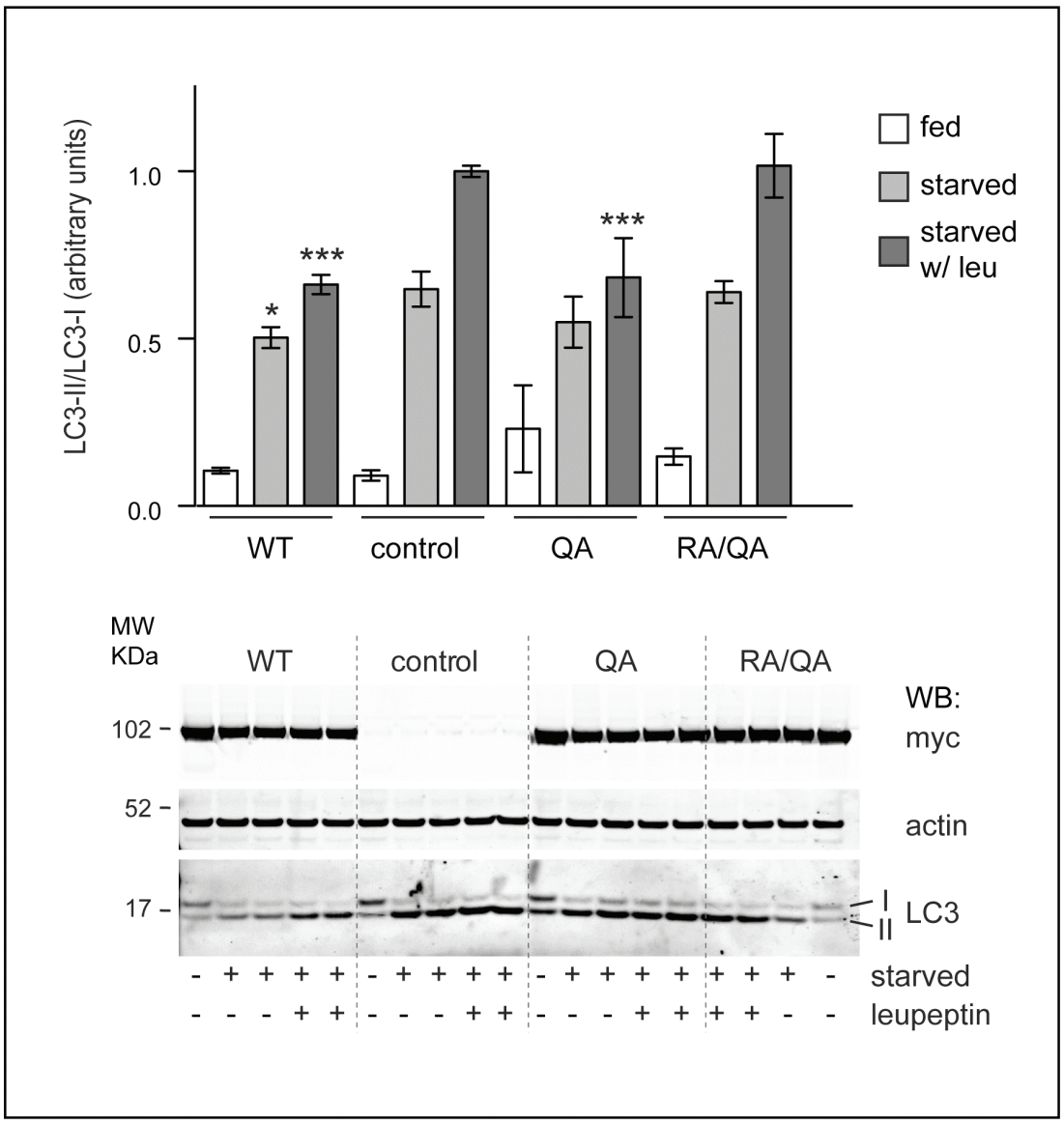

Figure 4-3 Over-expression of the double mutant TBC1D14RA/QA does not inhibit autophagosome formation

HEK293A cells were transfected with TBC1D14WT (WT), control renilla vector, TBC1D14Q508A (QA), or TBC1D14R472A/Q508A (RA/QA) constructs and starved for 2h with or without leupeptin (leu) to measure autophagic flux. The mean result of 3 experiments with each condition done in duplicate except for the fed condition is shown. A representative western blot of the transfected cell lysates is shown below using the antibodies indicated and the LI-COR system. Asterisks indicate results of unpaired Student's t-test compared to vector control EBSS with leupeptin: WT, $p<0.0001$; QA, $p=0.0002$; and WT EBSS vs. control EBSS: $p=0.0432$). Error bars indicate standard error of the mean (SEM).

4.3 siRNA mediated knock down of TBC1D14 enhances autophagy

To better study the role of TBC1D14 in autophagy an antibody was raised against a peptide from human TBC1D14. Rabbits were injected with three different peptides, two from the N-terminus (one rabbit each) of TBC1D14 and one from the C-terminus (two rabbits). Peptides were chosen based on calculations of antigenicity using the MacVector program. A cysteine residue was added to the N-terminus of the peptide to allow conjugation of the peptide to a sulfolink column for affinity purification of specific antibodies. The peptides were as follows:

STO289 (amino acids 81-101): CSAVHVRRKQSDSDLIPERA

STO290 (amino acids 116-136): CTEREQSVRKSSTFPRTGYD

STO291 and STO292 (amino acids 671-691) CLTALQKDSREMEKGSPSLR

I tested the rabbit sera by western blot for detection of endogenous TBC1D14 with lysates from HEK293A cells mock transfected, or after TBC1D14 was knocked down with a siRNA pool consisting of 4 different oligos (Fig. 4-4). Cells were transfected with 50nM of the siRNA pool twice over the course of 3 days to achieve efficient

protein depletion. Western blots were then done using the four different rabbit sera diluted 1:100 in 5% milk. TBC1D14 is a 78 kDa protein and a band of this size, which disappears upon siRNA knock down of TBC1D14 can be detected with both STO298 and STO291 (Fig. 4-4, red asterisks). However, STO289 also detects many unspecific bands at around that size, therefore STO291 was used for all further experiments. STO291 was affinity purified using the peptide the rabbits were injected with covalently conjugated to a sulfolink column (Pierce) according to the manufacturers instructions.

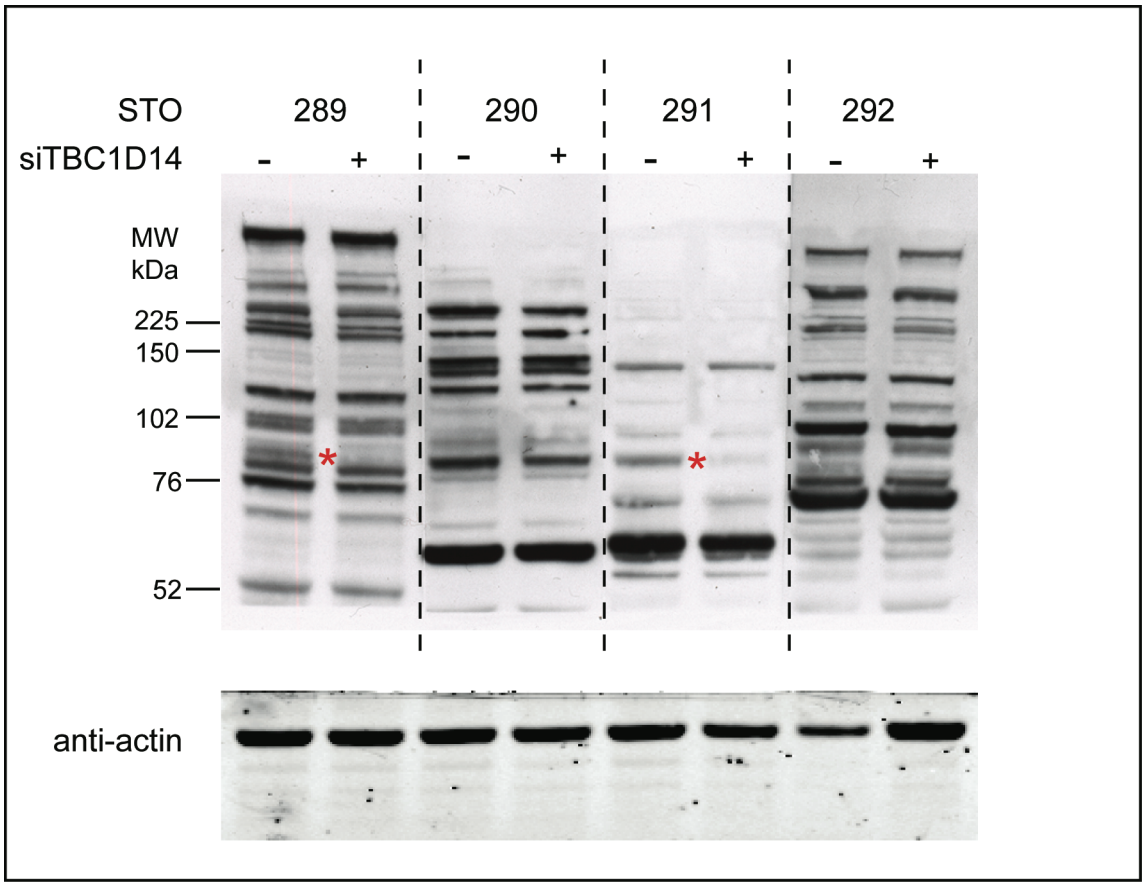

Figure 4-4 STO289 and STO291 rabbit sera detect endogenous TBC1D14 by western blot

HEK293A cells were transfected with a siRNA pool consisting of 4 individual duplexes targeting different regions of TBC1D14 or mock transfected. Transfections were done on day 1 and 2 using Oligofectamine and 50nM pooled siRNA. On day 4 after a 72h knock down period cells were harvested for western blot analysis. The membrane was probed with the 4 different rabbit sera (STO289-292) diluted 1:100 in 5% milk and HRP-conjugated secondary antibodies specific for rabbit immunoglobulins.

Red asterisks indicate a band that is the right size to be TBC1D14 and is not present when TBC1D14 is depleted in the knocked down cells. Dashed lines indicate where the membrane was cut. The lower part of the membrane was stained for actin as a loading control.

Next, I wanted to test whether siRNA mediated knock down of TBC1D14 could enhance autophagy in HEK293A cells. First, I deconvoluted the siRNA pool against TBC1D14 to determine which duplex would work most effectively when used alone instead of the pool. HEK293A cells were transfected as described above with either 50nM siRNA pool or 50nM of one of the siRNA duplexes. The membrane was blotted with anti-TBC1D14 antibody and Ponceau staining served as a control for protein loading. Duplex 12 showed a good depletion of the TBC1D14 protein in two independent experiments and was chosen for all future siRNA knock-down assays.

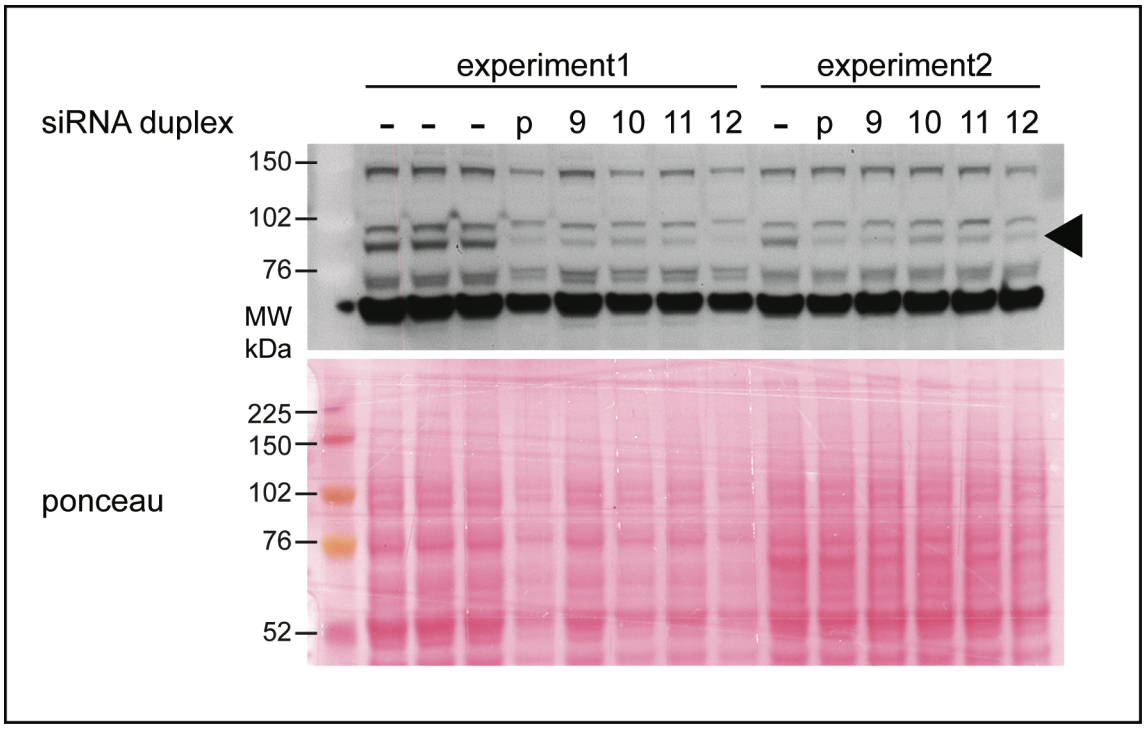

Figure 4-5 Deconvolution of a siRNA pool targeting TBC1D14

HEK293A cells were transfected with a siRNA pool against TBC1D14 as described in Figure 4-4 or with 50nM of the individual siRNA duplexes. Shown are western blots using anti-TBC1D14 from two independent experiments. p = siRNA pool; number indicates the duplex number given by the manufacturer. Arrowhead indicates TBC1D14 band. Ponceau staining was performed before antibody staining (lower panel).

To test whether TBC1D14 knock down has any effect on autophagy I chose to use endogenous LC3 lipidation as a readout. HEK293A cells were transfected with a siRNA oligo targeting TBC1D14 twice as described above and LC3 lipidation was measured by western blot using the LI-COR system. Knock down of TBC1D14 was confirmed by blotting with anti-TBC1D14 antibody using HRP-labelled secondary antibodies and 5% milk to block because the TBC1D14 antibody does not work with the LI-COR system.

Knock down of TBC1D14 leads to a significant increase in autophagosome formation in starved conditions with or without leupeptin but has no effect on basal autophagy in fed cells (Fig. 4-6). This suggests that TBC1D14 controls autophagosome formation induced by starvation but not in basal homeostatic autophagy. Consistent with this notion, over-expressed TBC1D14 does not inhibit basal autophagosome formation (Fig. 4-4). Alternatively, autolysosome formation could be inhibited leading to a block in LC3 turnover but this is highly unlikely since I have shown above that TBC1D14 over-expression affects autophagosome formation and not maturation.

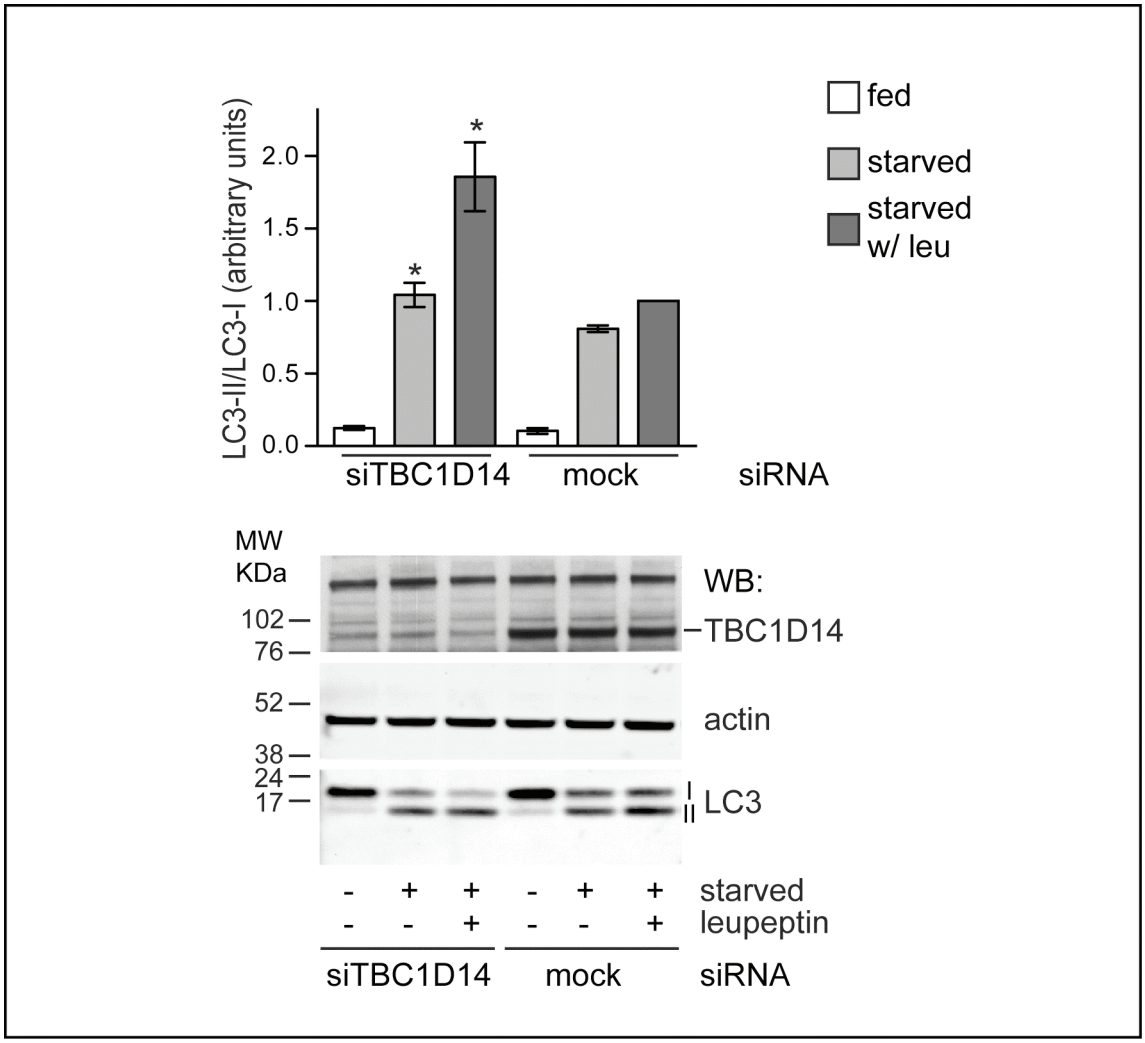

Figure 4-6 siRNA mediated knock down of TBC1D14 leads to increased autophagosome formation upon starvation

HEK293A cells were transfected with a single duplex targeting TBC1D14 or mock transfected, left in fill medium, starved in EBSS with or without leupeptin (leu) for 2h and harvested. Endogenous LC3 conversion was measured by western blot. The graph shows the mean of 5 independent experiments (n=5). A representative blot is shown. Asterisks indicate results of paired Student's t-test, starved p=0.0323; starved with leupeptin p=0.0224. Error bars indicate standard error of the mean (SEM).

4.4 Endogenous TBC1D14 localises to the Golgi and endosomes

Using the STO291 antibody against TBC1D14 I investigated the intracellular localisation of endogenous TBC1D14. I stained HEK293A cells using a standard PFA-fixation based protocol and observed TBC1D14 in a juxta-nuclear position, a punctate pool, and in the nucleus. To further characterise the juxta-nuclear pool of TBC1D14 I then labelled the cells with antibodies recognising a marker of the cis and medial Golgi cisternae anti-GM130 and a marker of the trans-Golgi network (TGN) anti-TGN46. Indeed, TBC1D14 shows good co-localisation with the Golgi and TGN and this pool seems to increase upon nutrient starvation suggesting that TBC1D14 cycles between the Golgi/TGN and a peripheral pool and re-distributes to the Golgi/TGN upon starvation (Fig. 4-7).

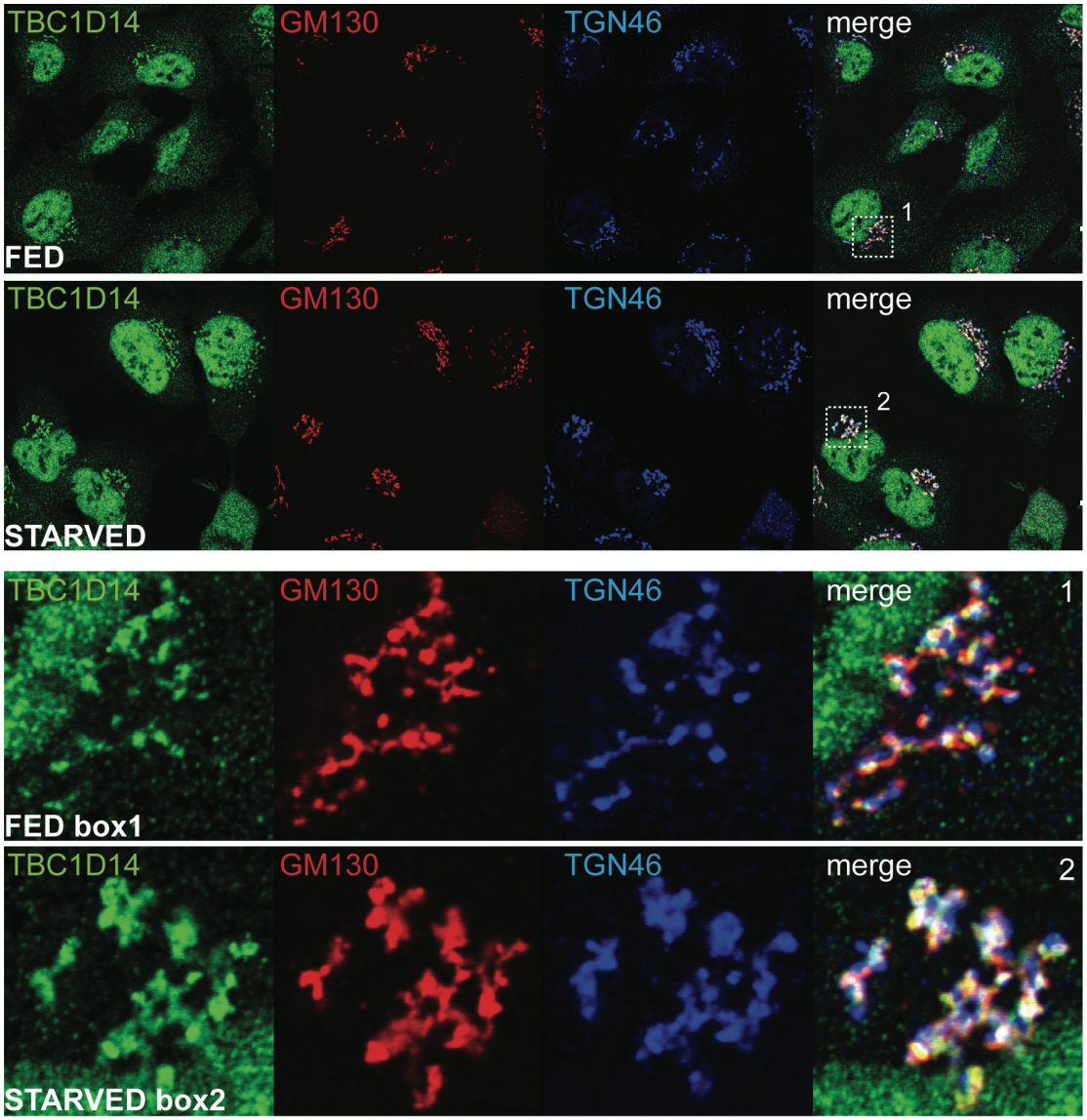

Figure 4-7 Endogenous TBC1D14 localises to the Golgi and TGN, a peripheral punctate pool and the nucleus

HEK293A cells were starved for 2h in EBSS or not, labelled with antibodies against TBC1D14 (green), GM130 (red) and TGN46 (blue) and, imaged using confocal microscopy. Note that the Golgi/TGN pool, and the extent of co-localisation with TGN46 and GM130 increase upon starvation. Merged box 1 (fed) and box 2 (starved) are shown below.

To make sure that this antibody is specific in immunofluorescence, HEK293A cells were knocked down with siRNA against TBC1D14 or not and labelled with STO291. The Golgi/TGN fraction and part of the peripheral pool of TBC1D14 were strongly

depleted in the knocked down cells (Fig. 4-8b). The nuclear staining was not reduced upon TBC1D14 knock down suggesting that this signal is unspecific. Some of the peripheral staining may be unspecific as well as it didn't disappear completely. Alternatively, the depletion of TBC1D14 may not be 100% although it does seem efficient as assessed by western blot analysis using post-nuclear supernatant of cells from the same knock-down experiment (Fig. 4-8d).

In addition to TBC1D14 cells were labelled with anti-mAtg9 to investigate the possibility that TBC1D14 regulates mAtg9 trafficking. mAtg9 is a transmembrane protein that cycles between the TGN and endosomes re-distributing to the endosomal pool upon starvation [41]. This movement is dependent on the presence of ULK1 since knock down of ULK1 leads to an increase of mAtg9 in the TGN even in starved cells. However, mAtg9 traffic is not affected by TBC1D14 knock down (Fig. 4-8b). mAtg9 disperses normally in cells lacking TBC1D14 and is found on the TGN in fed cells consistent with the observation that TBC1D14 depletion does not induce basal autophagy (Fig. 4-6). While knock-down of ULK1 leads to concentration of mAtg9 on the TGN it does not alter TBC1D14 trafficking as it appears to be more concentrated in the TGN area after starvation similarly to cells that were not depleted of ULK1 (Fig. 4-8c).

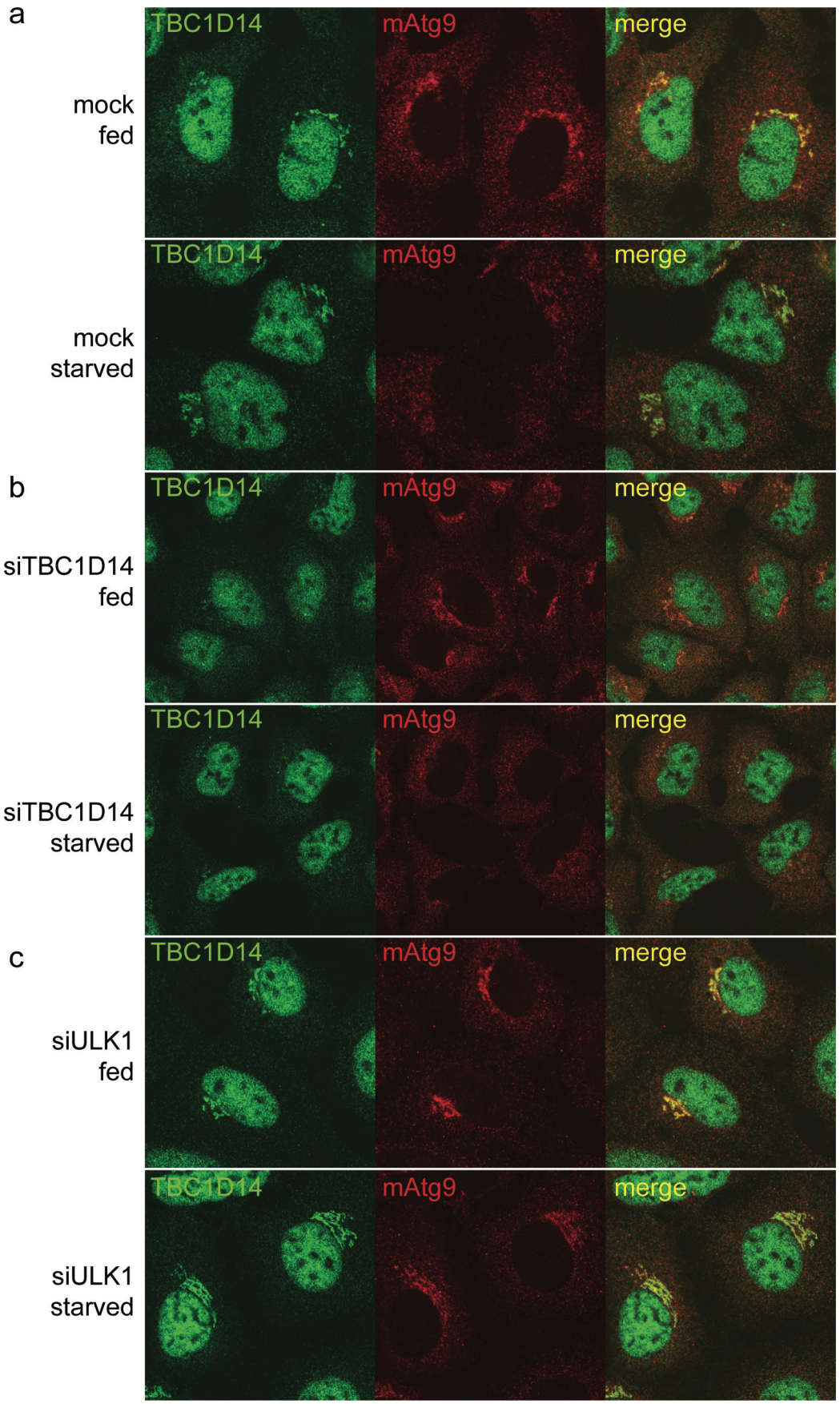
a
mock
fed
TBC1D14
mAtg9
merge
mock
starved
TBC1D14
mAtg9
merge
b
siTBC1D14
fed
TBC1D14
mAtg9
merge
siTBC1D14
starved
TBC1D14
mAtg9
merge
c
siULK1
fed
TBC1D14
mAtg9
merge
siULK1
starved
TBC1D14
mAtg9
merge

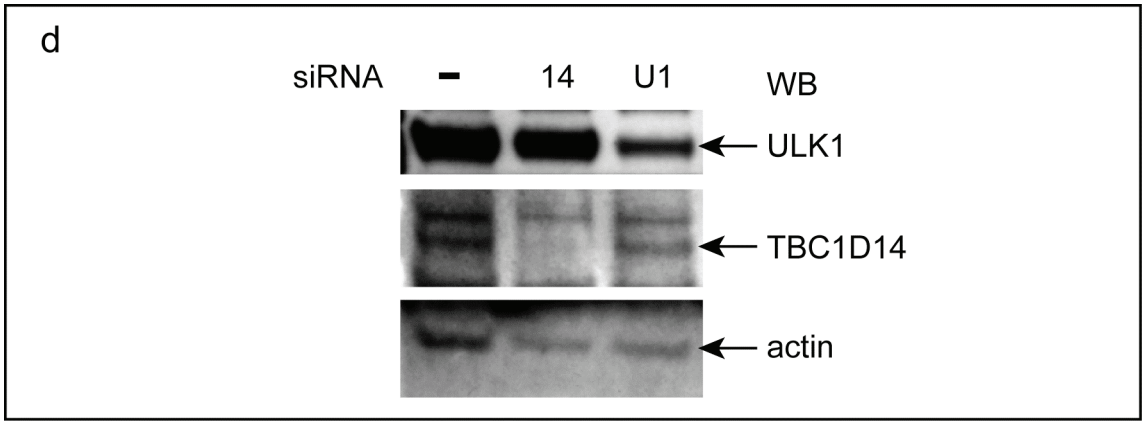

Figure 4-8 siRNA mediated knock down of TBC1D14 does not alter mAtg9 trafficking

HEK293A cells were transfected for 72h with **(a)** mock transfected using Oligofectamine without RNA, or single siRNA duplexes against **(b)** TBC1D14 (50nm), or **(c)** ULK1 (50nm). Cells were incubated in full medium, or for 2 h with EBSS, and labelled with antibodies against endogenous TBC1D14 (green) and mAtg9 (red) followed by specific fluorescently tagged secondary antibodies. **(d)** In parallel, cells were harvested for western blot analysis to confirm the knock down efficiency. Post-nuclear supernatants were run on SDS-PAGE and membranes were labelled with anti-ULK1, anti-TBC1D14, and anti-actin. – indicates mock transfected, 14 indicates siTBC1D14, U1 indicates siULK1. Note: the nuclear staining of TBC1D14 is non-specific as siRNA mediated knockdown of TBC1D14 did not decrease it. ULK1 knockdown prevents the starvation-induced dispersal of mAtg9 away from the TGN (lower panel in (c)) whereas knockdown of TBC1D14 does not.

4.5 TBC1D14 binds ULK1 via its TBC domain

TBC1D14 interacts with ULK1 in a yeast-2-hybrid assay and co-localises with it when over-expressed in HEK293A cells. Since both anti-ULK1 and anti-TBC1D14 antibodies were raised in rabbit it was not possible to look at whether the endogenous proteins co-localise. However, I wanted to confirm the interaction of ULK1 with TBC1D14 by co-immunoprecipitation. Therefore, HEK293A cells were transfected with human HA-ULK1 and GFP-TBC1D14 as well as truncation mutants of TBC1D14 containing the TBC domain only (GFP-TBC1D14-TBC) or the N-terminal domain alone (GFP-

TBC1D14-N) to determine where ULK1 binds. Unfortunately, neither the ULK1 nor TBC1D14 antibodies efficiently immuno-precipitate the endogenous proteins so I used anti-HA to pull down over-expressed HA-ULK1 and test whether GFP-TBC1D14 co-immunoprecipitates with it. Anti-FLAG was used as a negative control. Co-immunoprecipitation was carried out over night at 4ºC with antibodies bound to protein G-sepharose beads and post-nuclear whole cell lysates. GFP-TBC1D14 co-immunoprecipitates with ULK1 via its TBC domain but not its N-terminal domain (Fig. 4-9). To test the possibility that this interaction is regulated by starvation, and therefore the activation status of ULK1 (see Introduction and [83]), the cells were starved for 2h in EBSS before lysis. However, the interaction efficiency is the same in fed and starved cells suggesting that TBC1D14 binds ULK1 constitutively (Fig. 4-9a).

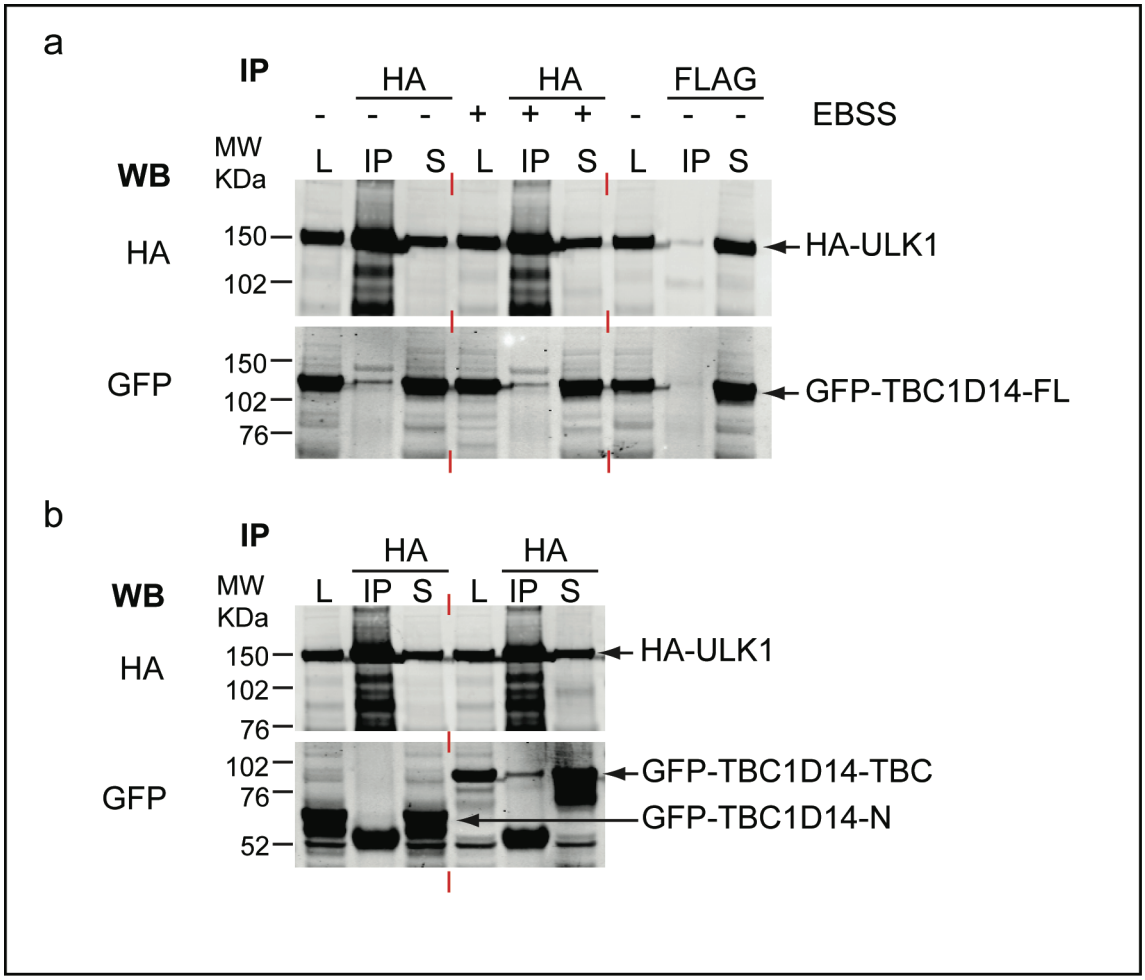

Figure 4-9 TBC1D14 binds ULK1 via its TBC domain
(a, b) HEK293A cells were transfected with HA-ULK1 and the indicated GFP-TBC1D14 construct. Proteins were allowed to express for 24h and cells were starved in EBSS for 2h or not. Cell lysates were then immunoprecipitated with anti-HA or anti-FLAG antibodies. L=3% lysate; IP=immunoprecipitated pellet; S=3% supernatant, unbound fraction. Membranes were labelled with antibodies against HA and GFP using the LI-COR system. **(a)** Full length GFP-TBC1D14 co-immunoprecipitates with ULK1 in both fed and starved conditions and there is no difference in binding efficiency. No HA- or GFP-tagged protein was co-immunoprecipitated when an irrelevant antibody, anti-FLAG, was used. **(b)** The C-terminal TBC domain (amino acids 224-669) but not the N-terminus (amino acids 1-223) of TBC1D14 binds to ULK1.

To assess the localisation of the fragments of GFP-TBC1D14 they were transfected into HEK293A cells and processed for confocal microscopy. As expected, full length GFP-TBC1D14 forms tubules like the myc-TBC1D14 does and recruits ULK1. The N-

terminal domain of TBC1D14 is diffusely cytosolic whereas the C-terminal TBC domain forms tubules (Fig. 4-10). However, the tubules formed by the TBC domain alone are mostly concentrated in the juxta-nuclear position suggesting that there is a signal in the N-terminus, or the last 24 amino acids of TBC1D14 that leads to transport of the protein away from the microtubule organising centre (MTOC), or prevents and regulates retrograde transport. As expected from my co-immunoprecipitation experiments the over-expressed TBC domain also recruits ULK1.

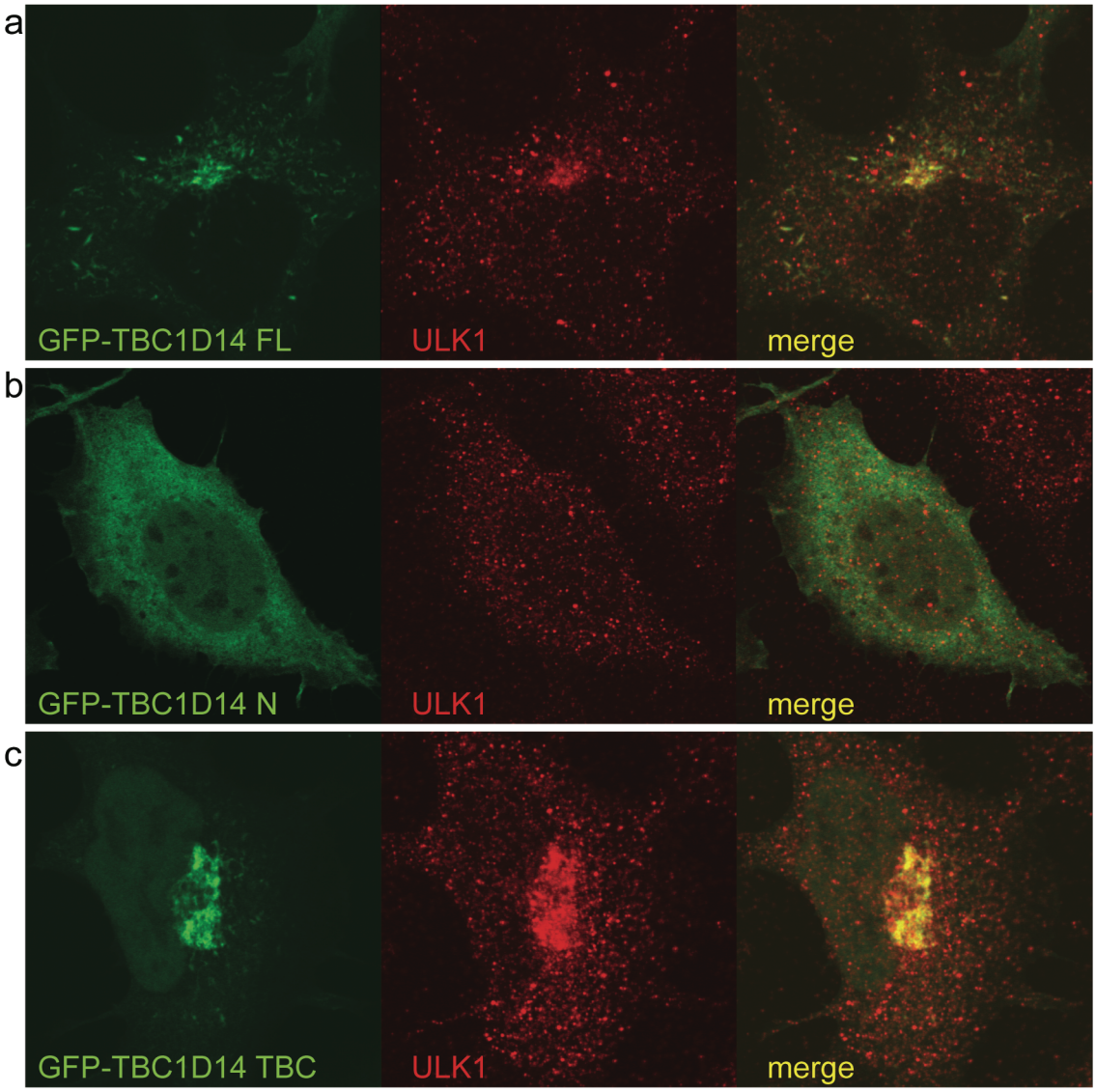

Figure 4-10 Subcellular distribution of TBC1D14 truncation mutants

HEK293A cells were transfected with **(a)** full length GFP-TBC1D14, **(b)** GFP-TBC1D14-N, which comprises the N-terminus from amino acids 1-223, or **(c)** GFP-TBC1D14-TBC, which comprises the C-terminal TBC domain from amino acids 224-669. Cells were then starved for 2h in EBSS and stained with anti-ULK1 (red).

Preliminary data suggests that over-expression of either truncation mutant alone does not inhibit autophagosome formation (Fig. 4-11). HEK293A cells were transfected with the truncation mutants and full length GFP-TBC1D14 to assess their effect on LC3 lipidation via western blot. As expected the full length GFP-TBC1D14 like myc-TBC1D14 inhibits autophagosome formation. The two truncation mutants GFP-TBC1D14-N and GFP-TBC1D14-TBC, however, do not. Although, this experiment would have to be repeated it seems that the TBC domain alone is not sufficient to inhibit autophagy but requires some signal or function of the N-terminus or very C-terminal amino acids.

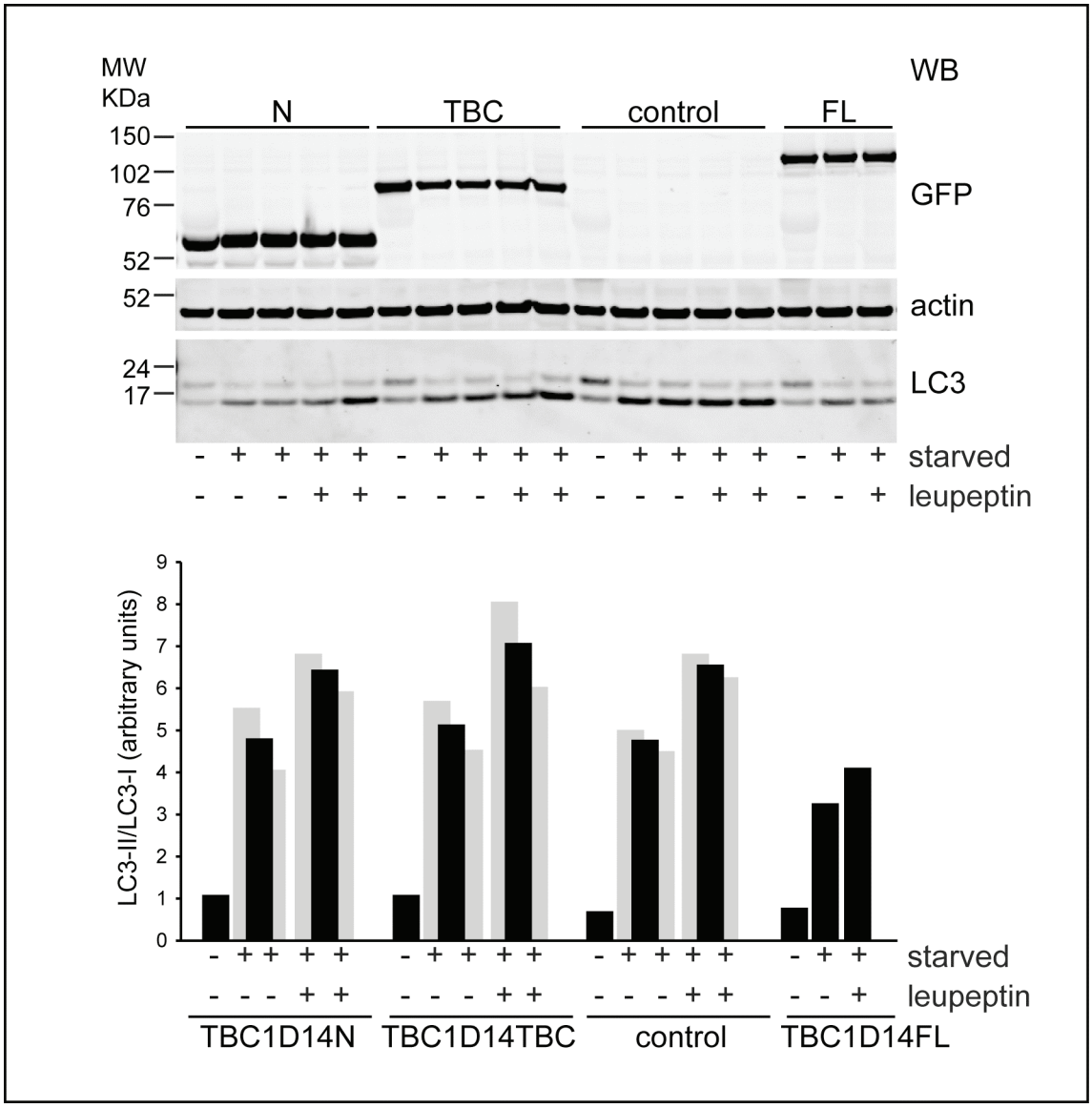

Figure 4-11 Over-expression of the TBC domain of TBC1D14 does not inhibit LC3 lipidation

HEK293A cells were transfected with full length GFP-TBC1D14 (TBC1D14FL), GFP-TBC1D14-N comprising the N-terminus of TBC1D14 (amino acids 1-223), or GFP-TBC1D14-TBC containing only the TBC domain (amino acids 224-669). Cells were left in DMEM (single well), starved (duplicate wells), or starved with leupeptin (duplicate wells) for 2h. Single wells were used for the full length protein. Membranes were revealed with anti-GFP, anti-actin and anti-LC3 using the LI-COR system. N=GFP-TBC1D14-N, TBC=GFP-TBC1D14-TBC, control=renilla vector control, FL=GFP-TBC1D14. Quantification done with Metamorph software is shown in the lower panel. Grey bars indicate values for each replicate, black bars indicate average of duplicates or single replicate.

4.6 *In vitro* GAP activity assay for TBC1D14

The target Rab for TBC1D14 has not been identified. Therefore, I wanted to do an *in vitro* GAP assay using purified recombinant TBC1D14 protein to identify the target Rab. TBC1D14 was cloned into pBacPAKGST vector and N-terminally tagged GST-TBC1D14 was purified by the protein purification facility at the London Research Institute (LRI) from insect cell lysates over-expressing it. The GST was cleaved off to elute untagged TBC1D14 using 3C-protease taking advantage of a 3C cleavage site, which is located C-terminally to the GST-protein in the vector. Insect cells were used for expression of GST-TBC1D14 because the protein cannot be expressed in bacteria (personal communication F. Barr; University of Liverpool, UK).

Recombinant purified Rab GTPases were provided by Prof. F. Barr (University of Liverpool, UK), and loaded with a mixture of [γ^{32}P]GTP and cold GTP. I tested a library of 48 Rab GTPases incubated with or without (buffer alone) TBC1D14 protein for 1 hour at 30ºC to allow GTP hydrolysis. The specific activity of each reaction was calculated as described in Materials and Methods and proteins were pelleted using activated charcoal slurry and ^{32}P released into the supernatant buffer through GTP hydrolysis was measured. GAP activity was calculated by dividing the amount of GTP hydrolysed by the specific activity (see Materials and Methods for a detailed description of the calculations). As a positive control TBC1D20 was used, which is known to act on Rab1b and an increase in ^{32}P counts in the supernatant can be seen [200] (Fig. 4-12). Unlike the other Rabs, Rab21 has very high intrinsic GTPase activity. TBC1D14 did not activate any of the Rab GTPases. This could be due to protein concentration being

too low, because the protein lost its GAP activity during purification, or due to TBC1D14 not having GAP activity at all. The assay was repeated by Dr. Shin-ichiro Yoshimura (University of Liverpool, UK) in a different buffer, with higher protein concentration using GST-TBC1D14 rather than untagged protein but still no GTPase activation by TBC1D14 was seen.

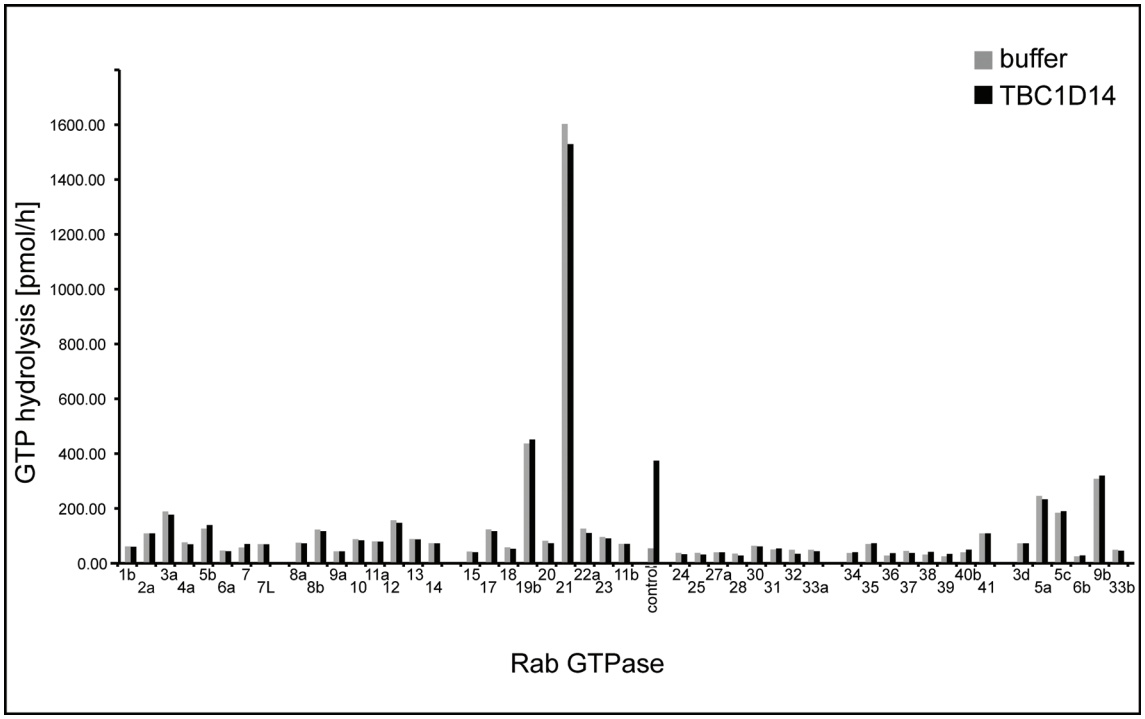

Figure 4-12 *In vitro* GAP activity assay with TBC1D14 against the Rabome
Recombinant TBC1D14 protein was purified from Sf9 and High5 insect cells (pooled) by the LRI protein purification service. 5µg of each Rab GTPase was loaded with [γ^{32}P]GTP and cold GTP (1:5). 200ng of TBC1D14 (black bars), or empty buffer (grey bars) was added to each Rab followed by 1h incubation at 30ºC. 2.5µl of each GAP reaction was counted to allow calculation of the specific activity of each reaction. 5µl of each GAP reaction was added to 800µl activated charcoal slurry, spun down and 400µl of the supernatant buffer containing released free ^{32}P, as a result of GTP hydrolysis, was counted. GAP activity was calculated by dividing the amount of GTP hydrolysed by the specific activity [251]. Control is TBC1D20 incubated with Rab1b, which is known to be its target [200]. All reactions were done in duplicate and shown is the average of the two.

4.7 Yeast-2-hybrid screen to identify Rab binding partners of TBC1D14

In another approach to identify the Rab GTPase target of TBC1D14, a yeast-2-hybrid screen was done by Dr. Shin-ichiro Yoshimura (a collaborator at the University of Liverpool, UK). The screen was done in the same way as described in Figures 3-6 and 3-8 using TBC1D14R472A as bait against a library of Rab GTPases. The RA mutant was used because the interaction between RabGAP and Rab is thought to be stabilised by removal of the arginine finger [204]. TBC1D14 binds specifically to Rab11a and Rab11b but no other Rabs tested (Fig. 4-13). It is particularly significant that Rab25, which is closely related to Rab11 and is sometimes called Rab11c, did not bind TBC1D14.

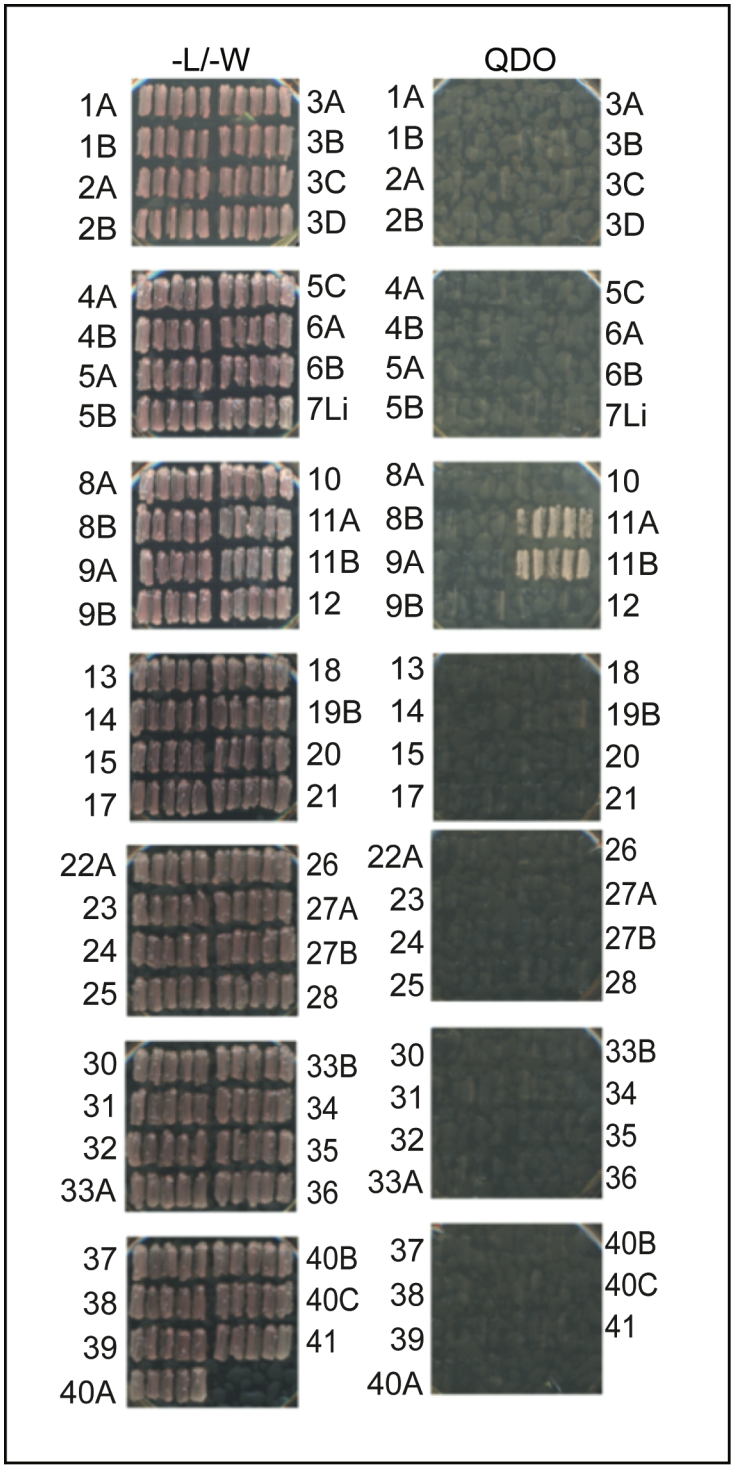

Figure 4-13 TBC1D14 binds to Rab11a and 11b

(a) A yeast-two-hybrid screen to identify Rab binding partners of TBC1D14 was done by Shin-ichiro Yoshimura (University of Liverpool, UK). Cells were transfected with the indicated active (QA) Rab constructs (prey) and TBC1D14R472A (bait) and selected for double transfected cells on plates lacking leucine and tryptophan (-L/-W left). Each box shows five colonies streaked on both selective media.

Binding of the TBC1D14 to the Rab allows growth on quadruple drop out medium (QDO) lacking leucine, tryptophan, histidine and adenine (right panel).

4.8 TBC1D14 co-localises with Rab11 in HEK293A cells

To confirm the finding that TBC1D14 binds Rab11a and Rab11b (now called Rab11 when both isoforms are meant) I looked at the endogenous proteins by indirect immunofluorescence in HEK293A cells. To that end, cells were stained with anti-TBC1D14, and anti-Rab11 antibodies. Rab11 is found on recycling endosomes, the pericentriolar endocytic recycling compartment (ERC) and the TGN [271, 272]. I found some overlap of TBC1D14 with Rab11 in the MTOC region and also on peripheral recycling endosomes (Fig. 4-14). Note, not all recycling endosomes are TBC1D14 positive and the co-localisation is often partial but this may be expected since a GAP only acts at a specific step during vesicle traffic, and endosomes are mosaic structures containing various subdomains [193].

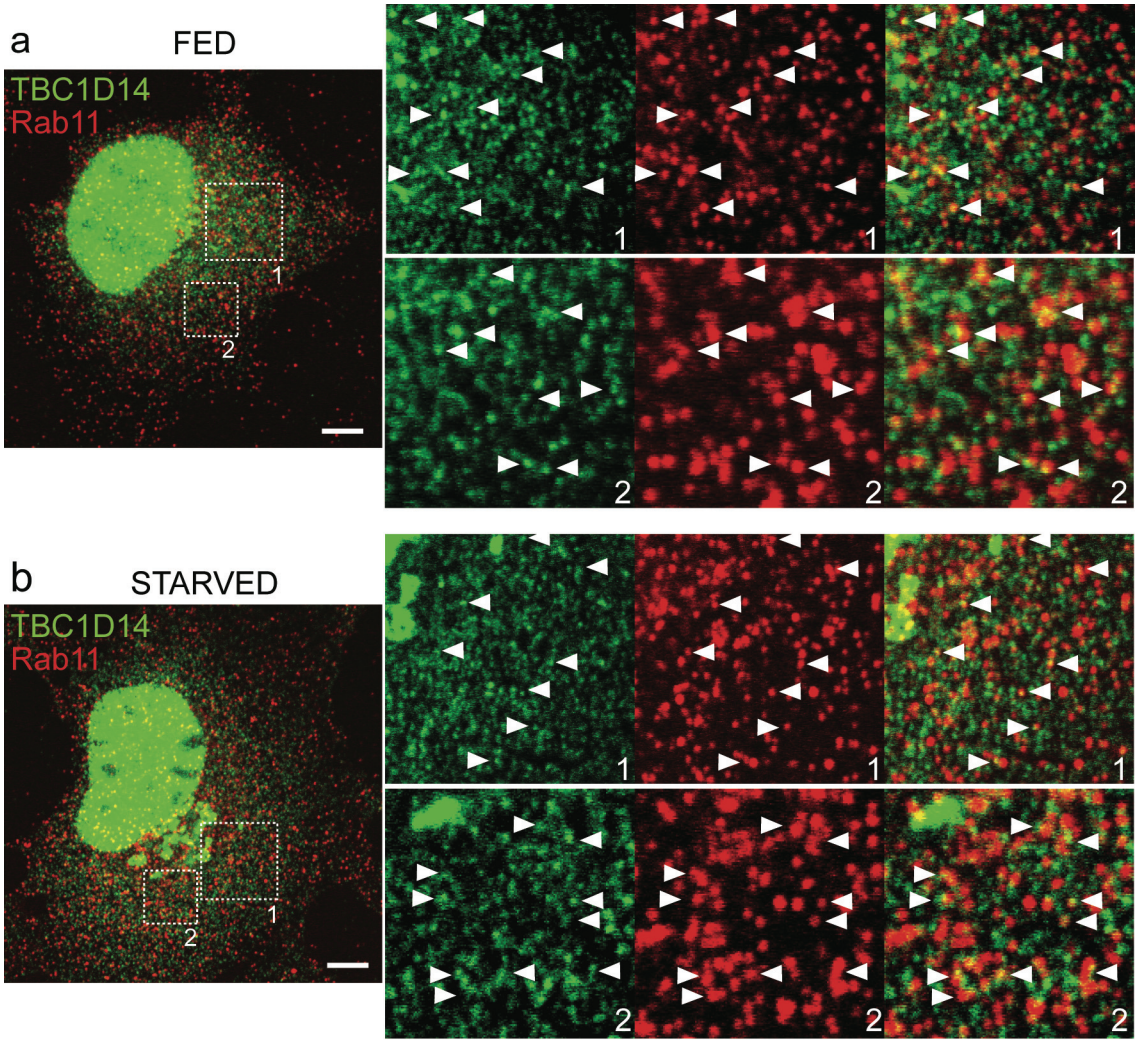

Figure 4-14 TBC1D14 co-localises with Rab11 in HEK293A cells
HEK293A cells were labelled with anti-TBC1D14 (green) and anti-Rab11 (red) antibodies and were **(a)** left in DMEM for 2h (fed), or **(b)** starved for 2h in EBSS. Panels on the right show enlarged boxes indicated. Arrowheads point to Rab11-positive recycling endosomes that contain TBC1D14.

This commercial Rab11 antibody probably recognises both isoforms of Rab11 as they are very similar and only differ in 19 amino acids in the C-terminus, although the immunogen used by the manufacturer contains some of the divergent amino acids. Unfortunately, it is not specified which isoform was used as a template to synthesise the antigenic peptide. Both isoforms are expressed in HEK293A cells as shown by western blot analysis with two different isoform specific antibodies (Fig. 4-15). However, the

isoform specific antibodies used for immuno-blotting only work for immunofluorescence analysis after permeabilisation of cells with saponin. As this leads to loss of TBC1D14 staining because its membrane association is not strong enough (data not shown) I could not do co-localisation experiments using these isoform specific antibodies.

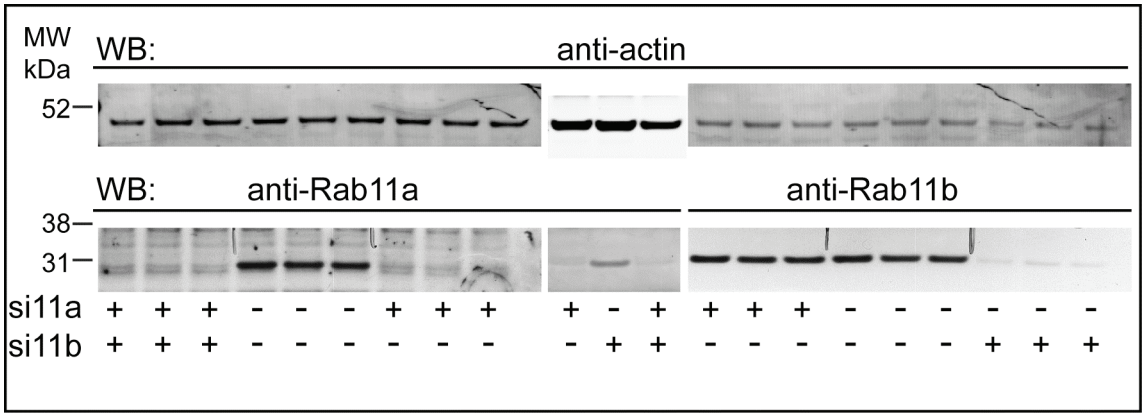

Figure 4-15 HEK293A cells express both Rab11 isoforms
HEK293A cells were transfected with no siRNA, siRNA against Rab11a (25nM), Rab11b (25nM), or both (25nM each) twice and after 72h harvested for western blot analysis. Membranes were labelled with antibodies specific against Rab11a or Rab11b and actin. si11a=siRab11a, si11b=siRab11b, WB=western blot.

4.9 Conclusion

I have confirmed that TBC1D14 is a general inhibitor of autophagosome formation and its effect is not limited to an inhibition of LC3 lipidation. Using an antibody against TBC1D14 I found that it localises to the Golgi/TGN and recycling endosomes. TBC1D14 binds both Rab11 isoforms but no other Rab GTPases in yeast-2-hybrid experiments and co-localises with Rab11 in HEK293A cells. Mutation of the two

catalytic residues arginine 472 and glutamine 508 rescues inhibition of autophagy most likely by abolishing GAP activity.

Chapter 5. TBC1D14 regulates autophagosome formation via ULK1 and Rab11-positive recycling endosomes

5.1 Aim

TBC1D14 binds Rab11, which is involved in endocytic recycling of proteins such as the Transferrin receptor (TfnR) back to the plasma membrane via the endocytic recycling compartment (ERC). Recycling endosomes (REs) have never been implicated in autophagy. However, TBC1D14 co-localises with Rab11 on REs and negatively regulates autophagy. Therefore, I investigated the role of REs and Rab11 in autophagosome formation and how TBC1D14 regulates this process.

5.2 TBC1D14 tubulates recycling endosomes

Since endogenous TBC1D14 is localised to Rab11-positive REs I hypothesised that the tubules induced by TBC1D14 over-expression are tubulated REs. To test this, HEK293A cells were transfected with myc-TBC1D14 and stained with anti-TBC1D14 and anti-Rab11 or anti-TfnR, which is a cargo of REs (Fig. 5-1). Transfected cells can easily be recognised by the appearance of tubules throughout the cells. These tubules contain the TfnR and are Rab11 positive confirming that they are REs. Interestingly, the TfnR completely disperses in untransfected starved cells (Fig. 5-1b) whereas Rab11 does not. Endogenous TBC1D14 shows little overlap with the pericentriolar ERC

because it is mostly localised to the Golgi and TGN. It remains unclear why the over-expressed protein preferentially localises to REs and the ERC and tubulates those two but not the Golgi or TGN.

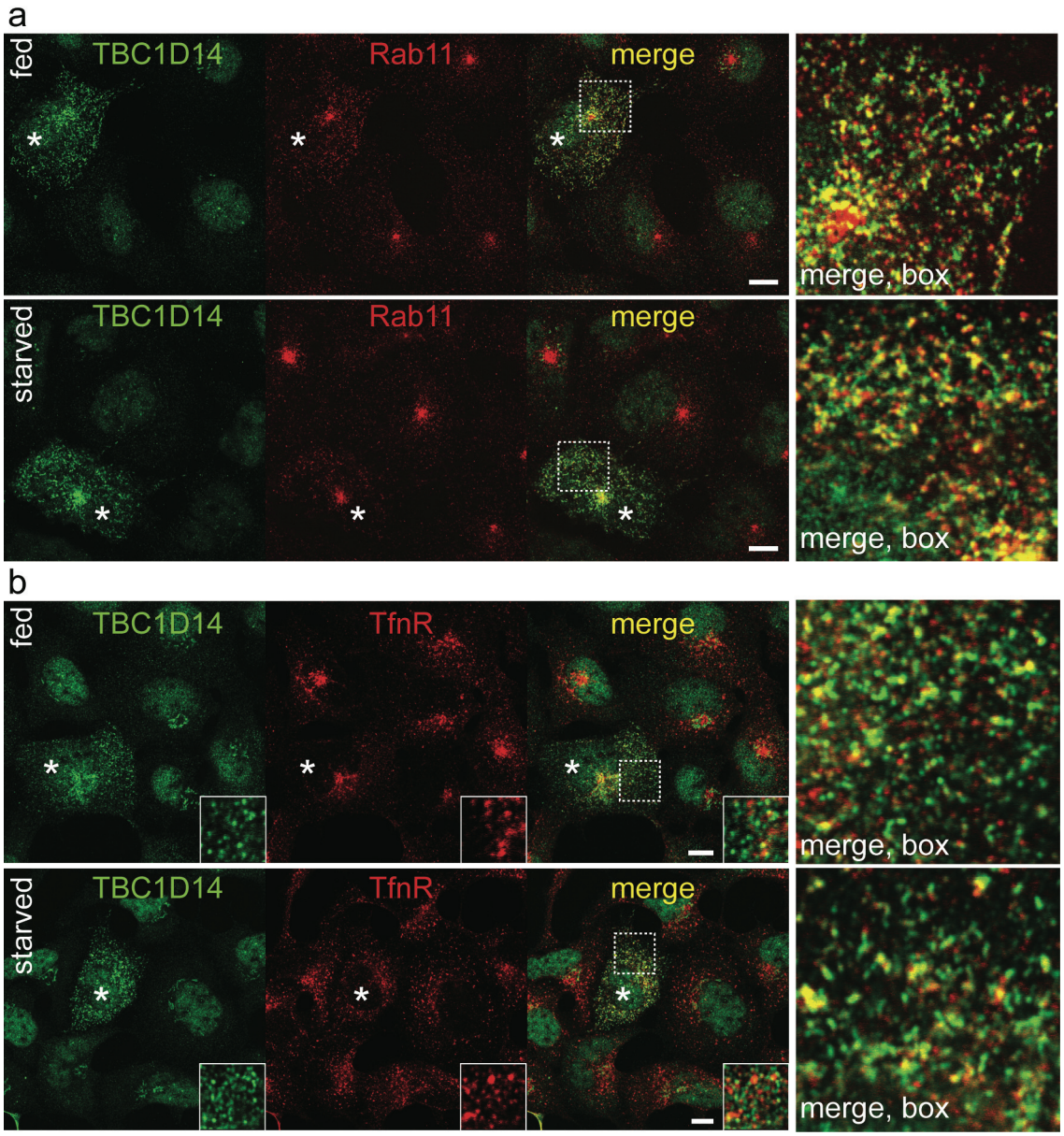

Figure 5-1 TBC1D14 over-expression tubulates recycling endosomes
(a) HEK293 cells were transfected with myc-TBC1D14 and 24h later starved in EBSS or not, and labelled with antibodies against TBC1D14 (green) and Rab11 (red). **(b)** Same as in (a) but cells were labelled with anti-Transferrin receptor (TfnR) antibody. Small boxes on panel show enlarged TfnR-

positive endosomes with endogenous TBC1D14 from untransfected cells. Asterisks indicate transfected cells. Boxes on transfected cells in merged panels are enlarged on the right. Scale bars are equal to 10μm.

I hypothesised that inactivation of Rab11 by TBC1D14 leads to tubulation of REs and the ERC either causing a defect in budding of vesicles, enhanced homotypic fusion between them or leading to a defect in vesicle transport. Furthermore, TBC1D14 may be recruited to REs by Rab11 as it does not seem to have any membrane association domains. To test this I transfected cells with siRNAs against Rab11a and Rab11b prior to transfection with GFP-TBC1D14. Indeed, knock down of Rab11 prevents TBC1D14 from tubulating endosomes and leads to a cytosolic localisation of the over-expressed protein (Fig. 5-2a) strongly supporting the hypothesis that TBC1D14 is a Rab11-GAP. Over-expression of the TBC1D14RA/QA double mutant still leads to RE tubulation, as TBC1D14RA/QA is probably still able to bind Rab11, perhaps even more strongly [204]. Even though TBC1D14RA/QA may not inactivate Rab11, it may prevent binding of Rab11 effectors. Also, it is likely that Rab11 is part of a Rab cascade similar to the Rab5-Rab7 cascade in early to late endosome maturation [205, 206] and that failure to inactivate Rab11 stops this cascade still leading to endosome tubulation.

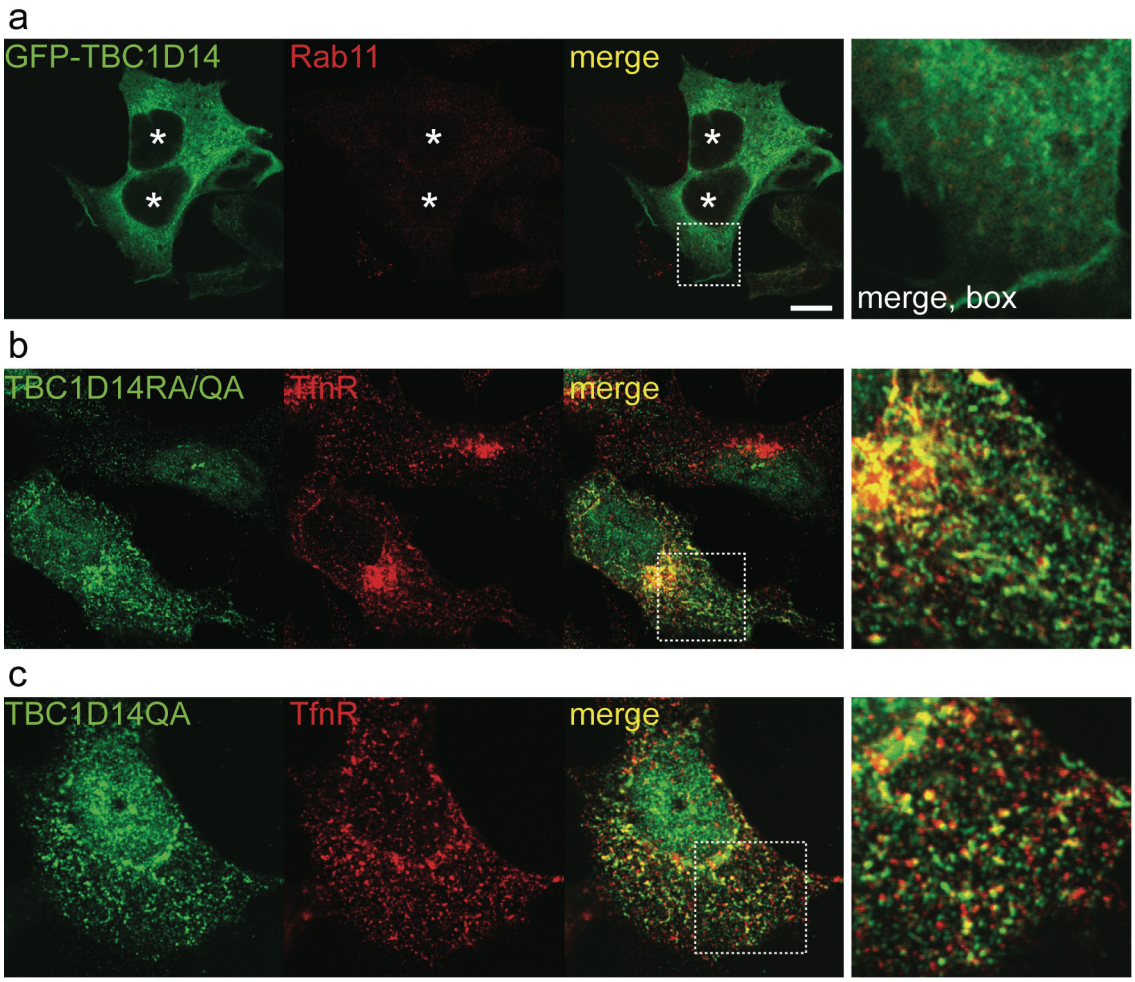

Figure 5-2 Depletion of Rab11 prior to TBC1D14 expression prevents tubulation of REs

(a) Cells were transfected with siRNA duplexes against Rab11a and Rab11b (25nm each) on day 1 and 2 and subsequently transfected with GFP-TBC1D14 on day 3. On day 4 (72h knock down, 24h expression) cells were labelled with anti-TBC1D14 and anti-Rab11 antibodies. Scale bar is equal to 10µm. **(b,c)** HEK293A cells were transfected with **(b)** myc-TBC1D14R472A/Q508A or **(c)** myc-TBC1D14QA and labelled with anti-TBC1D14 and anti-TfnR antibodies.

Lastly, if Rab11 inactivation is the cause of tubulation of REs by TBC1D14 then loss of Rab11 should have the same phenotype. Indeed knock down of Rab11 in HEK293A cells revealed that REs are more tubulated in the absence of Rab11 although the tubules are not as extreme as in the case of TBC1D14 over-expression (Fig. 5-3). Furthermore, the endosomal pool of TBC1D14 is greatly diminished and probably reduced to

background staining in the Rab11 depleted cells suggesting that RE association of TBC1D14 is dependent on binding to Rab11. The Golgi pool of TBC1D14 on the other hand remains the same in knocked down compared to control cells.

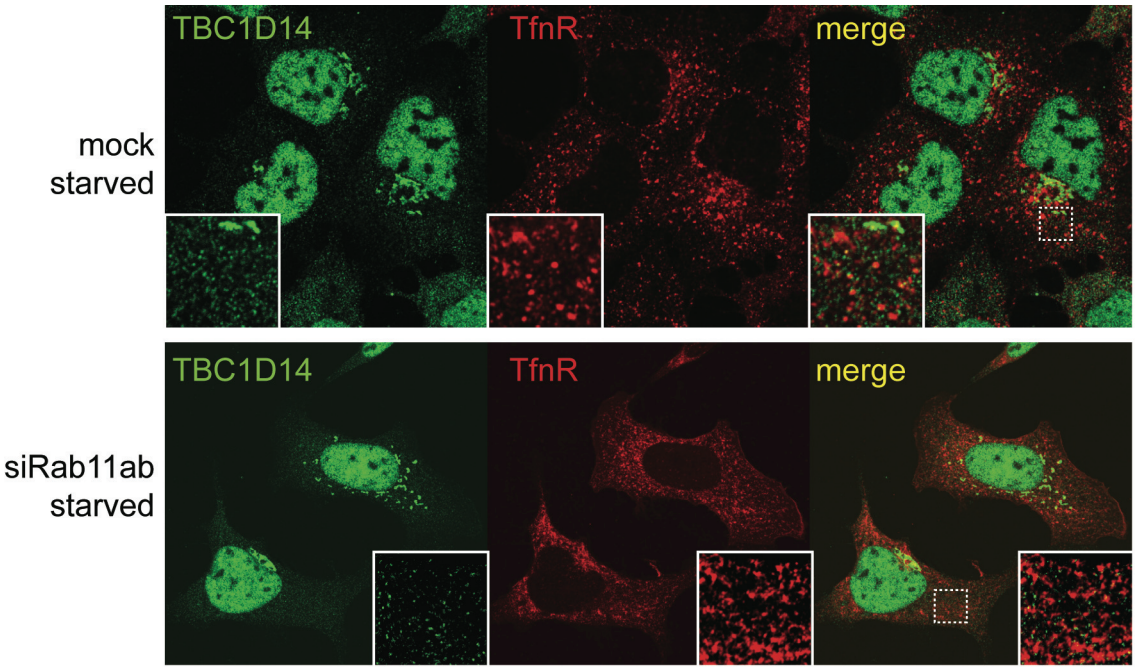

Figure 5-3 siRNA mediated knock down of Rab11 tubulates TfnR-positive REs
HEK293 cells were transfected with single siRNA duplexes against Rab11a and Rab11b (25nm each) for 72h as described before. Cells were incubated in EBSS for 2 h, and stained with antibodies against endogenous TBC1D14 (green) and TfnR (red). While TfnR-positive endosomes are tubulated in the absence of Rab11, TBC1D14 seems to be present on the Golgi still.

5.3 Transferrin but not epidermal growth factor is delivered to TBC1D14 tubules and Tfn recycling is delayed

To test whether tubulated REs are functional I looked at uptake of the ligand Transferrin (Tfn) and another extracellular cargo, epidermal growth factor (EGF). EGF is taken up by receptor mediated endocytosis and delivered to early endosomes just like Tfn is but

from there the two ligands follow different trafficking routes. Tfn is sorted away to be recycled to the plasma membrane via the ERC while EGF follows the degradative route via MVBs to the lysosome.

Serum starved HEK293A cells transfected with GFP-TBC1D14 were incubated in the presence of fluorescently labelled Tfn and EGF for 30 sec (this being the zero minute timepoint without chase) or 15 min, and then chased in serum free medium without fluorescent ligands for 5min, 45min, or 1h and 45min (Fig. 5-4). After 0min both Tfn and EGF can be seen in small vesicles just below the plasma membrane and some co-localisation is observed, as expected. After a 15min pulse with the ligands, plus a 5min chase, Tfn is found in the ERC and REs as well as TBC1D14 tubules, whereas EGF is in endosomes separate from Tfn. After 45min chase most of the Tfn has been recycled back to the extracellular medium in the untransfected cells whereas it is retained in the GFP-TBC1D14 positive tubular REs. EGF degradation is much slower so that it can still be observed in endosomes after 45min and this is not affected in GFP-TBC1D14 transfected cells. After 1h and 45min of chase all the Tfn is apparently recycled even in the transfected cells whereas some EGF is still located in what are probably late endosomes/MVBs. This finding that Tfn can be delivered to TBC1D14 tubules and is recycled eventually but with much delay supports my hypothesis that TBC1D14 structures are tubulated REs. Also, EGF trafficking in transfected cells is indistinguishable from untransfected cells suggesting that other internalisation routes are not affected by TBC1D14 over-expression and, importantly, that late endosomes and lysosomes are intact.

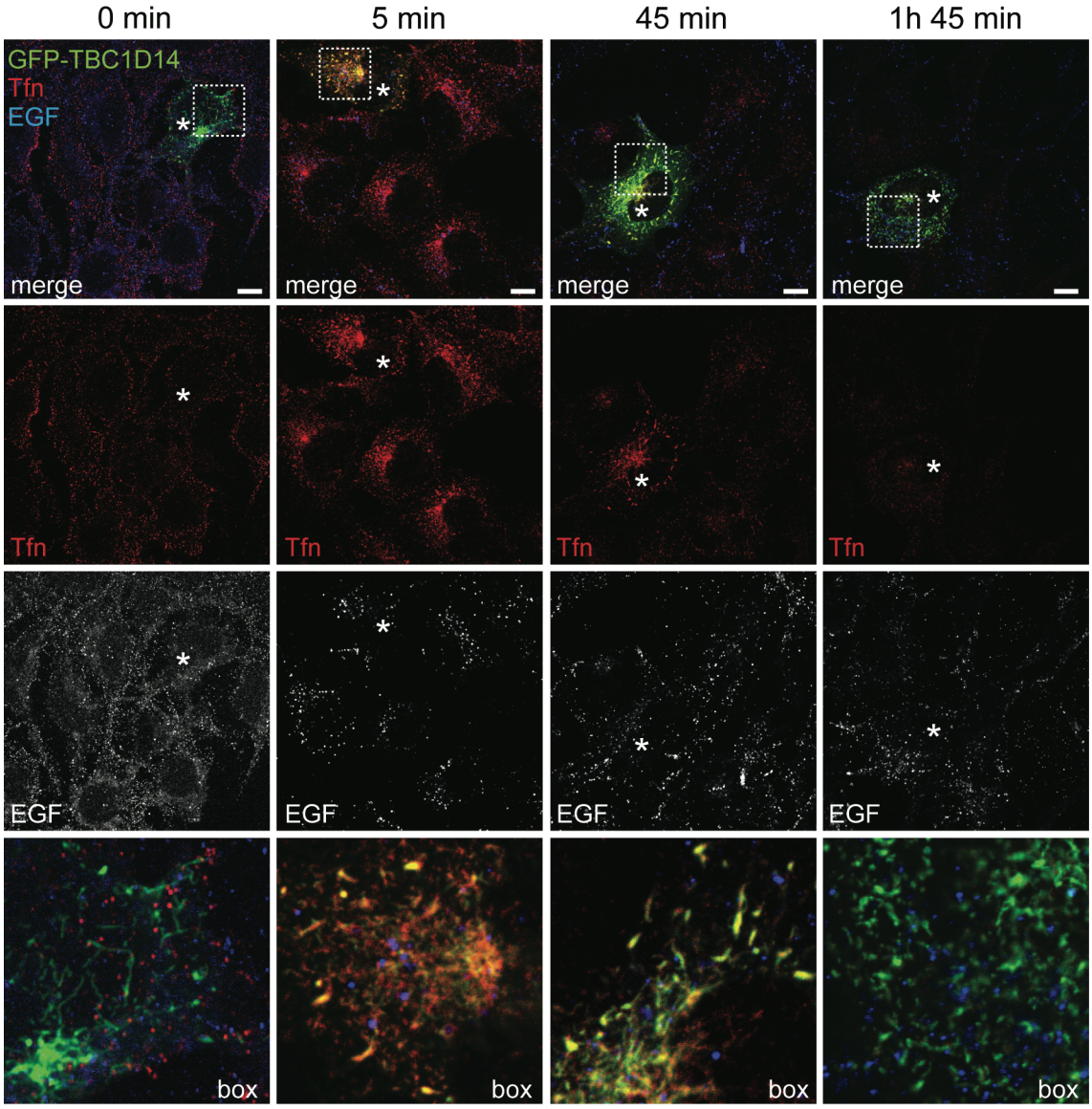

Figure 5-4 Tfn recycling via TBC1D14 tubules is delayed whereas EGF trafficking is unaffected

HEK293A cells were transfected with GFP-TBC1D14 and 24h later allowed to internalise fluorescently labelled Alexa647-Transferrin (Tfn, red) and Alexa555-epidermal growth factor (EGF, blue). Tfn and EGF were applied to the cells for 30 seconds at room temperature, and then cells were fixed (0min). Or cells were allowed to internalise Tfn and EGF for 15 minutes at 37˚C, washed and then chased for 5min, 45min, or 1h 45min in serum free medium at 37˚C. Asterisks indicate transfected cells. Indicated boxes are enlarged in bottom panel. Scale bars are equal to 10µm.

To confirm these results I also performed a biochemical assay following the recycling of radioactively labelled [^{125}I]Tfn in myc-TBC1D14, myc-TBC1D14RA/QA, renilla

vector, and Rab11aN124I transfected cells. Rab11aN124I is a dominant negative mutant of Rab11a, which cannot bind nucleotides and is expected to impair Tfn recycling since another dominant negative mutant Rab11S25N was shown to delay Tfn recycling [272]. All [^{125}I]Tfn handling was done by Dr. Minoo Razi (LRI).

Serum starved transfected HEK293A cells were allowed to internalise [^{125}I]Tfn for 10min at 37ºC followed by two acid washes at 4ºC to remove plasma membrane bound [^{125}I]Tfn. These washes were counted and added to the calculations. Cells were then chased at 37ºC for 20, 50, or 110 minutes in either serum free DMEM, which for this duration does not induce autophagy, or EBSS, which will induce autophagy quickly. The [^{125}I]Tfn released at each time point was counted in the medium and at the end cells were lysed and the total lysate was also counted. The percent recycled [^{125}I]Tfn was determined by dividing the cpm in the medium (adding all counts from previous time points if applicable) by the total cpm (lysate+medium). The amount of internalised versus bound (lysate/lysate+acid washes), which gives an indication of how efficient uptake was for each condition, was found to be approximately 65% for all conditions (data not shown) suggesting that endocytosis and surface receptor availability is not affected in |TBC1D14 transfected cells.

Tfn recycling was delayed in Rab11aN124I expressing cells compared to control cells, as expected, and also in TBC1D14 expressing cells although not as strongly (Fig. 5-5). The mutant TBC1D14RA/QA impaired Tfn recycling as efficiently as the wild type. There may be a slight difference between fed and starved chase conditions but the

experiment would have to be repeated to confirm this. Although the RA/QA mutant protein is expected to have no GAP activity I have shown above that it still tubulates REs and may therefore still cause a delay in Tfn recycling.

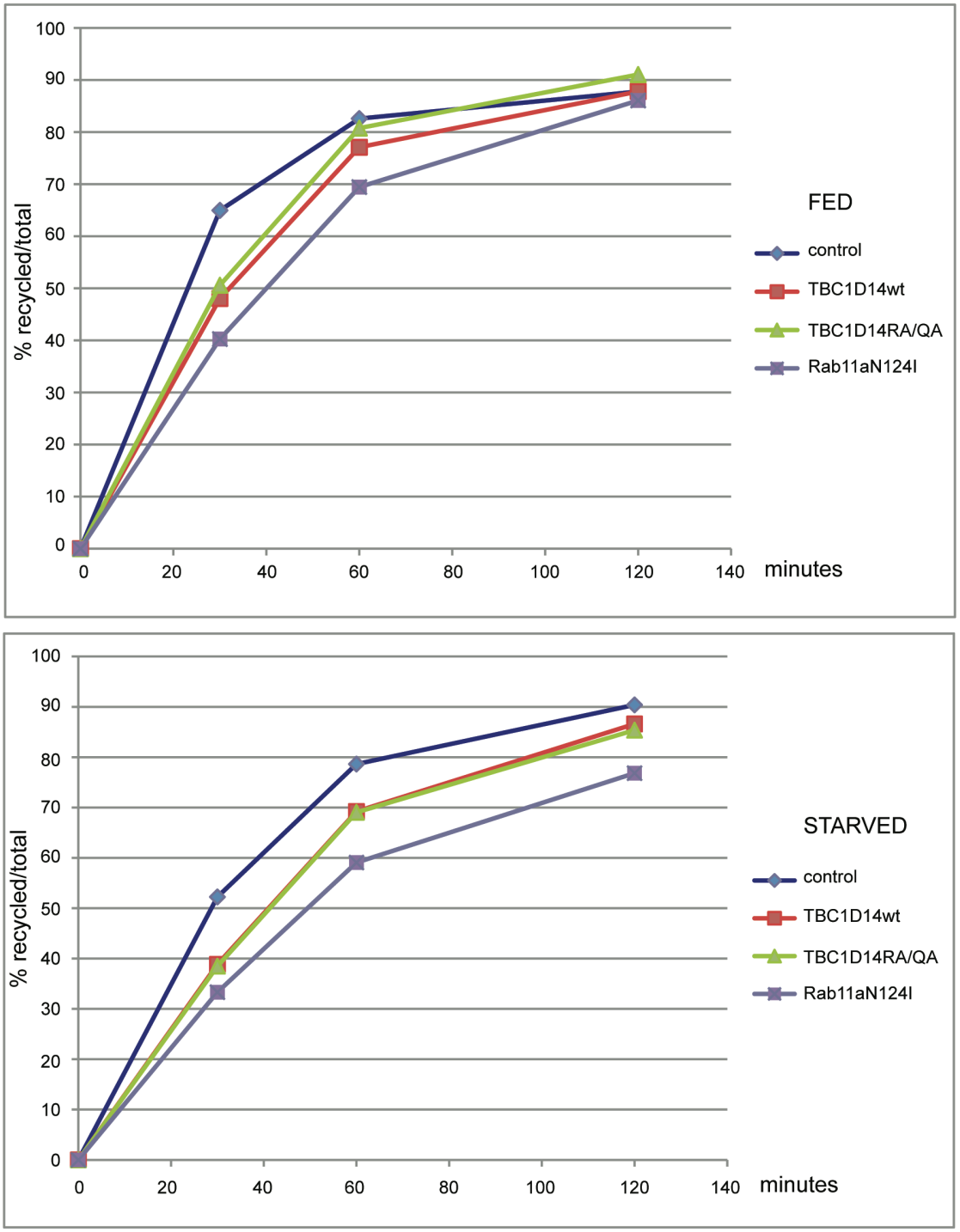

Figure 5-5 Tfn recycling is delayed in TBC1D14 over-expressing cells

HEK293A cells were transfected with renilla vector control, myc-TBC1D14, myc-TBC1D14R472A/Q508A or Rab11aN124I. After 24h expression transfected cells were serum starved for 2h and incubated with [^{125}I]Tfn for 10min at 37ºC to allow uptake. Then, cells were put on ice and acid washed twice with the acid wash measured by gamma counting. Cells were chased in serum free medium (fed; top) or EBSS (starved; bottom) for 20, 50, or 110 min. At each time point the supernatant medium containing recycled [^{125}I]Tfn was removed for gamma counting and the cells were lysed to count intracellular [^{125}I]Tfn. All conditions were done in duplicates and the average was used for calculations. The percentage of recycled [^{125}I]Tfn was calculated by dividing CPM^{medium} + CPM^{medium} of previous time points, if applicable, by $CPM^{medium\ all\ time\ points}$ + $CPM^{cell\ lysate}$. This number was multiplied by 100 to display % values.

To further investigate the nature of the TBC1D14-induced tubules I performed electron microscopy (EM) with the help of Dr. Minoo Razi (LRI). HEK293A cells transfected with either GFP or GFP-TBC1D14 were incubated with HRP-Tfn, gold-labelled anti-EGFR, and human EGF to stimulate uptake of the latter, for 2 hours continuously. This allows internalisation of labelled Tfn and EGFR and achieves a steady state distribution of the two markers. Fixed cells were then prepared for EM and the HRP reaction was done, which will cause HRP-Tfn to appear dark in the EM pictures. We did not observe any tubulation in the GFP transfected cells (not shown) but saw a tubulated endosome containing HRP-Tfn but not gold anti-EGFR in the GFP-TBC1D14 transfected cells (Fig. 5-6). I would hypothesise that this cell is transfected with GFP-TBC1D14 and that the tubule seen corresponds to the tubules seen by confocal microscopy but further experiments, including correlative light and EM, could confirm this.

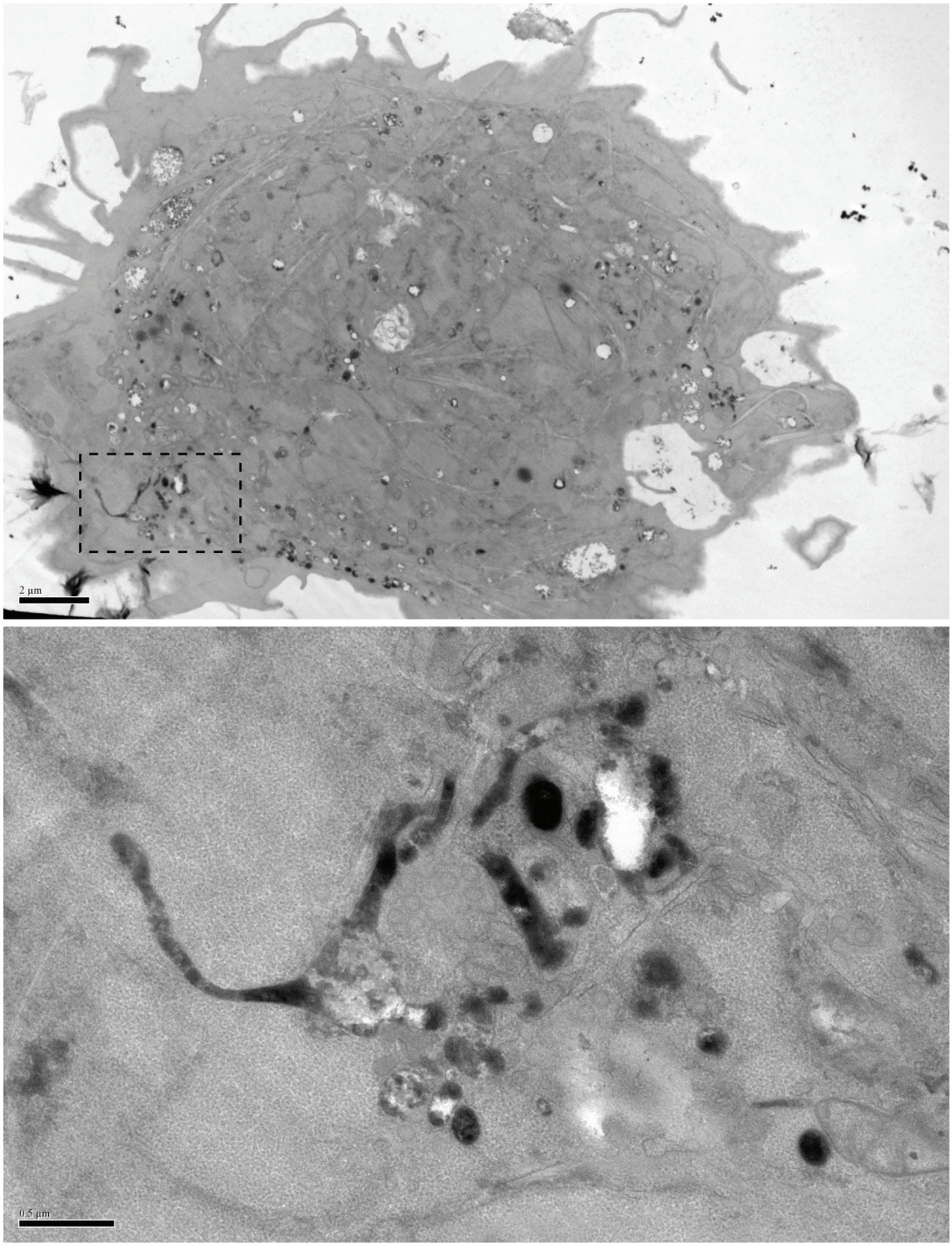

Figure 5-6 Putative GFP-TBC1D14 tubular RE revealed by EM

HEK293A cells were transfected with GPF-TBC1D14 and 24h later cells were serum-starved for an hour and stimulated with HRP conjugated Tfn and human EGF (Sigma) in the presence of gold-anti-EGFR (clone 108) for 2hrs. Cells were fixed in 0.1M cacodylate containing 2% paraformaldehyde and 2% glutaraldehyde. HRP-Transferrin stimulated cells were incubated with hydrogen peroxide and DAB as

described by Graham and Karnovsky (1966) [273, 274], and were then embedded by standard procedures [275]. Thin (70nm) sections were imaged using a transmission electron microscope. Top panel shows the whole cell with the marked box enlarged below. Scale bars represent top=2µm, bottom=500nm.

5.4 Over-expression of dominant negative Rab11 inhibits autophagosome formation

TBC1D14 over-expression leads to tubulation of REs in a Rab11 dependent manner and causes inhibition of autophagosome formation. This implies that Rab11 itself must be involved in autophagosome formation. Therefore, I tested Rab11 mutants for their effect on autophagy. As mentioned above Rab11N124I is a dominant negative mutant, which is unable to bind nucleotides, and should essentially have the same effect as TBC1D14 when over-expressed. Rab11Q70A is a dominant active mutant that preferentially binds GTP rather than GDP. Rab7 has been shown to be essential for late endosome-autophagosome fusion [183, 184] and similarly it has been suggested that Rab11 mediates MVB-autophagosome fusion [216], therefore, I included a dominant negative form of Rab7 (Rab7T22N), which prevents autophagosome maturation leading to an accumulation of LC3-II because it is not degraded in autolysosomes. Indeed, over-expression of Rab7T22N leads to accumulation of LC3-II even in fed cells as expected (Fig. 5-7). However, in my hands, the block of autophagosome-lysosome fusion induced by excess Rab7T22N seems to be incomplete as LC3-II accumulates even further when leupeptin is added to the starvation medium.

Compared to Rab7T22N the dominant negative form of Rab11 has a very different effect on autophagy in HEK293A cells. Over-expression of Rab11aN124I and

Rab11bN124I robustly inhibits autophagosome formation and not maturation, as there is a strong reduction of LC3-II even in the presence of leupeptin. As seen with TBC1D14 over-expression there is no difference in basal autophagy between control and transfected fed cells. Over-expression of wild type Rab11 enhanced autophagy but the constitutively active mutant Rab11aQ70A had no effect on LC3 lipidation.

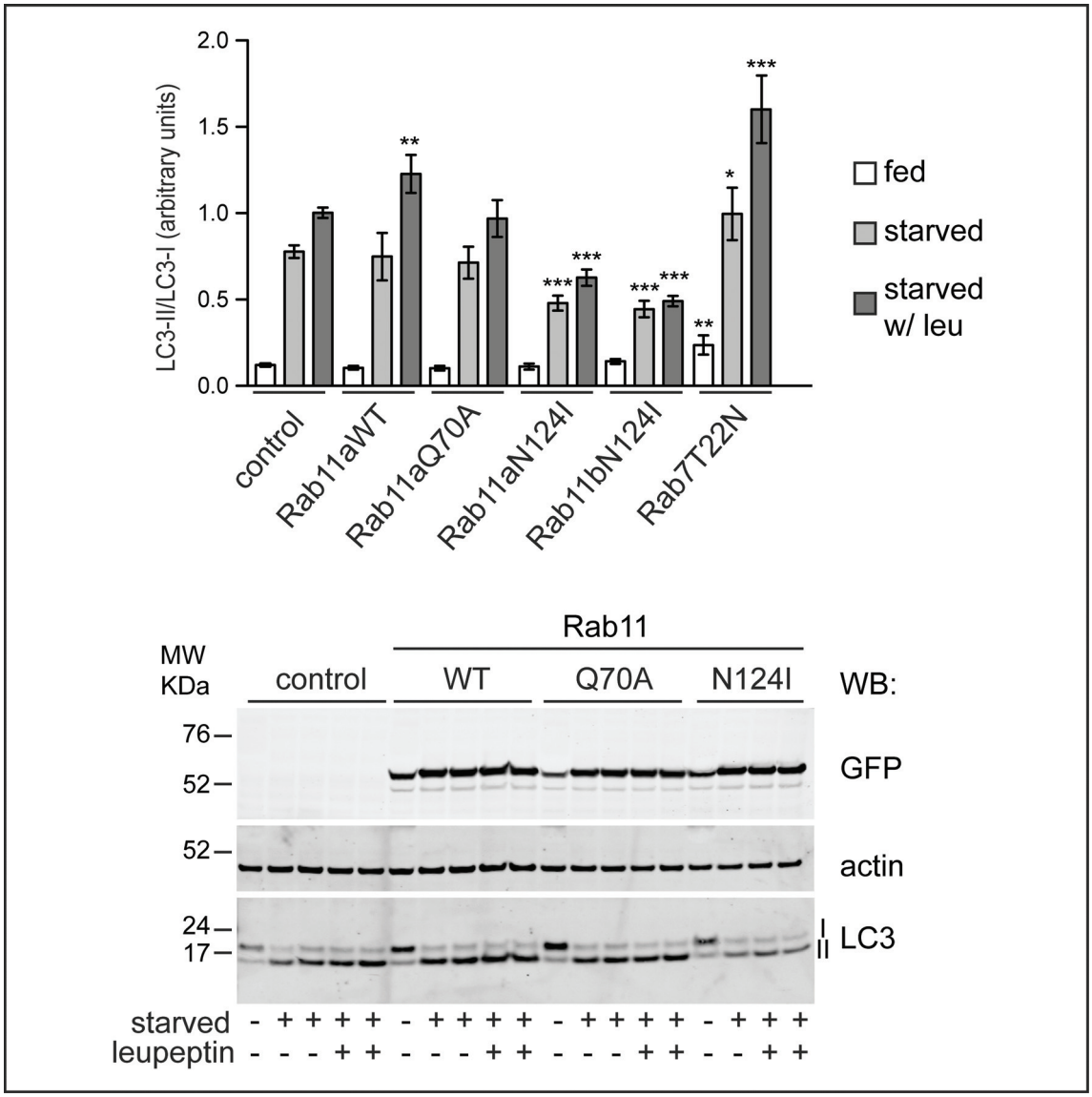

Figure 5-7 Inactive over-expressed dominant negative Rab11 inhibits autophagy
HEK293A cells were transfected with the indicated GFP-tagged Rab construct, Rab11a wild type (Rab11aWT), Rab11aQ70A (GTP-bound), Rab11aN124I, Rab11bN124I (nucleotide empty), or Rab7T22N (GDP-bound). 24h later cells were starved in EBSS with or without leupeptin (leu).

Endogenous LC3 conversion was measured by western blot using anti-LC3. The mean of at least 3 independent experiments is shown with the starved and starved with leupeptin samples done in duplicates. Asterisks indicate results of unpaired Student's t-test comparing to the vector control (fed vs. fed; starved vs. starved; etc.). Rab11aWT starved with leupeptin $p=0.0096$; Rab11aN124I starved $p<0.0001$; starved with leupeptin $p<0.0001$; Rab11bN124I starved $p<0.0001$; starved with leupeptin $p<0.0001$; Rab7T22N fed $p=0.001$; starved $p=0.0443$; starved with leupeptin $p<0.0001$. Error bars indicate SEM. A representative western blot is shown using anti-GFP antibody to detect transfected Rab proteins, anti-actin, and anti-LC3 antibodies to detect the respective endogenous proteins.

The above result strongly suggests that Rab11 is a positive regulator of autophagosome formation. To investigate further whether it is essential for autophagy HEK293A cells were depleted of Rab11a and 11b by siRNA mediated knock down and LC3 lipidation was measured. However, biochemical analysis was not feasible because there was a significant amount of cell death in Rab11 knock down cells. This could be due to the role of Rab11 in cytokinesis [276, 277] as many multinucleated or apoptotic cells are observed by immunofluorescence (not shown). Indeed, when TBC1D14 is highly over-expressed, some cells are also multi-nucleated (Fig. 3-4). Alternatively, redundancy between Rab11 and Rab25, which are very similar [196] may explain why knock down of the former has no effect. Rab11 and Rab25 may use the same effectors but, whereas these are sequestered by dominant negative Rab11, they are freely available to interact with Rab25 in Rab11 siRNA treated cells. Knock down of all three Rab proteins may be more effective or use of different RNA duplexes since many siRNAs have off target effects. Knock down over a shorter time period than the 3 days used for this experiment may allow biochemical analysis.

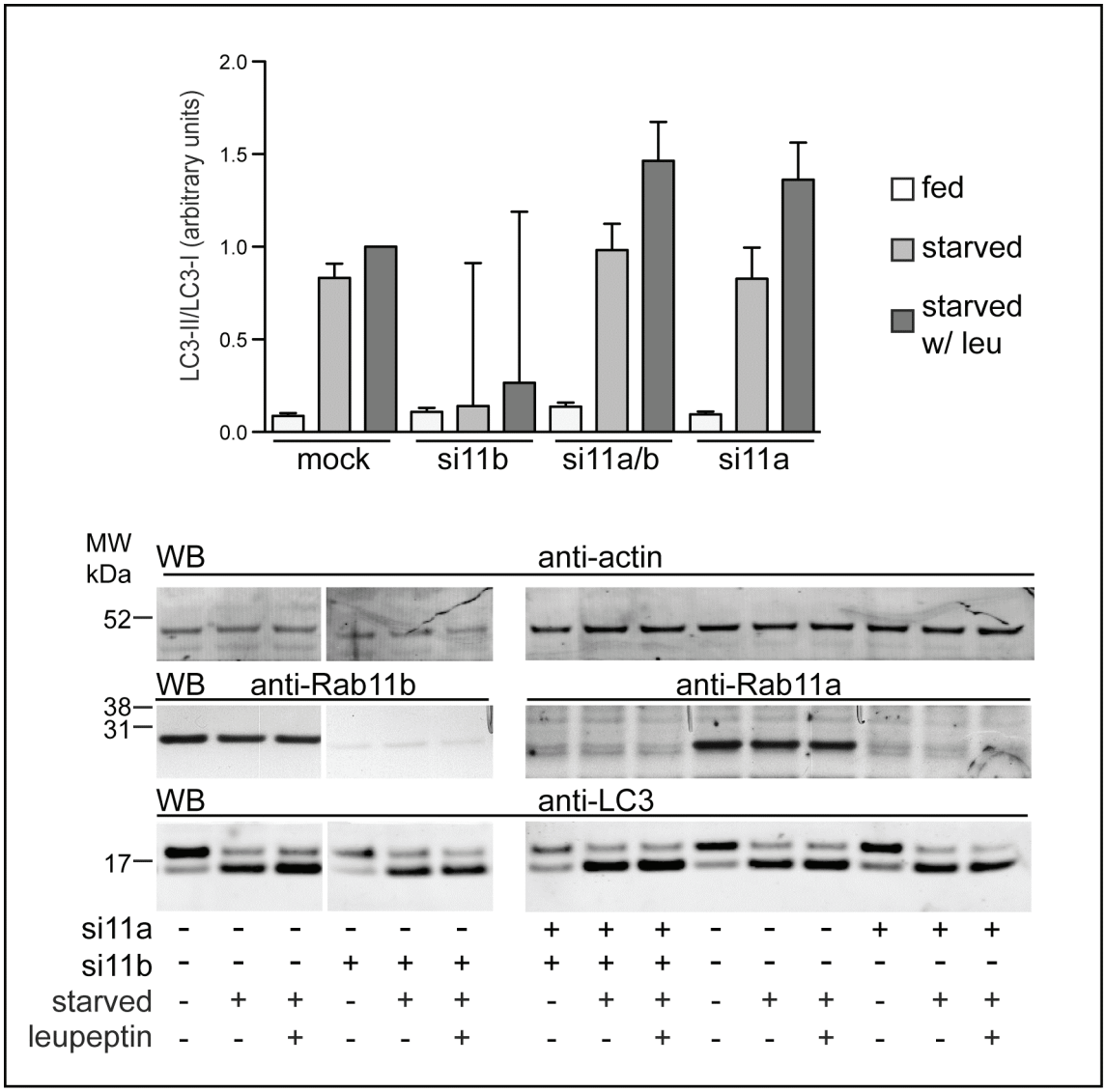

Figure 5-8 siRNA mediated knock down of Rab11 had no robust inhibitory effect on autophagy

HEK293A cells were transfected with the indicated siRNA as described above and left in full medium, starved, or starved with leupeptin (leu) for 2h before lysis. Western blot analysis was performed using the LI-COR system for quantification of actin and LC3. HRP-conjugated secondary antibodies and d ECL reagent were used to detect anti-Rab11a and anti-Rab11b. si11a=siRab11a, si11b=siRab11b, si11a/b=siRab11a and 11b, mock=mock transfected. Data represents the mean of 6 independent experiments. Error bars represent SEM. Paired Student's t-test detected no significance. Membrane blotted with anti-Rab11b on the left is one membrane but was partly flipped (last 3 lanes were loaded the other way round) for clarity.

5.5 Over-expression of constitutively active Rab11 can not rescue TBC1D14 induced inhibition of autophagosome formation

I have shown that TBC1D14 inhibits autophagosome formation when over-expressed, and tubulates REs in a Rab11 dependent manner suggesting that it acts a Rab11-GAP. Therefore, I hypothesised that by-passing Rab11 inactivation by over-expressing a constitutively active mutant Rab11Q70A, which preferentially binds GTP rather than GDP, should rescue the inhibition of autophagosome formation induced by TBC1D14. Similarly, ULK1 sequestration may also be contributing to the phenotype and providing excess ULK1 by over-expressing it may rescue autophagy inhibition. To test these hypotheses, HEK293A cells were transfected with myc-TBC1D14 as before either alone or together with Rab11aQ70A, Rab11bQ70A, myc-ULK1, or HA-ULK1 and assayed for LC3 conversion as described above. Both ULK1 constructs were used because the myc-tagged one contains mouse ULK1 whereas the HA-tagged one contains the human homologue even though their amino acid sequences are very similar.

Co-transfection of Rab11Q70A did not rescue inhibition of autophagosome formation, and the reduction in LC3 lipidation was comparable to TBC1D14 alone (Fig. 5-9). This may be due to sequestration of effectors of Rab11 and/or TBC1D14, so that a functional Rab11 effector platform cannot form. ULK1 co-transfection with TBC1D14 on the other hand was able to rescue autophagy inhibition and induced even higher rates of LC3 conversion than observed in control cells. Even under fed conditions basal

autophagy was enhanced in ULK1-TBC1D14 over-expressing cells, which is not seen when ULK1 alone is over-expressed [20, 21].

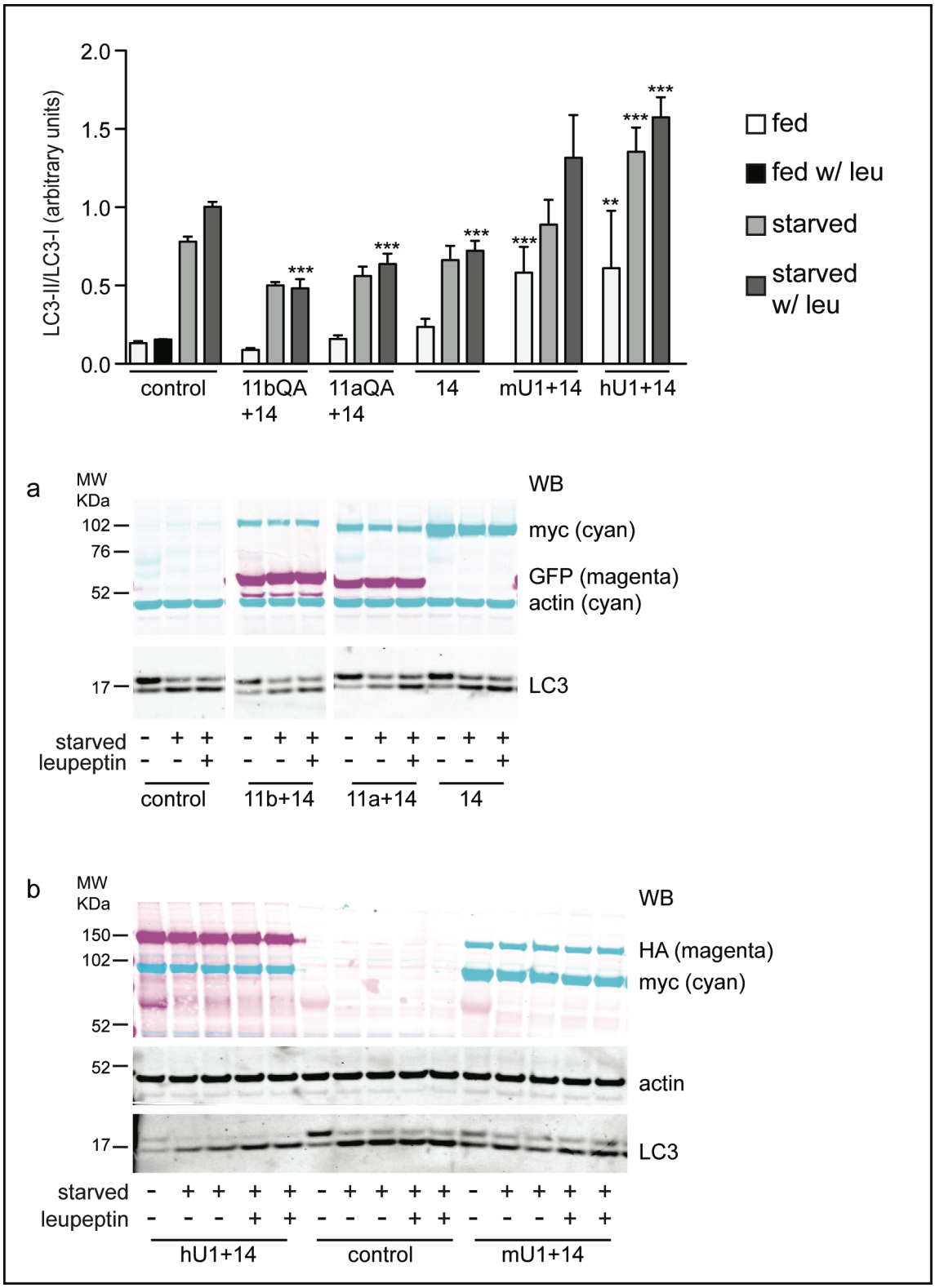

Figure 5-9 Over-expression of constitutively active Rab11 does not rescue TBC1D14 induced inhibition of autophagosome formation by TBC1D14 but over-expression of ULK1 does

HEK293A cells were transfected with renilla vector (control), GFP-Rab11bQ70A and myc-TBC1D14 together (11bQA+14), GFP-Rab11aQ70A and myc-TBC1D14 together (11aQA+14), myc-TBC1D14 alone (14), human HA-ULK1 and myc-TBC1D14 together (hU1+14), or mouse myc-ULK1 and myc-TBC1D14 together (mU1+14). Cells were processed as usual for LC3 western blotting. Membranes were incubated with antibodies against actin and LC3 as indicated, followed by antibodies against myc, GFP, and HA to detect over-expressed proteins using the LI-COR system. Secondary antibodies labelled with two different infrared fluorophores were used and polyclonal antibodies (myc and HA) were pseudo-coloured magenta, monoclonal antibodies were pseudo-coloured cyan and the two pictures were overlaid showing the over-expressed proteins. The actin band is still visible in the top blot as membranes were not stripped after LC3 and actin quantification but labelled with anti-myc, anti-HA, and anti-GFP. **(a)** Representative western blot of TBC1D14 over-expression with constitutively active Rab11Q70A. **(b)** Representative western blot of TBC1D14 over-expression with either HA-ULK1 or myc-ULK1. Data represents mean of 3 independent experiments and error bars represent SEM. Asterisks indicate results from unpaired Student's t-test comparing fed control to fed condition, starved with leupeptin (leu) control to starved with leupeptin condition, etc. GFP-Rab11bQ70A and myc-TBC1D14 starved with leupeptin $p<0.0001$; GFP-Rab11aQ70A and myc-TBC1D14 starved with leupeptin $p<0.0001$; TBC1D14wt starved with leupeptin $p=0.0002$; myc-ULK1 and myc-TBC1D14 fed $p<0.0001$; HA-ULK1 and myc-TBC1D14 fed $p=0.0046$, starved $p<0.0001$, and starved with leupeptin $p<0.0001$.

Despite the ability of excess ULK1 to rescue inhibition of autophagy induced by TBC1D14 it is unlikely that ULK1 sequestration is the sole reason for inhibition of autophagosome formation since over-expression of the TBC domain of TBC1D14, which still binds ULK1, does not inhibit autophagy (Fig. 4-11). This raises the question whether the TBC domain alone localises to the same compartment as full length TBC1D14 or whether it is found on a different organelle such as the Golgi apparatus. After all endogenous TBC1D14 localises to the Golgi and it is conceivable that the N or C-terminal domains of this protein, which are missing in the TBC construct, somehow regulate its localisation. Were this the case failure to tubulate REs may the reason that there is no inhibition on autophagosome formation when the TBC domain alone is over-

expressed. Therefore, cells were transfected with GFP-TBC1D14-TBC and labelled with anti-TfnR to investigate whether the TBC domain localises to the pericentriolar ERC like the full length protein or to a different compartment. Indeed, the TBC domain alone localises to a TfnR-positive structure (Fig. 5-10). Interestingly, this juxta-nuclear pool appears larger than the normal ERC observed in untransfected cell suggesting that RE movement away from it is blocked or transport towards it enhanced.

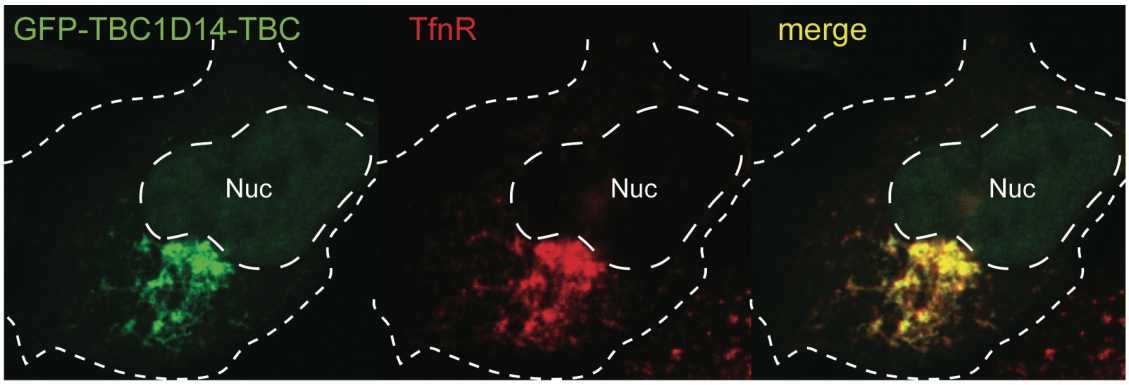

Figure 5-10 The TBC domain of TBC1D14 alone can tubulate REs
HEK293A cells were transfected with GFP-TBC1D14-TBC (amino acids 224-669) (green), fixed and labelled with anti-TfnR antibody (red). The cell border and the nucleus (Nuc) are indicated by dotted lines. Note that there is an untransfected cell in the south east corner of the image.

5.6 Over-expression of TBC1D14 does not affect other cellular trafficking pathways

As shown in Figure 5-4 EGF uptake and trafficking was not affected by TBC1D14 over-expression. To confirm that TBC1D14 acts in Rab11-dependent RE trafficking only I investigated the distribution of several markers of other intracellular trafficking pathways in TBC1D14 expressing cells. HEK293A cells were transfected with myc- or

GFP-TBC1D14, starved for 2 hours or not and fixed. Cells were then labelled with the corresponding antibody to a range of markers for subcellular compartments. With the exception of CI-MPR and LAMP2 only starved cells are shown for marker proteins that do not change distribution upon starvation (Fig. 5-11).

The cation-independent mannose-6-phosphate (M6P) receptor (CI-MPR) shuttles between the TGN and endosomes to target M6P labelled lysosomal enzymes to the lysosome [278]. It is sorted in the early endosomes to be transported back to the TGN (see Introduction section 1.2.1) and unlike TfnR does not change its distribution upon starvation (Fig. 5-11a). TBC1D14 over-expression does not disturb the localisation of CI-MPR although these TBC1D14-positive tubules can often be found juxta-posed to CI-MPR-positive vesicles. TfnR and CI-MPR are both found in early endosomes but probably only the TfnR-positive endosomal subdomain is tubulated by TBC1D14. Another early endosomal protein early endosomal autoantigen 1 (EEA1) which is an effector of Rab5 [279] behaves similarly to CI-MPR in that it can be found in close proximity to TBC1D14-positive tubules but is not affected by its over-expression (Fig. 5-11b). Finally, EGFR, which localises to both early and late endosomes/MVBs, can be found in some TBC1D14 tubules but this is probably because unlike CI-MPR it is not actively sorted to a subdomain of the early endosome but follows the degradative route passively as endosomes mature from early to late to lysosomes (Fig. 5-11c). However, this degradative route itself is not affected by TBC1D14 over-expression as the late endosomal protein Rab7 and the lysosomal associated membrane protein 2 (LAMP2) are distributed normally in transfected cells (Fig. 5-11d,e). Note, that LAMP2 shows a much more peripheral distribution after starvation due to autolysosome formation.

The Golgi and TGN were labelled with antibodies against Golgi matrix protein of 130 kDa (GM130) and trans-Golgi network integral membrane protein 2 of 46 kDa (TGN46), respectively [280, 281] (Fig. 5-11f,g). Surprisingly, TBC1D14 tubules do not substantially co-localise with GM130 or TGN46, as is the case for endogenous TBC1D14. This preference of over-expressed TBC1D14 to localise to Rab11-positive compartments rather than the Golgi/TGN may be due to titration of an essential effector that keeps TBC1D14 on the Golgi/TGN or directs it there. However, this is purely speculative. Interestingly, the Golgi appears to be fragmented in some but not all TBC1D14 over-expressing cells but it is unclear what leads to this differential phenotype. It may possibly be cell cycle specific but this was not investigated. The other possibility is that TBC1D14 has a role in Golgi stability as has been reported before by Haas et al. [200], even though it did not bind any known Golgi localised Rabs in a yeast-2-hybrid assay (Fig. 4-13).

Finally, TBC1D14 tubules do not overlap with the ER protein calreticulin suggesting that the secretory pathway is intact in TBC1D14 over-expressing cells (Fig. 5-11h).

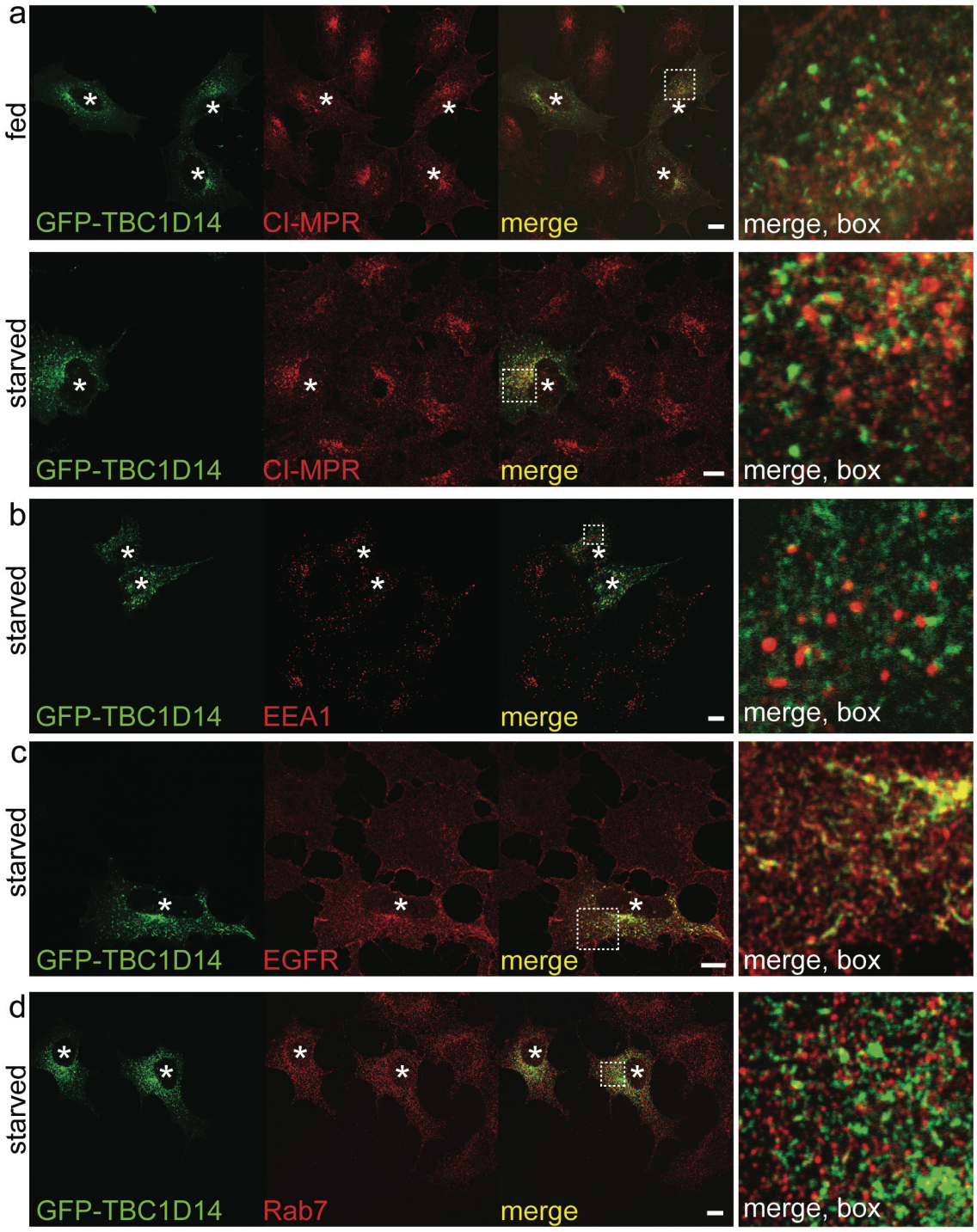
a
fed
GFP-TBC1D14
CI-MPR
merge
merge, box
starved
GFP-TBC1D14
CI-MPR
merge
merge, box
b
starved
GFP-TBC1D14
EEA1
merge
merge, box
c
starved
GFP-TBC1D14
EGFR
merge
merge, box
d
starved
GFP-TBC1D14
Rab7
merge
merge, box

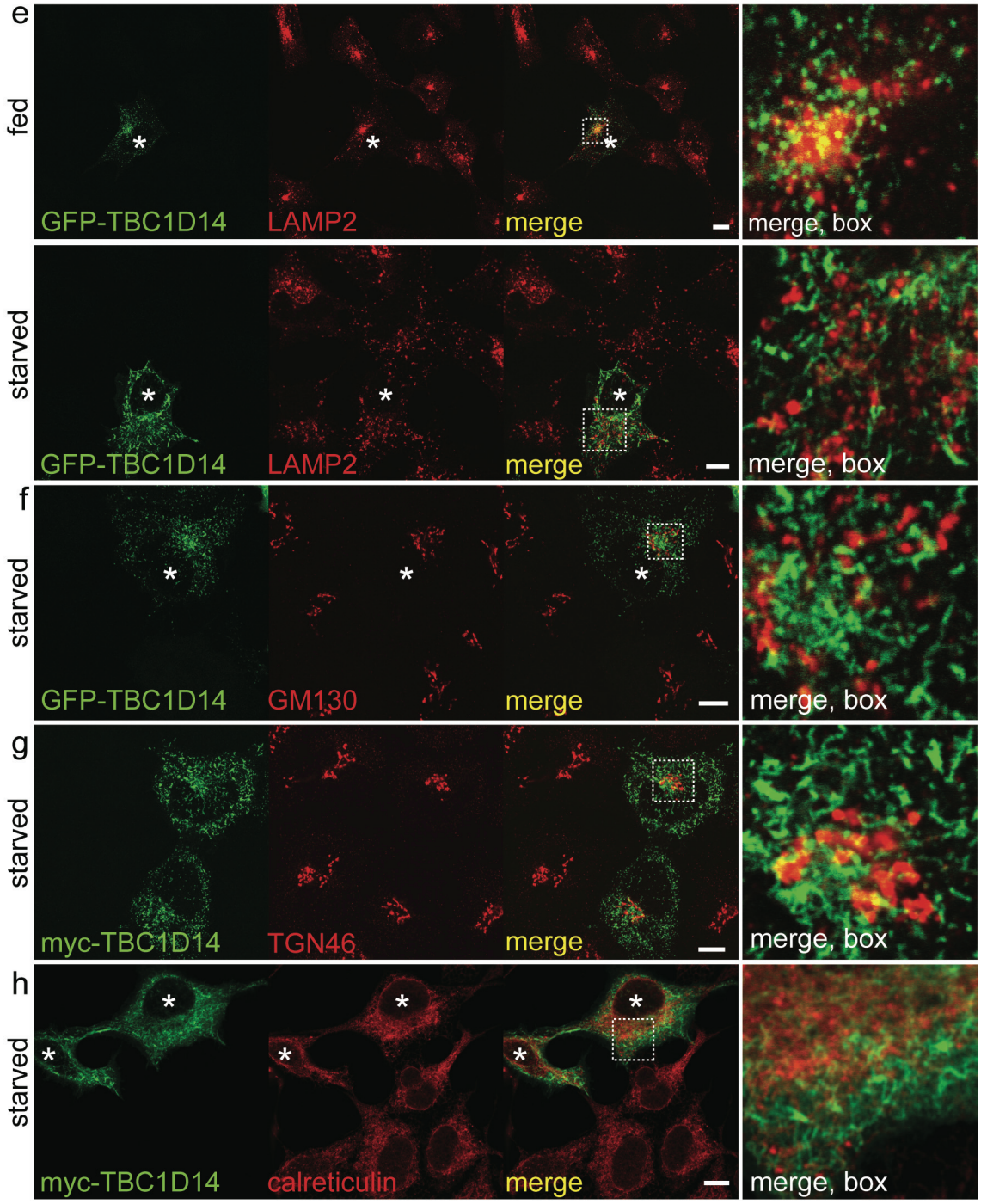

Figure 5-11 TBC1D14 over-expression does not disturb several other intracellular trafficking pathways

HEK293A cells were transfected with GFP or myc-TBC1D14 (green) and 24h later starved for 2h in EBSS where indicated. Cells were then labelled with antibodies against (red) the **(a)** CI-MPR (cation independent-mannose-6-phosphate receptor), **(b)** EEA1 (early endosomal autoantigen 1), **(c)** EGFR (epidermal growth factor receptor) **(d)** Rab7 **(e)** LAMP2 (lysosomal associated membrane protein 2), **(f)** GM130 (Golgi matrix protein of 130 kDa), **(g)** TGN46 (trans-Golgi network integral membrane protein 2

of 46 kDa), and **(h)** calreticulin. Asterisks indicate transfected cells, with enlarged inset on right indicated as boxes on the merged panel. Scale bars are equal to 10μm.

5.7 TBC1D14 tubules do not co-localise with early autophagic markers DFCP1 or WIPI2

So far I have shown that over-expression of TBC1D14 tubulates Rab11-positive REs, sequesters ULK1 and leads to inhibition of autophagosome formation. However, this population of REs has not been previously linked to autophagy, so I investigated the role of REs in autophagosome formation.

The phosphatidylinositol-3-kinase (PI3K) complex apart from the ULK1 kinase complex is also essential for initiation of autophagy (see Introduction section 1.1.3). This second complex contains the class III PI3K vps34, which creates phosphatidylinositol-3-phosphate (PI3P) on isolation membranes and autophagosomes. WIPI2 and DFCP1 are two PI3P-binding autophagy proteins, which localise to isolation membranes dependent on PI3K activity. The ULK1 and PI3K complexes most likely act somewhat in parallel [80], very early in autophagosome formation, so I investigated whether WIPI2 or DFCP1 would localise to TBC1D14 induced tubular REs together with ULK1.

TBC1D14 was over-expressed in HEK293A cells, which were starved and labelled with antibodies against ULK1 and WIPI2. WIPI2 is mostly cytosolic and diffuse in fed cells but forms distinct puncta on isolation membranes upon starvation [57]. These WIPI2 puncta co-localise with ULK1 in most cases, however, WIPI2 is not observed on TBC1D14 tubules suggesting that autophagosome formation is blocked by TBC1D14

over-expression before the two pathways converge (Fig. 5-12a). TBC1D14 was found to share some sequence similarity with a yeast protein sbe22p in a PSI blast. Interestingly, sbe22p was found in a yeast-2-hybrid assay to bind Atg18p, which is the yeast homologue of WIPI2 but I could not confirm this interaction by co-immunoprecipitation in HEK293A cells. There is also no substantial co-localisation between endogenous TBC1D14 and WIPI2 although some WIPI2 puncta can be observed in close proximity to the Golgi/TGN pool of TBC1D14 (Fig. 5-12b, insets 1 and 2).

DFCP1 localises to the same structures as WIPI2 but because there is no antibody against DFCP1 available myc-TBC1D14 was over-expressed in HEK293A cells stably expressing GFP-DFCP1 [69]. Immunofluorescence staining with anti-myc and anti-TBC1D14 specific antibodies revealed that DFCP1 does not localise to tubulated REs (Fig. 5-12c, inset 1) and does not co-localise with endogenous TBC1D14 endosomal puncta but the DFCP1 Golgi pool shows good overlap Golgi localised TBC1D14 (Fig. 5-12c, inset 2).

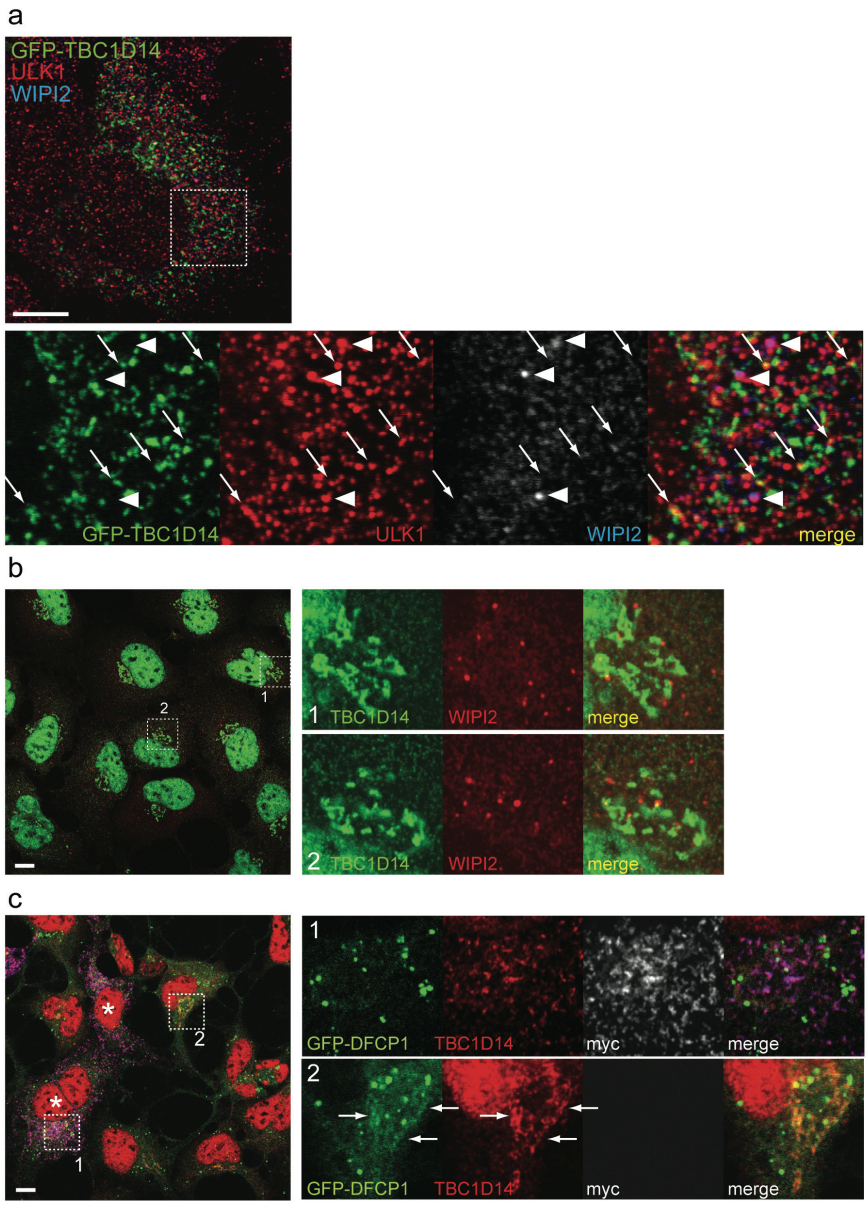

Figure 5-12 PI3P binding proteins WIPI2 and DFCP1 do not localise to TBC1D14 tubules

(a) HEK293A cells were transfected with GFP-TBC1D14, starved for 2h in EBSS and labelled with anti-ULK1 (red) and anti-WIPI2 antibody (blue in merge). WIPI2 co-localises with ULK1 in cytosolic puncta (arrowheads) but is not recruited to TBC1D14 induced ULK1-positive tubules (arrows). **(b)** HEK293A cells were starved for 2h in EBSS, fixed, and labelled with antibodies against WIPI2 and TBC1D14. Dotted boxes 1 and 2 are enlarged on the right. **(c)** Cells stably expressing GFP-DFCP1 (201 cells) were transfected with myc-TBC1D14, starved and stained with antibodies against myc (blue) and TBC1D14 (red). Transfected myc-positive cells are marked with an asterisk. GFP-DFCP1 puncta do not co-localise with myc-TBC1D14 tubules (inset 1) but endogenous TBC1D14 shows overlap with GFP-DFCP1 in the Golgi/juxta-nuclear region in untransfected cells (inset 2, arrows). Scale bars are equal to 10µm.

TBC1D14 over-expression does not seem to inhibit WIPI2 and DFCP1 puncta formation dramatically but appears to reduce the number of GFP-LC3 positive autophagosomes. This suggests that the PI3K pathway is unaffected and WIPI2 as well as DFCP1 can localise normally to IMs in TBC1D14 over-expressing cells. However, these isolation membranes may not be able to progress to become autophagosomes because TBC1D14 over-expression blocks other essential autophagic functions most likely involving the ULK1 kinase complex. To test this hypothesis TBC1D14 transfected starved 2GL9 cells were labelled with anti-WIPI2 antibody and the number of WIPI2 positive isolation membranes was counted. Indeed preliminary data suggests that there are slightly more WIPI2 puncta in TBC1D14 over-expressing cells and that less of those have acquired GFP-LC3, which localises to autophagosomes at a later stage than WIPI2 (Fig. 5-13). Whereas in untransfected cells on average 64% of WIPI2 spots were also positive for GFP-LC3, this was significantly reduced in transfected cells to 57%.

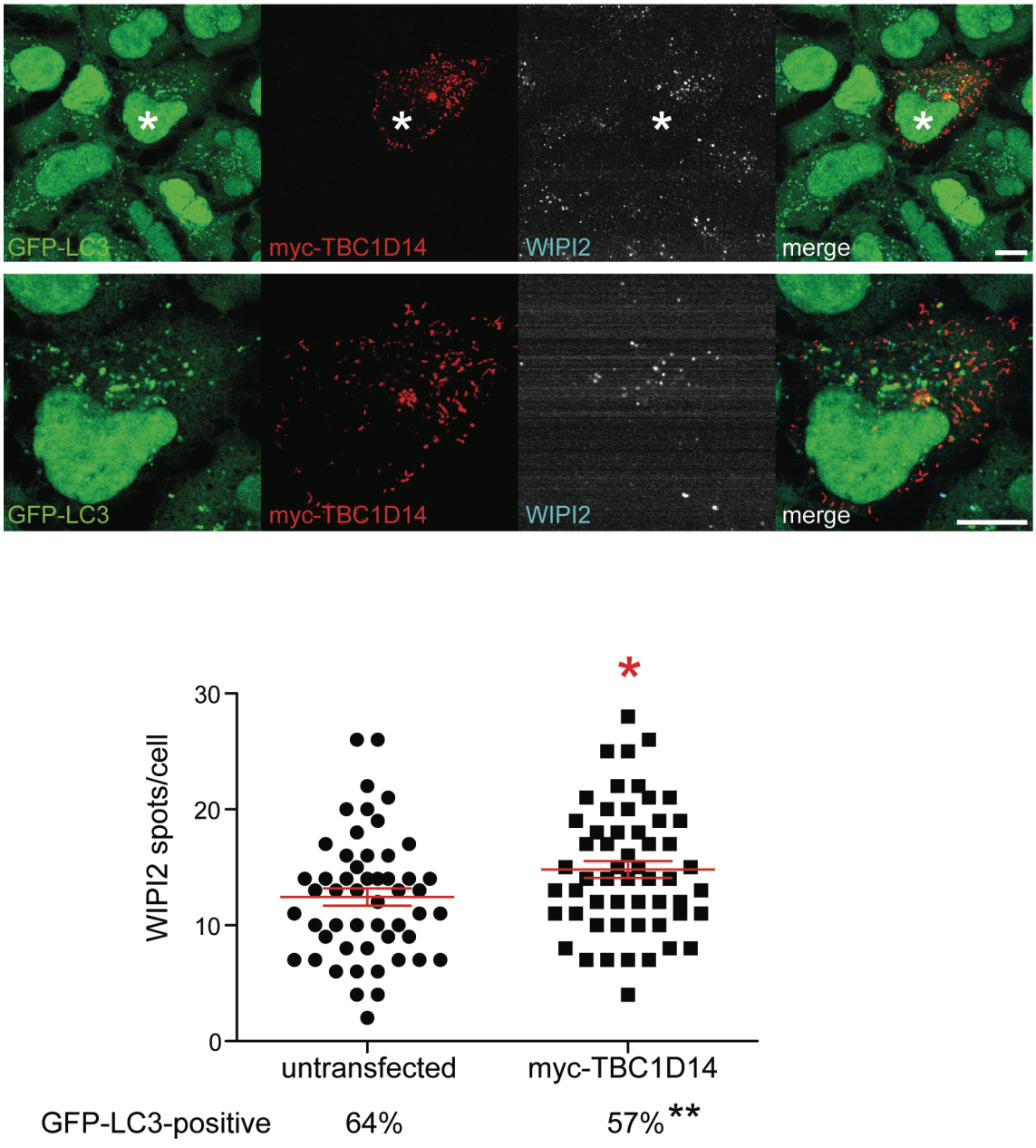

Figure 5-13 WIPI2 puncta accumulate in TBC1D14 over-expressing cells

2GL9 cells were transfected with myc-TBC1D14 and starved for 2h in EBSS. Cells were labelled with anti-myc (red) to detect transfected cells (marked by a white asterisk) and anti-WIPI2 antibodies. A representative image used for spot counting is shown above with the transfected cell enlarged underneath. The number of WIPI2 spots were counted in 52 untransfected and 55 transfected cells on the same cover slip and classified as GFP-LC3-positive or negative. In untransfected cells 64.3% (±2.3% SEM) of WIPI2 spots were GFP-LC3 positive compared to 56.9% (±1.6% SEM) in myc-TBC1D14 transfected cells. Black asterisks indicate result of unpaired Student's t-test with p=0.0084. Scale bars are equal to 10µm. A distribution of spot count per cell is shown below. Each data point represents the number of WIPI2 puncta per cell. Red asterisk indicates significant accumulation of WIPI2 spots in TBC1D14 transfected

cells as calculated by an unpaired Student's t-test. p=0.0247. Red line indicates mean number of WIPI2 spots per cell. Mean untransfected=12.44 (±0.7427); mean transfected=14.82 (±0.7308). Error bars indicate SEM.

5.8 mAtg9 and ULK1 localise to REs

Another early acting autophagy protein is mAtg9. This transmembrane protein cycles between the TGN and an endosomal pool and disperses to endosomes upon starvation (see Introduction section 1.1.5.1). Although mAtg9 has been shown to localise to late endosomes it can also be found to co-localise extensively with REs labelled by TfnR (Fig. 5-14a). In starved HEK293A cells labelled with antibodies against endogenous ULK1, mAtg9, and TfnR, mAtg9 seems to be localised on subdomains of REs rather than cover the entire surface and almost every RE observed contains such a mAtg9 subdomain (Fig. 5-14ii). ULK1 also localises to REs and can occupy the same area as mAtg9 or be on a different domain (Fig. 5-14i and iii). This localisation seems to be starvation-independent as both proteins are also found on REs in fed cells (data not shown), however, closer investigation and quantification of mAtg9 overlap on REs in fed versus starved cells may reveal subtle differences.

When TBC1D14 is over-expressed REs are tubulated and sequester ULK1, however, mAtg9 is not localised to tubules (Fig. 5-14b). Interestingly, mAtg9 dispersal is not affected by TBC1D14 over-expression suggesting that its trafficking to other compartments such as late endosomes is intact but it cannot reach REs that are tubulated. I hypothesise that REs provide an autophagy signalling platform containing

both ULK1 and mAtg9, which can induce autophagosome formation upon nutrient deprivation. This signalling platform is disrupted by TBC1D14 over-expression and Rab11 inactivation leading to a block of autophagosome formation.

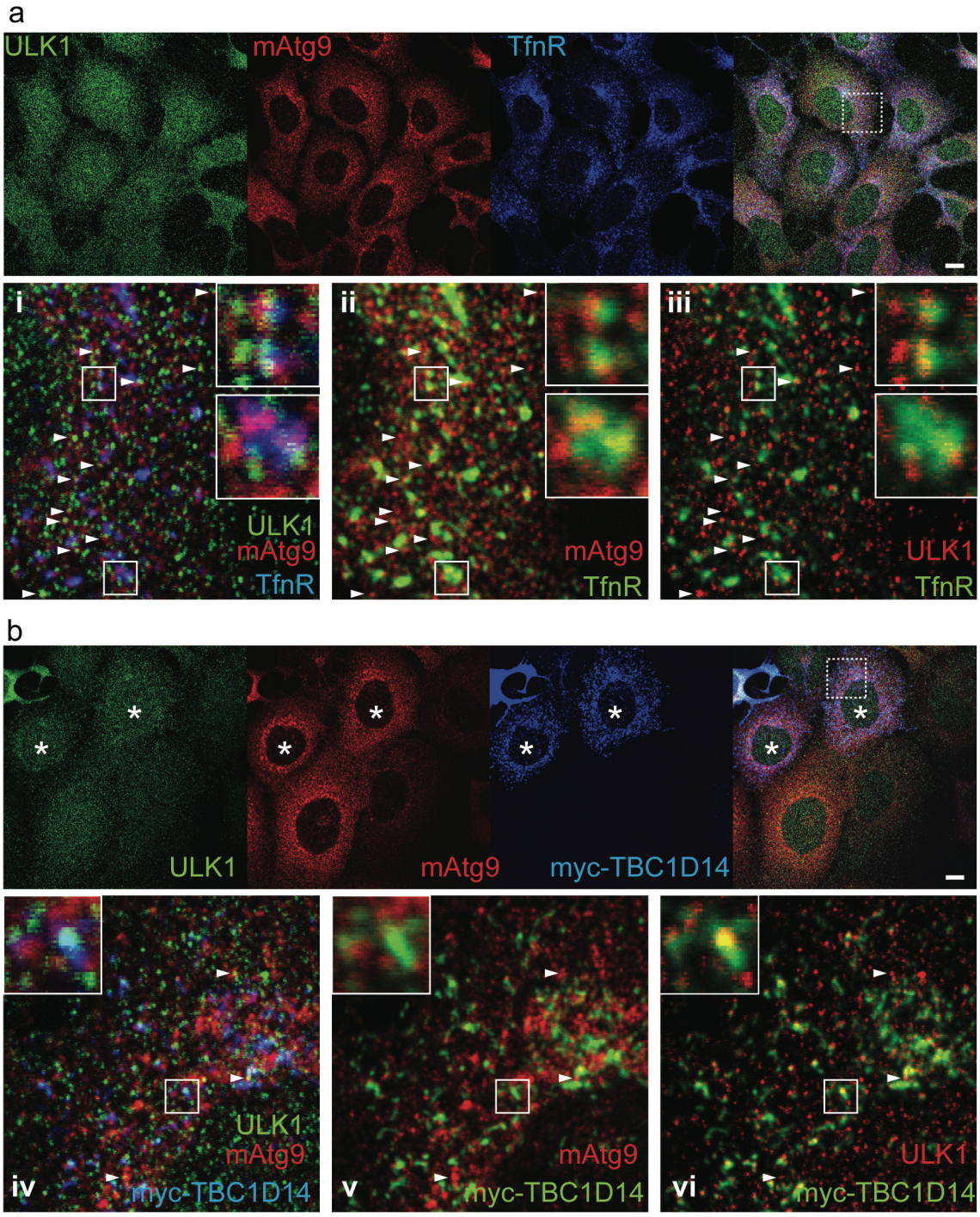

Figure 5-14 mAtg9 and ULK1 localise to REs, but TBC1D14 tubules contain only ULK1

(a) HEK293A cells were starved for 2h in EBSS, fixed and labelled with antibodies against ULK1 (green), mAtg9 (red) and TfnR (blue). Inset i) shows the triple-labelled merge. Insets ii) and iii) were pseudo-coloured for clarity so that TfnR (green) is shown with ii) mAtg9 (red), and iii) ULK1 (red). Arrowheads indicate i) TfnR, ii) mAtg9 and iii) ULK1 positive puncta. Two enlarged images of REs are shown (top inset corresponds to top box). **(b)** Same as in (a) but HEK293 cells were transfected with myc-TBC1D14, and labelled with anti-myc instead of TfnR. Inset iv) shows triple labelled merge. Inset v) shows mAtg9 (red) and myc-TBC1D14 (green) tubules, which do not overlap, and vi) shows ULK1 (red) co-localised on myc-TBC1D14 (green) tubules. Enlarged images of a RE-tubule are shown as indicated. Asterisks in **(b)** indicate myc-TBC1D14 transfected cells. Scale bars are equal to 10μm.

5.9 TfnR and Rab11 show partial co-localisation with GFP-LC3

Since REs contain two early autophagy proteins ULK1 and mAtg9 it is tempting to speculate that REs can not only act as a platform to activate downstream signalling to induce autophagosome formation but also provide membrane to expanding isolation membranes. To test this hypothesis 2GL9 cells were starved for two hours and labelled with anti-TfnR. Partial co-localisation of TfnR with GFP-LC3 positive autophagosomes can be observed in these cells (Fig. 5-15a). Likewise when 2GL9 cells were starved for 2h, fixed, treated with saponin briefly to reduce cytosolic Rab11 background and labelled with isoform specific anti-Rab11a or anti-Rab11b and anti-TfnR antibodies, GFP-LC3 spots can be observed that contain all three markers (Fig. 5-15b). This suggests that REs may provide membrane to expanding IMs and/or autophagosomes directly but are probably not the sole membrane donors. Alternatively, the partial co-localisation observed between RE markers and GFP-LC3 positive autophagosomes may be due to engulfment of REs by autophagosomes as this cannot be distinguished from membrane incorporation by immunofluorescence microscopy.

Myc-TBC1D14 shows no substantial co-localisation with GFP-LC3 but is sometimes observed in close proximity to GFP-LC3 puncta and endogenous TBC1D14 also shows very little overlap with GFP-LC3 (Fig. 5-15c). This may be due to TBC1D14 acting in a different step in RE trafficking and no longer associating with Rab11 on autophagosomes or because of the interaction with Rab11 is too transient to detect reliably.

Furthermore, because GFP-LC3 is quenched in an acidic environment such as the autolysosome it can only reveal immature AVs. To investigate whether TBC1D14 can be found on mature autophagosomes I transfected HEK293A cells with an mRFP-EGFP-LC3 tandem-fluorescent construct (tf-LC3). Because mRFP is not quenched in autolysosomes mature autophagosomes will appear red, whereas immature autophagosomes will appear yellow. Again, no co-localisation of endogenous TBC1D14 with either population of AVs was observed (Fig. 5-15d)

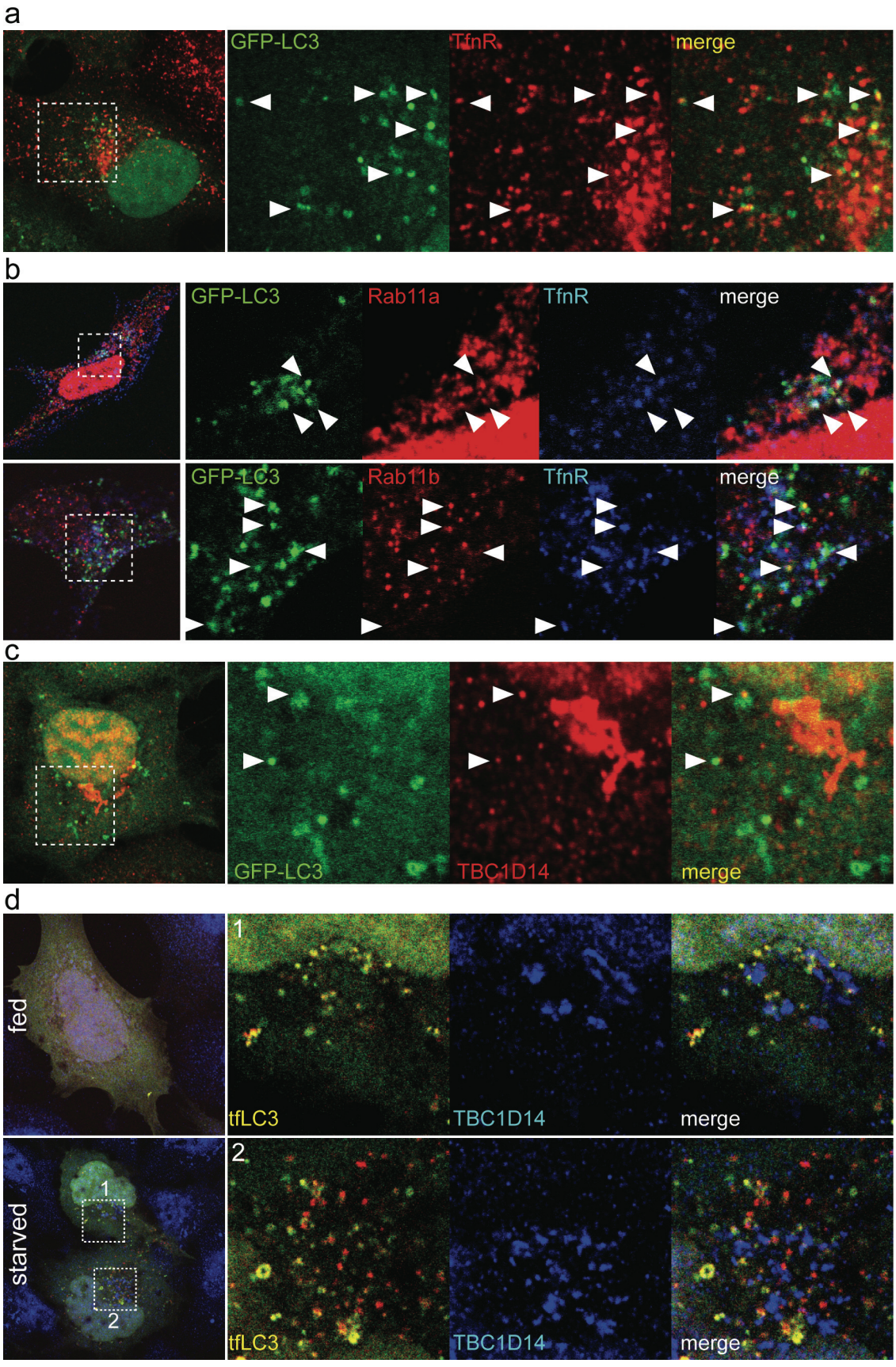
a
GFP-LC3
TfnR
merge
b
GFP-LC3
Rab11a
TfnR
merge
GFP-LC3
Rab11b
TfnR
merge
c
GFP-LC3
TBC1D14
merge
d
fed
1
tfLC3
TBC1D14
merge
starved
1
2
2
tfLC3
TBC1D14
merge

Figure 5-15 TfnR and Rab11 show partial co-localisation with GFP-LC3
(a) 2GL9 cells were starved for 2h in EBSS, fixed, and labelled with anti-TfnR antibody (red). TfnR partially co-localises with GFP-LC3 positive autophagosomes (arrowheads). **(b)** 2GL9 cells were starved for 2h in EBSS, treated with 0.2% saponin/PIPES to reduce cytosolic staining, fixed and labelled with antibodies against Rab11a (red, top) or Rab11b (red, bottom) and TfnR (blue). Rab11 and TfnR partially co-localise with GFP-LC3 positive autophagosomes (arrowheads). Note that although the anti-Rab11a and anti-Rab11b antibodies are isoform specific by western blot (Fig. 4-15) I have not tested whether they also specifically recognise the native isoforms in immunofluorescence experiments. **(c)** 2GL9 cells were starved for 2h in EBSS, fixed, and labelled with anti-TBC1D14 (red). TBC1D14 shows very little co-localisation with GFP-LC3 positive autophagosomes (arrowheads). **(d)** Cells were transfected with tfLC3, fixed, stained for TBC1D14 and starved for 2h in EBSS (bottom image) or not (top image). The tfLC3 is visualized in the green and red channel, which is shown merged. Enlarged insets (1) and (2) are from starved cells.

5.10 Conclusions

I have shown a role for REs in autophagy, which I propose act as signalling platforms to induce autophagy and may provide parts of the autophagosomal membrane. Two early autophagy proteins ULK1, and mAtg9, localise to Rab11-positive REs. The RabGAP protein TBC1D14, binds to Rab11, and tubulates TfnR/Rab11-positive REs when over-expressed. Tubulated REs sequester ULK1 but not the other early autophagy proteins mAtg9, WIPI2, or DFCP1 nor the later acting protein LC3. Autophagy is inhibited by TBC1D14 over-expression at an early step during formation or expansion and not during maturation. In agreement with the data suggesting TBC1D14 is a GAP or an effector for Rab11, I have shown that a dominant negative mutant of Rab11 inhibits autophagosome formation.

I propose a model whereby a population of ULK1 and mAtg9 is resident on the REs in both fed and starved conditions. ULK1 is recruited to the REs by TBC1D14. Upon nutrient starvation ULK1 is activated and moves to the site of autophagosome formation or recruits Atg proteins to form IMs de novo. mAtg9, which localises to REs and other endosomal populations may be a nutrient sensor on these vesicles that can activate autophagy when cells are deprived of nutrients.

Chapter 6. ULK1 knock-out mice

6.1 Aim

ULK1 or its homologues is essential for autophagy in HEK293A and HeLa cells as well as *S. cerevisiae, D. discoideum, C. elegans,* and *D. melanogaster* [20, 22-26]. In mice ULK1 has been shown to regulate axon extension in primary neurons in culture, purified from mouse brain [90]. However, whereas invertebrates have one Atg1 homologue there are at least two but possibly up to five Atg1 homologues in vertebrate organism, which in mice and humans are called ULK1, ULK2, ULK3, ULK4 and STK36. To investigate the specific functions of ULK1 in mice, animals lacking the ULK1 protein were created (ULK1KO) by Dr. Edmond Chan and I analysed whether they have any specific defects.

6.2 ULK1 knock-out mice appear healthy, are fertile, and undergo autophagy

ULK1KO mice were created by injecting 129 embryonic stem (ES) cells with a gene trap insertion in the ULK1 gene (clone AC0566, Sanger institute gene trap resource) into C57BL/6J blastocysts to create chimeric mice. Gene trapping is a method of creating embryonic stem cells with a random insertion of a well defined reporter cassette. This cassette contains a splice acceptor site from an *engrailed 2* (*En2*) intron located 5′ to a promoterless β-gal/neo (or β-geo) fusion construct, followed by a poly-

adenylation signal from an SV40 virus gene. Once this cassette is inserted in an exon or more often an intron of a gene X this will lead to splicing events creating a fusion transcript consisting of the upstream 5' exon(s) of gene X, followed by the β-gal/neo reporter/resistance gene, followed by a poly-A stretch, which leads to translation termination. This transcript will be under the endogenous promoter of gene X and the β-gal product can then serve not only as a reporter to confirm insertion of the gene trap cassette but also as an indicator of the expression pattern of gene X. Trapped ES cells can be selected using neomycin as the neomycin transferase in the β-geo fusion protein confers neomycin resistance but cells will be selected regardless of whether the insertion occurred intergenically or intragenically. Insertion of the gene trap at the 5' end is more likely to lead to total loss of function of a gene but there is always a small possibility that inactivation is incomplete. In clone AC0566 that was used to create ULK1KO mice the gene trap cassette inserted at the beginning of the ULK1 gene intronically after exon 3 creating a fusion protein of the first 81 amino acids of ULK1, the β-galactosidase and neomycin transferase (Fig. 6-1). This results in a short truncation of the kinase domain of ULK1 (spanning from amino acids 16-278) and is expected to lead to complete loss of function. However, both heterozygous and homozygous ULK1KO mice show no obvious phenotypes and are fertile. ULK1KO mice were backcrossed into the C57BL/6J strain for 10 generations (n=10), which should result in a 99.9% C57BL/6J background but still no phenotype was observed. Detailed post-mortem analysis by the histopathology laboratory at LRI (see Appendix) also revealed no abnormalities in ULK1KO mice.

There are several explanations for the lack of a severe phenotype in ULK1KO mice. Firstly, there is a small possibility that the gene was not completely inactivated by the gene trap insertion but this is unlikely given the upstream 5' location of the reporter cassette and its location inside the kinase domain. Secondly, the only ES cells to survive the selection process may have carried a mutation or polymorphism that leads to enhanced ULK2 expression or another compensating mechanism. Thirdly, compensation may have occurred during development leading to an increase in ULK2 levels. Lastly, ULK1 dependency for autophagic function may be a feature applying to immortalised cells in culture and not *in vivo* for unknown reasons but possibly linked to the immortalisation process.

Intron: 1.5 kb of Mouse En2 intron 1
SA: splice acceptor of mouse En2 exon 2
β-gal/neo: fusion of β-galactosidase and neomycin transferase
pA: SV40 polyadenylation signal

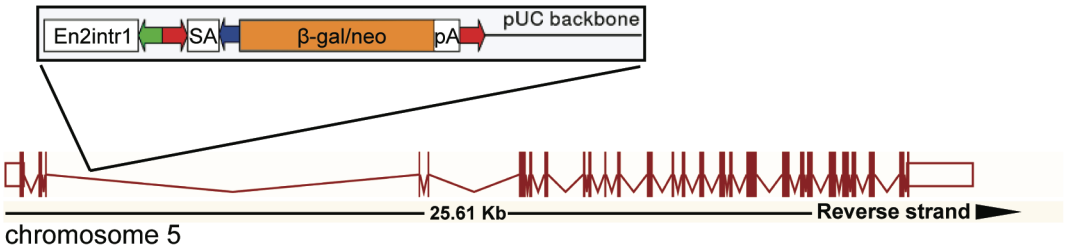

ULK1 mus musculus

MEPGRGGVETVGKFEFSRKDLIGHGAFAVVFKGRHREKHDLEVAVKCINKK
NLAKSQTLLGKEIKILKELKHENIVALYDFQ

GENE TRAP

EMANSVYLVMEYCNGGDLADYLHTMRTLSEDTVRLFLQQIAGAMRLLHSKG
IIHRDLKPQNILLSNPGGRRANPSNIRVKIADFGFARYLQSNMMAATLCGSP
MYMAPEVIMSQHYDGKADLWSIGTIVYQCLTGKAPFQASSPQDLRLFYEKN
KTLVPAIPRETSAPLRQLLLALLQRNHKDRMDFDEFFHHPFLDASTPIKKSPP
VPVPSYPSSGSGSSSSSSSASHLASPPSLGEMPQLQKTLTSPADAAGFLQG
SRDSGGSSKDSCDTDDFVMVPAQFPGDLVAEAASAKPPPDSLLCSGSSLV
ASAGLESHGRTPSPSPTCSSSPSPSGRPGPFSSNRYGASVPIPVPTQVHNY
QRIEQNLQSPTQQQTARSSAIRRSGSTSPLGFGRASPSPPSHTDGAMLARK
LSLGGGRPYTPSPQVGTIPERPSWSRVPSPQGADVRVGRSPRPGSSVPEH
SPRTTGLGCRLHSAPNLSDFHVVRPKLPKPPTDPLGATFSPPQTSAPQPCP
GLQSCRPLRGSPKLPDFLQRSPLPPILGSPTKAGPSFDFPKTPSSQNLLTLL
ARQGVVMTPPRNRTLPDLSEASPFHGQQLGSGLRPAEDTRGPFGRSFSTS
RITDLLLKAAFGTQASDSGSTDSLQEKPMEIAPSAGFGGTLHPGARGGGAS
SPAPVVFTVGSPPSGATPPQSTRTRMFSVGSSSSLGSTGSSSARHLVPGA
CGEAPELSAPGHCCSLADPLAANLEGAVTFEAPDLPEETLMEQEHTETLHS
LRFTLAFAQQVLEIAALKGSASEAAGGPEYQLQESVVADQISQLSREWGFAE
QLVLYLKVAELLSSGLQTAIDQIRAGKLCLSSTVKQVVRRLNELYKASVVSCQ
GLSLRLQRFFLDKQRLLDGIHGVTAERLILSHAVQMVQSAALDEMFQHREG
CVPRYHKALLLLEGLQHTLTDQADIENIAKCKLCIERRLSALLSGVYA

Blue highlighting indicates alternate exons.
Red highlighting indicates amino acids encoded across a splice junction.
GENE TRAP indicates where the gene trap cassette was inserted.

Figure 6-1 ULK1 knock-out mice were created using gene trapped ES cells
ES cells were obtained from the Sanger institute gene trap resource and injected into C57BL/6J blastocysts to create chimeric mice harbouring a disrupted ULK1 gene in the germ line. The gene trap

cassette has inserted in an intronic region after exon 3 in a very upstream 5' region of the ULK1 gene, which is found on chromosome 5 in mice and contains 28 exons encoding a 1051 amino acid protein. In the ULK1 knock-out mice instead, a fusion protein containing the first 81 amino acids of ULK1 followed by the β-galactosidase-neomycin transferase fusion protein is transcribed. Importantly, the ULK1 gene was interrupted at the N-terminal region of the kinase domain, which should essentially inactivate the protein.

To investigate whether basal autophagy is impaired in ULK1KO mice several tissues were analysed for LC3 lipidation by western blotting. For this wild type, heterozygous and knock-out sex-matched littermates were sacrificed, and organs or tissues were removed and shock-frozen in liquid nitrogen. Tissues tested included: whole brain, heart, liver, lung, kidney, pancreas, and skeletal muscle from the thigh. Tissues were then lysed in 4 to 5 times their weight of TNTE and homogenised using a polytronic homogeniser. Protein content in cleared lysates was measured by Bradford assay and 60µg protein was loaded per lane. Membranes were blotted with antibodies against ULK1, actin as a loading control, and LC3. No differences in basal LC3 lipidation between wild type, heterozygous and knock-out mice could be observed in any of the tissues tested (Fig. 6-2). Ponceau staining of membranes revealed two thick bands running at roughly the same size as LC3, which probably represent haemoglobin. In tissues where haemoglobin is particularly high, the LC3 antibody bound inefficiently and the western blot staining could probably not reveal all LC3 bound to the membrane. In the liver, LC3-II is much more prevalent and no LC3-I could be detected. Actin staining for the pancreas was uneven and there may have been some degradation in the heterozygous and knock-out samples, which could be due to handling differences. ULK1 could not be visualised in all tissues even though it is reported to be expressed ubiquitously (Fig. 6-2). This may reflect different protein levels or be due to the

appearance of different background bands. However, this analysis was only done once and should be repeated optimising ULK1 blotting.

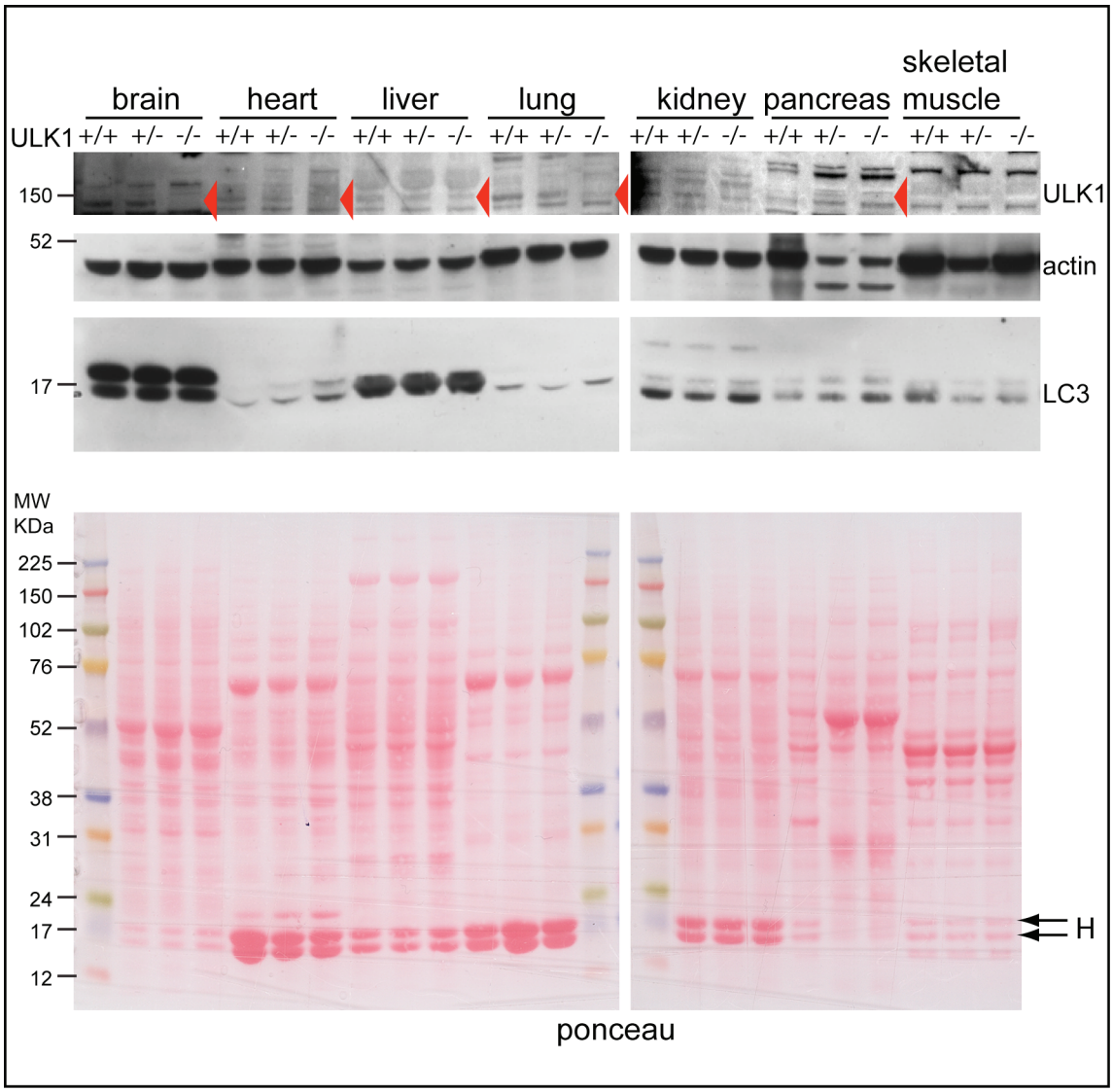

Figure 6-2 Basal autophagy is not affected in ULK1KO mouse tissues
A wild type, a heterozygous, and a knock-out mouse were sacrificed, and organs or tissues were removed and shock-frozen in liquid nitrogen. Tissues tested were: whole brain, heart, liver, lung, kidney, pancreas, and skeletal muscle from the thigh. Tissues were then lysed in 4 times their weight of TNTE containing protease and phosphatase inhibitors except for the liver with 5 times its weight in TNTE because of relatively high protein content. Tissue lysates were homogenised using a polytronic homogeniser and cleared by short centrifugation for 5 min. at 2500g. All these steps were done at 4ºC. Protein content in cleared lysates was measured by Bradford assay and samples were heated to 65ºC for 15min. in 5X sample buffer. 60µg of protein was loaded in each lane and membranes were stained with ponceau (shown below) and afterwards labelled with anti-ULK1, anti-actin, and anti-LC3 antibodies. ULK1 band

where detectable is indicated by red arrowheads. In tissues with high haemoglobin content (marked by H and two arrows) the LC3 band was hard to visualise as the large haemoglobin band probably prevents efficient anti-LC3 binding. This analysis was done once with 3 littermate sex-matched mice.

6.3 ULK1KO mice have reduced thymic cellularity but the T cell populations look normal

Some post-mortem reports on ULK1KO mice that had died of old age stated that in several cases they had a small thymus, which was never reported for wild type mice. Furthermore, during the course of this investigation another group reported reticulocyte maturation defects in ULK1KO mice [81] although they only observed this in a mixed C57B/6, 129Sv, and FVB/N background mouse strain but not a pure C57BL/6J strain (personal communication). These findings prompted me to investigate the hematopoietic system of ULK1KO mice more closely. I first investigated the thymus, which is the site of T cell maturation in which autophagy plays an important role [244, 282]. Thymi were removed from ULK1 wild type (WT), heterozygous (HET), and knock-out (KO) sex matched littermates and processed through a 70μm mesh into fresh medium to obtain primary thymocytes. Red blood cells (RBCs) were removed by incubation in RBC lysis buffer for 5 min. This buffer is slightly hypotonic leading to RBC lysis with minimal effects on other cells. Some thymocytes were left in full medium or starved for 2.5 hours in EBSS with leupeptin lysed and analysed by anti-LC3 western blotting. No difference in basal autophagy between WT, HET, or KO fed thymocytes could be observed (Fig. 6-3a). Autophagy seems to be slightly enhanced in all starved thymocytes with a slight increase in lipidated LC3 in ULK1KO cells compared to cells that have some ULK1. ULK1 staining revealed that HET thymocytes

have half as much ULK1 protein as WT cells with the band disappearing completely in the KO cells, as expected. However, this analysis should be optimised and repeated to allow quantification of LC3 conversion.

For FACS analysis 10^6 thymocytes from each mouse were labelled with anti-CD4 and anti-CD8 antibodies to reveal the major T cell populations and FACS profiles were acquired for 1min each with gates set on live single cells. The FACS profile of ULK1WT, HET, or KO thymi revealed no substantial differences in the percentage of mature CD4+ (~10%) and CD8+ T (~5%) cells or immature double positive (~77%) T cells (Fig. 6-3b). Since autophagy may also act as a type II programmed cell death pathway and enhanced autophagy in starved ULK1KO thymocytes may lead to enhanced apoptosis the cells were also labelled with AnnexinV and DAPI. Early apoptotic cells display phosphatidylserine (PS) on their surface, which is only located to the inner plasma membrane leaflet in healthy cells and AnnexinV binds PS therefore labelling early apoptotic cells specifically. DAPI binds DNA and reveals necrotic or late apoptotic bodies. However there was no difference in the percentage of apoptotic CD4+ or CD8+ T cells between ULK1WT, HET or KO thymi (Fig. 6-3c) nor in the double positive or double negative thymocyte populations (not shown). There do seem to be less T cells in total however in the ULK1KO thymus (137,464 cells) compared to the ULK1WT thymus (176,513 cells) with the HET thymus having an intermediate phenotype (154,715 cells).

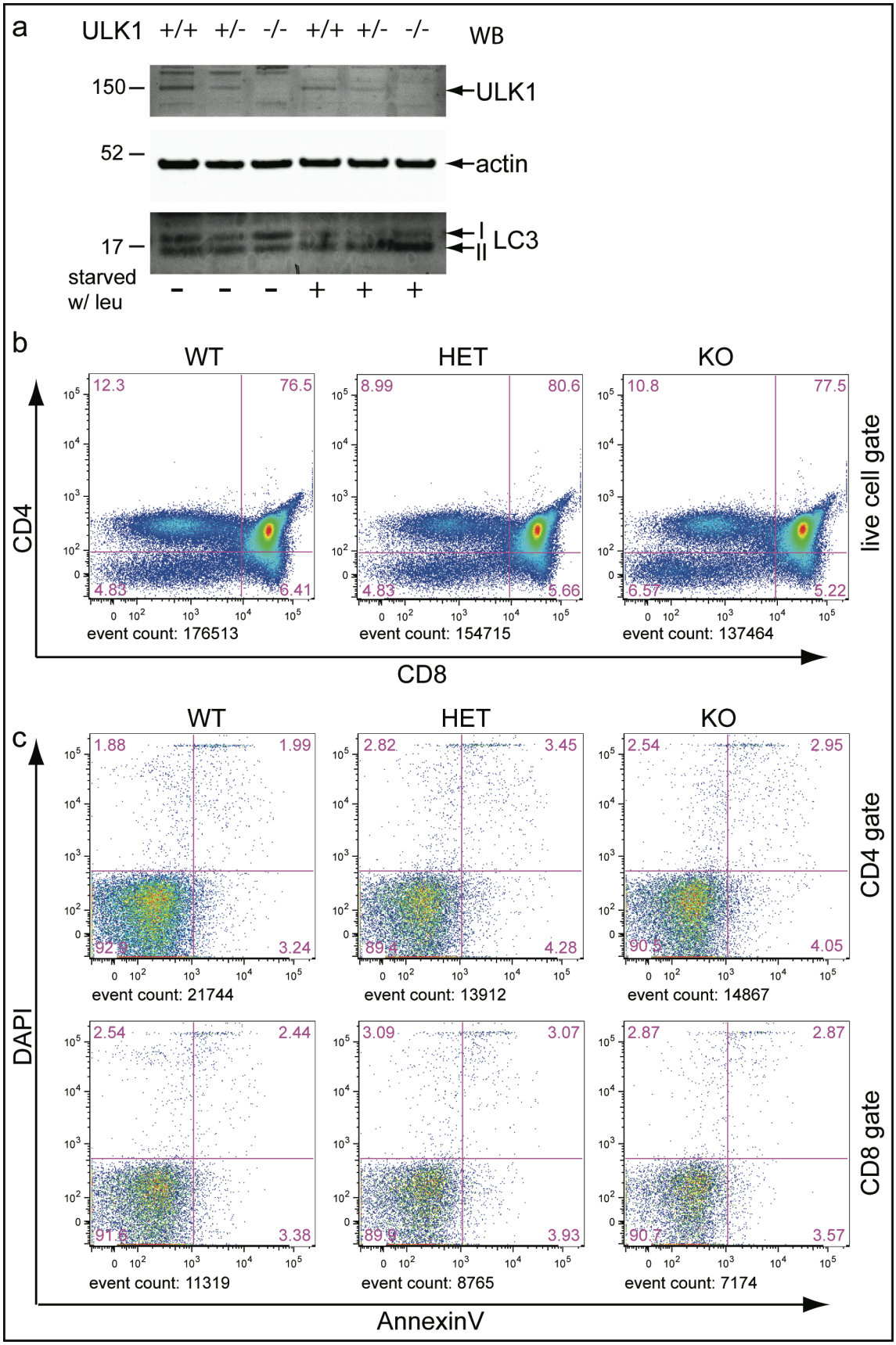
a
ULK1 +/+ +/- -/- +/+ +/- -/-
WB
150
ULK1
52
actin
17
I
II
LC3
starved
w/ leu
- - - + + +
b
WT
HET
KO
12.3
76.5
4.83
6.41
event count: 176513
8.99
80.6
4.83
5.66
event count: 154715
10.8
77.5
6.57
5.22
event count: 137464
CD4
CD8
live cell gate
c
WT
HET
KO
1.88
1.99
92.9
3.24
event count: 21744
2.82
3.45
89.4
4.28
event count: 13912
2.54
2.95
90.5
4.05
event count: 14867
2.54
2.44
91.6
3.38
event count: 11319
3.09
3.07
89.9
3.93
event count: 8765
2.87
2.87
90.7
3.57
event count: 7174
DAPI
AnnexinV
CD4 gate
CD8 gate

Figure 6-3 ULK1KO thymocytes can undergo autophagy
Thymi were removed from ULK1 wild type (WT), heterozygous (HET), and knock-out (KO) sex-matched littermates and processed through a 70μm mesh to harvest thymocytes. Cells were incubated for 5min in red blood cell (RBC) lysis buffer to remove RBCs. **(a)** One group of thymocytes was starved for 2.5h in EBSS with leupeptin (leu) or left in full medium, lysed and run on SDS-PAGE for western blotting with anti-LC3, anti-actin, and anti-ULK1 antibodies. **(b,c)** The other group was labelled with DAPI, AnnexinV, and antibodies against CD4 and CD8 for FACS analysis. 10^6 cells were resuspended in FACS buffer and the FACS profile was acquired for 1 min each with gates set on single live cells. **(b)** FACS profiles of CD4 and CD8 positive T cell populations of ULK1WT, HET and KO thymi. **(c)** FACS analysis of T cell apoptosis for CD4+ gate (top) and CD8+ gate (bottom).

As shown above there was no difference in basal autophagy in thymocytes lacking ULK1 as compared to the wild type cells. However, since the vast majority of thymocytes consist of T cells it would probably not be detectable by western blot analysis if there were a defect in autophagy in a small population of cells such as dendritic cells or thymic epithelial cells, which use autophagy to present endogenous antigens via MHC-II molecules to CD4+ T cells [244]. To look at different subpopulations of thymocytes cells were FACS sorted by the LRI sorting facility into CD4+, CD8+, double positive and double negative cells. Not enough cells could be harvested for LC3 western blot analysis but as in the previous experiment (and as noted in the post-mortem report) there seemed to be about 3 times less cells in the ULK1KO and HET thymi as compared to the WT thymus (Table 2). However, this data is preliminary and needs further confirmation.

Table 6-1 Thymocyte FACS sorting reveals lower total cellularity in ULK1HET and KO thymi

Thymocytes from entire thymi of ULK1WT, HET, and KO mice were labelled with anti-CD4, and anti-CD8 antibodies and FACS sorted into the four different populations. Cells were counted during sorting and the total numbers are shown in this table.

	WT	HET	KO
Double positive T cells	$13.4x10^6$ (82%)	$3.4\ x10^6$ (67%)	$3.2\ x10^6$ (57%)
CD4+ T cells	$1.7\ x10^6$ (10%)	895000 (17%)	$1.02\ x10^6$ (18%)
CD8+ T cells	613000 (4%)	340000 (7%)	360000 (6%)
Double negative cells	679000 (4%)	450000 (9%)	$1.08\ x10^6$ (19%)
Total cellularity	$16.4\ x10^6$	$5.1\ x10^6$	$5.7\ x10^6$

6.4 ULK1KO mice have less mature T cells

It has been shown that T cells derived from Atg5 knock-out (Atg5KO) mice deficient in autophagy are reduced in number but develop normally and only when they reach the peripheral circulation and spleen show defects in survival and proliferation [283]. Therefore, I next investigated mature T cells from the spleen of ULK1KO mice. The ULK1 deficient mice had been reported to have mild splenomegaly [81] and indeed this is the case in our strain as well as observed repeatedly (Fig. 6-4a). Splenocytes from sex-matched littermates were FACS sorted into CD4, CD8, CD19 and triple negative cell populations. CD19 labels mostly B cells, which are practically absent in the thymus but abundant in the spleen where they act as co-activators of naïve T cells. The four subpopulations including whole splenocytes before sorting were harvested for western blot analysis to assess autophagic activity via LC3 lipidation. A Bradford assay was used to quantify protein concentration in each sample and 75µg protein was loaded in each well unless the volume would have exceeded 60µl (the maximum that can be

added to a well). All three cell types CD4+ and CD8+ T cells as well as B cells had mostly lipidated LC3-II indicating that they are undergoing basal autophagy (Fig. 6-4b). Starvation in culture did not seem to induce any more autophagy in these cells. Triple negative cells, which constitute a mixture of other cell types also showed basal autophagy in WT as well as ULK1KO cells and a two hour treatment with EBSS with leupeptin also did not increase autophagic activity dramatically. However, LC3 lipidation measurements should be repeated for quantification and statistical analysis.

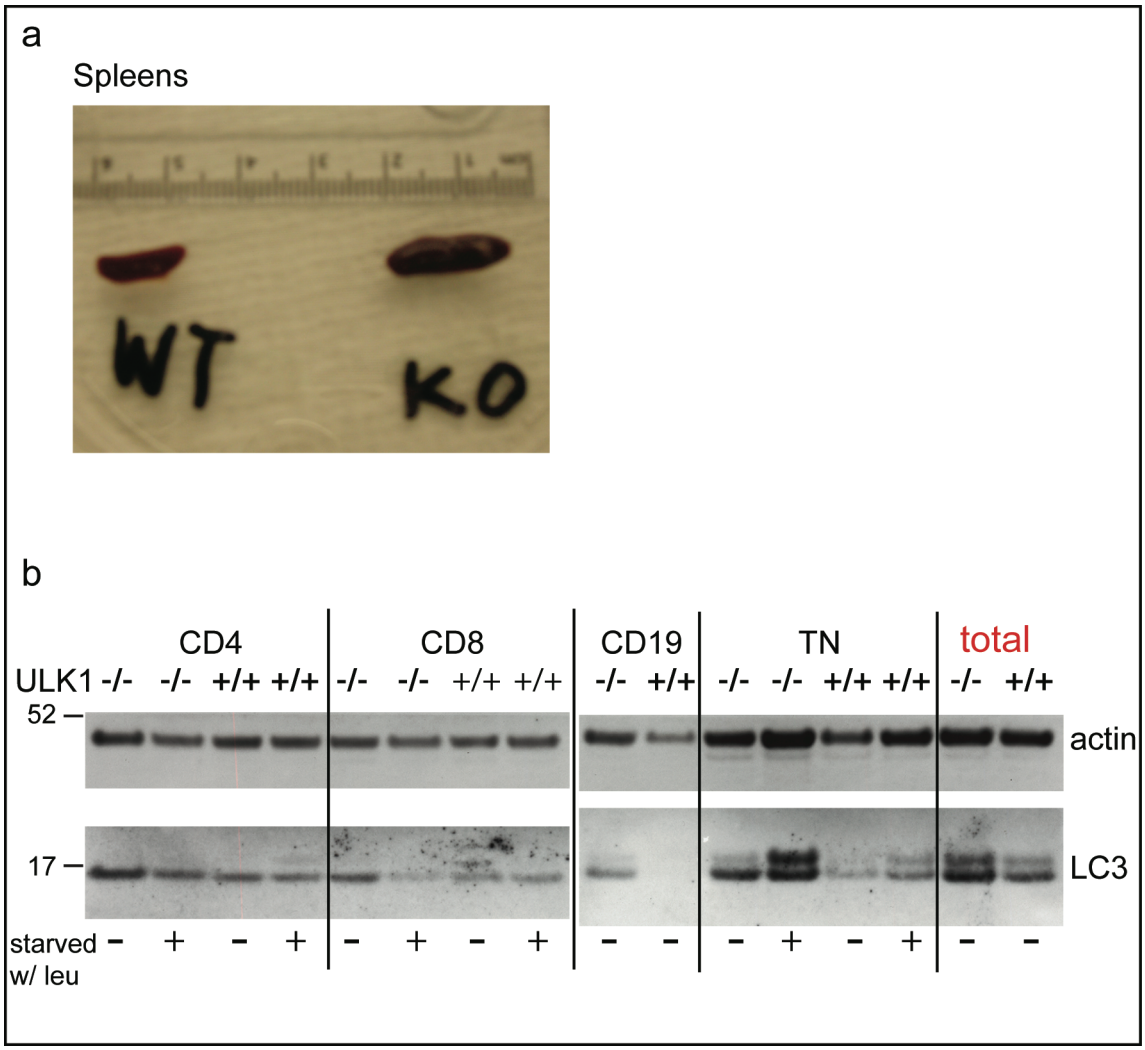

Figure 6-4 ULK1KO mice have splenomegaly but mature T cells from the spleen of ULK1KO mice can undergo autophagy

(a) Spleens from ULK1WT and KO sex-matched littermates. **(b)** Western blot for LC3 and actin with splenocytes from ULK1WT and KO littermates. Splenocytes were FACS sorted using antibodies against CD4, CD8, and CD19 (B cells and follicular dendritic cells) and starved for 2h in EBSS with leupeptin or left in full RPMI for 2h as was done with a fraction of unsorted splenocytes (total). Equal protein was loaded (75µg) except for samples with low protein concentration as assessed by a Bradford assay, in which case 60µl were loaded onto the gel. All 3 subpopulations and the triple negative (TN) cells were run on SDS-PAGE and membranes were blotted with anti-LC3 and anti-actin.

To investigate whether peripheral T cells are affected by the absence of ULK1 splenocytes from wild type, heterozygous, and knock-out littermate mice were analysed by FACS. Cells were labelled for CD4 and CD8 T cell markers, for CD19 a B cell and follicular dendritic cell marker and for DAPI and AnnexinV to analyse apoptosis. The FACS profile of WT, HET, and KO splenocytes revealed that there are indeed less CD4 (WT~15%, KO~10%) and CD8 (WT~8%, KO~5%) positive T cells in spleens of KO mice as they are reduced in percentage as well as number (Fig. 6-5). The HET splenocytes show an intermediate phenotype and these results are reproducible (n=2) suggesting that ULK1 may be involved in T cell development, selection, and/or survival. CD19 positive B cells and follicular dendritic cells, which assist in B cell maturation [284], were not affected by lack of ULK1.

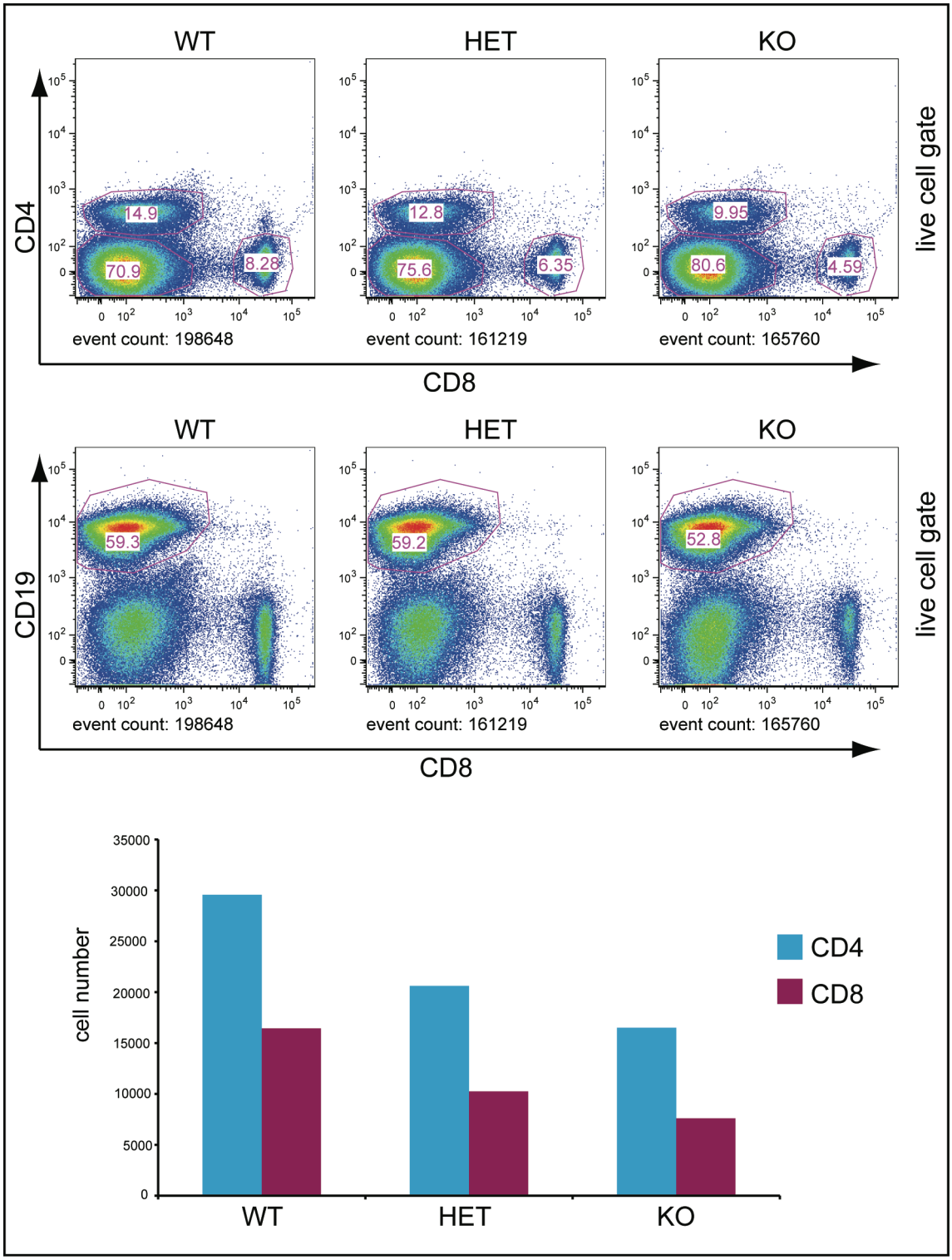

Figure 6-5 Peripheral CD4 and CD8 positive T cell numbers are reduced in ULK1KO mice

Spleens were removed from ULK1 wild type (WT), heterozygous (HET), and knock-out (KO) sex-matched littermates and processed through a 70µm mesh to harvest splenocytes. Cells were incubated for 5min in RBC lysis buffer to remove RBCs. These cells were labelled with antibodies against CD4, CD8,

and CD19 for FACS analysis. 10^6 cells were resuspended in FACS buffer and the FACS profile was acquired for 1 min each. The graph shows total numbers of CD4+ and CD8+ T cells, which are reduced in ULK1HET and KO mice compared to the WT as was seen repeatedly (n=2).

6.4.1 ULK1KO splenocytes show enhanced apoptosis

As mentioned above these splenocytes were also labelled with DAPI and AnnexinV to analyse the amount of apoptosis. When gated on CD4+, CD8+, or CD19+ cells more apoptotic CD4+, and CD8+ T cells are observed in the spleens of KO mice compared to WT animals with the HETs again showing an intermediate phenotype. CD19+ B cells show no substantial enhancement in apoptosis (Fig. 6-6). Both early apoptosis (AnnexinV positive) and late apoptosis or necrotic cell death (AnnexinV positive and high DAPI) are enhanced in the ULK1KO splenocytes, which could explain the reduced numbers of T cells in the KO spleen. However, it cannot be excluded that there is also a proliferation defect.

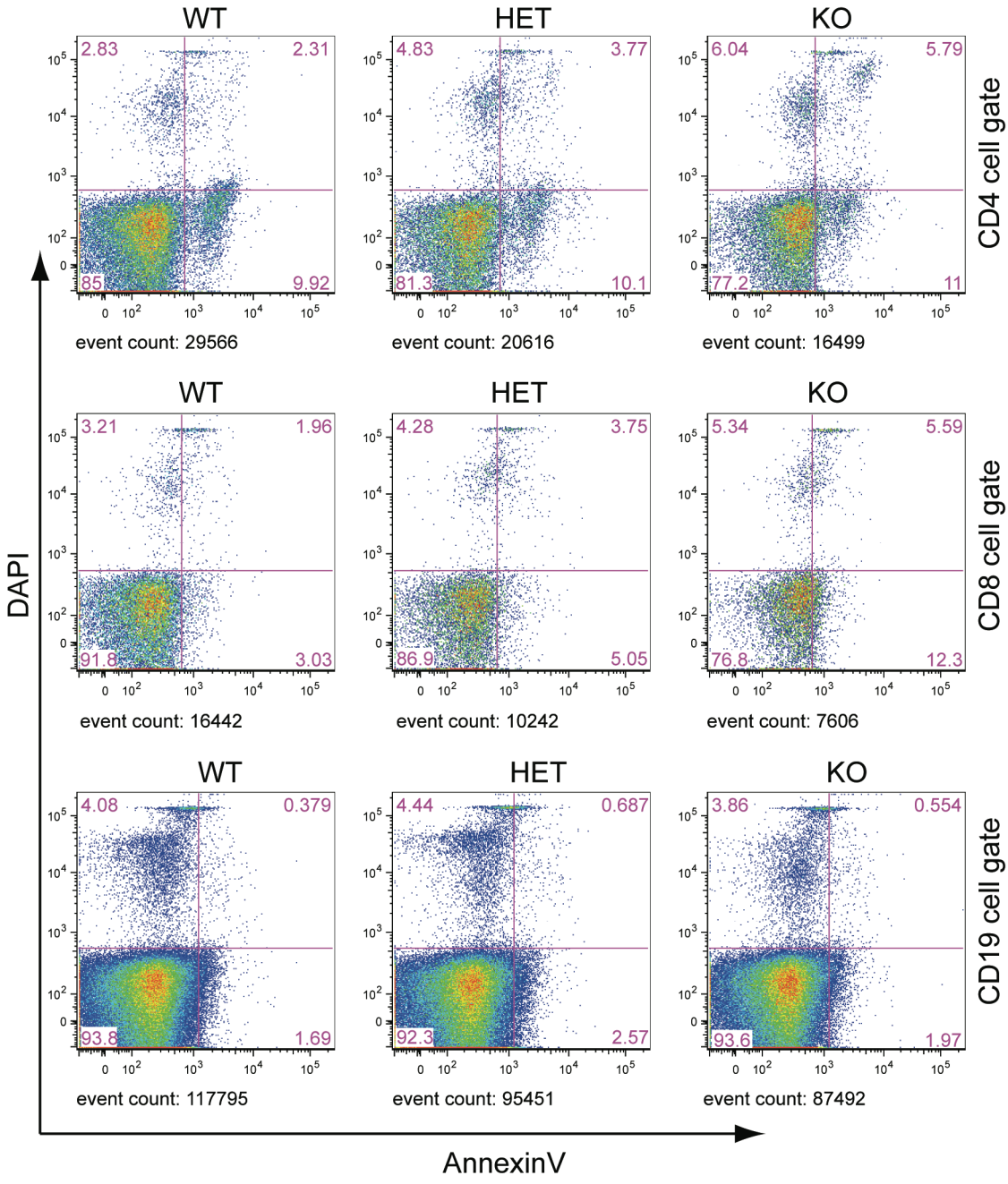

Figure 6-6 Peripheral T cells from ULK1KO mice show enhanced apoptosis
The same splenocytes as in Figure 6-5 were labelled with AnnexinV and DAPI for FACS analysis. 10^6 cells were resuspended in FACS buffer and the FACS profile was acquired for 1min each. Gates were set on, CD4 positive T cells (top), CD8 positive T cells (middle), or CD19 positive B cells.

6.5 ULK1KO splenocytes show a significant deficit in response to TCR stimulation compared to WT cells

To confirm these preliminary results, and obtain further insight into the ability of ULK1KO T cells to be activated, I investigated their response to T cell receptor (TCR) stimulation. TCR can be stimulated experimentally by activating anti-CD3ε and co-stimulatory signals, which are normally provided by antigen presenting cells (APCs) [285]. Anti-CD3ε diluted in PBS was bound to 96-well plates over night in various concentrations via serial dilution. Splenocytes were harvested from ULK1WT or KO littermate mice and $0.5x10^6$ cells were added to each well in full medium. RBCs were not lysed by incubation in RBC-lysis buffer as in previous experiments to prevent even minimal damage to other splenocytes. Cells were incubated for 72 hours during which anti-CD3ε will activate the TCR leading to T cell activation, proliferation, and cytokine secretion. Essential co-stimulatory signal are provided by APCs present in the splenocyte preparation. After 3 days the amount of metabolically active cells per well was measured using the CellTitre-Glo® luminescent cell viability assay. This assay determines the amount of ATP in the sample, which is directly proportional to the amount to metabolically active live cells. Luminescence was measured using an Envision plate reader. Although activation of T cells may also lead to proliferation of co-stimulatory APCs through cytokine secretion the bulk of the proliferating cells are probably T cells.

The response of ULK1KO splenocytes is significantly impaired compared to wild type cells (Fig. 6-7). In ULK1WT cultures an increase in cell number is first observed after

stimulation with about 0.5µg/ml anti-CD3ε peaking at 2.5µg/ml. This is significantly delayed in ULK1KO cultures, whose number only peak at a concentration of 5-10µg/ml anti-CD3ε possibly due to a reduction in cell proliferation or enhancement of apoptosis or induction of anergy a state of non-responsiveness that can be induced in lymphocytes [286].

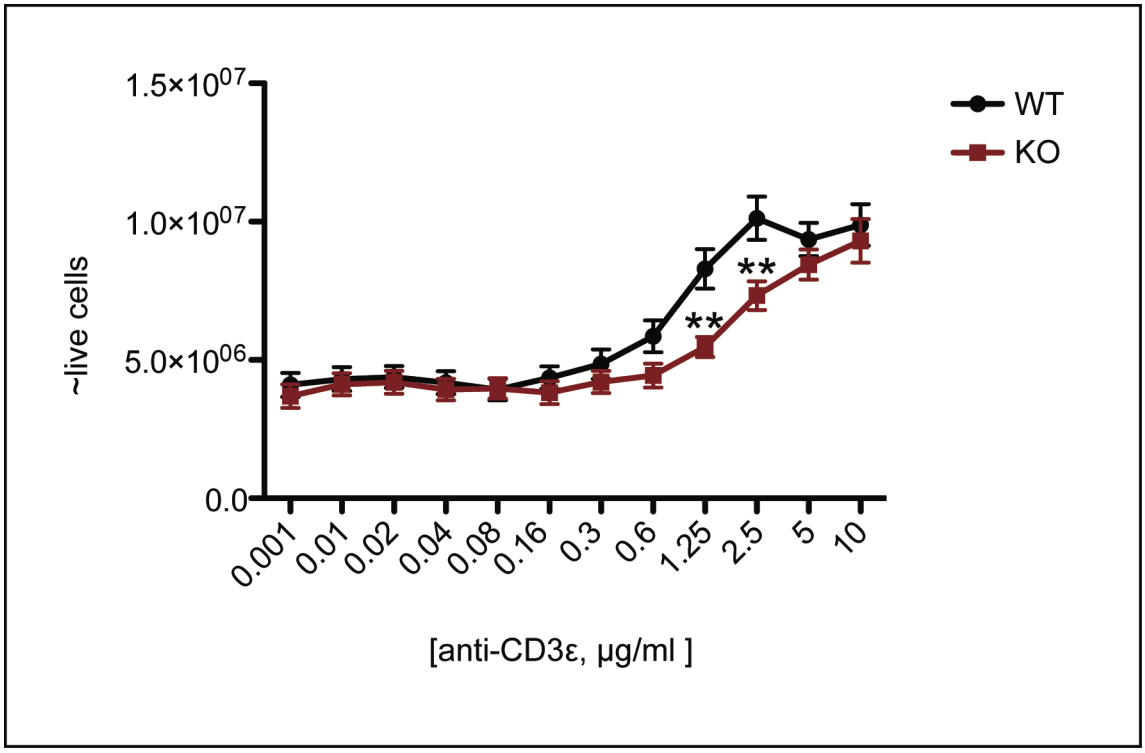

Figure 6-7 ULK1KO splenocytes show an impaired response to TCR stimulation with anti-CD3ε

Spleens were removed from ULK1WT and KO sex-matched littermates and passed through a 70µm mesh to obtain splenocytes. Red blood cells were not removed by lysis to avoid damage to other splenocytes. $0.5x10^6$ cells were plated per well of a 96-well plate, which had been coated over night with the indicated concentration of anti-CD3ε in PBS. Cells were incubated for 72h in normal growth conditions with each concentration done in triplicate. CellTitre-Glo reagent was added to each well according to the manufacturers instructions and luminescence was measured using an Envision plate reader. Y-axis shows luminescence intensity, which is directly proportional to live metabolically active cells. Shown is the mean of 4 independent experiments (n=4) and error bars represent SEM. Asterisks indicate result of two-way ANOVA analysis with p=0.0429 overall, and Bonferroni posttests results for 1.25µg/ml $p<0.01$; for 2.5µg/ml $p<0.01$.

6.5.1 The FACS profile of anti-CD3ε stimulated splenocytes suggests that there is more apoptosis in ULK1KO cells

The above result suggests that either ULK1KO splenocytes undergo more apoptosis or proliferate less upon anti-CD3ε stimulation. To address this question the FACS profiles of various concentrations were analysed. Splenocytes were treated as described above and while 3 wells per condition were used for the CellTitre-Glo assay the remaining well was prepared for FACS analysis. The cells were labelled with antibodies against CD4, CD8, and with a nucleic acid binding dye TO-PRO3 to identify late apoptotic and necrotic cells. Reflecting the previous results, the percentage of both CD4 (WT~12%, KO~5% at 0.07µg/ml anti-CD3ε) and CD8 (WT~7%, KO~2% at 0.07µg/ml anti-CD3ε) positive T cells was lower in ULK1KO splenocytes. T cell populations are activated and proliferate upon anti-CD3ε stimulation in KO cultures but at a lower rate than the in the WT and they never reach the same levels as ULK1WT cultures (CD4+: WT~20%, KO~11% at 10µg/ml anti-CD3ε; CD8+: WT~24%, KO~18% at 10µg/ml anti-CD3ε) (Fig. 6-8a).

The late apoptotic/necrotic marker TO-PRO3 revealed that there are more dead cells in the ULK1KO wells than in the WT wells at low (WT~5%, KO~8% at 0.07µg/ml anti-CD3ε) as well as at high concentrations of anti-CD3ε (WT~9%, KO~16% at 10µg/ml anti-CD3ε; Fig. 6-8b). Only the CD4 positive T cell population is shown in Figure 6-8b but the CD8 positive population looks very similar (data not shown). Most dead cells are not CD4 positive but in any case I would expect late apoptotic or necrotic T cells revealed by this analysis not to display T cell markers anymore. This strongly suggests

that there is more apoptosis in ULK1KO spleens compared to the WT but does not exclude additional proliferation defects.

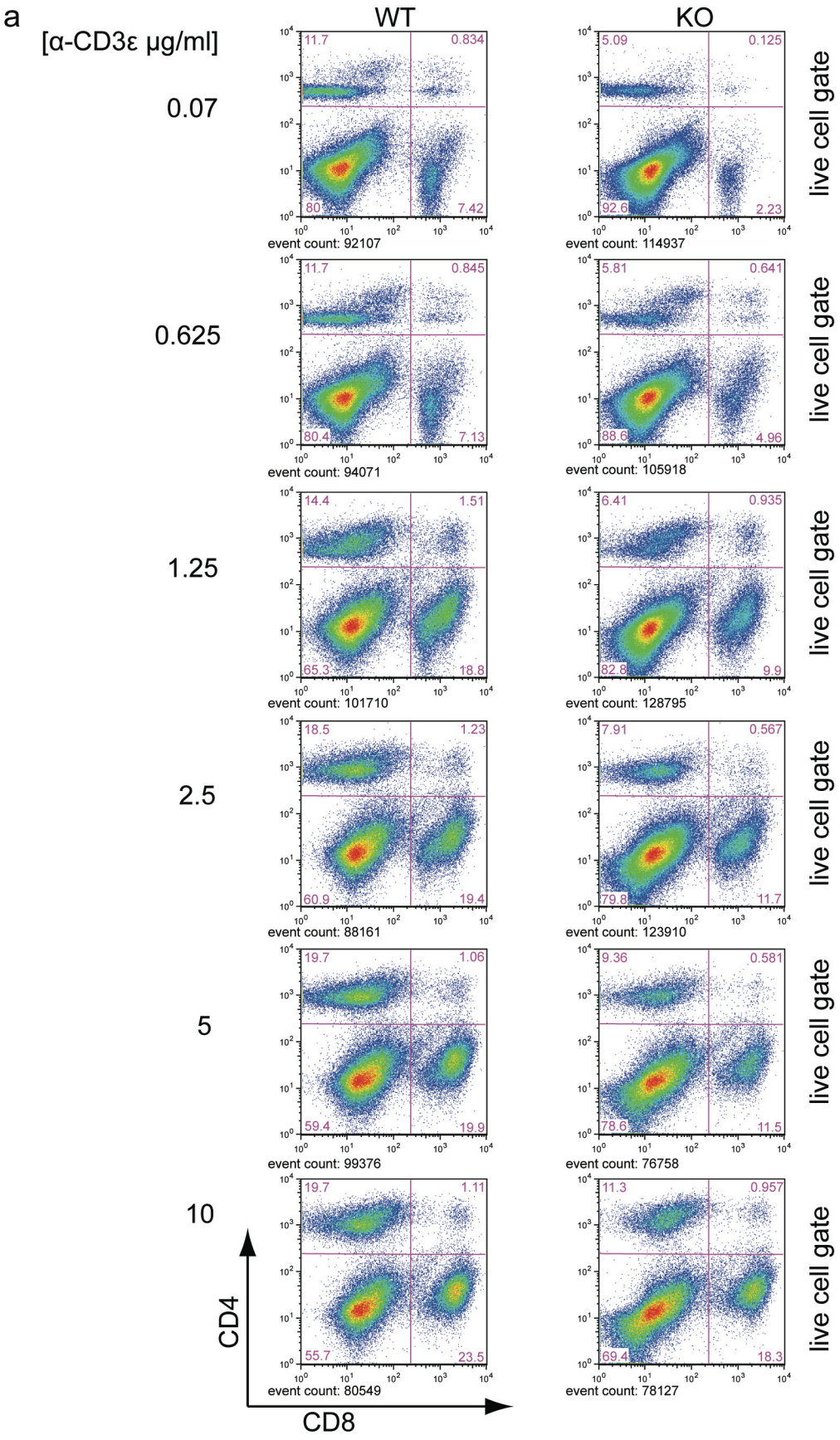
a
[α-CD3ε µg/ml]
WT
KO
0.07
11.7
0.834
80
7.42
event count: 92107
5.09
0.125
92.6
2.23
event count: 114937
0.625
11.7
0.845
80.4
7.13
event count: 94071
5.81
0.641
88.6
4.96
event count: 105918
1.25
14.4
1.51
65.3
18.8
event count: 101710
6.41
0.935
82.8
9.9
event count: 128795
2.5
18.5
1.23
60.9
19.4
event count: 88161
7.91
0.567
79.8
11.7
event count: 123910
5
19.7
1.06
59.4
19.9
event count: 99376
9.36
0.581
78.6
11.5
event count: 76758
10
19.7
1.11
55.7
23.5
event count: 80549
11.3
0.957
69.4
18.3
event count: 78127
live cell gate
CD4
CD8

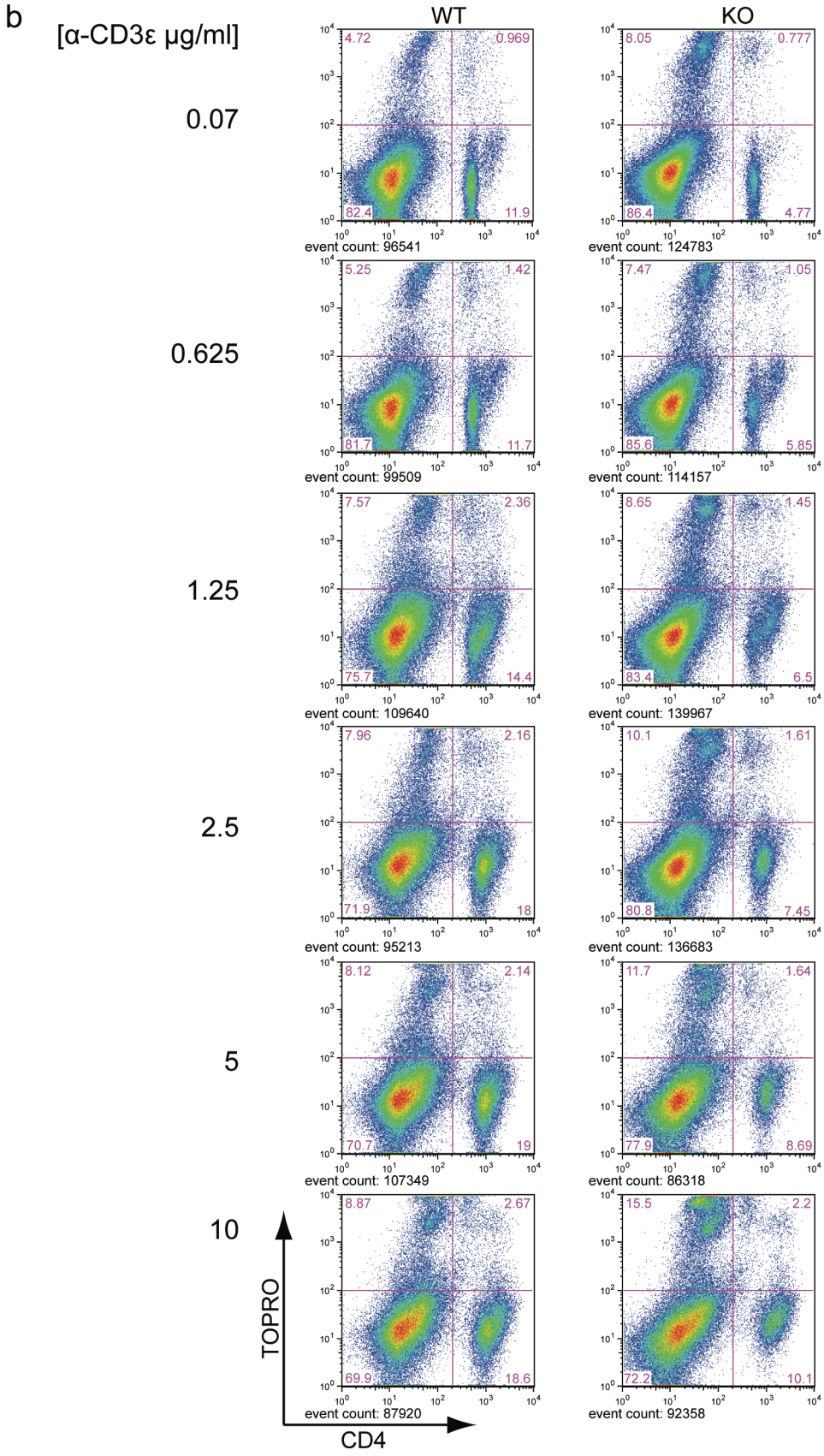
b
[α-CD3ε μg/ml]
WT
KO
0.07
4.72
0.969
82.4
11.9
event count: 96541
8.05
0.777
86.4
4.77
event count: 124783
0.625
5.25
1.42
81.7
11.7
event count: 99509
7.47
1.05
85.6
5.85
event count: 114157
1.25
7.57
2.36
75.7
14.4
event count: 109640
8.65
1.45
83.4
6.5
event count: 139967
2.5
7.96
2.16
71.9
18
event count: 95213
10.1
1.61
80.8
7.45
event count: 136683
5
8.12
2.14
70.7
19
event count: 107349
11.7
1.64
77.9
8.69
event count: 86318
10
8.87
2.67
69.9
18.6
event count: 87920
15.5
2.2
72.2
10.1
event count: 92358
TOPRO
CD4

Figure 6-8 Anti-CD3ε stimulated ULK1KO splenocytes show enhanced apoptosis
Splenocytes were treated the same as in Figure 6-7 and while 3 wells were used for the CellTitre-Glo assay, one well per condition was prepared for FACS analysis, which was performed for the indicated anti-CD3ε concentrations. Cells were labelled with antibodies against CD4, CD8, and a nucleic acid binding dye TO-PRO3, which stains late apoptotic and necrotic cells. **(a)** FACS profile of splenocytes illustrating CD4 and CD8 cell populations. **(b)** FACS profile of cells illustrating CD4 and TOPRO positive cells.

6.6 CFSE proliferation assay shows impairment in ULK1KO cells

Another way to measure cell proliferation and survival is by incorporation of the fluorescent dye carboxyfluorescein succinimidyl ester (CFSE), which is retained in the cytosol [287]. Therefore, fluorescence intensity is reduced by half after every cell division and this can easily be measured by FACS analysis.

Splenocytes from ULK1WT and KO littermates were labelled with CFSE and cultured in various conditions for 4 days. The different conditions were: no treatment (no cell divisions are expected without stimulus); anti-CD3ε; anti-CD3ε with co-stimulatory anti-CD28; anti-CD3ε with growth factor IL-2; phorbol 12-myristate 13-acetate (PMA) with ionomycin. As described above anti-CD3ε leads to activation of TCR signalling together with its co-activator anti-CD28. CD28 on antigen presenting cells (APCs) present in the culture can provide this co-stimulatory signal but exogenous addition of anti-CD28 should enhance the stimulatory signal. IL-2 is an important cytokine that is massively produced by T cells and other cells after activation leading to T cell proliferation and survival. PMA activates protein kinase C (PKC) due to its similarity to diacylglycerol (DAG) and ionomycin is an ionophore leading to enhanced intracellular

calcium levels. These last two events are usually the downstream signalling events of TCR activation but PMA/ionomycin addition can by-pass these signalling events to elucidate whether any block in T cell activation is downstream or upstream of kinase signalling.

The response of ULK1KO CD4-positive T cells to anti-CD3ε and anti-CD3ε/anti-CD28 is dramatically impaired compared to control cells as the peaks of the dividing cells are much reduced (Fig. 6-9a). This seems to be rescued by supplementing IL-2 or by addition of PMA/ionomycin suggesting that ULK1KO splenocytes have a defect in IL-2 signalling or production. Interestingly, when the total cell number is calculated it seems that IL-2 administration could not really rescue CD4+ T cell expansion, as T cell numbers were not increased in IL-2 treated wells compared to untreated wells (Fig. 6-9b). However, the proliferative ability of ULK1KO CD4+ T was rescued by IL-2 addition since there is a large peak of dividing cells in the CFSE assay suggesting that cells underwent cell division but died or became anergic and therefore could not expand. The ULK1HET cells again show an intermediate phenotype to the ULK1KO (not shown). Note also that in the anti-CD3ε, or anti-CD3ε/anti-CD28 treated wells small peaks can be observed but no T cell expansion is taking place suggesting that they may be able to proliferate but may undergo apoptosis or anergy much more than ULK1WT cells.

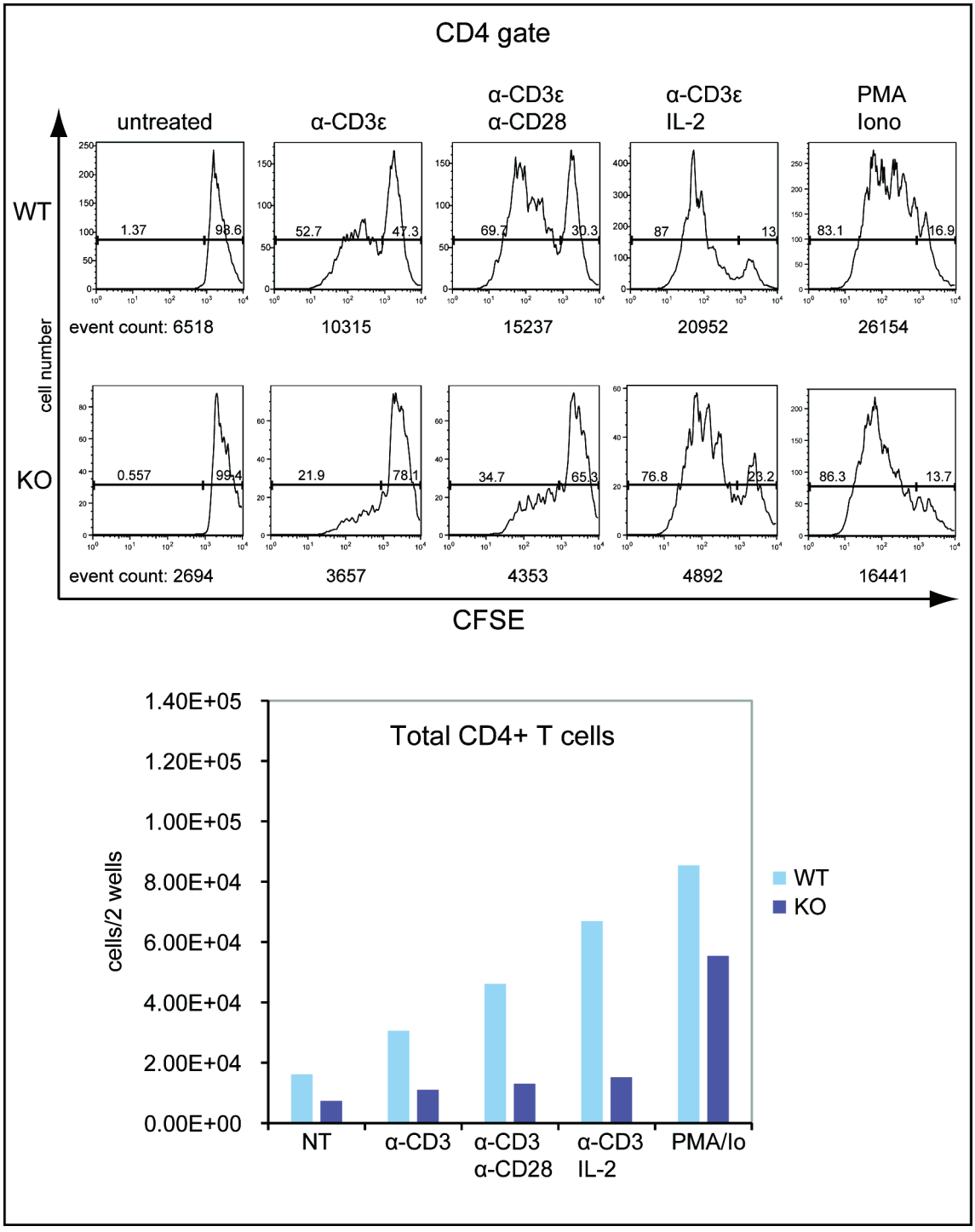

Figure 6-9 ULK1KO CD4 positive T cells show an impaired response to TCR stimulation

Spleens were removed from WT and KO sex-matched littermates and processed through a 70µm mesh to obtain primary splenocytes. Cells were labelled with CFSE and anti-CD4 and $0.2x10^6$ cells per well were cultured for 4 days under the following conditions in duplicates: no treatment (NT); 5µg/ml plate bound anti-CD3ε alone, or with 1µg/ml plate-bound anti-CD28, or with 100U/ml recombinant IL-2; 10ng/ml PMA with 300ng/ml of ionomycin. Shown is the number of cells with diluted CFSE staining gated on the

CD4+ population (top) and in the graph below the total number of CD4+ T cells pooled from 2 wells after the treatment. Total CD4+ T cells were calculated using small beads that were added to the cells (see Material and Methods).

6.7 ULK1KO mice show normal thymic morphology but may have less autophagosomes in thymic cells of non-T cell origin

Thymic epithelial cells (TECs) have been shown to be important in presentation of endogenous antigens to CD4+ T cells leading to negative selection and apoptosis if its T cell receptor recognises the auto-antigen [244, 282]. TECs use autophagy to process endogenous antigens to be loaded on MHC-II molecules for T cell presentation. Therefore, if there were a specific defect of autophagy in TECs of ULK1KO mice this would not be detectable by LC3 western blotting as they make up less than 5% of cells in the thymus but it would lead to auto-reactive T cells leaving the thymus and reaching the peripheral T cell pool. This may lead to autoimmune disease or, more likely [244], to induction of apoptosis in the auto-reactive T cells by cells such as regulatory T cells. This could explain the above results and therefore I wanted to investigate autophagy in TECs.

As seen in Figure 6-3b about 95% of cells in the thymus are mature (CD4 or CD8 positive) or immature (CD4 and CD8 double positive) T cells. The other 5% contain among other cell types the TEC and dendritic cells. Because the population of TECs is so small and GFP-LC3/ULK1KO mice were not yet available electron microscopic (EM) analysis of ULK1WT and KO thymi was performed to obtain preliminary results.

Thymi were removed from sex-matched littermate mice and fixed immediately in PFA/glutaraldehyde. All further processing for EM and image acquisition was done by Ken Blight in the electron microscopy unit at LRI and standard procedures were used. Figure 6-10 shows representative EM images of sections of ULK1WT (Fig. 6-10a) and ULK1KO (Fig. 6-10b) thymi. The over-all structure of the ULK1KO thymus looks normal mostly consisting of small spheroid T cells interspersed by TECs and other cells with dendritic morphology. Because TECs and dendritic cells extend branch like structures in between the immature T cells to make contact with as many cells as possible the nucleus of these cells is usually not in the plane of section and only cytoplasmic regions are easily seen. In the ULK1WT thymus the areas of cytoplasm between T cells, which are hypothesised to be TECs or dendritic cells (DCs), contain many autophagosomes, and one case of an autophagosome engulfing a mitochondrion can be seen (Fig. 6-10a, iii). Autophagosomes were identified by having diverse contents of similar electron density as the cytoplasm, even though the double membrane cannot always be resolved. Also, considering that there are professional phagocytes such as DCs and macrophages present in the thymus, it is hard to distinguish an autophagosome from a phagosome if the double membrane is not resolved, except when structures such as mitochondria are engulfed, as they are not expected to be released to the extracellular space. In this preliminary experiment, many fewer autophagosomes were seen in ULK1KO thymus sections suggesting that ULK1 may be more essential in TEC autophagy than in other cells. The cell in panel vi may contain numerous autolysosomes although normally autolysosomes have more homogenous contents than in this example. Alternatively, these organelles could be secretory lysosomes found in natural killer cells and cytotoxic T lymphocytes [288].

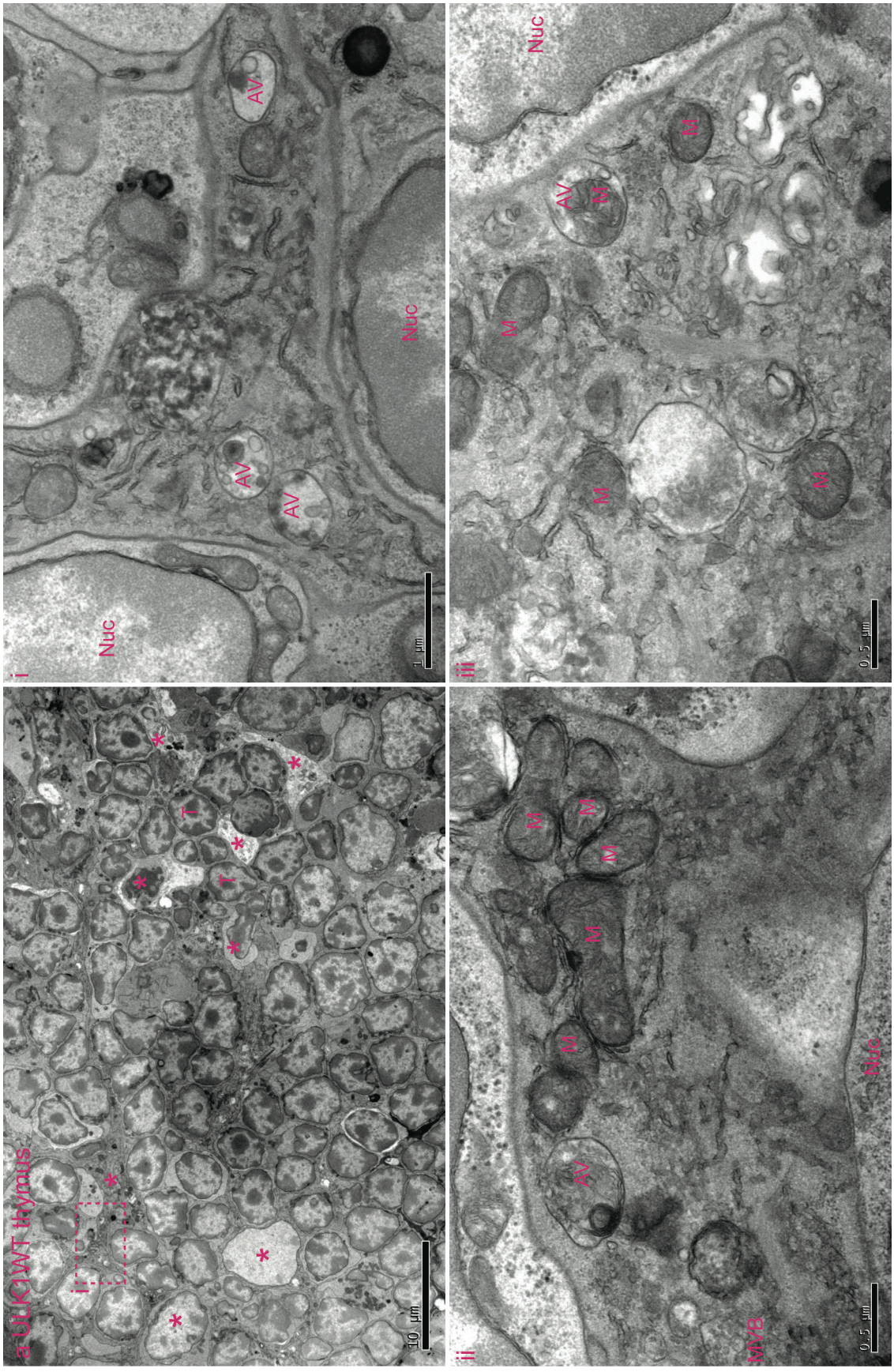
a UBKWT thymus
i
ii
iii
iv
AV
Nuc
M
T
1 µm
10 µm
0,5 µm
MV8

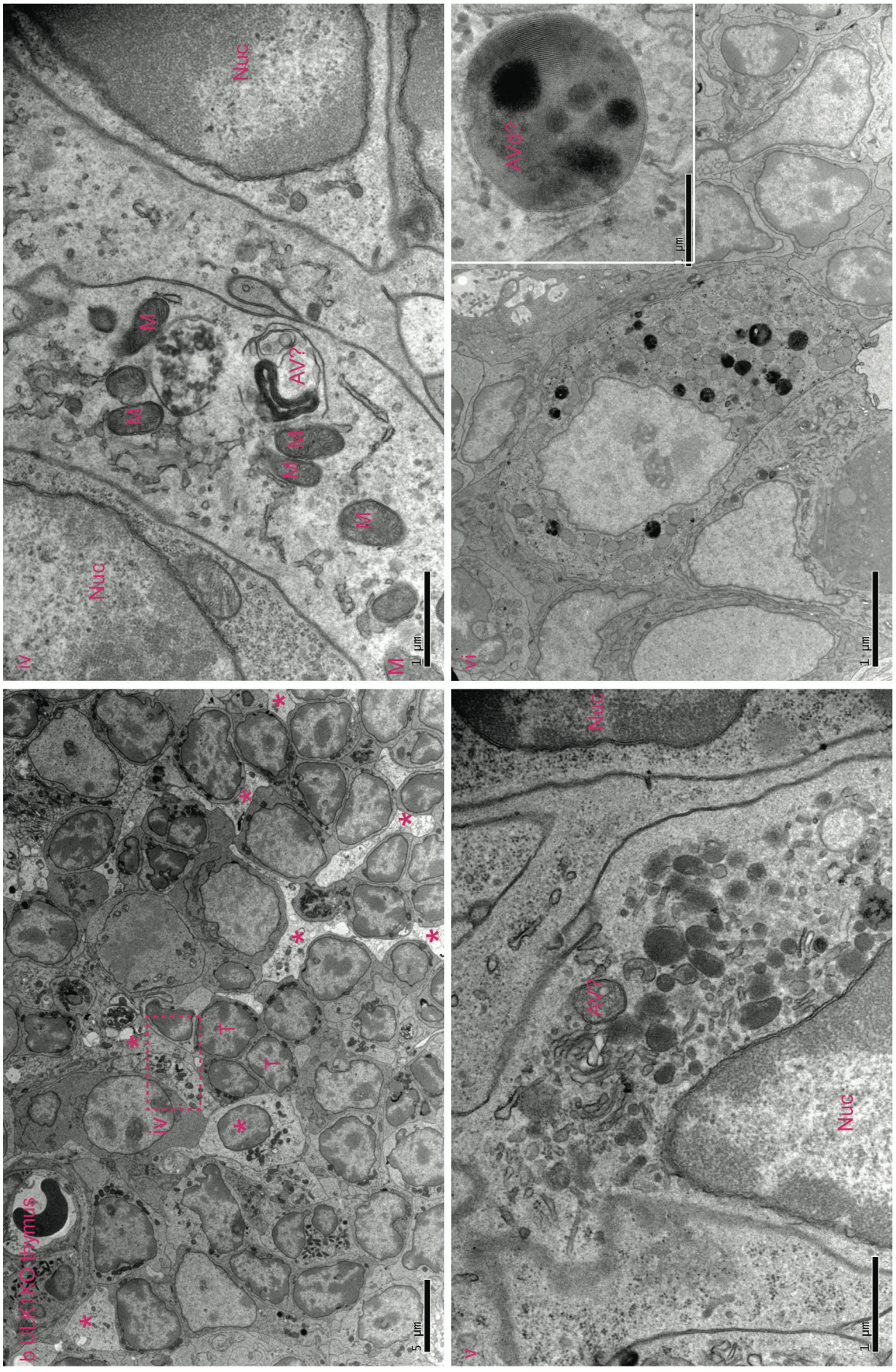
b ULK1KO thymus
5 µm
iv
Nuc
M
M
M
M
M
AV?
M
M
1 µm
v
Nuc
AV?
Nuc
1 µm
vi
AV?
1 µm
1 µm
IV
V
T
T
T

Figure 6-10 EM analysis of a ULK1KO thymus suggests a reduction in autophagosomes in TECs
Thymi were removed from ULK1WT and KO sex-matched littermates and fixed immediately in PFA/glutaraldehyde according to standard procedures. **(a)** Section of ULK1WT thymus with 3 enlarged images i-iii. The area enlarged in image i is indicated by a dashed box in the zoomed out picture **(b)** Section of a ULK1KO thymus. The area enlarged in image iv is indicated by a dashed box in the low magnification picture. T indicates putative T cells (based on morphology) but only two examples are labelled in (a) and (b); asterisks indicate interspersed cells with dendritic morphology, which at least in part represent TECs; Nuc indicates nuclei; AV indicates autophagosomes; AVd indicates autolysosomes; M indicates mitochondria. Note an autophagosome engulfing a mitochondrion in image iii.

6.8 Conclusion

ULK1KO mice appear healthy under conventional laboratory conditions, they are fertile and can undergo basal autophagy. This is surprising because ULK1 is essential in all invertebrate organisms and vertebrate cells in culture tested so far. This discrepancy may be explained by the presence of several ULK1 homologues in mammalian genomes especially ULK2, which shares more than 50% homology with ULK1 although ULK2 does not seem to be essential for autophagy in HEK293A cells. This observation is, however, consistent with results from independently created ULK1KO mice [81]. ULK1 mice show mild splenomegaly as reported previously and seem to have reduced thymic cellularity as was reported for mice with an Atg5 deficient thymus although thymic T cell populations appear to undergo normal development. Interestingly though, peripheral CD4+ and CD8+ T cells in the spleen of ULK1KO mice are reduced compared to wild type animals and show a significantly impaired response to TCR stimulation, which may be due to reduced survival or proliferation of ULK1KO T cells.

Based on my data on T cell apoptosis, survival, proliferation, and EM analysis of a ULK1KO thymus I propose three hypotheses that may explain this phenotype: 1) Thymic epithelial cells are autophagy compromised leading to inefficient removal of auto-reactive T cells and subsequent induction of apoptosis or anergy in these cells upon auto-antigen encounter in the periphery, 2) IL-2 signalling or production are impaired in ULK1KO T cells or other IL-2 producing cells leading to inefficient activation and proliferation of T lymphocytes, 3) ULK1 has been proposed to play a role primarily in mitophagy and it may be that the presence of damaged mitochondria in cells with a high metabolic rate such as activated T cells leads to cellular damage and apoptosis [81] although this remains to be tested.

Chapter 7. Discussion

In this study I aimed to further elucidate the membrane trafficking events involved in autophagosome formation. As a main approach to answer these questions an over-expression screen with all putative human RabGAPs was performed to identify those that inhibit autophagosome formation through Rab GTPase inactivation and one GAP TBC1D14 was studied in detail.

I have shown that 11 out of 38 putative human RabGAPs inhibit starvation induced autophagy by 40% or more when over-expressed in 2GL9 cells. One of those TBC domain containing proteins is TBC1D14, whose function was previously unknown. Over-expression of TBC1D14 inhibits autophagosome formation, long lived protein degradation, and depletion of the protein enhances autophagy. TBC1D14 binds Rab11 and tubulates recycling endosomes (REs) in a Rab11 dependent manner. The endogenous protein localises to the Golgi/TGN and endosomes. ULK1 is sequestered by TBC1D14 induced tubulated REs but is also found on REs normally together with mAtg9. I hypothesise that mAtg9 and ULK1 coordinate autophagosome formation using REs as a signalling platform and/or as a membrane source for phagophores.

To study the role of the important autophagy kinase ULK1 *in vivo,* mice with a disrupted ULK1 gene were created by Dr. E. Chan. Despite ULK1 being essential for autophagy in HeLa and HEK293A cells, mice lacking ULK1 appear healthy and are fertile. However, I've shown that ULK1KO mice have less CD4 and CD8-positive T

cells and show defects in mature T cell proliferation upon TCR stimulation and/or survival whereas B cell numbers are unaffected.

In conclusion, I have performed a comprehensive analysis revealing RabGAPs involved in autophagosome formation. One of those TBC1D14 is a novel effector of Rab11 and I show for the first time an essential role of Rab11 and REs in autophagosome formation. Further analysis is necessary to elucidate whether REs are novel membrane donors for IM expansion or whether they serve as a signalling platform for the ULK1 kinase complex. *In vivo* ULK1 seems to have an especially important role in the adaptive immune system that ULK1KO mice cannot compensate for.

7.1 Identification of 11 RabGAPs that inhibit autophagy when over-expressed in 2GL9 cells

The screen I performed identified 11 RabGAPs that inhibit autophagy as assessed by GFP-LC3 lipidation when over-expressed in 2GL9 cells (Fig. 3-1). To confirm that the reduction in autophagosome formation observed was due to Rab GTPase inactivation eight mutants, which should lack catalytic GAP activity, were tested for their ability to rescue this inhibition. Indeed, seven out of these eight no longer reduced LC3-II formation confirming that they act on a Rab GTPase involved in autophagosome formation. The remaining three inhibitory RabGAPs were not tested as the catalytic residues could not be easily distinguished and the mutant construct was not available. I believe that the large number of RabGAPs (~30%) inhibiting LC3 lipidation highlights the important point that autophagosome formation is a complex, multi-step process that

may well require the activity of several Rab proteins. Phylogenetic analysis of the TBC proteins that inhibit autophagosome formation revealed that they do not fall into a specific subfamily of RabGAPs, and share no common domains other than the TBC domain.

Within the group of 11 RabGAPs classified as having a substantial effect on GFP-LC3 lipidation, the role of TBC1D14 in autophagosome formation was studied in detail and will be discussed below. TBC1D14 was chosen because it binds and co-localises with ULK1, whose activation is the most upstream event in autophagosome formation [98]. Out of the other ten RabGAPs a few show partial co-localisation with GFP-LC3 and published data supports my findings that some of these may have a role in autophagy.

TBC1D7 was shown to inhibit the TSC1 complex, which in turn controls mTOR activity [75]. It is not entirely clear what the molecular mechanism for this inhibition is but it may be through regulation of Rab17 activity. Rab17 was shown to be the target of TBC1D7 regulating cilia formation [201] but I have also shown that over-expression of a dominant negative mutant Rab17N132I inhibits autophagosome formation (Fig. 3-9). Also, TBC1D7 shows some juxta position with GFP-LC3 (Fig. 3-2a). Taken together this suggests that TBC1D7 and Rab17 may also be involved in induction of autophagy possibly through regulating mTOR activity via the TSC1/2 complex.

TBC1D17 shows partial co-localisation with GFP-LC3 puncta (Fig. 3-2b) and has been shown to bind Rab5 [196], which has been previously shown to have a role in the removal of aggregated mutant huntingtin (Htt) by selective autophagy [217]. In

accordance with Rab5 binding, myc-TBC1D17 can be seen on the plasma membrane and a punctate pool (Fig. 3-2b and 3-3b). However, two other Rab5 GAPs, RN-tre and RabGAP5 [197, 289] had only a mild inhibitory effect and were not amongst the top 11 candidates (Fig. 3-1). Interestingly, Htt has been shown to be important for activation of Rab11 [290], as in Huntington's disease patient fibroblasts, Rab11 activity was diminished and Tfn recycling was inhibited.

The RabGAPs TBC1D10A, B and, C were all shown to act on Rab35 [199], which was shown to regulate TfnR recycling [202]. It is possible that Rab35-positive REs have a similar function in autophagy as Rab11-positive REs, which I have shown to be involved in autophagosome formation. However, over-expression of inactive Rab35N120I did not inhibit LC3 lipidation, on the contrary, it slightly enhanced it (Fig. 3-9). Further experiments would be necessary to clarify the role of the TBC1D10 family and Rab35 in autophagosome formation such as siRNA mediated knock down of Rab35 or over-expression of different mutants.

The target Rab GTPase of TBC1D9 is not known and its function remains unknown. It seems to localise to a juxta-nuclear compartment (Fig. 3-2d and 3-3d) but was not found to be involved in Golgi maintenance [200]. TBC1D9 contains two GRAM domains, which are PI lipid binding domains.

TBC1D9B shows partial co-localisation with GFP-LC3 (Fig. 3-2f) positive autophagosomes and like TBC1D9 has two GRAM domains, which could enable it to bind to PI3P on the phagophore although this needs to be confirmed. The target Rab of

TBC1D9B is not known but it binds Rab22a indicating that it may act on this Rab GTPase (personal communication F. Barr; University of Liverpool, UK). Interestingly, Rab22a was found to be necessary for autophagosome formation as siRNA mediated knock down inhibited GFP-LC3 spot formation in 2GL9 cells (N. McKnight, LRI, unpublished data). Rab22a was shown to be involved in recycling of proteins endocytosed by clathrin independent mechanisms [291]. This particular recycling route does not affect TfnR and acts independently of Rab11. However, a dominant negative mutant Rab22aS19N had no effect on LC3 lipidation when over-expressed in HEK293A cells but closer investigation or use of a different mutant, which is unable to bind nucleotides may confirm a role for TBC1D9B and Rab22a in autophagosome formation.

TBC1D4 (also called AS160) is involved in glucose transporter 4 (GLUT4) trafficking and was shown to act on Rab2a, Rab8a, Rab10 and Rab14 [264]. Rab2a and Rab14 are closely related to Rab11 [196, 292], and Rab8a and Rab10 also have roles in endocytic recycling [194, 265, 266] further suggesting a more general role of REs in autophagosome formation, which is not limited to Rab11 alone. Interestingly, a closely related GAP TBC1D1 similarly regulates GLUT4 trafficking but had no effect on LC3 lipidation when over-expressed but this may be due to complementary regulation of TBC1D4 and TBC1D1 by growth factors [293] with a specialised role for TBC1D4 in autophagy.

RUTBC1/SGSM2 was reported to bind to Rab11 and Rab4, which are involved in endocytic protein recycling [267], and I observed partial co-localisation of RUTBC1

with GFP-LC3 puncta (Fig. 3-2h), suggesting that similarly to TBC1D14 it is involved in RE traffic and autophagy. However, unlike TBC1D14, RUTBC1 did not induce tubule formation or co-localise with ULK1 (Fig. 3-3g). Further investigation and identification of the target Rab for RUTBC1 are necessary to confirm its exact role in autophagosome formation.

Lastly, TBC1D16 shows GAP activity towards Rab36 (personal communication F. Barr, University of Liverpool, UK). This small GTPase was shown to localise to the Golgi/TGN and cause juxta-nuclear accumulation of late endosomes and lysosomes when over-expressed [258]. However, my experiments using over-expressed TBC1D16 or constitutively active Rab36Q182A suggest that both are also involved in autophagosome formation (Fig. 3-1 and 3-9). I did not see an accumulation of myc-TBC1D16 in the Golgi area but further analysis is required to determine its localisation and confirm its target Rab (Fig. 3-2i and 3-3h).

In summary, none of the TBC proteins tested co-localise dramatically with GFP-LC3 or ULK1-positive autophagosomes except for TBC1D14. However, TBC1D7 and TBC1D14 show some juxta-position to GFP-LC3 puncta and TBC1D17, TBC1D4, TBC1D9B and RUTBC1 show partial co-localisation with GFP-LC3 positive autophagosomes (Fig. 3-2). Co-localisation may be partial due to the transient interaction of the GAPs with their cognate Rab GTPases or because they act at a different step during autophagosome formation and do not localise permanently to the phagophore.

7.2 A yeast-2-hybrid screen identifies 17 RabGAPs interacting with ULK1

In primary cultured cerebellar granule neurons ULK1 was shown to form a protein complex with Syntenin1, SynGAP, and Rab5 in which SynGAP acts as a Rab5-GAP [90]. However, SynGAP does not have a classical RabGAP TBC domain but a RasGAP domain and it can also act on Ras. While, SynGAP seems to be brain specific, I could confirm the interaction of ULK1 with Syntenin1 in HEK293A cells via co-immunoprecipitation (Fig. 3-5). Therefore, I hypothesised that ULK1 may form a similar complex with a Rab and RabGAP in other cell types to regulate autophagy.

Interestingly, in a yeast-2-hybrid screen ULK1 was found to interact with 17 out of 35 human RabGAPs tested (Fig. 3-6). The large number of interactors could partly be due to the possibility that ULK1 can regulate other membrane trafficking events by binding to different RabGAPs, such as regulating neuronal vesicular traffic during axon extension as mentioned above. Alternatively, it is possible that ULK1 binds to TBC domains directly, which have a high similarity in their tertiary structure. This binding may normally be prevented in mammalian cells by compartmentalisation or inaccessibility due to binding of other co-factors. Indeed, I have shown that ULK1 binds to the TBC domain of TBC1D14 (Fig. 4-9), which I have also shown to be the only TBC protein that shows substantial co-localisation with ULK1 (Fig. 3-3 and 3-4).

Another yeast-2-hybrid analysis I performed (Fig. 3-8), revealed that Syntenin1 binds Rab5, as has been reported previously [90], and Rab33, both of which have been shown

to be involved in autophagy [217, 222]. ULK1 does indeed bind the RabGAPs RN-tre and TBC1D22B, suggested to act on Rab 5 and Rab33, respectively ([289] and personal communication F. Barr, University of Liverpool, UK), and I speculate that such Rab-RabGAP-ULK1 complexes may exists in HEK293A cells. However, neither of these RabGAPs, nor the corresponding inactive Rab GTPases, inhibit LC3 lipidation when over-expressed in HEK 293A or 2GL9 cells (Fig. 3-1 and 3-9), and therefore these Rab-RabGAP pairs may regulate other membrane trafficking steps such as endocytosis in which ULK1 also plays a role in neurons [93].

Finally, as not all the TBC proteins that bind ULK1 inhibit autophagosome formation (Fig. 3-7) I suggest that ULK1 sequestration by over-expressed RabGAPs is not the main mechanism for this inhibition. This is supported by the fact that the RA mutant proteins, and the RA/QA mutant in case of TBC1D14, do not inhibit LC3 lipidation confirming that Rab inactivation rather than ULK1 sequestration is causing impaired autophagosome formation (Fig. 3-1 and 4-3).

7.3 The function of TBC1D14

Previous to this study the function of TBC1D14 was not known even though its TBC domain has been crystallised and solved [198]. I have shown that over expression of TBC1D14 leads to an inhibition of autophagosome formation as assessed by two robust autophagy readouts (Fig. 3-1 and 4-2); LC3 lipidation and long lived protein degradation. Furthermore, siRNA knock down leads to an increase in autophagosome

formation (Fig. 4-6) supporting the role of TBC1D14 as a negative regulator of autophagy

By yeast-2-hybrid, and co-immunoprecipitation assays I show that TBC1D14 binds ULK1 directly via its C-terminal TBC domain (Fig. 3-6 and 4-9). However, sequestration of the ULK1 kinase complex alone is unlikely to be the sole mechanism for inhibition of autophagosome formation by TBC1D14. The over-expressed TBC domain is localised predominantly in a juxta-nuclear pool and sequesters ULK1 but it does not seem to be sufficient for inhibition of autophagosome formation as over-expression of the TBC domain does not inhibit LC3 lipidation (Fig. 4-11). I hypothesise that TBC1D14 exhibits its autophagy inhibitory function on peripheral endosomes or tubules and the mislocalisation of the TBC domain on the juxta-nuclear ERC prevents this.

Inhibition of autophagosome formation by TBC1D14 is likely due to inhibition of Rab11 functions, as I have shown that Rab11 inactivation itself leads to inhibition of autophagosome formation (Fig. 5-7), and TBC1D14 is a negative regulator of Rab11. There are two main possibilities as to how TBC1D14 inhibits Rab11 and the trafficking steps regulated by Rab11: As a Rab11-GAP or as a Rab11 effector.

The target Rab GTPase of TBC1D14 is not known and attempts to purify recombinant TBC1D14 from bacteria for *in vitro* GAP assays have failed due to aggregation of the protein (personal communication F. Barr, University of Liverpool, UK). Therefore, I performed an *in vitro* GAP assay with TBC1D14 purified from insect cells using the

baculovirus expression system (Fig. 4-12). However, no GAP activity could be detected against any of the 47 Rabs tested, either because the purified TBC1D14 was not active, because there was not enough GAP protein per reaction, or because it does not have GAP activity *in vivo*.

My findings that mutation of both the arginine finger and glutamine thumb in the TBC domain of TBC1D14 abolished its ability to inhibit LC3 lipidation suggest that it does have GAP activity, which is dependent on these conserved catalytic residues (Fig. 4-3). For all the other GAPs tested mutation of a single one of those residues was sufficient to inactivate the protein (Fig. 3-1). However, It is likely that TBC1D14 has a slightly different catalytic domain than other TBC proteins as its arginine and glutamine residues are oriented at a different angle than the other two TBC domains so far crystallised [198] although more TBC domain structures would have to be solved and analysed accordingly to confirm this hypothesis.

Even though I could not show *in vitro* GAP activity of TBC1D14 against Rab11, indirect evidence supports the hypothesis that it could be a Rab11-GAP.

Firstly, yeast-2-hybrid analysis undertaken by one of our collaborators S. Yoshimura (University of Liverpool, UK), revealed that TBC1D14 binds specifically to Rab11a and Rab11b but not to any other Rabs including Rab25 (also called Rab11c) the most closely related GTPase (Fig. 4-13).

Secondly, over-expressed TBC1D14 tubulates TfnR- and Rab11-positive REs and is also localised to these tubules but is diffusely cytosolic in cells that have previously been depleted of Rab11 using siRNAs (Fig. 5-2). I hypothesise that TBC1D14 localises

to REs by binding to Rab11 and inactivates Rab11 leading to impaired vesicle budding or a block of vesicle transport away and tubulation of REs. This is supported by the fact that Rab11 depletion by siRNA also leads to tubulation of REs in the absence of excess inhibitory TBC1D14 (Fig. 5-3).

Therefore I have confirmed that Rab11 depletion and its inactivation by over-expressing TBC1D14, which I hypothesise to be a putative Rab11-GAP, both lead to tubulation of TfnR positive REs. However, the double mutant TBC1D14RA/QA, which I speculate to lack GAP activity, still tubulates TfnR-positive REs when over-expressed although it does not inhibit autophagosome formation (Fig. 4-3 and 5-2). This may be explained by the fact that the double mutant protein is expected to bind Rab11 even more strongly than the wild type due to the absence of the two protruding A and Q catalytic residues [204]. Binding of TBC1D14, therefore, could prevent specific effector binding to the Rab11 GTP bound form still leading to an inhibition of RE trafficking.

On the other hand, it has been shown that another TBC protein TBC1D15 exhibits *in vitro* GAP activity towards Rab11a and Rab11b (F. Barr unpublished, University of Liverpool, UK). If the hypothesis that one RabGAP acts on one Rab family were true, then this would suggest that TBC1D14 is not the Rab11-GAP. However, this hypothesis remains to be proven, as there are several cases where multiple TBC proteins have been suggested to act on the same Rab. For example, RN-tre and RabGAP-5 in mammals, and TBC-2 in *C. elegans*, were shown to have GAP activity against Rab5 [197, 289, 294]. Similarly, TBC1D15, TBC1D2, and TBC1D5 have been suggested to be Rab7-GAPs [295-297]. There may be differences between cell types and organisms involved in these discrepancies but it may also be that the one GAP for one Rab hypothesis needs

to be revised and adjusted to the possibility that there may be regulatory mechanisms allowing different GAPs to act on the same Rab.

An alternative possibility is that TBC1D14 is an effector of active GTP-bound Rab11 and is recruited by it to inactivate a Rab immediately upstream of it. Such Rab cascades have been described for example in yeast where Ypt32 (the homologue of Rab11) recruits Gyp1 (homologous to TBC1D22A/B) to inactivate the upstream Ypt1 (homologous to Rab1) [207]. Intriguingly, Ypt1 has been shown to be recruited to the yeast phagophore and functions in autophagy [74]. The same study also found that Trs85, a subunit of the TRAPPIII complex, which acts as a Ypt1 GEF is recruited to the yeast phagophore assembly site (PAS). Interestingly, TBC1D14 was found to bind the human homologue of Trs85 and another subunit of the TRAPP complex TPPC3 in a GST pull down assay done by Sharon Tooze (LRI). The heavy chain subunit of cytoplasmic dynein was also pulled down suggesting that TBC1D14 may act as an adaptor linking Rab11 to the microtubule cytoskeleton similarly to Rab11FIP2, which links it to the motor protein myosin V [298]. Another protein that was pulled down by GST-TBC1D14 is Annexin2, which is involved in positioning of TfnR/Rab11-positive REs [299]. However, this experiment should be repeated to confirm these interactions.

In conclusion, I have shown that TBC1D14 is a negative regulator of Rab11 either by acting as a Rab11-GAP or an effector of Rab11. Both over-expression of TBC1D14 and dominant negative Rab11 lead to inhibition of autophagosome formation. Therefore, I speculate that the main cause for inhibition of autophagosome formation by TBC1D14 is perturbation of Rab11 function and REs. Endogenous TBC1D14 localises to REs and

the Golgi complex. The role of TBC1D14 on the Golgi complex is unknown but TBC1D14 redistribution to the Golgi complex upon starvation may be important for initiation of autophagy possibly because this allows Rab11 to function in autophagosome formation when TBC1D14 is not inhibiting it on the peripheral REs.

7.4 The role of TBC1D14 and REs in autophagy

My results showing a perturbation of REs raised the question about whether other trafficking pathways are disturbed by TBC1D14 over-expression. Immunofluorescence staining against markers of several intracellular compartments showed that their distribution is unperturbed in TBC1D14 transfected cells with the exception of the Golgi apparatus, which seemed to be fragmented in some cells as has been reported previously [200]. It would therefore be interesting to investigate whether TBC1D14 also has a role in Golgi stability or the secretory pathway in addition to its function in endocytic recycling.

I have shown that TBC1D14 is an effector of Rab11 and impairs endosomal recycling and autophagy when over-expressed (Fig. 5-4 and 5-5). In accordance with this I found that over-expression of dominant negative constructs of Rab11 (Rab11N124I) also inhibits autophagosome formation (Fig. 5-7). Rab11 was previously shown to be involved in fusion of MVBs with autophagosomes in human leukemic K562 cells [216]. However, this is clearly not the case in HEK293A cells as addition of leupeptin to block autophagic flux did not lead to accumulation of LC3-II in Rab11N124I expressing cells

unlike in cells expressing inactive Rab7T22N, which blocks late endosome-autophagosome fusion [183, 184].

In agreement with my hypothesis that Rab11 functions in autophagosome formation over-expression of wild type Rab11 increased LC3-II levels (Fig. 5-7). However, over-expression of a constitutively active protein Rab11Q70A had no effect on LC3 lipidation. This may be due to the fact that Rab11 probably does not act alone but in a Rab cascade as described above and failure of Rab11 to be deactivated leading to disruption of this cascade could prevent it from acting in autophagosome formation. Furthermore, excess active Rab11 may lead to depletion of essential effectors that specifically bind to GTP-bound form of Rab11 and perturb the pathway.

No significant inhibitory effect on autophagy could be observed after siRNA mediated knock down of Rab11a, Rab11b, or both (Fig. 5-8). However, biochemical analysis was hampered by the fact that the 72 hour knock down caused cell death leaving many multinucleated cells among the surviving population. This is probably due to the role of Rab11 in cytokinesis [277], which is not so pronounced during the relatively short 24 hour over-expression of dominant negative Rab11N124I or TBC1D14.

I hypothesised that TBC1D14 inhibits autophagosome formation through inactivating Rab11 and therefore performed rescue experiments on TBC1D14 over-expressing cells with constitutively active Rab11: The excess active Rab11Q70A may then overcome TBC1D14 inactivation. However, this was not the case, and it is likely that depletion of

effectors by active Rab11Q70A prevented rescue of autophagosome formation (Fig. 5-9).

Since ULK1 is sequestered by TBC1D14-induced tubular REs, I also tested whether over-expression of ULK1 together with TBC1D14 could prevent inhibition of LC3 lipidation, which indeed seems to be the case. Interestingly, simultaneous expression of ULK1 and TBC1D14 significantly increased basal autophagy under fed conditions (Fig. 5-9), which is not observed when ULK1 alone is over-expressed [20, 21]. Perhaps TBC1D14 sequesters inhibitory factors allowing ULK1 to induce autophagosome formation in fed conditions or TBC1D14 interferes with a negative feedback loop that may be normally induced by ULK1 over-expression. However, the signalling events downstream of the ULK1 kinase complex are poorly understood making it difficult to test these hypotheses. In this experiment I tested both HA-tagged human ULK1 and myc-tagged murine ULK1, firstly, because the TBC1D14 construct contains the human protein sequence, and secondly, to confirm that the newly cloned HA-ULK1 behaves similarly to the previously studied myc-ULK1. As expected, since these proteins are highly conserved between mouse and human (90% amino acid sequence identity) the phenotypes observed were comparable. These results would suggest that ULK1 sequestration is one of the major factors leading to inhibition of autophagy by TBC1D14 but the situation seems to be more complex as the TBC domain alone does not seem to inhibit autophagy even though it is able to sequester ULK1. Since the TBC domain localises exclusively to the pericentriolar ERC and not peripheral TfnR-positive REs, which seem to be reduced or absent, I speculate that the peripheral distribution of TBC1D14-tubules and ULK1 sequestration on these peripheral tubules leads to a block in autophagosome formation (Fig. 4-10).

The autophagy specific PI3K pathway, which is required for autophagosome induction in addition to the ULK1 kinase complex, did not seem to be affected by TBC1D14 over-expression, as the two autophagy specific PI3P effector proteins DFCP1 and WIPI2 respond normally to starvation by localising to punctate phagophores. However, my preliminary data shows that there are more WIPI2 puncta in TBC1D14 over-expressing cells, and that compared to the control significantly fewer of these WIPI2 puncta have acquired LC3 (Fig. 5-13). This implies that in the TBC1D14 expressing cells WIPI2 puncta accumulate because formation into LC3-positive autophagosomes is blocked, or halted at an early stage after WIPI2 acquisition but before LC3 recruitment. This result is strengthened by the notion that TBC1D14 over-expression disrupts the ULK1 kinase complex, but not PI3K signalling and that these two pathways act partly in parallel, perhaps independently of each other. At some point however, the two must converge for IMs to mature into autophagosomes.

Another early acting autophagy protein is mAtg9, which localises to the IM from the beginning but remains transiently associated with the autophagosome throughout formation. I show that mAtg9 localises to REs in HEK293A cells together with ULK1 but often occupying different subdomains of the RE membrane (Fig. 5-14). Since both ULK1 and mAtg9 act early in autophagosome formation and are essential for autophagy in HEK293A cells, this suggest that REs are important for phagophore formation and initiation of autophagosome formation through Atg protein assembly. mAtg9 and ULK1 are associated with TfnR-positive REs in the periphery but less so on the ERC in both fed and starved conditions. An important question is whether ULK1 is able to recruit REs from the ERC upon starvation as TfnR dispersal is observed after EBSS treatment.

Or alternatively, whether ULK1, which becomes active upon nutrient deprivation causes retention of REs in the periphery blocking retrograde traffic to the ERC so that the REs can function in autophagosome formation. Similar questions can be asked for the role of mAtg9 on REs but it is striking that while ULK1 is sequestered by TBC1D14 induced tubulated REs mAtg9 is not.

From my thesis work the most important question remaining concerns the exact function of REs in autophagosome formation and I could envisage two scenarios, which incorporate my data and recent advances.

The first possible scenario is that REs provide membrane to the phagophore and autophagosomes directly. This is supported by recent findings that plasma membrane derived endocytic vesicles provide membrane for autophagosome precursors [127]. In this study they also show that the clathrin coat machinery is necessary for autophagosome formation and since clathrin coated vesicles can also form on recycling endosomes and recruit Tfn [300] it is possible that similar mechanisms are involved in the supply of both endosomal and plasma membranes to IMs. Indeed I show that some Rab11/TfnR-positive REs co-localise with GFP-LC3 upon starvation (Fig. 5-15). As is the case with plasma membrane derived vesicles not all autophagosomes contain the RE markers Rab11 and TfnR.

Accumulating evidence suggest autophagosomal membranes can be recruited from different sources and that not one single compartment provides the membrane for all autophagosomes. I speculate that REs may be an additional source of autophagosomal

membrane. If this were the case it raises the question as to whether REs provide membrane just for phagophore precursor formation where early Atg proteins assemble, or also for phagophore expansion, or both. If indeed REs were to provide a substantial amount of membrane to autophagosomes this raises the question of whether mechanisms exist to specifically exclude RE resident proteins from the autophagosome membrane as has been shown for ER and mitochondrial membrane proteins [123, 124, 130].

The second possibility is that REs act as nutrient sensors that can activate autophagy proteins such as ULK1 and mAtg9 upon starvation and provide a signalling platform for the assembly of Atg protein complexes. REs and other endosomal vesicles that continuously shuttle between intracellular compartments and the plasma membrane are well equipped to monitor nutrient status. Since the transmembrane protein mAtg9 localises to Rab7, Rab9, CI-MPR, and Rab11 positive endosomal populations it is an ideal candidate to be the prime nutrient sensor, which activates autophagy upon starvation. This is supported by my data suggesting that Rab11 and TBC1D14 are involved in starvation-induced autophagy but not basal autophagosome formation. However, further work is needed to confirm or reject these hypotheses and it is also possible that a combination of both theories is true. Interestingly, a recent study showed a functional connection between the REs and the intermediate compartment between the ER and cis-Golgi [301] raising the possibility that TBC1D14 may be involved in membrane traffic between these compartments.

In conclusion, I have shown for the first time a role for REs in autophagy, which I propose act as a signalling platforms to induce autophagy by regulating the localisation of ULK1 and/or providing membrane to the phagophore. TBC1D14 is a novel effector of Rab11 and inhibits autophagosome formation when over-expressed in HEK293A cells, as does dominant negative Rab11N124I. Over-expression of TBC1D14 leads to tubulation of REs and sequestration of ULK1 to subdomains of these tubules. No other autophagy proteins tested localise to tubulated REs but both ULK1 and mAtg9 can be found on REs normally. A model, which summarises my data is depicted in Figure 7-1.

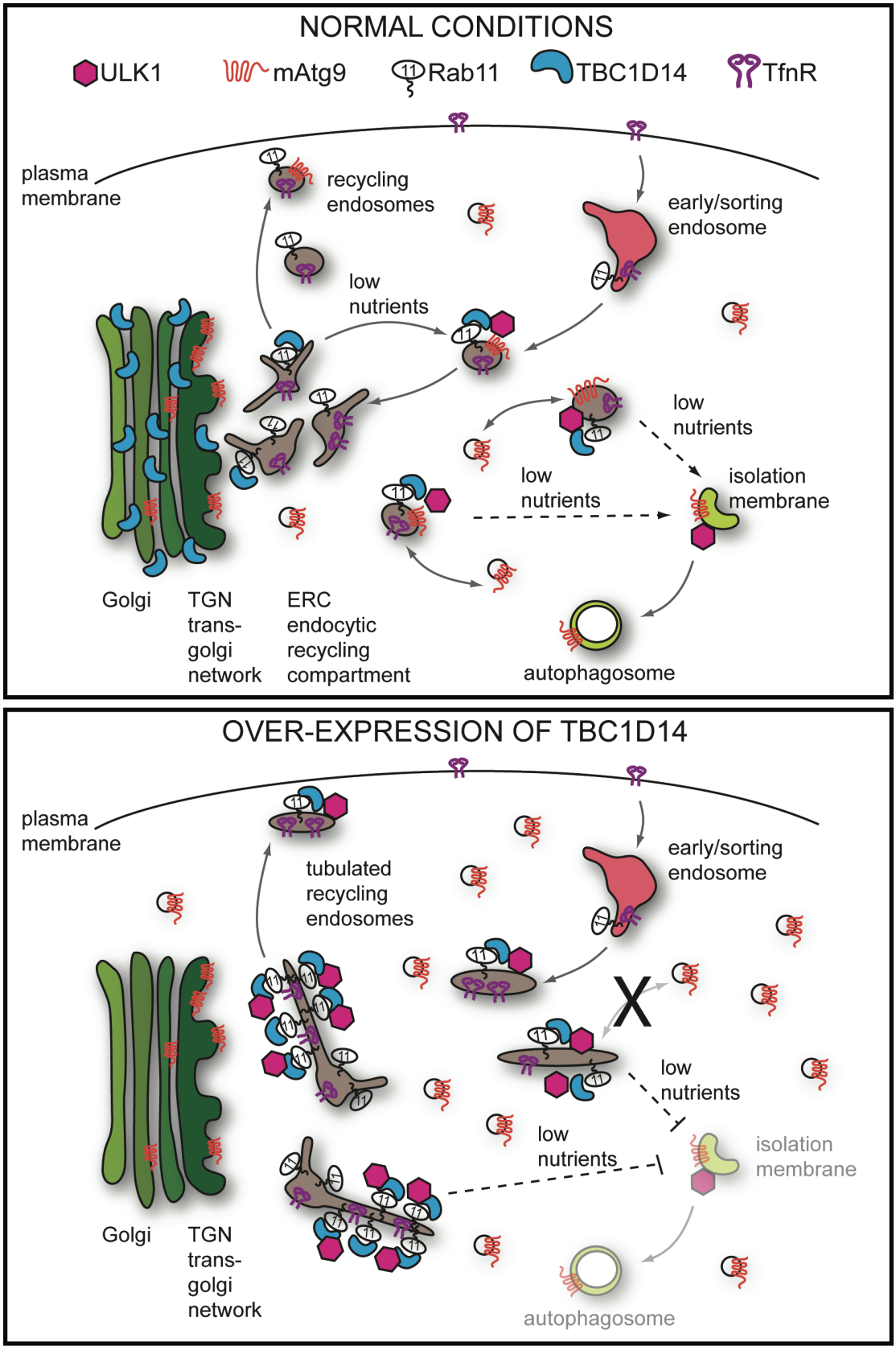

Figure 7-1 Model for the role of REs in autophagosome formation
I propose the following model: a population of ULK1 and mAtg9 is resident on REs in both fed and starved conditions. ULK1 is recruited to the REs by TBC1D14, whereas TBC1D14 is recruited by Rab11.

Upon nutrient starvation ULK1 is activated and moves to the site of autophagosome formation or recruits other Atg proteins to REs, which then contribute membrane to IM formation and expansion. Over-expression of TBC1D14 in both fed and starved conditions tubulates REs and sequesters ULK1 on these tubules. Furthermore, the association of mAtg9 with this compartment is disrupted. The exact activation state of ULK1 on the tubulated REs remains to be elucidated but none of the other early Atg proteins tested localise to tubulated REs.

7.5 ULK1 knock-out mice

To better understand the role of ULK1 in autophagy *in vivo,* mice lacking a functional ULK1 gene (ULK1KO) were created by E. Chan (LRI) using gene trapped embryonic (ES) stem cells (Fig. 6-1). These mice appear healthy, are fertile and able to undergo basal autophagy in various tissues analysed (Fig. 6-2). This is surprising since acute knock down of ULK1 using siRNA leads to a loss of autophagy in HEK293A and HeLa cell lines [20]. Various mouse models with deletions of essential autophagy genes indicate that complete loss of autophagy leads to post-natal fatality for example in Atg5 and Atg7 knock-out mice [8, 9], or death during early embryogenesis such as in the Beclin1 deficient animals and mice with an oocyte specific Atg5 deletion [102, 137, 138]. Therefore, it was unexpected that ULK1 knock-out mice show no obvious phenotypes. This may be due to the presence of ULK2, which is highly homologous to ULK1 (51% overall, 78% in the kinase domain). Even though siRNA mediated knock down of ULK2 in HEK293A cells does not lead to an impairment of autophagy, ULK1 and ULK2 may be partially redundant *in vivo.* A possible explanation for this is that acute knock down of ULK1 does not allow enough time for cultured cells to adapt and up-regulate the ULK2 gene or that they simply lack the ability to do so. Alternatively, the ES cells used to create chimeric mice may have been inadvertently selected for those that had up-regulated ULK2 functions because the others were not viable.

The only phenotype that has been reported for ULK1 knock-out in mice is a defect in reticulocyte maturation specifically the failure to remove mitochondria through mitophagy [81]. I did not investigate whether our mice show the same phenotype but I also observed a similar degree of splenomegaly as reported by Kundu and colleagues. Note however, that they can only observe these phenotypes in a mixed genetic background but not in a pure C57BL/6J background. Our ULK1 mice were back-crossed for ten generations (n=10), which should lead to a >99% pure C57BL/6J genetic background. Certain phenotypes, especially neurological phenotypes, are only manifested consistently in a pure genetic background. However, even after ten generations no obvious phenotype was observed even though ULK1 was shown to be essential for axon extension in primary cerebellar granule neurons [90].

However, post-mortem reports on mice that died of old age were done by the scientific officer in the mouse facility and suggested that ULK1KO animals have a small thymus. This was reported exclusively for knock-out and some heterozygous mice, while no other abnormalities were consistently observed. Splenomegaly was not observed probably because this phenotype seems to be much reduced in older mice (my personal observations). The histopathology unit at LRI also reported no major abnormalities in ULK1KO mice but this analysis did not include thymus and spleen as I had removed them for FACS analysis (see Appendix). Tissue sections should be done however to determine if there are histopathological abnormalities. Splenomegaly in young mice may be due to stress-induced erythropoiesis caused by the presence of damaged mitochondria, which subsides at an older age when the erythropoietic system can no longer cope. However, this was not further investigated. On the other hand FACS

analysis did confirm reduced thymic cellularity although this experiment was only done once. Despite the reduced cell number the percentages of CD4+, CD8+ and double positive (immature) T cells in the thymus of ULK1KO mice is comparable to wild type animals (Fig. 6-3) suggesting that T cell development is normal. Basal and starvation-induced autophagy are both readily observed in ULK1WT and KO thymocytes and there may even be an increase in the starvation response of the latter. However, this experiment would have to be repeated and quantified for statistical analysis to draw a final conclusion.

While immature T cell populations in the ULK1KO thymus were similar in percentage to the WT, a decrease in percentage and number of mature T cells in the spleen of ULK1KO mice was observed. Like thymocytes, splenocytes of ULK1KO mice can undergo basal autophagy as LC3-II is observed in these cells (Fig. 6-4). Treatment with EBSS did not seem to induce autophagy in total splenocytes or FACS purified CD4+, or CD8+ T cells. In fact, both these T cell populations seemed to have mostly LC3-II and little or no LC3-I suggesting rapid autophagic turn-over. However, this experiment should be repeated to enable statistical analysis. A high percentage of splenocytes consists of CD19+ B cells but this population was not altered in number or percentage in ULK1KO spleens compared to the wild type. Enhanced apoptosis was observed in ULK1KO T cells (both CD4+, and CD8+) compared to WT cells but not in B cells, indicating that the reduction in number is due to cells dying rather than a defective proliferation.

These results were reproducible but to investigate whether these changes were statistically significant and whether ULK1KO T cells could respond normally to activating stimuli I performed anti-CD3ε-titration experiments. Anti-CD3ε is an antibody that cross-links the T cell receptor (TCR) and induces T cell activation and proliferation. Indeed, cell proliferation can be observed with rising anti-CD3ε concentrations administered to splenocytes in culture over 3 days. That the majority of proliferating cells in these cultures are T cells was confirmed by FACS analysis, but cytokine and growth factor secretion by T cells will also induce proliferation of other splenocytes such as B cells and fibroblasts. The response in ULK1WT splenocytes peaks at 2.5µg/ml anti-CD3ε compared to ULK1KO splenocytes, which peak at a concentration of 10µg/ml suggesting a considerable impairment in the response to TCR stimulation (Fig. 6-7). This assay measures the number of live cells after 3 days in culture but cannot distinguish whether ULK1KO have proliferated less or whether they have undergone more apoptosis. However, FACS analysis of the same cells again indicates enhanced cell death although an additional proliferative defect cannot be excluded (Fig. 6-8).

To further analyse the response of ULK1KO T cells to TCR stimulation a CFSE proliferation assay was performed showing again that the response of ULK1KO cells is impaired (Fig. 6-9). Individual CFSE peaks indicate that some T cells were able to divide but no expansion of cell number took place. This could not be rescued by addition of anti-CD28 co-stimulatory signal, which is provided by APCs in the culture. Exogenous IL-2 addition, which is the major T cell growth factor also failed to rescue T cell expansion. Bypassing TCR/CD3 signalling with PMA/ionomycin largely rescued the T cell responses suggesting that mitogen-activated protein (MAP) kinase activation

and Ca^{2+} mobilisation can overcome the defects observed in ULK1KO cells. These findings are similar to results from Atg5 deficient T lymphocytes [283] but while it is likely that Atg5KO cells cannot undergo classical autophagy this was not shown by the authors and would be in contrast to ULK1KO T cells, which are autophagy competent.

In summary I have shown, that T but not B lymphocytes from ULK1KO mice have impaired responses to TCR/CD3 stimulation and undergo more apoptosis both when activated and at steady state. Similar defects have been reported in Atg5KO T cells but it has been unclear whether this represents a specialised function of Atg5 or is applicable to the process of classical autophagy. My results would support the latter but more autophagy genes should be analysed to confirm this. On the other hand ULK1KO T cells seem to be able to form LC3-II positive autophagosomes as efficiently as wild type cells but it is still possible that they fail to respond to autophagy inducing, but presently unknown, stimuli leading to enhanced cell death and/or proliferation defects or anergy.

Another possibility is that the differences observed between ULK1KO and ULK1WT T cells are due to impaired negative selection in the ULK1KO thymus leading to release of auto-reactive T cells into the peripheral lymphoid organs. Negative selection is mediated by thymic epithelial cells (TECs), which rely partly at least on autophagy to present self-antigens to immature T cells. T lymphocytes recognising such auto-antigens undergo apoptosis to prevent auto-immune disease. Autophagy defects in TECs could therefore lead to an increase in auto-reactive T cells in the periphery but these would be induced to undergo apoptosis or anergy by regulatory T cells, which are another line of

defence to prevent autoimmune disease. In support of this hypothesis, I observed less autophagosomes in EM images of an ULK1KO thymus than in the wild type thymus when looking specifically at TECs and other APCs in the thymus. However, this experiment has only been done once and the data remains preliminary. ULK1KO mice do not show autoimmune disease but this may be explained by the fact that there are other mechanisms to prevent this such as the regulatory T cells or lack of co-stimulatory B cells. Furthermore, CD8-positive T cells are also reduced in number and show impaired responses to TCR stimulation in ULK1KO mice but these cells do not rely on MHC class II presented antigen recognition as do the CD4-positive T cells (Fig. 6-5 and 6-7). This could be explained by a lack of co-stimulation by CD4-positive helper T cells, which are necessary for CD8-T cell responses. It would be interesting to challenge ULK1KO mice with an infectious agent or a vaccine and study the immune response *in vivo* but under clean laboratory conditions they do not seem to succumb to infection more than wild type mice.

In conclusion, I have shown that ULK1KO CD4 and CD8-positive mature T cells have an impaired response to TCR stimulation and are reduced in number. This suggests that ULK1 plays a critical role in the adaptive immune system, which ULK1KO mice cannot compensate for even though they can compensate for loss of ULK1 in most tissues and remain capable to undergo autophagy. It remains to be elucidated what the exact role of ULK1 in T cell biology is and whether it involves classical autophagy or represents a separate function of the ULK1 protein.

Appendix

Cell Death and Differentiation (2009) 16, 956–965

www.nature.com/cdd

Review

Vesicular trafficking and autophagosome formation

A Longatti[1] and SA Tooze*,[1]

The source of the autophagosome membrane, and the formation of the autophagosome remain the most important questions for understanding autophagy. Fundamentally, the process of autophagosome formation is similar between yeast and mammalian cells and many of the proteins involved (called the autophagy-related (Atg) proteins) are known, having been first discovered in yeast. However, both in yeast and mammalian cells, the molecular details are missing to explain how the double-membrane autophagosome is formed. Important advances in our understanding of the formation process have recently been obtained, and here, we review and interpret these data in the context of well-known paradigms of membrane trafficking to develop some hypothetical models for how an autophagosome forms in mammalian cells.
Cell Death and Differentiation (2009) **16,** 956–965; doi:10.1038/cdd.2009.39; published online 17 April 2009

In mammalian cells, autophagy is an inducible cell survival pathway that relies on the lysosomal degradation pathway for its execution (Figure 1). Autophagosomes sequester cytosolic components constitutively, or during the times of nutrient deprivation or stress, and fuse with the endosomal and lysosomal system to acquire degradative enzymes to digest the sequestered material.[1] In mammalian cells, autophagy is initiated by the formation or elongation of the isolation membrane (IM), also called a phagophore. In yeast, the IM arises from the yeast pre-autophagosomal structure (PAS),[2] the PAS is defined as the initial site of autophagy-related (Atg) protein recruitment. In mammalian cells, so far there is no evidence for a PAS, and so the mammalian IM could either be derived from the equivalent of the yeast PAS, or be, in fact, the PAS itself. One of the major differences between yeast and mammalian autophagy seems to be that, in yeast, all autophagosomes apparently arise from a single PAS, whereas in mammalian cells, it appears that they can be generated anywhere in the cytoplasm. The IM is induced to grow and expand into a double-membrane vesicle (Figure 1). Expansion of the IM requires a unique set of proteins and is followed by the closure of the double membrane forming a spherical immature autophagosome. The full molecular details of how the IM expands and closes remain to be understood. Autophagy is completed by fusion of autophagic vacuole (AV)i (immature autophagosomes) with endosomes and lysosomes, forming an AVd (degradative autophagosome) or autolysosome, followed by consumption of the content, and release of amino acids and other building blocks into the cytosol.

Much of the molecular details about the autophagosome formation were originally obtained in the yeast. Among the 31 Atg proteins in yeast, 18 have been shown to be involved in autophagosome formation (Atg1-10, Atg12-14, Atg16-18, Atg29, and Atg31).[3,4] Most, if not all, of these proteins are recruited to the PAS, on which some remain throughout the autophagosome maturation and can be used as markers, in particular, Atg8 (or microtubule-associated protein light chain 3 (LC3) in mammals). Genetic and biochemical studies have elucidated many of the interactions between these proteins as well as the sequence of their action, allowing a hierarchy to be established. However, this hierarchy reveals a complex interrelationship of the Atg proteins and the molecular events they mediate, which do not occur in a linear sequence. All the data to date suggest that the hierarchy in yeast and mammalian cells are identical or very similar. Owing to this complex hierarchy, the most 'upstream' event, the initiating event in autophagosome formation, has been so far impossible to identify. The identification of this initiating event combined with an increased understanding of what the IM/PAS is, the sequence of recruitment of Atg proteins to IMs, and the source of components allowing expansion could finally define the mysterious membrane source of the autophagosome.

Molecular Machinery Required for Induction of Autophagy

Recent data have dramatically expanded our knowledge of how the Atg proteins function to expand the IM into an autophagosome. This has mostly come about through work

[1]Cancer Research UK, London Research Institute, Secretory Pathways Laboratory, 44 Lincolns Inn Fields, London WC2A 3PX, UK
*Correspondence: S Tooze, Secretory Pathways Laboratory, Cancer Research UK, London Research Institute, 44 Lincolns Inn Fields, London WC2A 3PX, UK.
Tel: +44 207 269 3122; Fax: +44 207 269 3417; E-mail: sharon.tooze@cancer.org.uk
Keywords: autophagy; autophagosome; isolation membrane; phagophore; membrane trafficking; Atg proteins
Abbreviations: Atg, autophagy-related; AV, autophagic vacuole; AVi, immature AV; AVd, degradative AV; BIF-1, Bax-interacting factor 1; DFCP1, Double FYVE domain-containing protein 1; ERGIC, ER–Golgi intermediate compartment; ESCRT, endosomal sorting complex required for transport; FIP200, focal adhesion kinase family interacting protein of 200 kD; IM, isolation membrane; LC3, microtubule-associated protein light chain 3; PAS, pre-autophagosomal structure; PE, phosphatidylethanolamine; PI3P, phophatidylinositol-3-phosphate; SNARE, soluble *N*-ethylmaleimide-sensitive factor attachment protein receptors; TGN, trans-Golgi network; TOR, target of rapamycin; TP53INP2, tumour protein 53 induced nuclear protein 2; ULK, unc-51-like kinase; UVRAG, ultraviolet irradiation resistant-associated gene; VMP1, vacuolar membrane protein 1; Vps, vacuolar protein sorting; WIPI, WD-repeat protein interacting with phosphoinositides
Received 22.12.08; revised 02.3.09; accepted 12.3.09; Edited by M Piacentini; published online 17.4.09

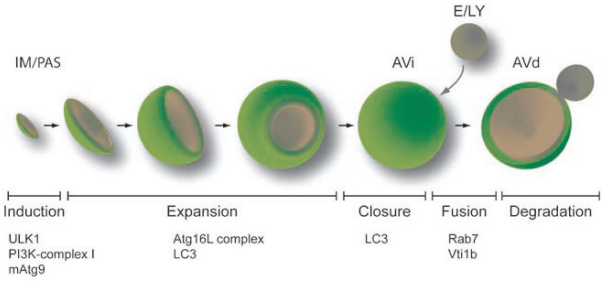

Figure 1 Scheme of macroautophagy pathway in mammalian cells. Autophagy is initiated during an induction phase on IMs/PAS (isolation membranes/pre-autophagosomal structures) that serves both as a signalling platform and a membrane source/acceptor compartment (see Figure 2 for IM-associated molecules). The source of the IM is unknown. During the expansion phase, the IM grows sequestering cytosolic components (for simplicity the sequestered cytosolic components are not illustrated). The possible mechanisms for expansion of the double-membrane IM are addressed in Figure 4. After closure of the expanded IM, the immature autophagosome (AVi) fuses with the endosomal compartments (E) and lysosomes (LY), becoming a degradative autophagosome AVd. Degradation of the sequestered cytosolic components occurs in the AVd as it matures into an autolysosome. At the final stage, the AVd is shown in cross-section to aid visualization of the membrane fusion event(s)

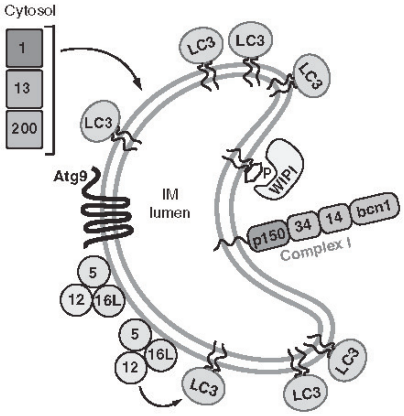

Figure 2 Proteins localized to the isolation membrane (IM). Proteins required for the expansion of the IM are shown on the membrane by their mode of association (if known). For example, the PI3K complex I associates with the membrane through p150, which has an N-terminal myristoylation acceptor sequence,[79] LC3 is bound through PE, and mAtg9 has six transmembrane domains. It is not known how ULK1 or the Atg16L complexes are associated with the membrane. 1, ULK1; 5, Atg5; 12, Atg12; 13, Atg13; 16L, Atg16L; 200, FIP200; 34, Vps 34; 14, Atg14; bcn1, Beclin1

on (1) the two ubiquitin-related pathways (the Atg5-12 and Atg8-PE (Atg8-phosphatidylethanolamine) conjugation systems); (2) the regulation of the class III phosphatidylinositol-3-phosphate (PI3P) kinase complex I (PI3K complex I), which forms PI3P, an essential phospholipid for IM expansion, and its interactors; (3) the transmembrane protein, mammalian Atg (mAtg)9; and (4) the Atg1 kinase homologues, unc-51-like kinase (ULK)1 and ULK2. As in yeast, these are all present on the IM (Figure 2). We will briefly review advances in the field with emphasis on how our knowledge about these molecules has increased our understanding of the formation and expansion process.

Ubiquitin-like conjugation pathways. In the first ubiquitin-related system, Atg12 is conjugated to Atg5 by the combined action of Atg7 and Atg10 (E1 and E2-like enzymes, respectively). The Atg5-12 conjugate, the formation of which is essentially constitutive, associates with Atg16L, and this trimeric complex homodimerizes to form a multimeric 800 kDa complex called the Atg16L complex.[5] The second ubiquitin-related system leads to the conjugation of LC3 (the homologue of Atg8 in yeast) to the lipid PE by Atg7 and Atg3, the latter of which acts as an E2-like enzyme in this conjugation reaction. The lipidated form of LC3 is referred to as LC3-II and localizes to autophagosomal membranes, whereas the unlipidated, cytosolic form is called LC3-I. Importantly, recent data suggests that the Atg16L complex associates with the IM by an unknown mode of recognition, possibly involving Rab33b (see below), and here it can act as a novel E3-like enzyme allowing the recruitment of the Atg3 (E2)-LC3 intermediate to the substrate PE in the membrane, thus determining the site of LC3 lipidation.[6,7]

Elongation of the IM requires the Atg16L complex[8] and LC3-II/Atg8-PE. The properties of the Atg16L complex suggest that it may provide a way to determine where the autophagosome membrane expansion starts. Atg8-PE has fusogenic properties,[9] which could catalyse the elongation process. Recently, it was shown that ectopic localization of Atg16L to the plasma membrane promoted recruitment of LC3-II to this site: Atg16L was targeted to the plasma membrane by the addition of a C-terminal prenylation motif (CAAX) derived from K-Ras.[8] The Atg16L-CAAX fusion protein, through Atg12, recruited GFP-LC3 to the plasma membrane, where it was lipidated by the Atg3-catalysed transfer to PE. Interestingly, GFP-LC3 lipidation was starvation-independent and insensitive to wortmannin, which inhibits the PI3K complex I, suggesting that the main output of PI3P formation is the localization of the Atg16L complex to the PI3P-rich IM. In addition, the expression of the Atg16L-

CAAX-containing complex inhibited the starvation-induced formation of LC3-positive autophagosomes in the cytosol, presumably by competition for the endogenous pools of Atg4, Atg7, and Atg3.

The lipidation of LC3 (and its paralogues GATE-16, GABARAP, and Atg8L) requires prior cleavage by Atg4, a cysteine protease. Importantly, Atg4 can also act on LC3-II to release LC3 from PE, and therefore from the autophagosomal membrane. The removal of LC3-II from the autophagosome is required for its subsequent fusion with the endosome/lysosome.[10] There are four members of the Atg4 family, Atg4a–d, also called the autophagins1–4,[11] and among these Atg4b seems to have the broadest specificity.[12–14]

The Atg4b-dependent cleavage of LC3 requires the catalytic residue, Cys74, and mutation of this residue has been shown to inhibit the cleavage of LC3-II and GABARAP-II *in vitro* and *in vivo* in cell culture model systems. Overexpression of Atg4b was also found to inhibit the lipidation of LC3,[14] and the formation of GFP-LC3-positive autophagosomes.[15] The expression of the catalytically inactive mutant, Atg4b-C47A, however, provided a more interesting phenotype. Although there was no effect on the Atg16L complex formation or its recruitment to autophagosomes, the lifetime of the Atg5-12 conjugate on membranes increased from 5 min to 20 min in cells overexpressing Atg4b-C47A. In these overexpressing cells, autophagosomes were readily detected and a larger percentage of open IMs were found. Although the length of the IMs was not altered after Atg4b-C74A expression, the closed autophagosomes were smaller than those seen in control cells. mAtg9 localization was not affected and ULK1 colocalization with Atg5 was also not perturbed.[15] Note, ULK1 is also recruited to Atg5-positive autophagosomes formed in cells expressing conjugation-defective Atg5-K130R mutant, which has mini-IMs.[8]

Lastly, in mouse embryonic fibroblasts (MEFs) isolated from Atg3 $^{-/-}$ mice several important observations were made about the inter-relationship between the Atg5-12 and LC3/Atg8 conjugation systems, and the role of these systems in autophagy. In the Atg3 $^{-/-}$ MEFs, there was a reduced conjugation of Atg12 to Atg5, and no LC3-II, GABARAP-II, or GATE16-II could be detected. However, under starvation conditions, autophagosomes were detected by EM analysis, but they were smaller than in wild-type (wt) cells. Atg5 and Atg16L were recruited to and remained longer on IMs compared with IMs in wt MEFs. Interestingly, in Atg3 $^{-/-}$ cells, IMs were reported to be abnormally shaped, curling around multiple sections of cytosol, and appeared either open ended or multi-lamellar.[16]

These data provide evidence that the elongation and closure of the IM is controlled by the Atg16L complex and by the LC3-lipidation system. The intimate inter-relationship between these two systems is essential for the formation of properly shaped and sealed autophagosomes. Interestingly, alteration of either complex results in the formation of visibly aberrant IMs, and, in all cases, the formation of these IMs remains sensitive to wortmannin. Two conclusions can be drawn from these experiments, first, LC3 is required for closure of the IM, and second the expansion of the IM is dependent on PI3P production at the site of recruitment.

Although the production of LC3-II is required for autophagy, and LC3-II is a bona fide marker for autophagosomes, recent reports have shown that the reverse is not the case. LC3-II can form and accumulate in the absence of autophagosomes, and in some cases, LC3-II levels were found to be insensitive to inhibitors of lysosomal enzymes in 'autophagic-flux' assays.[17–20] In another example, phagocytosis involving activation of the Toll-like receptor signalling cascade resulted in the recruitment of LC3-II to the phagosome, in an Atg5, Atg7 and Beclin1-dependent reaction.[21] The recruitment of LC3-II to the membrane did not result in the formation of double-membrane autophagosomes, but rather resulted in an enhanced fusion of the phagosomes with late endosomes. This observation suggests that the conjugation of LC3 to PE can occur on membranes that are either unrelated to IMs or to autophagosomal membranes, or on membranes that may be defective IMs unable to recruit the remaining machinery to make autophagosomes. The lack of LC3-II turnover in these cases also suggests that the Atg4b machinery is prevented from acting on LC3-II on these membranes, and/or that there is no fusion of the membranes with endosomes or lysosomes.

PI3K complex I and PI3P-effectors. In yeast, production of PI3P by the class III PI3-k complex I (consisting of Vps34, Vps15, Vps30/Atg6, Atg14) is essential for autophagy. Complex II (consisting of Vps34, Vps15, Vps30/Atg6, Vps38) produces the same lipid species, but has been shown to be required for the endosomal vacuolar protein sorting (Vps)-pathway. The mammalian homologues of Vps34 and Vps15, the shared lipid kinase and regulatory subunits, are called Vps34, and p150, respectively. Beclin1, the mammalian homologue of Vps30, has been the cornerstone for the advances in our understanding of the PI3K complex I in autophagy, and has been shown to be regulated by interaction with Bcl2,[22] and JNK1.[23] Importantly, however, the orthologues of Atg14 and Vps38 have only been identified recently to be Atg14/Barkor and ultraviolet irradiation resistant-associated gene (UVRAG), respectively.[24–26]

UVRAG, the homologue of Vps38, has a role in endocytosis[27] and autophagy.[26] Recent data suggest that its role in both pathways may be mediated by interaction with the class C Vps complex, providing a means to coordinate the two pathways to achieve a maximal autophagic response.[27] In contrast, Itakura *et al.*[24] did not detect a role for UVRAG in autophagy and further work is required to clarify this issue. Interestingly, UVRAG was shown to interact with Bax-interacting factor 1 (BIF-1), also known as endophilin B1.[28] BIF-1 was shown to be required for autophagy and was found on the surface of autophagosomes, colocalized with GFP-Atg5 and GFP-LC3. This exciting result suggests that recruitment of BIF-1 through UVRAG provides machinery to deform membranes, as BIF-1 has a N-BAR domain. BAR domains are modular protein domains, which bind membranes and cause them to undergo curvature.[29] Interestingly, BIF-1 is also required for COPI vesicle budding through interaction with ARF-GAP, the GTPase activating protein for the small GTPase, ARF, thus providing additional support for its role in membrane deformation. Finally, BIF-1 was proposed to interact with mAtg9,[30] a multi-spanning transmembrane Atg protein, which cycles between the

trans-Golgi network (TGN) and endosomes, and is present on autophagosomes after starvation.[31]

The mammalian homologue of Atg14,[24] also called Barkor,[25] plays a key role in the function of the mammalian PI3K complex. The presence of either Atg14/Barkor or UVRAG seems to be mutually exclusive. Thus, it seems that the two PI3K complexes found in mammalian cells are analogous to the yeast PI3K complexes I and II. Atg14/Barkor, which, interestingly, is only found on autophagosome membranes after starvation, can localize to membranes independent of Vps34 and Beclin1. In addition, the levels of Atg14 influence the stability of both Beclin1 and Vps34.[24] Thus, understanding how Atg14 is localized to the IMs may be the key for understanding the dynamics of PI3P production at the IMs. Another important question is whether, like UVRAG, Atg14 can recruit a BIF-1-like protein, and whether mAtg9 cycling from the TGN to endosomes and autophagosomes influences Atg14 recruitment.

In the autophagy pathway, PI3P produced by PI3K complex I is thought to be present on the IM as well as on elongating autophagosomes. Interestingly, in yeast, PI3P is preferentially localized to the inner autophagosomal membrane,[32,33] where it recruits Atg18 along with Atg2.[34] This recent data raises questions about where the PI3K complex I is localized on the autophagosomal membrane, and whether it produces the lipid only on the inner membrane, or all over the autophagosome, followed by segregation to the inner membrane. A localized production would obviate the need for redistribution, but require targeting of PI3K to the inner membrane. Atg18 associates with PI3P directly, whereas it has been proposed that Atg2 may associate with an unknown component on the IM.[32] This unknown component may provide a clue as to how the distinct populations of PI3P are generated and recognized specifically by the autophagy machinery, and address the mystery of how and why a specific population of PI3P can recruit unique downstream effectors to catalyse autophagy.

So far, in yeast, the main direct effector of autophagosomal PI3P is the Atg18-Atg2 complex. In mammalian cells, the orthologue of Atg18 was identified to be WD-repeat protein interacting with phosphoinositides (WIPI)-49,[35] also called WIPI-1, which is a member of a family of four proteins called WIPI-1–4.[36] Overexpressed WIPI-1 is localized to Rab5 and Rab9-positive membranes,[35] and is recruited to GFP-LC3-positive autophagosomes.[36] Two Atg2 homologues exist in mammalian cells, which have not yet been studied, but which are predicted to contain an N-terminal Vps13-like domain. Interestingly, although the function of this short domain is not known, Vps13 functions in the endosome to Golgi transport in yeast. Further work is required on the WIPI family and mAtg2 to uncover their role in PI3P-dependent autophagosome formation.

Lastly, another PI3P effector has been identified called DFCP1 (double FYVE domain-containing protein 1) that localizes to endoplasmic reticulum (ER), ER–Golgi intermediate compartment (ERGIC) and Golgi membranes (Figure 3).

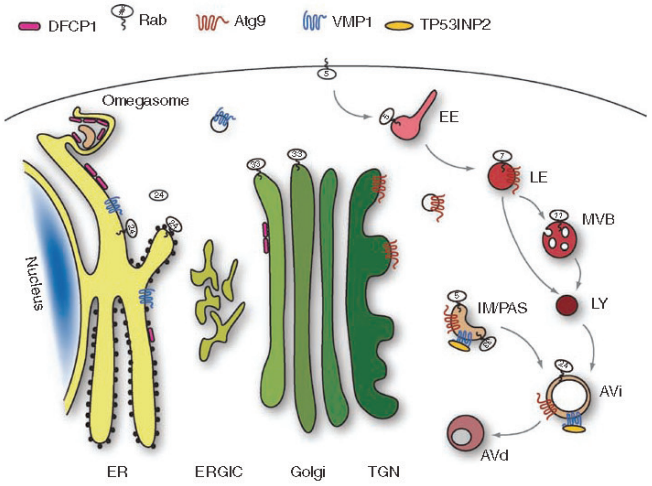

Figure 3 Intracellular localization of membrane-associated molecules involved in the formation and expansion of the isolation membrane. IM/PAS and autophagosomes are found distributed in the cytosol of mammalian cells, although there is some evidence that the maturing AVs are actively translocated to the perinuclear region. Shown is the subcellular localization of membrane proteins that are required for autophagy. Also included is TP53INP2, which associates with VMP. In many cases, the induction of autophagy causes a translocation of proteins to the IM or autophagosome from either the cytosol (LC3 and Rab proteins) or their steady-state location (mAtg9). Rab5, 7, 11, and 33 are efficiently geranylgeranylated, whereas Rab24 is inefficiently modified.[90] DFCP1 is thought to remain associated with the endoplasmic reticulum (ER) by binding to PI3P on the ER, and transiently interacting with the IM. For simplicity, the Atg proteins, except for Atg9, are not shown. TP53INP2, tumour protein 53-induced nuclear protein 2; VMP, vacuolar membrane protein; ERGIC; ER–Golgi intermediate compartment; TGN, trans-Golgi network; EE; early endosome, LE; late endosome, MVB; multi-vesicular body, LY; lysosome

After amino acid starvation, DFCP1 translocates to a punctate compartment, which has been suggested to be a platform for the expansion of IMs and recruitment of Atg proteins, in particular, LC3 and Atg5.[37] It remains to be determined what role this protein has in autophagosome formation, and whether this represents a specialized form of autophagy or whether DFCP1 is essential in all autophagic processes.

ULK1 and ULK2. In yeast, the serine/threonine kinase Atg1 is known to be a key effector for the induction of autophagy, acting downstream of the target of rapamycin (TOR) protein. Atg1 functions as part of a large complex with other Atg proteins, including Atg13 and Atg17. Recent studies have shown that the mAtg1 homologues, ULK1 and 2, have regulatory roles in autophagy and also have identified ULK1/2-interacting proteins.[19,38,39] Despite the high similarity between ULK1 and ULK2 (52% overall identity) they seem to have different roles, in particular, with regard to mAtg9 trafficking.[31] In addition, siRNA knockdown of ULK1 inhibits autophagy in HEK293A and HeLa cells, whereas ULK2 depletion does not.[39] The basis for these differences is not known. However, recent experiments have identified three new interacting proteins, which bind both ULK1 and ULK2: the novel mammalian Atg13 homologue (KIAA0652), focal adhesion kinase family interacting protein of 200 kD (FIP200), and Atg101 (see for review Chan and Tooze[40]).

Yeast Atg13 is a phosphoprotein that, after inactivation of TOR, is dephosphorylated, binds Atg1, and together with Atg17 regulates its activity to promote autophagy. The mAtg13 has recently been identified and was shown to be required for autophagy.[38,41–44] It binds ULK1 and ULK2 at the C-terminal domain (CTD) independent of its phosphorylation state; however, mAtg13 was shown to be a substrate for ULK1 and ULK2.[38,41–43] Interestingly, ULK1/2 and mAtg13 form a tight association with membranes and exhibit a partial colocalization.[38]

The FIP200 also interacts with ULK1 and ULK2,[19] and may be the mammalian equivalent of Atg17.[45] FIP200 is required for autophagy, and colocalizes with ULK1/2 and Atg16L on IMs. FIP200 also interacts with ULK1/2 in the CTD, and is required for the recruitment of ULK1/2 to IMs. In addition, it has been shown that ULK1-Atg13-FIP200 are present in a large complex that, in nutrient-rich conditions, contains mTOR.[42] Atg101, identified through its homology to a Atg1-binding protein in Drosophila, was shown to interact with the ULK1-Atg13-FIP200 complex in an Atg13 dependent manner.[44]

The identification and characterization of potential ULK1/2 effectors will allow a better understanding of the function of these kinases in autophagosome formation. The two most promising avenues would be a further understanding of the membrane association of ULK1/2, mAtg13, and mTOR, how and where the kinases are activated, and how their activity regulates the initiation of autophagy and expansion of the IM.

Transmembrane proteins. Two transmembrane proteins have so far been found to be involved in mammalian autophagy. One is the homologue of yeast Atg9,[46] called mAtg9,[31] or Atg9L1,[47] and the other is vacuolar membrane protein 1 (VMP1).[48] Although absent in yeast, there is a VMP1 homologue in *Dictyostelium discoideum*, which functions in organelle biogenesis, the secretory pathway, multicellular development and, potentially, in autophagy.[49] These proteins localize to different compartments in the cell, yet both contribute to the formation of autophagosomes (see Figure 3).

mAtg9 has six transmembrane domains with both the N and C-termini in the cytosol. Although its function is not yet known, mAtg9 cycles between the TGN and late endosomes in an ULK1-dependent manner, and relocates to a peripheral pool upon starvation or rapamycin treatment. This peripheral pool was shown to overlap with both GFP-LC3-positive, Rab7-negative and GFP-LC3-positive, Rab7-positive autophagosomes, representing AVis and AVds, respectively. siRNA-mediated knock down of mAtg9 resulted in an impairment of autophagy.[31] From the existing data in yeast, mAtg9 has been proposed to deliver lipids to the forming autophagosome,[50] an attractive hypothesis that remains to be tested experimentally in mammalian cells.

VMP1 is predicted to be a multi-spanning transmembrane protein, but unlike mAtg9, it localizes predominantly to the ER. The topology of VMP1 remains to be determined, however, the C-terminus contains a domain that interacts with Beclin1, suggesting that this domain is cytosolic. It was found that both VMP1 mRNA and protein levels increase after starvation. VMP1 has been shown to colocalize with LC3 and Beclin1 on autophagosome membranes.[51] Overexpression of VMP1 induces autophagosomes even under nutrient-rich conditions and this seems to be dependent on its direct binding to Beclin1. Importantly, depletion of VMP1 by RNAi inhibits autophagosome formation after starvation or rapamycin treatment. These findings suggest a role for VMP1 in recruitment of Beclin1 along with the other components of the PI3K complex I to the IM, which leads to the recruitment of further Atg-proteins.

Recently, a novel VMP1-interacting protein, called tumour protein 53-induced nuclear protein 2 (TP53INP2), has been identified and was discovered to be essential for autophagy.[52] Interestingly, TP53INP2 translocates from the nucleus to autophagosomes upon induction of autophagy, where it binds to LC3 and other LC3-family members (Gate-16, GABARAP), as well as VMP1. Therefore, TP53INP2 was proposed to act as a scaffold protein to recruit other Atg proteins to the IM. TP53INP2 is absent in ancient eukaryotes and it is tempting to speculate that it has evolved later to regulate the more diverse functions of autophagy in multicellular organisms.

It remains to be determined what the function of mAtg9 or VMP1 is; do they function as lipid carriers or provide platforms for recruitment of Atg-proteins and/or other effectors to the IM? Further study of these proteins and their binding partners should give us valuable information about autophagosome formation.

Membrane Trafficking Proteins Required for Autophagosome Formation

We propose four potential models to illustrate how an IM and autophagosome may form (see Figure 4). In developing each model, we have identified a set of common requirements, some of which are Atg proteins, and some based on data from other membrane trafficking and membrane biogenesis

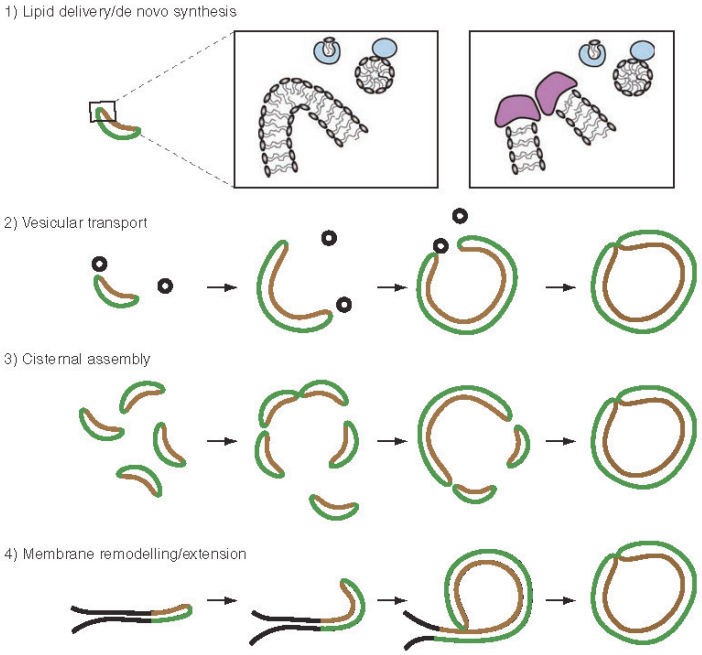

Figure 4 Four models for isolation membrane (IM) expansion. The mechanisms driving the growth and expansion of the IM are not well-understood. There are many potential scenarios by which the IM can expand, and as discussed in the text, we propose four possible alternative models. Model 1 is based on a *de novo* delivery of lipids by either lipid transfer proteins (light blue) to sealed bilayers (left side) or to open bilayers stabilized by a putative capping protein (purple). Models 2 and 3 both use conventional trafficking pathways through heterotypic fusion of vesicles (Model 2) or homotypic fusion (Model 3) of individual IMs. In Models 2 and 3, it is assumed that the IM is a pre-existing, and perhaps stable vesicle or double-membrane structure. Model 4 proposes that the IM is derived and expands from a compartment, such as the endoplasmic reticulum. Segregation of membrane proteins and lipids into the elongating tip, and retention of resident proteins and lipids would generate a unique membrane domain. This unique domain could either bend and enclose cytosol, while still attached to the donor organelle, and then pinch off, or first pinch off as a large sheet, and then undergo curvature and closure

pathways. For brevity, we have not included a comprehensive assessment of the role of the cytoskeleton in autophagosome formation. After a discussion below of the common requirements, we will discuss these models and hypothesize on the specific cellular machinery that would be required for each model.

Curvature machinery. Regardless of the mechanism by which autophagosomes are assembled, a principal requirement is a membrane deforming and/or lipid organizing machinery to induce membrane curvature. The best characterized curvature-generating machineries are coat protein complexes (clathrin, COPI, and COPII), and proteins or protein complexes capable of bending membranes, for instance ENTH and BAR domain-containing proteins.[29] So far, there are two main candidates known to be required for autophagy, which may drive IM curvature.

All Atg proteins, apart from LC3/Atg8, exhibit some preference for localization to the external surface of the nascent autophagosome.[8] The Atg16L complex, in particular, has been proposed to act as a proteinaceous coat.[53] Importantly, the complex dissociates from the membrane during the formation process, which is a common feature of other coat machinery. BIF-1 is a second possible candidate to fulfil this function, as it has a BAR and an SH3 domain, both of which are required to induce autophagosome formation through activation of the class III PI3K complex.[28] Interestingly, at least in yeast, PI3P seems to be localized primarily to the inner autophagosome bilayer.[32] Atg16L, BIF-1, or both together, combined with a differential distribution of lipid, could generate a lipid and protein asymmetry that could be responsible for driving membrane curvature intrinsically, or through the recruitment of additional proteins.

Expansion, closure, and fusion machinery. Another common requirement in all four models is for the machinery to expand and then close the nascent autophagosomes, allowing subsequent fusion with early and late endosomes,

lysosomes and multi-vesicular bodies (MVBs). Expansion and closure are sequential steps that are likely to be linked either through utilization of the same machinery or through interacting machinery. Although still one of the big questions, recent data provides some suggestion on how expansion of the IM may occur, and also begins to address how the closure of the IM occurs.

Microtubule-associated protein light chain 3. As discussed above, LC3 might be directly responsible for autophagosome closure,[6] possibly through its intrinsic hemifusion activity first shown *in vitro*.[9] In yeast, Atg8 has been shown to be responsible for PAS expansion, and the amount of Atg8 present directly determined the size of the completed autophagosome.[54] In contrast, in mammalian cells, IM expansion did not seem to be affected by LC3-II inactivation and further work is required to reconcile these differences.

ESCRT complex machinery. Several subunits of the endosomal sorting complex required for transport (ESCRT) are essential for autophagy. Deletion of vps28 (ESCRT-I), vps25 (ESCRT-II), vps32 (ESCRT-III), or vps4 (AAA-ATPase) results in accumulation of non-degradative autophagosomes in flies.[55] Likewise, loss of mSnf7-2 or overexpression of CHMP2B^{Intron5} (both subunits of ESCRT-III) in cortical neurons of mice led to a similar phenotype,[56] showing that a functional pool of MVBs is essential for autophagosome maturation by providing target organelles for fusion. Although the data suggests that loss of ESCRT function was a result of a fusion defect, it cannot be entirely excluded that there was also a closure defect, and expanded, but not closed, IMs accumulated. As the membrane topology of a closing autophagosome is similar to the inward budding vesicle on a late endosome (see Figure 4), we speculate that components of the ESCRT complex itself may be responsible for the final closure of autophagosomes. However, it has been shown that the deletion of ESCRT proteins in yeast does not seem to affect autophagy,[57,58] thus this hypothesis remains entirely speculative.

Rabs and SNAREs. The final two classes of common machinery are the Rab and soluble *N*-ethylmaleimide-sensitive factor attachment protein receptors (SNARE) proteins.[59] Both Rabs and SNAREs act in most, if not all, membrane trafficking pathways. Rab proteins are small molecular weight GTP-binding proteins, which act as molecular switches, mediating transport and fusion of vesicles. Relevant to this discussion are the data, which suggests that Rab proteins are crucial for developing subdomains on membranes to facilitate maturation; for example, during early to late endosome maturation, Rab5-positive domains give way to Rab7-positive domains.

Regarding autophagosome formation, the early endosomal protein Rab5 has been shown to act at early formation stages through Vps34, and regulates the conjugation of Atg12 to Atg5, possibly by promoting the recruitment of Atg12 or the conjugation machinery to the PI3P and Atg5-positive IM.[60]

The late endosomal Rab7 has been shown to be involved in late stages of autophagosome maturation, presumably by facilitating fusion of autophagosomes with late endosomes and lysosomes (Figure 3). Likewise, Rab11, which is present on MVBs in K562 cells may promote fusion of autophagosomes with MVBs.[61] Rab24 was initially shown to partially associate with GFP-LC3-positive autophagosomes.[62] Rab24 is usually localized to the ER, cis-Golgi, and ERGIC, but relocalizes to punctate structures after induction of autophagy through starvation or vinblastine treatment. However, it seems to be recruited mainly to fully formed degradative autophagosomes or autolysosomes, indicating that it is not involved in vesicular extension of the IM and its exact function remains to be elucidated.

Recent evidence suggest that Rab33 might play an important role in the targeting and recruitment of Atg16L to the IM.[63] It was shown that the Golgi residents (Rab33a and Rab33b) bind directly to Atg16L in a GTP-dependent manner and overexpression of GFP-Rab33b causes Atg16L recruitment to the Golgi. A constitutively active mutant of Rab33b (Rab33b-Q92L) significantly increased LC3-II levels regardless of the nutrient state, but did not lead to formation of LC3-positive puncta, normally found under starvation conditions. This indicates that the Atg16L complex was recruited and functional, but additional factors needed for autophagosome expansion were lacking, and therefore, no large LC3 puncta could be observed. In fact, overexpression of Rab33b-Q92L in full medium led to an accumulation of the autophagy substrate, p62/SQSTM1, suggesting an inhibition of constitutive, basal autophagy. However, after starvation, p62 was efficiently degraded indicating that perhaps when enough additional autophagy-factors were activated, the process could continue. Alternatively, the pathway for constitutive autophagy could be different from the inducible autophagy pathway, and a different set of proteins could be involved in autophagosome formation in each case.

Finally, many vesicular fusion steps in the cell are catalysed by the SNARE protein family. SNARE proteins drive membrane fusion through the formation of a four-member alpha helix bundle (the SNARE complex), comprised of cognate target and vesicle SNAREs (called t and vSNAREs, respectively) on opposing membranes, which is regulated by *N*-ethylmaleimide-sensitive factor (NSF). Both the distribution of each of the four SNAREs comprising the complex, and complex formation is a characteristic of each membrane compartment. In *Saccharomyces cerevisiae*, it has been shown that Sec18 (NSF) and Vti1 (a SNARE) are required for fusion of the AV to the vacuole;[64] however, no tSNARES could be detected on the PAS, suggesting that Rabs, NSF, or SNAREs are not involved in AV biogenesis.[58] Although in mammalian cells no data exists about the presence of SNAREs on the IM, Vti1b knockout mice accumulate autophagosomes, showing that this SNARE (and presumably its SNARE complex) is required for maturation, but not formation of autophagosomes.[65] This leaves open the question of the role of SNARE-mediated fusion events for expansion, assembly or closure during autophagosome formation.

Models for Autophagosome Formation

Model 1: lipid delivery/*de novo* synthesis. This model implies that the IM is elongated through the delivery of lipids,

lipid droplets, or micelles. Lipids from lipid droplets could be delivered by spontaneous exchange and insertion, or through lipid transfer proteins. Delivery of lipids to the outer leaflet will allow it to expand. However, for expansion of the inner leaflet, lipids delivered to the outer leaflet will have to undergo 'flip-flop' (see Figure 4, model 1). This could be accomplished by a lipid flippase enzyme.[66] Alternatively, we have speculated that the IM may be comprised of two distinct bilayers held in close proximity by a protein scaffold that could also act as a capping protein. This capping protein, or protein complex could receive lipids through a lipid transfer protein.

A third alternative is that, a close proximity of the IM to the lipid synthesis machinery in the ER could provide fatty acids for *de novo* autophagosomal membrane formation.

Recent studies by Axe *et al*.[37] have found that at least some autophagosomes seem to arise from ER membrane-associated cups, called omegasomes because of their shape. These omegasomes are highly enriched in PI3P and the PI3P-binding protein termed DFCP1, the marker for omegasomes, which might provide a signalling platform for autophagosome biogenesis (see Figure 3). However, additional experiments are required to determine the exact function of DFCP1 and the omegasomes, whether lipid synthesis occurs in or around these structures, or whether they might provide ER membrane itself to the autophagosome.

Yeast or mammalian screens have not revealed any protein machinery to support our first model, but the apparent scarceness of protein in the autophagosomal membranes[67,68] and the failure to identify a definitive membrane source for autophagosome biogenesis suggests that this hypothesis may be worth further investigation.

Model 2: vesicular transport. The second model proposes that the autophagosomal membrane is delivered to the growing IM through vesicular transport (Figure 4, model 2). In this case, one would expect a similar set of trafficking machinery to be necessary as in other regulated vesicular transport events. This includes cytoskeletal motor proteins to ensure directional transport, tethers to bridge the vesicle to the target, Rab GTPases and their effectors, as well as SNARE proteins to mediate homotypic and heterotypic fusion events.[59]

Microtubules have been shown to facilitate autophagosome formation in mammalian cells,[69,70] although it is not clear what role they have in AV formation. The motor protein required for transport of the autophagosome to the endosomal compartments has been identified as dynein;[71] however, there is no evidence yet that this motor is required for IM expansion or closure.

Interestingly, there may be a link, which has not yet been investigated, between microtubules and the Atg machinery. ULK1/Atg1 is not only an important early regulator of autophagy,[39,72,73] but has also been shown to be involved in neurite extension and axonal vesicular transport in the mouse and fly, respectively.[74,75] The Drosophila homologue of ULK1/Atg1 has recently been shown to mediate neuronal vesicular trafficking by binding and phosphorylating UNC-76, a kinesin heavy chain adaptor protein, and possibly other targets. This activated form of UNC-76 binds to synaptic vesicle proteins, and thereby links these vesicles to kinesin and the microtubule cytoskeleton for transport to the axon tip. Thus, it is tempting to speculate that ULK1 activity, which is a very early requirement in induction of autophagy, may promote transport of vesicles to the IM.

Lastly, of the Rab proteins listed above, Rab5 and Rab33b seem to be the most promising candidates. Rab proteins are recruited to specific membranes by a network of Rab effector proteins that form a membrane-specific platform.[76] No autophagy-specific Rab effectors have been identified, and thus it is not yet clear how these Rab proteins would be recruited to the IM.

Model 3: cisternal assembly. This model proposes that the autophagosome is assembled by homotypic fusion of special autophagy vesicles or discrete IMs. A similar model has been proposed earlier (see also Reggiori *et al*[58]). These vesicles are either constantly present in the cytoplasm and come together after induction of autophagy, or they are generated in response to autophagic stimuli. In the latter possibility, of course, the questions of how and where they would arise are raised, and their creation may involve special fission machinery. Otherwise, similar components would be needed, as in the vesicular transport model, with a homotypic instead of heterotypic fusion machinery.

Model 4: membrane remodelling/extension. In this model, the autophagosome is not so much generated by gradual expansion of the IM, but by extension and curvature of a pre-existing membrane sheet, or even by flattening an endosome-like structure. An analogy for such membrane remodelling/extension is the biogenesis of peroxisomes from specialized ER subdomains, in which ER-resident proteins are excluded and peroxisomal proteins get enriched.[77]

The first scenario (extension and curvature) would require some kind of selection and/or exclusion machinery to determine which lipids and proteins would enter into the autophagosome membrane and which would be excluded. The second possibility (flattening) would require a protein scaffold to deform the membrane and a mechanism to alter the lipid composition as the membrane changes shape. On the basis of immunofluorescence and EM data, it is often assumed that the IM is a crescent shaped membrane vesicle, distributed randomly throughout the cytoplasm.[8] In this scenario, however, the IM would be more like a signalling platform attached to the donor membrane structure. Seen in cross-section by EM, the sorted domain with its selective localization of proteins would resemble a cup-shaped structure.

Conclusions

Our first three hypothetical models are based on pre-existing, largely established mechanisms for lipid movement between membranes, and vesicular trafficking pathways. The last model is based on speculation, but was developed from the notion that the IM arises from the ER.[78] It should be noted that these models could coexist and drive different stages of autophagy. For example, biogenesis of the PAS/IM might use one mechanism, whereas expansion would employ another.

Further advances in our understanding could come from the identification of early intermediates, either visualized by sophisticated microscopy techniques, or using conventional approaches after manipulation of the process to accumulate intermediates. In addition, the continued identification of novel effectors of the key players will allow a greater understanding of the function of the proteins localized to the IM.

Acknowledgements. We thank members of the laboratory for helpful discussions, and Drs. Fiona McAlpine, Andrea Orsi, Ed Chan, and John Tooze for reading the manuscript and for their helpful comments. We thank Cancer Research UK for funding the research in the Tooze laboratory.

1. Mizushima N, Levine B, Cuervo AM, Klionsky DJ. Autophagy fights disease through cellular self-digestion. *Nature* 2008; **451**: 1069–1075.
2. Suzuki K, Kirisako T, Kamada Y, Mizushima N, Noda T, Ohsumi Y. The pre-autophagosomal structure organized by concerted functions of APG genes is essential for autophagosome formation. *EMBOJ* 2001; **20**: 5971–5981.
3. Klionsky DJ, Cregg JM, Dunn WA, Emr SD, Sakai Y, Sandoval IV *et al.* A unified nomenclature for yeast autophagy-related genes. *Dev Cell* 2003; **5**: 539–545.
4. Suzuki K, Kubota Y, Sekito T, Ohsumi Y. Hierarchy of Atg proteins in pre-autophagosomal structure organization. *Genes Cells* 2007; **12**: 209–218.
5. Mizushima N, Kuma A, Kobayashi Y, Yamamoto A, Matsubae M, Takao T *et al.* Mouse Apg16L, a novel WD-repeat protein, targets to the autophagic isolation membrane with the Apg12-Apg5 conjugate. *J Cell Sci* 2003; **116**: 1679–1688.
6. Fujita N, Itoh T, Omori H, Fukuda M, Noda T, Yoshimori T. The Atg16L complex specifies the site of LC3 lipidation for membrane biogenesis in autophagy. *Mol Biol Cell* 2008; **19**: 2092–2100.
7. Hanada T, Noda NN, Satomi Y, Ichimura Y, Fujioka Y, Takao T *et al.* The Atg12-Atg5 conjugate has a novel E3-like activity for protein lipidation in autophagy. *J Biol Chem* 2007; **282**: 37298–37302.
8. Mizushima N. Dissection of autophagosome formation using Apg5-deficient mouse embryonic stem cells. *J Cell Biol* 2001; **152**: 657–667.
9. Nakatogawa H, Ichimura Y, Ohsumi Y. Atg8, a ubiquitin-like protein required for autophagosome formation, mediates membrane tethering and hemifusion. *Cell* 2007; **130**: 165–178.
10. Kimura S, Noda T, Yoshimori T. Dissection of the autophagosome maturation process by a novel reporter protein, tandem fluorescent-tagged LC3. *Autophagy* 2007; **3**: 452–460.
11. Marino G, Uria JA, Puente XS, Quesada V, Bordallo J, Lopez-Otin C. Human autophagins, a family of cysteine proteinases potentially implicated in cell degradation by autophagy. *J Biol Chem* 2003; **278**: 3671–3678.
12. Hemelaar J, Lelyveld VS, Kessler BM, Ploegh HL. A single protease, Apg4B, is specific for the autophagy-related ubiquitin-like proteins GATE-16, MAP1-LC3, GABARAP and Apg8L. *J Biol Chem* 2003; **278**: 51841–51850.
13. Kabeya Y, Mizushima N, Yamamoto A, Oshitani-Okamoto S, Ohsumi Y, Yoshimori T. LC3, GABARAP and GATE16 localize to autophagosomal membrane depending on form-II formation. *J Cell Sci* 2004; **117**: 2805–2812.
14. Tanida I, Sou Y-S, Ezaki J, Minematsu-Ikeguchi N, Ueno T, Kominami E. HsAtg4B/HsApg4B/autophagin-1 cleaves the carboxyl termini of three human Atg8 homologues and delipidates microtubule-associated protein light Chain 3- and GABAA receptor-associated protein-phospholipid conjugates. *J Biol Chem* 2004; **279**: 36268–36276.
15. Fujita N, Hayashi-Nishino M, Fukumoto H, Omori H, Yamamoto A, Noda T *et al.* An Atg4B mutant hampers the lipidation of LC3 paralogues and causes defects in autophagosome closure. *Mol Biol Cell* 2008; **19**: 4651–4659.
16. Sou Y-S, Waguri S, Iwata J-I, Ueno T, Fujimura T, Hara T *et al.* The Atg8 conjugation system is indispensable for proper development of autophagic isolation membranes in mice. *Mol Biol Cell* 2008; **19**: 4762–4775.
17. Zeng X, Overmeyer JH, Maltese WA. Functional specificity of the mammalian Beclin-Vps34 PI 3-kinase complex in macroautophagy versus endocytosis and lysosomal enzyme trafficking. *J Cell Sci* 2006; **119**: 259–270.
18. Matsui Y, Takagi H, Qu X, Abdellatif M, Sakoda H, Asano T *et al.* Distinct roles of autophagy in the heart during ischemia and reperfusion: roles of AMP-activated protein kinase and Beclin 1 in mediating autophagy. *Circ Res* 2007; **100**: 914–922.
19. Hara T, Takamura A, Kishi C, Iemura S, Natsume T, Guan JL *et al.* FIP200, a ULK-interacting protein, is required for autophagosome formation in mammalian cells. *J Cell Biol* 2008; **181**: 497–510.
20. Ueno T, Wataru Sato W, Yasuo Horie Y, Masaaki Komatsu M, Isei Tanida I, Mitsutaka Yoshida M *et al.* Loss of Pten, a tumor suppressor, causes the strong inhibition of autophagy without affecting LC3 lipidation. *Autophagy* 2008; **4**: 692–700.
21. Sanjuan MA, Dillon CP, Tait SWG, Moshiach S, Dorsey F, Connell S *et al.* Toll-like receptor signalling in macrophages links the autophagy pathway to phagocytosis. *Nature* 2007; **450**: 1253–1257.
22. Pattingre S, Tassa A, Qu X, Garuti R, Liang XH, Mizushima N *et al.* Bcl-2 antiapoptotic proteins inhibit beclin 1-dependent autophagy. *Cell* 2005; **122**: 927–939.
23. Wei Y, Pattingre S, Sinha S, Bassik M, Levine B. JNK1-mediated phosphorylation of Bcl-2 regulates starvation-induced autophagy. *Mol Cell* 2008; **30**: 678–688.
24. Itakura E, Kishi C, Inoue K, Mizushima N. Beclin 1 forms two distinct phosphatidylinositol 3-kinase complexes with mammalian Atg14 and UVRAG. *Mol Biol Cell* 2008; **19**: 5360–5372.
25. Sun Q, Fan W, Chen K, Ding X, Chen S, Zhong Q. Identification of Barkor as a mammalian autophagy-specific factor for Beclin 1 and class III phosphatidylinositol 3-kinase. *Proc Natl Acad Sci USA* 2008; **105**: 19211–19216.
26. Liang C, Feng P, Ku B, Dotan I, Canaani D, Oh B-H *et al.* Autophagic and tumour suppressor activity of a novel Beclin1-binding protein UVRAG. *Nat Cell Biol* 2006; **8**: 688–698.
27. Liang C, Lee J-S, Inn K-S, Gack MU, Li Q, Roberts EA *et al.* Beclin1-binding UVRAG targets the class C Vps complex to coordinate autophagosome maturation and endocytic trafficking. *Nat Cell Biol* 2008; **10**: 776–787.
28. Takahashi Y, Coppola D, Matsushita N, Cualing HD, Sun M, Sato Y *et al.* Bif-1 interacts with Beclin 1 through UVRAG and regulates autophagy and tumorigenesis. *Nat Cell Biol* 2007; **9**: 1142–1151.
29. Itoh T, De Camilli P. BAR, F-BAR (EFC) and ENTH/ANTH domains in the regulation of membrane-cytosol interfaces and membrane curvature. *Biochimica et Biophysica Acta (BBA) - Mol Cell Biol Lipids* 2006; **1761**: 897–912.
30. Takahashi Y, Meyerkord CL, Wang HG. BARgaining membranes for autophagosome formation: regulation of autophagy and tumorigenesis by Bif-1/Endophilin B1. *Autophagy* 2008; **4**: 121–124.
31. Young ARJ, Chan EYW, Hu XW, chl R, Crawshaw SG, High S *et al.* Starvation and ULK1-dependent cycling of mammalian Atg9 between the TGN and endosomes. *J Cell Sci* 2006; **119**: 3888–3900.
32. Obara K, Ohsumi Y. Dynamics and function of PtdIns(3)P in autophagy. *Autophagy* 2008; **4**: 952–954.
33. Obara K, Noda T, Niimi K, Ohsumi Y. Transport of phosphatidylinositol 3-phosphate into the vacuole via autophagic membranes in Saccharomyces cerevisiae. *Genes Cells* 2008; **13**: 537–547.
34. Obara K, Sekito T, Niimi K, Ohsumi Y. The Atg18-Atg2 complex is recruited to autophagic membranes via phosphatidylinositol 3-phosphate and exerts an essential function. *J Biol Chem* 2008; **283**: 23972–23980.
35. Jeffries TR, Dove SK, Michell RH, Parker PJ. PtdIns-specific MPR pathway association of a novel WD40 repeat protein, WIPI49. *Mol Biol Cell* 2004; **15**: 2652–2663.
36. Proikas-Cezanne T, Waddell S, Gaugel A, Frickey T, Lupas A, Nordheim A. WIPI-1 (WIPI49), a member of the novel 7-bladed WIPI protein family, is aberrantly expressed in human cancer and is linked to starvation-induced autophagy. *Oncogene* 2004; **58**: 9314–9325.
37. Axe EL, Walker SA, Manifava M, Chandra P, Roderick HL, Habermann A *et al.* Autophagosome formation from membrane compartments enriched in phosphatidylinositol 3-phosphate and dynamically connected to the endoplasmic reticulum. *J Cell Biol* 2008; **182**: 685–701.
38. Chan EY, Longatti A, McKnight NC, Tooze SA. Kinase-inactivated ULK proteins inhibit autophagy via their conserved C-terminal domain using an Atg13-independent mechanism. *Mol Cell Biol* 2009; **29**: 157–171.
39. Chan EY, Kir S, Tooze SA. siRNA screening of the kinome identifies ULK1 as a multidomain modulator of autophagy. *J Biol Chem* 2007; **282**: 25464–25474.
40. Chan EY, Tooze SA. Evolution and expansion in Atg1 function. *Autophagy* 2009 (in press).
41. Chang Y-Y, Neufeld TP. An Atg1/Atg13 complex with multiple roles in TOR-mediated autophagy regulation. *Mol Biol Cell* 2009, E08-12-1250 (in press).
42. Hosokawa N, Hara T, Kaizuka T, Kishi C, Takamura A, Miura Y *et al.* Nutrient-dependent mTORC1 association with the ULK1-Atg13-FIP200 complex required for autophagy. *Mol Biol Cell* 2009, E08-12-1248 (in press).
43. Jung CH, Jun CB, Ro S-H, Kim Y-M, Otto NM, Cao J *et al.* ULK-Atg13-FIP200 complexes mediate mTOR signaling to the autophagy machinery. *Mol Biol Cell* 2009, E08-12-1249 (in press).
44. Mercer CA, Kaliappan A, Dennis PB. A novel, human Atg13 binding protein, Atg101, interacts with ULK1 and is essential for macroautophagy. *Autophagy* 2009 (in press).
45. Hara T, Mizushima N. Role of ULK-FIP200 complex in mammalian autophagy: FIP200, a counterpart of yeast Atg17? *Autophagy* 2009; **5**: 85–87.
46. Lang T, Reiche S, Straub M, Bredschneider M, Thumm M. Autophagy and the cvt pathway both depend on AUT9. *J Bacteriol* 2000; **182**: 2125–2133.
47. Yamada T, Carson AR, Caniggia I, Umebayashi K, Yoshimori T, Nakabayashi K *et al.* Endothelial nitric-oxide synthase antisense (NOS3AS) gene encodes an autophagy-related protein (APG9-like2) highly expressed in trophoblast. *J Biol Chem* 2005; **280**: 18283–18290.
48. Dusetti NJ, Jiang Y, Vaccaro MI, Tomasini R, Azizi Samir A, Calvo EL *et al.* Cloning and expression of the rat vacuole membrane protein 1 (VMP1), a new gene activated in pancreas with acute pancreatitis, which promotes vacuole formation. *Biochem Biophys Res Commun* 2002; **290**: 641–649.
49. Calvo-Garrido J, Carilla-Latorre S, Lazaro-Dieguez F, Egea G, Escalante R. Vacuole membrane protein 1 is an endoplasmic reticulum protein required for organelle biogenesis, protein secretion, and development. *Mol Biol Cell* 2008; **19**: 3442–3453.
50. Kim J, Huang WP, Stromhaug PE, Klionsky DJ. Convergence of multiple autophagy and cytoplasm to vacuole targeting components to a perivacuolar membrane compartment prior to *de novo* vesicle formation. *J Biol Chem* 2002; **277**: 763–773.

51. Ropolo A, Grasso D, Pardo R, Sacchetti ML, Archange C, Lo Re A *et al.* The pancreatitis-induced vacuole membrane protein 1 triggers autophagy in mammalian cells. *J Biol Chem* 2007; **282**: 37124–37133.
52. Nowak J, Archange C, Tardivel-Lacombe J, Pontarotti P, Pebusque MJ, Vaccaro MI *et al.* The TP53INP2 protein is required for autophagy in mammalian cells. *Mol Biol Cell* 2009; **20**: 870–881.
53. Reggiori F, Klionsky D. Autophagosomes: biogenesis from scratch? *Curr Opin Cell Biol* 2005; **17**: 1–8.
54. Xie Z, Nair U, Klionsky DJ. Atg8 controls phagophore expansion during autophagosome formation. *Mol Biol Cell* 2008; **19**: 3290–3298.
55. Rusten TE, Vaccari T, Lindmo K, Rodahl LM, Nezis IP, Sem-Jacobsen C *et al.* ESCRTs and Fab1 regulate distinct steps of autophagy. *Curr Biol* 2007; **17**: 1817–1825.
56. Lee J, Beigneux A, Ahmad S, Young S, Gao F. ESCRT-III dysfunction causes autophagosome accumulation and neurodegeneration. *Curr Biol* 2007; **17**: 1561–1567.
57. Epple UD, Eskelinen EL, Thumm M. Intravacuolar membrane lysis in Saccharomyces cerevisiae. Does vacuolar targeting of Cvt17/Aut5p affect its function? *J Biol Chem* 2003; **278**: 7810–7821.
58. Reggiori F, Wang CW, Nair U, Shintani T, Abeliovich H, Klionsky DJ. Early stages of the secretory pathway, but not endosomes, are required for Cvt vesicle and autophagosome assembly in Saccharomyces cerevisiae. *Mol Biol Cell* 2004; **15**: 2189–2204.
59. Cai H, Reinisch K, Ferro-Novick S. Coats, tethers, Rabs, and SNAREs work together to mediate the intracellular destination of a transport vesicle. *Dev Cell* 2007; **12**: 671–682.
60. Ravikumar B, Imarisio S, Sarkar S, O'Kane CJ, Rubinsztein DC. Rab5 modulates aggregation and toxicity of mutant huntingtin through macroautophagy in cell and fly models of Huntington disease. *J Cell Sci* 2008; **121**: 1649–1660.
61. Fader CM, Sanchez D, Furlan M, Colombo MI. Induction of autophagy promotes fusion of multivesicular bodies with autophagic vacuoles in k562 cells. *Traffic* 2008; **9**: 230–250.
62. Munafo DB, Colombo MI. Induction of autophagy causes dramatic changes in the subcellular distribution of GFP-Rab24. *Traffic* 2002; **3**: 472–482.
63. Itoh T, Fujita N, Kanno E, Yamamoto A, Yoshimori T, Fukuda M. Golgi-resident small GTPase Rab33B interacts with Atg16L and modulates autophagosome formation. *Mol Biol Cell* 2008; **19**: 2916–2925 E07-12-1231.
64. Ishihara N, Hamasaki M, Yokota S, Suzuki K, Kamada Y, Kihara A *et al.* Autophagosome requires specific early Sec proteins for its formation and NSF/SNARE for vacuolar fusion. *Mol Biol Cell* 2001; **12**: 3690–3702.
65. Atlashkin V, Kreykenbohm V, Eskelinen E-L, Wenzel D, Fayyazi A, Fischer von Mollard G. Deletion of the SNARE vti1b in mice results in the loss of a single SNARE partner, syntaxin 8. *Mol Cell Biol* 2003; **23**: 5198–5207.
66. Lenoir G, Williamson P, Holthuis J. On the origin of lipid asymmetry: the flip side of ion transport. *Curr Opin Chem Biol* 2007; **11**: 654–661.
67. Baba M, Osumi M, Ohsumi Y. Analysis of the membrane structures involved in autophagy in yeast by freeze-replica method. *Cell Struct Funct* 1995; **20**: 465–471.
68. Hirsimaki Y, Hirsimaki P, Lounatmaa K. Vinblastine-induced autophagic vacuoles in mouse liver and Ehrlich ascites tumor cells as assessed by freeze-fracture electron microscopy. *Eur J Cell Biol* 1982; **27**: 298–301.
69. Köchl R, Hu X, Chan E, Tooze SA. Microtubules facilitate autophagosomal formation and fusion of autophagosomes with endosomes. *Traffic* 2006; **7**: 129–145.
70. Fass E, Shvets E, Degani I, Hirschberg K, Elazar Z. Microtubules support production of starvation-induced autophagosomes but not their targeting and fusion with lysosomes. *J Biol Chem* 2006; **281**: 36303–36316.
71. Kimura S, Noda T, Yoshimori T. Dynein-dependent movement of autophagosomes mediates efficient encounters with lysosomes. *Cell Struct Funct* 2008; **33**: 109–122.
72. Kamada Y, Funakoshi T, Shintani T, Nagano K, Ohsumi M, Ohsumi Y. Tor-mediated induction of autophagy via an Apg1 protein kinase complex. *J Cell Biol* 2000; **150**: 1507–1513.
73. Scott RC, Juhasz G, Neufeld TP. Direct induction of autophagy by Atg1 inhibits cell growth and induces apoptotic cell death. *Curr Biol* 2007; **17**: 1–11.
74. Tomoda T, Kim JH, Zhan C, Hatten ME. Role of Unc51.1 and its binding partners in CNS axon outgrowth. *Genes Dev* 2004; **18**: 541–558.
75. Toda H, Mochizuki H, Flores III R, Josowitz R, Krasieva TB, Lamorte VJ *et al.* UNC-51/ATG1 kinase regulates axonal transport by mediating motor-cargo assembly. *Genes Dev* 2008; **22**: 3292–3307.
76. Grosshans BL, Ortiz D, Novick P. Rabs and their effectors: achieving specificity in membrane traffic. *Proc Natl Acad Sci USA* 2006; **103**: 11821–11827.
77. Geuze HJ, Murk JL, Stroobants AK, Griffith JM, Kleijmeer MJ, Koster AJ *et al.* Involvement of the endoplasmic reticulum in peroxisome formation. *Mol Biol Cell* 2003; **14**: 2900–2907.
78. Dunn Jr WA. Studies on the mechanisms of autophagy: formation of the autophagic vacuole. *J Cell Biol* 1990; **110**: 1923–1933.
79. Panaretou C, Domin J, Cockcroft S, Waterfield MD. Characterization of p150, an adaptor protein for the human phosphatidylinositol (PtdIns) 3-kinase. Substrate presentation by phosphatidylinositol transfer protein to the p150 PtdIns 3-kinase complex. *J Biol Chem* 1997; **272**: 2477–2485.
80. Erdman RA, Shellenberger KE, Overmeyer JH, Maltese WA. Rab24 is an atypical member of the Rab GTPase family. Deficient GTPase activity, GDP dissociation inhibitor interaction, and prenylation of Rab24 expressed in cultured cells. *J Biol Chem* 2000; **275**: 3849–3856.

Cell Research (2010) :1-4.

www.nature.com/cr

RESEARCH HIGHLIGHT

Autophagosome formation: not necessarily an inside job

Andrea Longatti[1], Andrea Orsi[1], Sharon A Tooze[1]

[1]*London Research Institute, Cancer Research UK, 44 Lincoln's Inn Fields, London WC2A 3PX, United Kingdom*
Cell Research advance online publication 14 September 2010; doi:10.1038/cr.2010.132

Autophagy is a highly conserved degradative process characterized by the formation of double membrane vesicles called autophagosomes. Autophagy occurs at a basal level in most cells and can be rapidly induced under stress conditions such as amino acid starvation. In multicellular organisms autophagy also plays a role in development, immunity, aging, and tissue homeostasis [1]. Autophagosomes start out as small membrane structures called phagophores or isolation membranes, which are expanded through an unknown mechanism to autophagosomes of various sizes but usually with a diameter of about 300-900 nm. Once mature, autophagosomes fuse with endosomes and lysosomes to form autolysosomes, leading to the degradation of the inner autophagosomal membrane along with all its contents by lysosomal hydrolases. The proteins involved in autophagosome formation were first characterized in yeast, where they are collectively known as Atg proteins. Many of them are conserved in higher eukaryotes. Atg proteins are recruited to, and function on the forming autophagosome sequentially, so that one can follow the formation process over time by following recruitment of the Atg proteins. For example, the Atg5-Atg12-Atg16 complex is recruited to the phagophore after the serine-threonine kinase Atg1 (ULK1 in mammalian cells), and the phosphatidylinositol-3 (PI3) kinase complex (Vps34, p150, Atg14 and Beclin1). In turn, the Atg5-Atg12-Atg16 complex is important for the subsequent recruitment of LC3 (Figure 1). LC3, typically tagged with GFP, is often used as a marker for autophagosomes because it remains associated with the autophagosomal membranes until it is degraded in the autolysosome.

Correspondence: Sharon A Tooze
Tel: +44 207 269 3122; Fax: +44 207 269 3417
E-mail: Sharon.tooze@cancer.org.uk

One of the most highly debated questions in the field concerns the origin of the autophagosomal membrane [2]. Efforts to answer this question are hampered by the fact that most Atg proteins are only transiently associated with phagophores and autophagosomes. Moreover, it is often difficult to distinguish between the membranes of the autophagosome itself and those of the organelles that have been engulfed to undergo degradation. Many different sources have been suggested since autophagosomes were first described in 1957, including the endoplasmic reticulum (ER) [3, 4], the Golgi apparatus and trans-Golgi network (TGN) [5], and the plasma membrane (PM) [6]. These early studies were descriptive and mostly based on electron microscopic observations.

However, more recent findings have given support to each one of the above hypothesized membrane origins, and outer mitochondrial membranes have been added to the possible candidates [7]. The ER hypothesis has recently gained support by electron tomography studies that showed close association and interconnections between the ER and the phagophore [8, 9]. Recent studies in yeast cells support the hypothesis that the Golgi and TGN are the origin of the autophagosomal membrane, as Golgi-derived secretory proteins were shown to be essential for autophagosome formation [10-12]. In mammals mAtg9, which is thought to deliver membrane to the phagophore, has been found to localize to TGN and to Rab7, Rab9, and CI-MPR-positive late endosomes [13].

A recent study in the August issue of *Nature Cell Biology* now provides new evidence for the PM as the origin of the autophagosomal membrane [14]. Ravikumar and colleagues performed a mass spectrometry analysis on cell lysates immunoprecipitated with an antibody against Atg16L1, and discovered that both clathrin heavy chain (CHC) and the adaptor protein AP2 co-immunoprecipitate with Atg16L1. CHC is part of a protein complex that is involved in vesicle budding from the PM, early tubular sorting endosomes, and the Golgi complex. Cargo recruitment to clathrin-coated vesicles on the PM and early endosomes (EE) is mediated by the adaptor protein AP2, while the closely related protein AP1 is specifically found on vesicles budding from the Golgi and the TGN. It would be interesting to know if AP2 is directly mediating the interaction between CHC and Atg16L, and if so what cargo, if any,

is recognized by AP2 in the Atg16L1-positive regions of the PM.

Furthermore, using siRNA-mediated knockdown of CHC, AP2 and another endocytic protein, Epsin1, they observed a decrease in autophagosomes mostly in basal but also in starvation conditions, thus providing an additional mechanistic link between endocytosis and autophagy. Importantly, siRNA-mediated knockdown of AP1 had no effect on autophagosome formation, excluding an involvement of Golgi-derived vesicles and suggesting a novel and specific role of the clathrin-AP2-Atg16 machinery in autophagy. Moreover, many Atg16L1 positive membranes were found near the PM. All together, these findings prompted the authors to investigate the possibility that the PM itself may provide membrane to autophagosomes.

Cholera toxin B subunit (CtxB) was used to identify endocytic vesicles coming from the PM and to assess whether Atg16L1 was found on these structures. CtxB binds the lipid GM1 on the plasma membrane and is internalized through clathrin-dependent and clathrin-independent mechanisms [15]. CtxB is then transported to the ER, first via EEA1-positive endosomes, and then through the TGN (Figure 1). After 10 min of internalization CtxB co-localizes with Atg16L1 and LC3. However, Atg16L1-positive CtxB vesicles did not co-localize with EEA1, suggesting they are either derived from earlier endocytic carriers or represent later stages of CtxB transport. Their proximity to the PM would suggest that they are indeed early endocytic carriers. Atg12 and Atg5, which form a complex with Atg16L1, can also be found co-localizing with CtxB, confirming that this is a functional autophagy complex.

Since CtxB is taken up from the extracellular space, it will get trapped in the lumen between the two autophagosomal precursor membranes (Figure 1). Indeed, electron microscopic analysis revealed autophagosomes labeled for both GFP-Atg16L1 and HRP-CtxB. It would be important in the future to understand whether any region of the PM or just GM1-containing CtxB-positive subdomains of the PM can contribute to autophagy. This raises an important issue, which was addressed in the recent papers proposing an involvement of ER [8, 9] and mitochondria [7]. In both cases resident proteins from the ER or mitochondria, respectively, were excluded from the newly formed autophagosomes.

To demonstrate that vesicles-containing Atg16L1 are derived from the PM, the authors investigated the effect

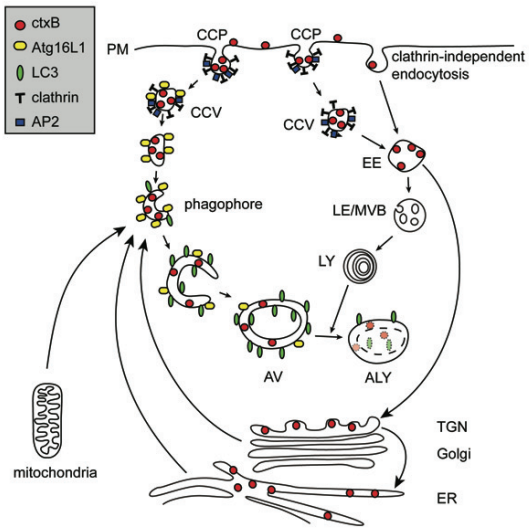

Figure 1 The plasma membrane contributes to phagophore precursor formation. Ravikumar and colleagues provide evidence that endocytic, plasma membrane (PM)-derived clathrin coated vesicles (CCVs) contribute to or form phagophore precursor structures. These are gradually expanded to become autophagosomes, which fuse with endosomes and lysosomes to degrade their contents. Other studies have proposed that the ER, Golgi/TGN, and mitochondria provide autophagosomal membranes supporting the hypothesis that several membrane sources are exploited by autophagy. Knockdown of factors essential for clathrin-mediated endocytosis such as clathrin heavy chain (CHC), AP2, and Epsin1 (not depicted) reduces phagophore precursors and autophagosome formation. Cholera toxin B subunit (CtxB) binds to the plasma membrane and is internalized via clathrin coated pits (CCPs) and clathrin-independent mechanisms. CtxB is delivered to the ER via early endosomes (EEs) and the TGN. Using CtxB as a marker for PM-derived endocytic vesicles, they show that these vesicles contribute to the formation of Atg16L1-positive phagophore precursors. Note that in this model, CtxB, and possibly other PM-derived proteins as well as extracellular fluids captured in the forming CCVs will be trapped between the inner and outer autophagosomal membrane. The consequence of the presence of this entrapped material, which will eventually be degraded in the autolysosome (ALY), is not known. LE/MVB = late endosome/multi-vesicular body; AV = autophagosome.

of dominant negative (DN) dynamin II and Dynasore, which block Dynamin-dependent membrane scission. Blocking vesicle scission by these means increased the co-localization of Atg16L1 with clathrin-coated vesicles and the plasma membrane. This suggests that Atg16L1 can be recruited to the PM, where it remains if the vesicles cannot bud off. As Dynamin II has been shown to be involved in vesicle formation from the PM and the TGN, as well as in exocytosis, the precise site-of-action of this DN-protein in this study remains to be directly demonstrated. However, since AP1-dependent pathways have been excluded by the authors, it is unlikely that these findings can be explained by dynamin II activities at the TGN. Similarly, Dynasore inhibits all Dynamins, including the mitochondrial Dynamin-like protein, DrpI and thus experiments using these inhibitors cannot alone differentiate between potentially contributing compartments. Most importantly, in support of the hypothesis put forward by the authors that PM indeed contributes to autophagosome initiation stages, the co-localization between GFP-Atg16L1 and tomato-LC3 was reduced in cells knocked down for Epsin1 or CHC although both populations of puncta are still found. Since the Atg16L1 complex is recruited to phagophores before LC3 and has been shown to determine the location of LC3 lipidation [16], this might suggest that the tomato-LC3-positive autophagosomes seen under these conditions form through an Atg16-independent pathway.

It would have been of interest to have capitalized on recent developments about the ULK1/2 kinase complex, investigating whether it can be found on these CtxB and Atg16L-positive phagophores or phagophore precursors. It has recently been shown that ULK1 and FIP200 drive the recruitment of all other Atg proteins [17], including Atg14 and the PI3 kinase complex. While inhibition with 3MA (which inhibits PI3P production by the PI3 kinase complex) decreased the number of Atg16L1-positive vesicles, the authors did not determine whether PI3P was on the early autophagosomal precursors. This could be resolved by looking at WIPI2, a specific effector of the autophagosomal PI3P pool [18].

An intriguing question that remains is whether these PM-derived vesicles fuse with pre-existing phagophores or whether endocytosed vesicles turn into autophagosomal precursors themselves. The same question would also apply to other donor compartments for autophagosomal membrane. Furthermore, it remains unclear whether PM derived vesicles can contribute to phagophore expansion or only to the formation of the precursor structure. A typical autophagosome of 400 nm in diameter has a surface area of about 500 μm^2 for each of the outer and inner membranes. In comparison, an average endocytic vesicle has a diameter of less than 100 nm, with a surface area of around 30 μm^2. This illustrates the quantity of such vesicles needed to form an entire autophagosome. However, given the highly dynamic nature of the PM and endosomal compartments, this may be feasible.

The finding that blocking clathrin-dependent endocytosis reduces the number of new autophagosomes by 30% suggests that the PM is not the exclusive source of membrane for autophagy. This is supported by recent publications, and numerous past ones [3, 4, 5, 6]. Ravikumar and colleagues [14] provide an intriguing model by which plasma membrane can be recruited to support autophagosome formation. As they suggest, this may be particularly important during enhanced autophagic activity when large amounts of membrane are needed; the PM, being a highly dynamic and large membrane reservoir, seems a reasonable candidate. However, the differential contribution of the PM to autophagy in basal vs. induced conditions was not fully explored and future studies will be required to establish this hypothesis. Another possibility is that different cell types use different membranes to form autophagosomes, or that different inducers of autophagy lead to the use of different donor membranes. The recent data certainly support the idea that several pathways for autophagosome formation might exist, including the ER, the Golgi, the mitochondria and the PM, and they could overlap to different extents. Such promiscuity would surely make autophagy an extremely adaptable process, able to function under a wide range of conditions, both ideal properties of an essential survival response.

Acknowledgments

We thank Cancer Research UK for funding the work in the author's laboratory. We thank the members of the Secretory pathways laboratory for support and advice. We thank Prof Vojo Deretic (University of New Mexico, USA) for his critical reading of the manuscript and discussion.

References

1 Mizushima N, Levine B, Cuervo AM, Klionsky DJ. Autophagy fights disease through cellular self-digestion. *Nature* 2008; **451**:1069-1075.
2 Longatti A, Tooze SA. Vesicular trafficking and autophagosome formation. *Cell Death Differ* 2009; **16**:956-965.
3 Dunn WA Jr. Studies on the mechanisms of autophagy: Formation of the autophagic vacuole. *J Cell Biol* 1990; **110**:1923-1933.
4 Novikoff AB, Essner E. Cytolysomes and mitochondrial degeneration. *J Cell Biol* 1962; **15**:140-146.
5 Locke M, Sykes AK. The role of the Golgi complex in the isolation and digestion of organelles. *Tissue Cell* 1975; **7**:143-158.
6 Quatacker JR. Formation of autophagic vacuoles during human corpus luteum involution. *Z Zellforsch Mikrosk Anat* 1971; **122**:479-487.
7 Hailey DW, Rambold AS, Satpute-Krishnan P, *et al*. Mitochondria supply membranes for autophagosome biogenesis during starvation. *Cell* 2010; **141**:656-667.
8 Hayashi-Nishino M, Fujita N, Noda T,

et al. A subdomain of the endoplasmic reticulum forms a cradle for autophagosome formation. *Nat Cell Biol* 2009; **11**:1433-1437.

9 Yla-Anttila P, Vihinen H, Jokitalo E, Eskelinen EL. 3D tomography reveals connections between the phagophore and endoplasmic reticulum. *Autophagy* 2009; **5**:1180-1185.

10 Geng J, Nair U, Yasumura-Yorimitsu K, Klionsky DJ. Post-golgi sec proteins are required for autophagy in *Saccharomyces cerevisiae*. *Mol Biol Cell* 2010; **21**:2257-2269.

11 van der Vaart A, Griffith J, Reggiori F. Exit from the golgi is required for the expansion of the autophagosomal phagophore in yeast *Saccharomyces cerevisiae*. *Mol Biol Cell* 2010; **21**:2270-2284.

12 Yen WL, Shintani T, Nair U, *et al*. The conserved oligomeric Golgi complex is involved in double-membrane vesicle formation during autophagy. *J Cell Biol* 2010; **188**:101-114.

13 Young ARJ, Chan EYW, Hu XW, *et al*. Starvation and ULK1-dependent cycling of mammalian Atg9 between the TGN and endosomes. *J Cell Sci* 2006; **119**:3888-3900.

14 Ravikumar B, Moreau K, Jahreiss L, Puri C, Rubinsztein DC. Plasma membrane contributes to the formation of pre-autophagosomal structures. *Nat Cell Biol* 2010; **12**:747-757.

15 Sandvig K, van Deurs B. Transport of protein toxins into cells: pathways used by ricin, cholera toxin and Shiga toxin. *FEBS Letters* 2002; **529**:49-53.

16 Fujita N, Itoh T, Omori H, *et al*. The Atg16L complex specifies the site of LC3 lipidation for membrane biogenesis in autophagy. *Mol Biol Cell* 2008; **19**:2092-2100.

17 Itakura E, Noboru Mizushima N. Characterization of autophagosome formation site by a hierarchical analysis of mammalian Atg proteins. *Autophagy* 2010; **6**:764-776.

18 Polson HE, de Lartigue J, Rigden DJ, *et al*. Mammalian Atg18 (WIPI2) localizes to omegasome-anchored phagophores and positively regulates LC3 lipidation. *Autophagy* 2010; **6**:506-522.

Molecular and Cellular Biology

Kinase-Inactivated ULK Proteins Inhibit Autophagy via Their Conserved C-Terminal Domains Using an Atg13-Independent Mechanism

Edmond Y. W. Chan, Andrea Longatti, Nicole C. McKnight, et al.
2009. Kinase-Inactivated ULK Proteins Inhibit Autophagy via Their Conserved C-Terminal Domains Using an Atg13-Independent Mechanism. Mol. Cell. Biol. 29(1):157-171.
doi:10.1128/MCB.01082-08.

MOLECULAR AND CELLULAR BIOLOGY, Jan. 2009, p. 157–171 Vol. 29, No. 1
0270-7306/09/$08.00+0 doi:10.1128/MCB.01082-08

Kinase-Inactivated ULK Proteins Inhibit Autophagy via Their Conserved C-Terminal Domains Using an Atg13-Independent Mechanism[▽]

Edmond Y. W. Chan,[†] Andrea Longatti,[‡] Nicole C. McKnight,[‡] and Sharon A. Tooze*

Secretory Pathways Laboratory, London Research Institute, Cancer Research UK, 44 Lincoln's Inn Fields, London WC2A 3PX, United Kingdom

Received 10 July 2008/Returned for modification 11 August 2008/Accepted 14 October 2008

The yeast Atg1 serine/threonine protein kinase and its mammalian homologs ULK1 and ULK2 play critical roles during the activation of autophagy. Previous studies have demonstrated that the conserved C-terminal domain (CTD) of ULK1 controls the regulatory function and localization of the protein. Here, we explored the role of kinase activity and intramolecular interactions to further understand ULK function. We demonstrate that the dominant-negative activity of kinase-dead mutants requires a 7-residue motif within the CTD. Our data lead to a model in which the functions of ULK1 and ULK2 are controlled by autophosphorylation and conformational changes involving exposure of the CTD. Additional mapping indicates that the CTD contains other distinct regions that direct membrane association and interaction with the putative human homologue of Atg13, which we have here characterized. Atg13 is required for autophagy and Atg9 trafficking during autophagy. However, Atg13 does not bind the 7-residue dominant-negative motif in the CTD of ULK proteins nor is the inhibitory activity of the CTDs rescued by Atg13 ectopic expression, suggesting that in mammalian cells, the CTD may interact with additional autophagy proteins.

During macroautophagy in mammalian cells, a membrane cisterna wraps around cytoplasmic material to form a nascent autophagosome, which then fuses with late endosomal structures to initiate the degradation of autophagosomal contents. The targets of macroautophagy (herein referred to as autophagy) can include long-lived proteins, organelles, ubiquitinated cellular substrates, and aberrant protein aggregates (7, 13, 15, 24, 26). Autophagy has been implicated in a number of medical contexts, such as cancer, neurodegeneration, and immunity (as recently reviewed in references 16, 19, and 21), raising interest in understanding its basic regulatory mechanisms.

The serine-threonine protein kinase Atg1 was originally identified as a critical autophagy regulator in genetic screens performed with the yeast *Saccharomyces cerevisiae* (17, 29, 31, 34). Autophagy in yeast is induced by nitrogen starvation or rapamycin treatment, and studies with yeast have shown that Atg1 functions at a regulatory step downstream of the nutrient-sensing signaling kinase TOR (target of rapamycin). Atg1 forms part of a complex that includes additional *aut*ophagy (Atg) proteins, such as Atg13, Atg17, Atg29, Atg31, Atg11, Atg20, and Atg24 (9–12, 22). While the proteins Atg17, Atg29, and Atg31 have autophagy-specific functions, Atg11, Atg20, and Atg24 function in the yeast autophagy-related CVT (cytoplasm-to-vacuole targeting) pathway, raising the possibility that a number of different Atg1-containing subcomplexes may exist in vivo to regulate distinct pathways. Atg1 also regulates the recycling of Atg9 between the preautophagosomal structure (PAS) and a peripheral pool via a mechanism involving Atg2, Atg18, and the phosphatidylinositol-3 kinase complex I (25). In addition, the localization of yeast Atg1 to the PAS can be regulated by cyclic AMP-dependent protein kinase-mediated phosphorylation in a starvation-dependent manner (2).

Although the role of Atg1 kinase activity has been controversial (1, 8), recent data have demonstrated that Atg1 acts in distinct kinase-dependent and kinase-independent roles (5, 11). Kinase-inactivated Atg1 was capable of directing the assembly of the PAS containing Atg8, Atg17, and Atg29, consistent with the proposal that Atg1 plays a structural role. However, the kinase activity of Atg1 was required to drive protein or membrane dynamics through disassembly or dissociation of Atg proteins from the PAS, a step which is required to produce fully formed autophagosomes.

Full kinase activity of Atg1 in yeast requires its binding partners Atg13 and Atg17 (10). Interestingly, the kinase activity of Atg1 is stimulated when autophagy is induced in yeast, and this correlates with increased binding of Atg1 to Atg13 and Atg17 upon autophagy induction (10, 11). Furthermore, the efficiency of Atg1-Atg13 binding is inversely correlated with levels of phosphorylation on Atg13 (10), leading to the model in which Atg13 is dephosphorylated upon autophagy induction, thereby promoting its ability to bind to and act as a cofactor for Atg1. The autophagy-dependent kinases and phosphatases controlling yeast Atg13 phosphorylation remain to be determined. However, Atg13 dephosphorylation has been shown to be TOR dependent (10).

The single Atg1 homologues of *Dictyostelium discoideum*, *Caenorhabditis elegans*, and *Drosophila melanogaster* have been confirmed to be key autophagy regulators (20, 23, 27). In contrast, mammals have at least two Atg1 homologues (6), Unc-51-like kinase 1 (ULK1) and ULK2, that share strong

* Corresponding author. Mailing address: Secretory Pathways Laboratory, London Research Institute, Cancer Research UK, 44 Lincoln's Inn Fields, London WC2A 3PX, United Kingdom. Phone: (44) 207 269 3122. Fax: (44) 207 269 3417. E-mail: sharon.tooze@cancer.org.uk.

† Present address: Strathclyde Institute of Pharmacy and Biomedical Sciences, University of Strathclyde, Glasgow, United Kingdom.

‡ These authors contributed equally to this work.

▽ Published ahead of print on 20 October 2008.

homology with the *C. elegans* Atg1 homologue Unc (uncoordinated)-51 (32). Whether ULK1 and ULK2 play similar roles for autophagy induction remains unclear.

We previously found that, in HEK293A cells, small interfering RNA (siRNA)-mediated knockdown of ULK1 was sufficient to reduce starvation-induced autophagy and inhibit the starvation-dependent redistribution of mammalian Atg9 (mAtg9) to a dispersed, peripherally localized pool (3, 37). In this cell system, knockdown of ULK2 had no effect on the induction of autophagy or mAtg9 traffic, suggesting a preferential role of ULK1 in autophagy. ULK1 and -2 have overlapping widespread mRNA expression patterns (35, 36). However, only ULK1 mRNA was upregulated in maturing reticulocyte cultures to promote autophagic clearance of mitochondria, indicating that some specificity exists in vivo (15). These authors went on to show that mice lacking ULK1 displayed abnormal erythrocyte maturation but were viable and without a developmental phenotype, in contrast with other models of mice deficient in autophagy genes (13, 14). These data suggest that ULK2 can support autophagic function in the absence of ULK1, implying a more specialized role for ULK1 in vivo (15). Although the precise roles of ULK1 and ULK2 require further clarification, our data on ULK1 and recent other data show that both of these proteins can localize to mammalian PASs (called isolation membranes, or phagophores) in a starvation-dependent manner (3, 6).

All Atg1 homologs share similar domain structures in which the kinase catalytic domain comprises the N-terminal one-third of the protein and the remaining two-thirds contain regulatory sequences. Comparison of the mouse ULK1 and ULK2 sequences with that of *C. elegans* Unc-51 has allowed the definition of a C-terminal domain (CTD) (222 residues long in mouse ULK1) that shows relatively high levels of conservation (32), suggestive of an important biological function. We previously described how the deletion of a three-residue PDZ binding motif at the CTD C terminus transforms ULK1 into a potent dominant inhibitor of autophagy (3). In *D. discoideum*, defects in development and autophagy found in Atg1 null cells could not be rescued with a mutant *D. discoideum* Atg1 containing a deletion of the last 40 amino acids of the CTD (30). A recent study has identified a novel ULK1-binding protein called FIP200 (focal adhesion kinase family-interacting protein of 200 kDa), which was required for starvation-induced autophagy, proper ULK1 phosphorylation, and ULK1 stability (6). FIP200 binding to ULK1 required the CTD, further supporting a role of the CTD in autophagy regulation.

In this study, we aimed to gain insight into the function of ULK1 and ULK2 for the regulation of autophagy by studying the role of their kinase activities and the regulation of these activities by the CTD. We demonstrated that complete ablation of ULK1 kinase activity results in decreased protein autophosphorylation and a potent dominant-negative effect on autophagy. Our further analysis has led to a working model in which autophosphorylation is critical for promoting a closed molecular conformation that regulates interactions of the CTD. In further support of this model, expression of the CTD from either ULK1 or ULK2 was sufficient to inhibit autophagy, and additional analysis has identified a 7-residue motif critical for this effect. We determined that this motif was distinct from other signals within the CTD that direct membrane binding of ULK1 and ULK2 and incorporation into large protein complexes.

To explore other mechanisms involved in the function of the CTD, we identified a putative human Atg13 orthologue that we confirmed is essential for autophagy by using siRNA depletion. In addition, we found that loss of human Atg13 affected the trafficking of mAtg9, as was previously observed after the loss of ULK1 (37). Although mAtg13 bound the CTDs of both ULK1 and ULK2, this interaction utilized sequences that were distinct from the dominant-negative 7-residue motif, and overexpression of Atg13 did not rescue the dominant-negative activity of the overexpressed CTDs. Thus, our data have identified a 7-residue motif in the ULK1 and ULK2 CTDs that engages a novel dominant-negative mechanism which is independent of Atg13 and membrane-associated components.

MATERIALS AND METHODS

Cell culture. HEK293A cells and their derivative cell line stably expressing enhanced green fluorescent protein (EGFP)-rat LC3 (293/GFP-LC3) have been described previously (3). Cells were maintained in Dulbecco's modified Eagle's medium with 10% fetal bovine serum, which also served as the full nutrient medium in the analytical experiments. Starvation medium consisted of Earle's balanced saline solution (EBSS), containing 0.5 mM leupeptin where indicated.

DNA constructs. Expression plasmids for N-terminal Myc epitope-tagged wild-type and kinase-dead (K46R) murine ULK1 (ULK1-K46R) have been described previously (3). ULK2 containing an N-terminal Myc tag was constructed by PCR from a full-length clone containing murine ULK2 (IMAGE:5709559) as the template. The CTDs of ULK1 and -2 were amplified from full-length cDNAs using PCR and cloned with an N-terminal Myc tag into a modified pcDNA3.1 or pRK5 backbone, respectively. Substitutions in the kinase domains of ULK1 and -2 were generated using a PCR site-directed mutagenesis kit (Stratagene), and additional deletion constructs were generated by isolating internal regions using PCR. We obtained a full-length cDNA containing the human putative Atg13 homolog KIAA0652 (pF1KSDA0652; Kazusa DNA Research Institute, Kisarazu, Japan). A C-terminal FLAG epitope tag was added onto the Atg13 open reading frame using PCR and cloned into a modified pcDNA3.1 vector. For biochemical analyses, cells were transfected using Lipofectamine 2000 (Invitrogen) according to the manufacturer's protocols and analyzed 24 h later.

siRNAs and knockdown determination. A pool of four siRNA duplexes (On-Target plus SMARTpool) targeting the putative human Atg13 (KIAA0652, Entrez nucleotide accession no. NM_014741) was obtained (Dharmacon). Two duplexes within this pool specific for KIAA0652 that were confirmed in multiple assays correspond to Duplex1 (5′-AGA CCA UCU UUG UCC GAA A-3′) (sense sequence 989 to 1007) and Duplex2 (5′-GAA GAA UGU CCG CGA GUU U-3′) (sense sequence 1398 to 1416). The siRNAs targeting human ULK1 have been described previously (3). Experimental and control siRNAs were transfected into HEK293 and 293/GFP-LC3 cells by use of a wet/reverse-knockdown protocol in which trypsinized cells in suspension are plated directly into an siRNA-Lipofectamine 2000 (Invitrogen) mixture. Fresh medium is replenished 24 h before the day of the experiment.

Confirmation of siRNA knockdown by reverse transcription-PCR was carried out by assaying message RNA levels in cell samples following 72 h of knockdown, as described previously (3), using Sybr green real-time PCR. QuantiTect (Qiagen Biotech) primer sets were obtained for detection of the putative Atg13 (KIAA0652) transcript and the beta-actin control.

Immunoprecipitations and in vitro kinase assays. Singly or doubly transfected cells were lysed in ice-cold TNTE (20 mM Tris, pH 7.5, 150 mM NaCl, 0.3% [vol/vol] Triton X-100 [TX-100], 5 mM EDTA) containing Complete EDTA-free protease inhibitor cocktail (Roche) and PhosStop phosphatase inhibitor cocktail (Roche). Lysates cleared by centrifugation were incubated with protein G-Sepharose beads coupled to anti-Myc monoclonal 9E10 or anti-FLAG monoclonal M2 (Sigma-Aldrich) antibody for 1 h and then washed three times with TNTE. For coimmunoprecipitation studies, proteins were eluted using 3× sodium dodecyl sulfate (SDS) sample buffer (with heating to 65°C for 5 min) and analyzed by SDS-polyacrylamide gel electrophoresis (SDS-PAGE).

For in vitro kinase assays, following the three TNTE washes, immunoprecipi-

tates were further washed once with kinase reaction buffer (KRB) (20 mM HEPES, pH 7.5, 20 mM $MgCl_2$, 25 mM beta-glycerophosphate, 2 mM dithiothreitol, 100 μM sodium orthovanadate) and then incubated at a final volume of 20 μl in KRB containing 20 μM ATP, 5 μg myelin basic protein (MBP), and 5 μCi [γ-^{32}P]ATP at 30°C for 15 min. For mixed-bead kinase reactions, immunoprecipitates of ULK1 and -2 and Atg13-FLAG were combined after the TNTE wash step, further washed in KRB, and then incubated in a 20-μl final volume of KRB containing 20 μM ATP at 30°C for 30 min. Reactions were stopped with the addition of 3× SDS sample buffer during heating to 65°C for 5 min. [^{32}P]-labeled reaction products were resolved on NuPAGE 4 to 12% bis-Tris gels in morpholinepropanesulfonic acid (MOPS)-SDS running buffer (Invitrogen). Mixed-bead reaction products were resolved by Laemmli SDS-PAGE. Proteins were transferred to polyvinylidene difluoride (PVDF) membranes and then analyzed using a phosphorimager scanner and anti-Myc immunoblotting.

Immunoblotting. To detect GFP-LC3 lipidation, 293/GFP-LC3 cells were lysed following various treatments in 1× SDS sample buffer. Lysates were then heated to 65°C for 5 min and passed through a 27-gauge needle five times to reduce viscosity before analysis by 10% Laemmli SDS-PAGE. To detect lipidation of endogenous LC3, HEK293A cells were lysed following treatments in ice-cold TNTE containing Complete EDTA-free protease inhibitor cocktail (Roche). Lysates cleared by centrifugation were mixed with 3× SDS sample buffer, heated to 100°C for 5 min, and then analyzed on either 12% Laemmli SDS-PAGE gels or 4 to 12% bis-Tris NuPAGE gels (morpholineethanesulfonic acid [MES]-SDS running conditions) (Invitrogen). Proteins were transferred to PVDF membranes. GFP-LC3 and endogenous LC3 were detected with 5F10 anti-LC3 monoclonal antibody (Nanotools, Teningen, Germany). Additional immunoblotting antibodies included anti-ULK1 polyclonal H-240 (Santa Cruz), anti-Myc 9E10 monoclonal, β-tubulin polyclonal (6046; Abcam, Cambridge, United Kingdom), anti-FLAG M2 monoclonal (Sigma-Aldrich), and antiactin monoclonal AC-40 (Sigma-Aldrich). Rabbit polyclonal antibodies toward human Atg13 (KIAA0652) were generated using the peptide sequence LAVHEKNVR EFDAFVETLQ. Following incubation with primary antibodies, signals were detected and quantified using secondary antibodies coupled to infrared chromophores and a two-channel scanning method (Licor Odyssey), as described previously (3). Statistical analyses for various pairwise comparisons were performed using Student's two-tailed *t* test on sample sets with equal variances.

Limited proteolysis. Cells were lysed in ice-cold TNT (50 mM Tris, pH 8.0, 150 mM NaCl, 0.5% TX-100) (without protease inhibitors) and then incubated with protein G-Sepharose beads coupled to 9E10 anti-Myc monoclonal antibody for 1 h. Immunoprecipitates were washed three times with TNT and then incubated in a 20-μl final reaction volume of TNT containing the concentrations of sequencing-grade chymotrypsin (Roche) indicated in Fig. 3 on ice for 15 min. Reactions were stopped (addition of 3× SDS sample buffer and heating to 100°C) and analyzed by SDS-PAGE and anti-Myc immunoblotting.

Long-lived protein degradation. Autophagy-dependent degradation of [^{14}C]valine-labeled cellular proteins in transfected 293/GFP-LC3 cells was measured as previously described (3).

Membrane association. Following transfection and treatments as indicated, 293/GFP-LC3 cells were scraped into ice-cold homogenization buffer (HB) (20 mM HEPES, pH 7.2, 1 mM EGTA, 5 mM $MgCl_2$, 150 mM KCl) containing Complete EDTA-free protease and PhosStop phosphatase inhibitors (Roche). Cells were disrupted by being passed 20 times through a 27-gauge needle and then cleared using a low-speed (1,000 × *g*) centrifugation. These cleared lysates were then centrifuged at 100,000 × *g* for 1 h (4°C) to obtain a crude membrane pellet and the resulting supernatant fraction. Where indicated, membrane pellets were further washed/extracted in HB containing either high salt concentrations or 1% TX-100 and then recentrifuged at 100,000 × *g*. Membrane pellets were finally resuspended in HB containing 1% TX-100. Membrane and supernatant fractions were mixed with 3× SDS sample buffer, heated to 65°C for 5 min, and resolved by SDS-PAGE for immunoblotting.

Native gel electrophoresis. Following transfection and treatments as indicated, HEK293A cells were lysed in ice-cold 1× native PAGE sample buffer (Invitrogen) containing 1% TX-100 and Complete EDTA-free protease and PhosStop phosphatase inhibitors. Cell lysates were precleared by centrifugation and then mixed with Coomassie G-250 dye additive (0.25% final) (Invitrogen) before being run on 3 to 12% Novex NativePAGE bis-Tris gels (Invitrogen) according to the manufacturer's protocols. Resolved proteins were transferred to PVDF membranes and detected with an anti-Myc monoclonal antibody, horseradish peroxidase-coupled secondary antibodies, and chemiluminescence.

Microscopic analysis of cell structures. For analysis of GFP-LC3-labeled autophagosomes using a Cellomics ArrayScan VTI high-content screening system (Thermo Scientific), 293/GFP-LC3 cells were seeded into 96-well tissue culture plates coated with poly-D-lysine-containing Lipofectamine-siRNA mixtures. Seventy-two hours after transfection, cells were starved, fixed, and analyzed using an automated calibrated quantitation algorithm (spot total intensity per object) (Thermo Scientific).

For confocal analyses, 293/GFP-LC3 cells or parental HEK293 cells were either plated onto glass coverslips and transfected with expression constructs or plated onto glass coverslips in an siRNA-Lipofectamine mixture. Following various treatments, cells were fixed and then further stained using 9E10 monoclonal Myc antibody, M2 monoclonal FLAG antibody, or a hamster anti-Atg9 monoclonal antibody generated by immunizing animals with a previously described C-terminal peptide (37). Samples were further analyzed using a confocal laser scanner fitted onto a Zeiss Axioplan 2 microscope.

RESULTS

Kinase function of ULK1. It was recently shown that in NIH 3T3 cells kinase-inactivated ULK1-K46N had dominant-negative properties on starvation-induced autophagy (6). Our previous data using a HEK293 cell system showed that the kinase-inactivated ULK1-K46R mutant behaved similarly to wild-type ULK1 in modulating autophagy (3). Our results also contrasted with the reported dominant-negative properties of ULK1-K46R in neurite outgrowth assays (32). Since ULK1-K46R displayed normal electrophoretic mobility (3), we hypothesized that ULK1-K46R had remaining kinase activity and we generated an additional kinase-inactivated mutant, ULK1-K46I. We examined the effects of these mutations by assaying the efficiency of immunoprecipitated ULK1 proteins to undergo autophosphorylation and to phosphorylate the generic substrate MBP. The K46R substitution inactivated these in vitro kinase activities only partially, while the K46I mutation produced stronger inactivation (Fig. 1A).

Kinase function in ULK1ΔCTD. We previously demonstrated that deletion of the ULK1 CTD generates a potent dominant-negative molecule, ULK1ΔCTD (3). We questioned whether the CTD modulated kinase activity, possibly via an intramolecular interaction. We observed that deletion of the CTD in ULK1 increased autophosphorylation levels (approximately 2.8-fold), while phosphorylation of MBP was reduced approximately 80% following deletion of the CTD (Fig. 1B). From these data, we speculated that loss of the CTD produced a kinase with an altered conformation in which the kinase domain has increased accessibility to the spacer domain for autophosphorylation and a decreased ability to phosphorylate substrates.

Kinase function in full-length ULK1. Since our in vitro data indicated that the K46R and K46I substitutions had various severities, we retested these mutants for their effect on starvation-induced autophagy in 293/GFP-LC3 cells (3). In this cell system, we can assess autophagy activation by measuring the conversion of its unmodified (GFP-LC3-I) form to its modified, lipidated species (GFP-LC3-II). Strikingly, we observed that ULK1-K46I exhibited strong dominant-negative properties compared to both the wild-type control and ULK1-K46R (Fig. 2A). In addition, ULK1-K46I displayed faster electrophoretic mobility, consistent with decreased autophosphorylation in vivo, than wild-type ULK1 and ULK1-K46R. These data demonstrate that strong inactivation of catalytic activity is required to transform ULK1 into a dominant-negative protein.

To understand further this dominant inhibitory effect, we performed a deletion analysis of ULK1-K46I. We determined

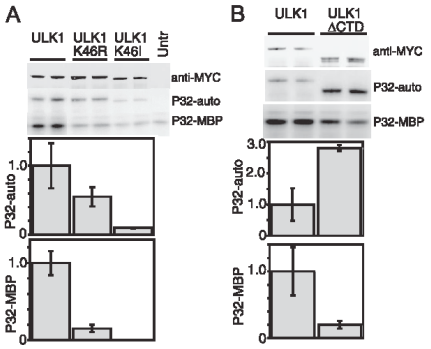

FIG. 1. In vitro kinase activities of ULK1 mutants. (A and B) HEK293A cells were transfected with Myc-tagged ULK1 constructs, lysed, and used for immunoprecipitation reactions. Immunoprecipitates were incubated in an in vitro kinase reaction mixture containing [^{32}P]ATP and the generic substrate MBP. Reaction products were resolved on SDS-PAGE gels (top). Anti-Myc immunoblotting was performed as a control to quantify the amount of ULK1 protein precipitated. Phosphorimager analysis detected levels of ULK1 autophosphorylation (P32-auto) and MBP phosphorylation (P32-MBP). Specific activities (in relative units) are expressed as the amount of phosphorylation normalized to the amount of Myc-tagged ULK1 per reaction (corrected for background activities detected in a parallel control reaction performed with untransfected cells [Untr] [not shown in panel B]). Each bar represents results from three independent samples ± standard deviations, and each experiment was reproduced a minimum of two times.

that ULK1-K46I lost approximately 50% of its potency to inhibit GFP-LC3-II upon deletion of its CTD (Fig. 2B). An equivalent loss of potency was seen with ULK1-K46I lacking the C-terminal 50 amino acids [ULK1-K46I(1–1001)]. Finer mapping determined that dominant-negative potency was similarly lost after the deletion of 10 residues from the ULK1 C terminus (ERR-STOP mutant). However, deletion of the PDZ binding motif from ULK1-K46I (LSG-STOP) had no effect on dominant-negative function. Thus, the ability of kinase-inactive, nonautophosphorylated ULK1 to inhibit autophagy depended upon a small region just inside its C terminus. In conjunction with our in vitro kinase data showing altered autophosphorylation efficiency following CTD deletion, we proposed a working model in which the CTD is normally folded back to keep the protein in a more closed conformation. Full kinase inactivation of ULK1 leads to a loss of autophosphorylation and a conformational change that causes the CTD to be abnormally exposed, revealing cryptic binding sites within the CTD that then recruit and titrate out other essential autophagy proteins.

Limited proteolysis reveals a conformational change in ULK1-K46I. To probe for possible conformational changes, we performed limited proteolysis on immunoprecipitated ULK1 compared to ULK1-K46I and ULK1-K46R. Treatment of immunoprecipitated wild-type Myc-ULK1 with low concentrations of chymotrypsin resulted in the loss of the full-length protein and generated distinct protected fragments ranging between 60 and 70 kDa in apparent molecular mass (Fig. 3B). Using the relative mobilities of previously described ULK1 deletion constructs, such as ULK1ΔCTD [ULK1(1–828)], ULK1(1–427), and ULK1(1–351), for comparison (Fig. 3A), we observed that the larger predominant digestion products are approximately 420 to 500 residues in length. Digestion of wild-type Myc-ULK1 with higher concentrations of enzyme generated smaller protected digestion products of approximately 350 to 380 residues. Digestion of Myc-ULK1-K46I also resulted in the loss of the full-length protein. However, distinct protected fragments were not detected efficiently, which is consistent with the idea that internal regions of the kinase-inactivated mutant were more accessible to protease. Digestion of Myc-ULK1-K46R yielded an intermediate phenotype, suggesting that the closed molecular conformation of our working model is altered only mildly when the kinase is partially inactivated.

Kinase inactivation in full-length ULK2. Hara et al. (6) recently reported that kinase-inactivated ULK2 also exhibited dominant-negative properties on autophagy. Given our observed differential effects of kinase inactivation in the context of ULK1, we performed a similar analysis using ULK2. We confirmed that the mutation of K39 in ULK2 to R or I resulted in the partial or full inactivation, respectively, of in vitro autophosphorylation and MBP phosphorylation activities (Fig. 4A). We next tested the effects of wild-type ULK2 and these kinase mutants on starvation-induced autophagy in 293/GFP-LC3 cells (Fig. 4B). Surprisingly, overexpression of wild-type ULK2 enhanced the levels of GFP-LC3-II following amino acid starvation. This enhancing effect was not seen with the ULK2-K39R mutant (which contains partially inactivated kinase activity). In agreement with our ULK1 results, ULK2-K39I produced strong inhibitory effects on starvation-induced GFP-LC3 lipidation. Strong and weak effects on autophosphorylation could also be observed as differences in electrophoretic mobilities for overexpressed ULK2-K39I and -K39R, respectively (Fig. 4B).

Analysis of ULK2 reveals both differences and similarities to ULK1. Consistently with recent observations showing the localization of ULK2 on Atg16L-positive-forming autophagosomes (also termed isolation membranes, or phagophores) (6) and our results with ULK1 (3), we could detect a proportion of ULK2 on GFP-LC3-labeled autophagosomes in starved 293/GFP-LC3 cells (Fig. 4C). Overexpressed ULK2 did not promote GFP-LC3 lipidation under full nutrient conditions (zero time point) but appeared to enhance the response following amino acid starvation (Fig. 4D). Using deletion analysis, we observed that ULK2 lacking its C-terminal three residues (ATV) similarly enhanced starvation-induced GFP-LC3 lipidation (Fig. 4E). Thus, while deletion of the C-terminal PDZ motif modulated ULK1 function (3), residues at the extreme C terminus of ULK2 were not required to enhance GFP-LC3 lipidation. A ULK2ΔCTD mutant had no effect on GFP-LC3 lipidation, in contrast with ULK1ΔCTD (Fig. 4F), which has dominant inhibitory properties (3). These data on wild-type and ΔCTD deletion mutants indicate that overexpression of ULK1 and ULK2 may have distinct effects on autophagy. In contrast, kinase-inactivated forms of ULK1 and ULK2 are both strong dominant-negative inhibitors of autophagy, as evidenced by their ability to block starvation-induced GFP-LC3 puncta (Fig. 4G). Finally, similarly to ULK1, limited pro-

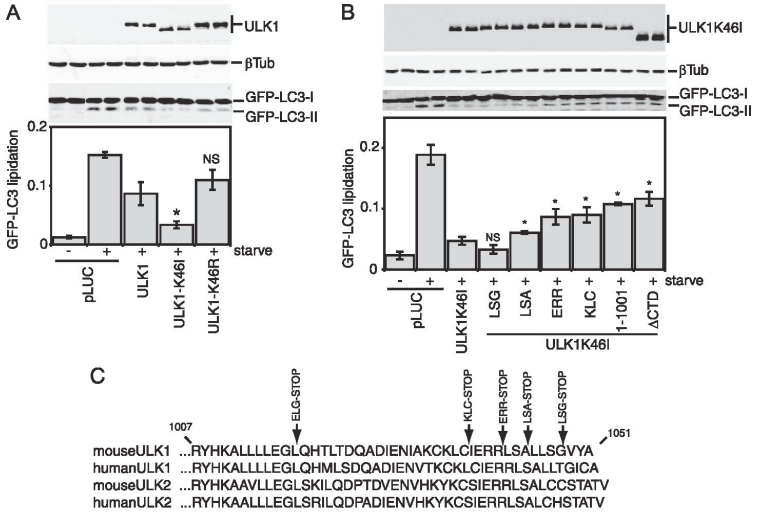

FIG. 2. Inhibition of GFP-LC3 lipidation by ULK1-K46I. (A and B) 293/GFP-LC3 cells were transfected with a control plasmid expressing luciferase (pLUC) or the indicated Myc-tagged ULK1 constructs. Twenty-four hours after transfection, cells were either left alone or starved for 2 h in EBSS containing leupeptin and lysed for SDS-PAGE analysis of GFP-LC3 lipidation (conversion of GFP-LC3-I to GFP-LC3-II) by use of anti-LC3 antibodies. The membrane was also probed with anti-Myc and -β-tubulin (βTub) antibodies. GFP-LC3 lipidation is quantified as follows: GFP-LC3-II/(GFP-LC3-I + GFP-LC3-II). Each bar represents results from three independent samples ± standard deviations. (A) *, $P < 0.05$; NS, $P = 0.20$ (in pairwise comparisons with wild-type ULK1). (B) *, $P < 0.05$; NS, $P = 0.18$ (in pairwise comparisons with full-length ULK1-K46I). (C) Alignments show C-terminal amino acid residues from CTDs of ULK1 and ULK2. Positions of stop codons used to generate various C-terminal truncations are indicated at the top. ULK1(1–1001) is missing its C-terminal 50 residues; ΔCTD is a deletion of the entire CTD and corresponds to amino acids 1 to 828 of ULK1. The EGL-STOP mutant is further studied in Fig. 6F.

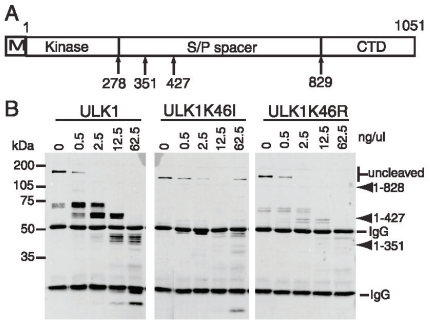

FIG. 3. Differential sensitivities of ULK1 kinase mutants to limited proteolysis. (A) Schematic showing the domain structure of ULK1, including the N-terminal Myc tag (M), the kinase domain, the serine- and proline-rich spacer domain (S/P spacer), and the conserved CTD. Positions of stop codons used by Chan et al. (3) to generate various deletion mutants are indicated at the bottom. (B) ULK1 constructs transfected into 293A cells were immunoprecipitated and then incubated with the indicated concentrations of chymotrypsin for 15 min on ice. Reaction products were resolved on SDS-PAGE gels and detected by anti-Myc immunoblotting. Molecular mass markers are indicated on the left. The relative mobilities of the uncleaved proteins, previously described ULK1 truncation mutants, and the heavy and light immunoglobulin G (IgG) chains are shown on the right.

teolysis of immunoprecipitated wild-type Myc-ULK2 generated protected fragments of roughly 60 to 75 kDa in apparent molecular mass (Fig. 4H). Immunoprecipitated Myc-ULK2-K39I could also be digested by chymotrypsin (note the loss of the full-length protein), but smaller protected fragments did not accumulate, consistent with our model that kinase-inactivated ULK2, like ULK1, has an altered protease-sensitive conformation.

Dominant-negative activity of the ULK CTDs depends on a short conserved sequence within the C terminus. In our model, as a result of a decreased kinase activity, an abnormally exposed CTD engages in uncontrolled interactions with essential autophagy regulatory components, thereby halting the pathway. Supporting this model, overexpression of the CTD alone from either ULK1 (amino acids 829 to 1051) or ULK2 (amino acids 811 to 1037) resulted in a strong dominant-negative effect on starvation-induced GFP-LC3 lipidation (Fig. 5A). The CTD of ULK1 or ULK2 also inhibited starvation-induced protein degradation (Fig. 5B). Overexpression of the ULK1 CTD inhibited lipidation of endogenous LC3 to similar extents, as previously described for N-terminal ULK1 dominant-negative fragments (3), such as ULK1(1–351) (Fig. 5C).

To investigate this dominant-negative mechanism, we performed a deletion analysis of the ULK1 CTD. Similarly to observations from a deletion analysis of full-length ULK1-K46I, removal of the PDZ binding motif (LSG-STOP) and the

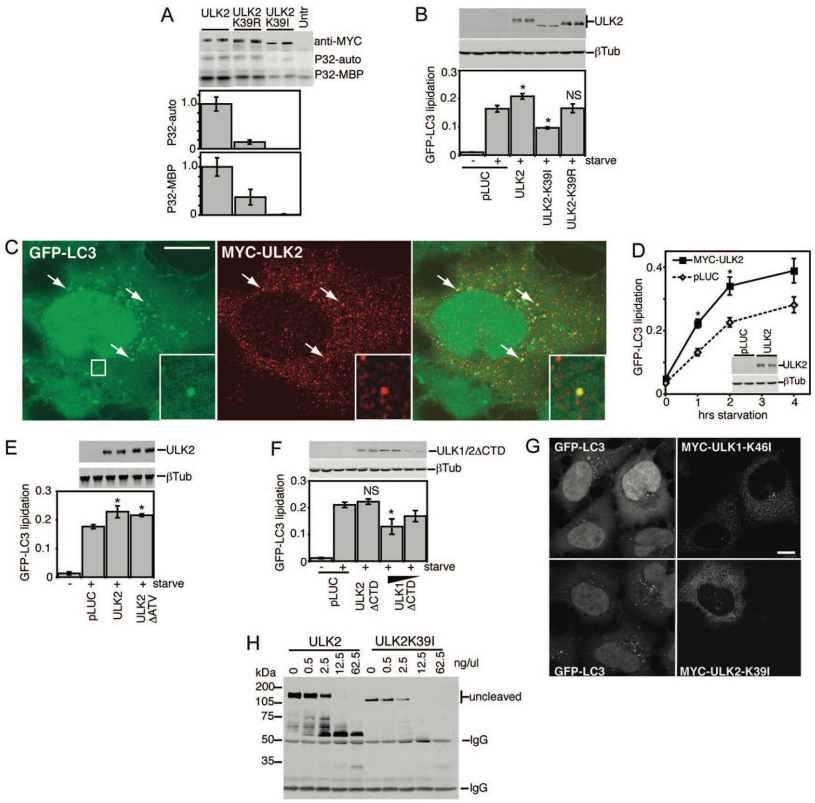

FIG. 4. Autophagy regulatory roles of wild-type and kinase-dead ULK2. (A) In vitro autophosphorylation and MBP kinase activities for ULK2 constructs were measured as described in the legend for Fig. 1. (B, D, E, and F) Modulation of GFP-LC3 lipidation by ULK constructs was detected as described in the legend for Fig. 2. (B) *, $P < 0.05$; NS, $P = 0.94$ (in pairwise comparisons with pLUC-transfected, starved cells). (D) *, $P < 0.03$ in pairwise comparisons with pLUC-transfected cells at the same time point. (E) *, $P < 0.06$ in pairwise comparisons with pLUC-transfected, starved cells. (F) *, $P < 0.02$; NS, $P = 0.42$ (in pairwise comparisons with pLUC-transfected, starved cells). (C) In 293/GFP-LC3 cells starved in EBSS-leupeptin for 2 h, Myc-tagged ULK2 could be observed on multiple cytoplasmic structures, a portion of which colocalized with GFP-LC3, as indicated by arrows and the boxed inset. Bar = 10 μm. (G) Myc-tagged ULK1-K46I or ULK2-K39I inhibited the formation of cytoplasmic GFP-LC3-labeled autophagosomes in starved 293/GFP-LC3 cells. Bar = 10 μm. (H) Limited proteolysis of wild-type ULK2 and ULK2-K39I, assayed as described in the legend for Fig. 3. Untr, untransfected; P32-auto, ULK1 autophosphorylation; P32-MBP, MBP phosphorylation; βTub, β-tubulin; IgG, immunoglobulin G.

next 4 amino acid residues (LSA-STOP) had no effect on the dominant-negative potency of the CTD (Fig. 5D). However, removal of the C-terminal 10 residues (ERR-STOP) began to rescue the dominant-negative activity, and further truncation (KLC-STOP) produced a stronger reversion of the dominant-negative activity. This region contains a 7-residue motif (IER RLSA) that is entirely conserved between the CTDs of ULK1 and ULK2 from human and mouse (Fig. 2C). Using the CTD of ULK2 (which is likely more ancestral than ULK1 [E. Y. W. Chan and S. A. Tooze, unpublished observations]) as a reference, we determined that the IERRLSA motif is perfectly conserved in a predicted avian ULK2 orthologue but displays clearly less conservation in the predicted ULK2 orthologues of fish and is unrecognizable in the Atg1 orthologues of *D. melanogaster* and *C. elegans*. Thus, our deletion analysis demonstrated that the ability of the ULK1/2 CTDs to act as dominant-negative molecules is highly dependent upon a well-conserved 7-residue motif at the C terminus.

Membrane binding signal within the CTD. We next aimed to elucidate the dominant-negative mechanism of the ULK CTDs, which by deletion analysis appeared to require the same amino acid residues as kinase-inactivated ULK1 and -2. Our

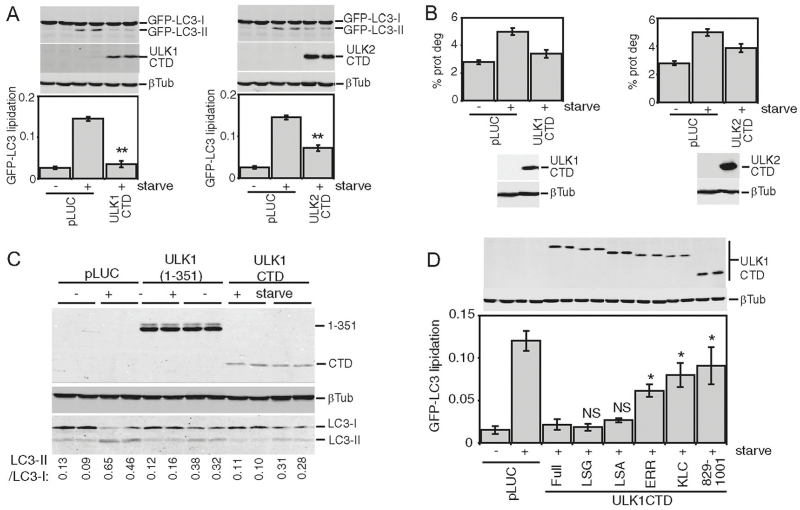

FIG. 5. CTDs of ULK1 and ULK2 inhibit autophagy. (A) Control (pLUC) and expression constructs for Myc-tagged ULK1 and ULK2 CTDs were transfected into 293/GFP-LC3 cells. Inhibition of starvation-induced GFP-LC3 lipidation was measured as described in the legend for Fig. 2. **, $P < 0.006$ in pairwise comparisons with pLUC-transfected, starved cells. (B) 293/GFP-LC3 cells transfected as described for panel A were labeled overnight with [^{14}C]valine. Cells were then either left untreated or starved in EBSS for 2 h, and autophagic degradation of long-lived proteins (prot deg) was analyzed. Cell samples transfected in parallel were used as a control to detect overexpressed constructs. Each bar represents the average from three independent samples ± the standard deviation. (C) HEK293A cells were transfected for 24 h with control pLUC plasmid, a Myc-tagged ULK1(1–351) deletion mutant as an internal control, or Myc-tagged ULK1 CTD. Cells were then left untreated or starved in EBSS-leupeptin for 2 h and then lysed for SDS-PAGE analysis of LC3 lipidation. The ratio of LC3-II/LC3-I measured for each sample is indicated at the bottom. (D) Myc-tagged ULK1 CTD constructs with C-terminal truncations were transfected into 293/GFP-LC3 cells, and GFP-LC3 lipidation was measured as described in the legend for Fig. 2. *, $P < 0.05$; NS, $P > 0.4$ (in pairwise comparisons with full-length-CTD-transfected, starved cells). A schematic of the truncations is shown in Fig. 2. βTub, β-tubulin.

previous data showed that localization of ULK1 to GFP-LC3-labeled structures was dependent on the CTD (3), so we investigated the relationship between dominant-negative activity and membrane association by using biochemical assays. We first confirmed that approximately 30% of the total overexpressed Myc-tagged ULK1 was associated with the crude membrane pellet in starved 293/GFP-LC3 cells (Fig. 6A), which was consistent with previous fractionation data from brain extracts (33). For control purposes, we observed that lipidated GFP-LC3-II was associated exclusively with crude membranes (relative to the soluble supernatant). Some GFP-LC3-I was also detected on the membranes, but this association could be disrupted by an additional salt wash of the pellet. Importantly, ULK1 and GFP-LC3-II were stably membrane bound even after a 0.5 M salt wash. We next confirmed that the association of ULK1 to crude membrane fractions was lost upon deletion of the CTD (Fig. 6B). However, deletion of the PDZ binding motif (LSG-STOP) or deletion of the last 50 amino acids [ULK1(1–1001)] of ULK1 did not disrupt membrane binding. Thus, ULK1 could still associate with membranes even after removal of C-terminal residues that are required for dominant-negative activity, suggesting that these functions were independent. Supporting the idea that altered membrane binding was not involved in the dominant-negative mechanism, kinase-inactivated forms of ULK1 and ULK2 were detected in the membrane fraction with an efficiency similar to that of wild-type proteins (Fig. 6C).

Since deletion of the entire CTD largely abolished membrane association, we questioned whether this region alone could bind membranes. Indeed, the CTD of ULK1 could be detected in the membrane pellets derived from extracts of starved 293/GFP-LC3 cells, and this association was salt resistant (Fig. 6D). As expected, an overexpressed ULK1 CTD reduced the amount of membrane-associated GFP-LC3-II. Expression of the ULK1 CTD clearly inhibited the formation of starvation-induced GFP-LC3-positive autophagosomes (Fig. 6E). Besides existing as a diffuse cytosolic pool, the ULK1 CTD could be observed on discreet puncta that colocalized with the remaining GFP-LC3 puncta, consistent with the idea that the CTD contains autophagosomal targeting signals. Membrane association was also confirmed biochemically for the ULK2 CTD (data not shown).

In agreement with deletion analysis of full-length ULK1, the last 50 residues of the ULK1 CTD C terminus were not required for membrane binding (Fig. 6F), suggesting that membrane targeting signals were distinct from the region involved in dominant-negative interactions. To map further the minimal membrane targeting region, we analyzed the hydropathy pro-

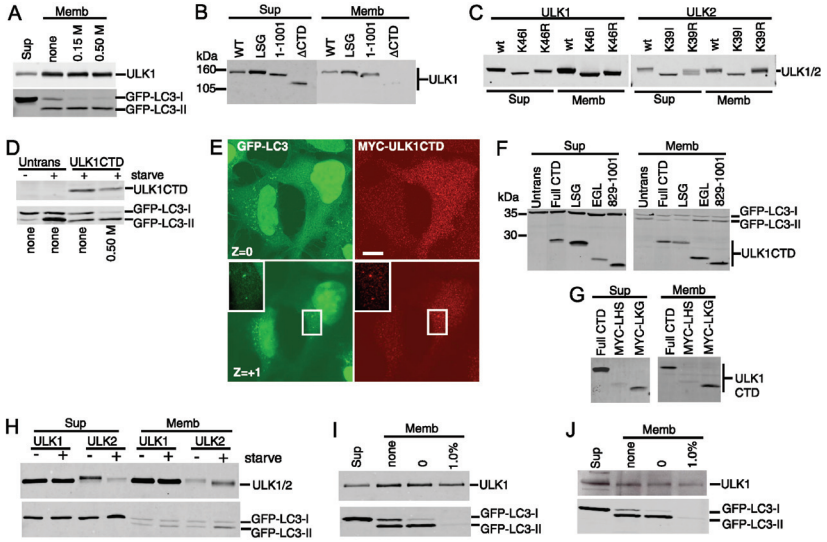

FIG. 6. Membrane targeting signal within the CTDs of ULK1 and ULK2. (A) 293/GFP-LC3 cells were transfected with Myc-ULK1 and starved in EBSS-leupeptin for 2 h. Cell homogenates were centrifuged at 100,000 × *g* to isolate membrane (Memb) and supernatant (Sup) fractions. Aliquots of the supernatant (representing 2% of the cell sample) and membrane (representing 10% of the cell sample) fractions were analyzed by SDS-PAGE. The top half of the blot was probed with anti-Myc and the bottom with anti-LC3. Where indicated, the membrane fraction was washed with HB containing 0.15 M or 0.5 M KCl. (B and C) Myc-tagged ULK1 and -2 constructs were transfected into cells and analyzed for membrane association as described above. (D) After transfection with Myc-tagged ULK1 CTD, cells were left untreated or starved in EBSS-leupeptin for 2 h. Where indicated, the membrane pellet was washed in HB containing 0.5 M KCl and analyzed as described above. (E) 293/GFP-LC3 cells were transfected with Myc-ULK1 CTD for 24 h and then starved in EBSS-leupeptin for 2 h before fixation and immunostaining with anti-Myc monoclonal antibody. In a *Z* section close to the substratum (*Z* = 0), ULK1 CTD strongly inhibited GFP-LC3 punctum formation. In the *Z* + 1 section, Myc-ULK1 CTD could be detected colocalizing with GFP-LC3-positive structures (inset). Bar = 10 μm. (F) Membrane associations of ULK1 CTD (Full CTD) and various C-terminal deletion constructs in starved 293/GFP-LC3 cells. See the schematic in Fig. 2 for the positions of inserted stop codons. The expression of ULK1 CTD was detected with anti-Myc, and GFP-LC3 was detected with anti-LC3. (G) Membrane associations of ULK1 CTD and two N-terminal deletion constructs, Myc-LHS (845–1051) and Myc-LKG (864–1051), in starved 293/GFP-LC3 cells. (H) 293/GFP-LC3 cells were transfected with full-length Myc-ULK1 or -ULK2 and then left untreated or starved in EBSS-leupeptin for 2 h before isolation of supernatant and membrane fractions. Expressed proteins were detected as described above. (I) Membrane association of transfected Myc-ULK1 in starved 293/GFP-LC3 cells. Membrane pellets were analyzed before washes (none) or following extraction in HB (0) or HB supplemented with 1.0% TX-100. (J) Membrane association of endogenous ULK1 was analyzed in untransfected, starved 293/GFP-LC3 cells following the fractionation and wash procedures described for panel I. WT, wild type; Untrans, untransfected.

file of the ULK1 CTD to identify regions amenable for deletion. Up to 35 amino acid residues (containing both a hydrophobic and a hydrophilic stretch) (MYC-LKG) could be removed from the N terminus of the ULK1 CTD without disruption of membrane binding (Fig. 6G). Thus, deletion analysis of the CTD N and C termini has further defined the membrane association region to amino acids 864 to 1001.

Although membrane binding did not appear to be critically involved in dominant-negative activity, we explored whether membrane association of ULK proteins was regulated upon induction of autophagy. Overexpressed ULK1 binding to membranes was unaltered following amino acid starvation (Fig. 6H). In contrast, overexpressed ULK2 exhibited both faster electrophoretic mobility and increased membrane association following amino acid starvation. These data suggest that, upon autophagy induction, ULK2 becomes partially dephosphorylated and more strongly associated with autophagosomal membranes, providing more evidence that ULK1 and ULK2 may have distinct roles in autophagy.

Further investigation unexpectedly revealed that the association of ULK1 to membrane fractions was resistant to extraction with 1% TX-100 (in contrast to lipidated GFP-LC3-II, which was no longer membrane bound) (Fig. 6I). This tight association of ULK1 to detergent-resistant membranes was confirmed for endogenous ULK1 (Fig. 6J). Note that membrane binding of endogenous ULK1 was not altered following amino acid starvation (data not shown).

ULK1 and -2 form distinct protein complexes. Since altered membrane binding did not appear to explain the dominant-negative effects of the ULK1/2 CTD or kinase-dead proteins, we investigated whether these mutant ULK proteins displayed altered protein complex formation. Using native polyacrylamide gels, we detected overexpressed ULK1 in two major species: a smaller population with an apparent molecular mass

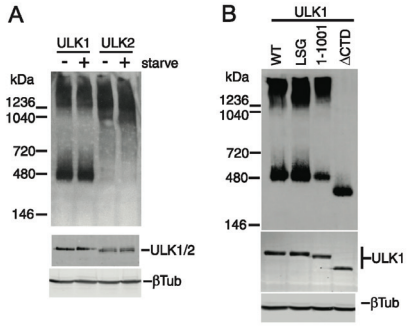

FIG. 7. Molecular complexes of ULK1 and ULK2 detected using native PAGE. HEK293A cells were transfected with ULK1 and ULK2 and starved for 2 h in EBSS where indicated (A) or ULK1 constructs (B) before lysis in native gel sample buffer. Complexes were resolved on native PAGE gels and then detected by immunoblotting with anti-Myc antibody (top). Positions of native-gel molecular mass markers are indicated on the left. As a control, aliquots of lysates were resolved by conventional SDS-PAGE to detect overexpressed proteins (anti-Myc) and total protein (β-tubulin [βTub]) (bottom). WT, wild type.

of 400 to 500 kDa, and a larger complex migrating with an apparent molecular mass of >1,200 kDa (Fig. 7A). By comparison, overexpressed ULK2 in native gels was detected primarily as one protein species migrating at >1,000 kDa. Although these protein complexes were not altered following amino acid starvation, these results suggest that ULK1 and ULK2 enter into distinct molecular complexes. Interestingly, and in contrast with wild-type ULK1, kinase-inactivated ULK1-K46I and ULK1-K46R existed primarily as a larger 1,200-kDa species (data not shown), raising the possibility that altered protein complexes were related to our dominant-negative mechanism. However, ULK1 lacking its C-terminal 50 residues still entered into two molecular complexes, similarly to the wild type, indicating that the C-terminal dominant-negative IERRLSA motif was not involved in these molecular interactions (Fig. 7B). Further deletion of the entire CTD prevented ULK1 from entering into the high-molecular-mass complex, indicating a requirement for sequences within the CTD between amino acids 829 and 1001.

Putative human homologue of Atg13. Our deletion analyses indicated a requirement of amino acid residues within the CTD C terminus for dominant-negative activity. Recent findings have shown that C-terminal residues of yeast Atg1 direct binding to Atg13 (5). Thus, we questioned whether an Atg13 orthologue was involved in the dominant inhibitory mechanism of the ULK1/2 CTDs. Using both *Schizosaccharomyces pombe* and *Saccharomyces cerevisiae* Atg13 protein sequences, we searched the genomes of higher organisms using repetitive rounds of PSI-BLAST for an mAtg13 orthologue. In the first round of iteration, we identified a putative orthologue in *D. melanogaster* (CG7331) in addition to orthologues in mice (Entrez protein database accession no. NP_663503.1) and humans (Entrez protein database accession no. NP_055556.2/KIAA0652), which have both been annotated as the gene products of *harbinger transposase derived 1* (*HARBI1*). Harbi1 (Entrez protein database accession no. AAH02378) had previously been identified as the putative human Atg13 orthologue (18). The *D. melanogaster* CG7331 protein was found in a systematic characterization of protein interactions to bind *D. melanogaster* Atg1 (28), supporting its role as a putative Atg13 orthologue. Bioinformatic analysis of current genome information revealed that the putative vertebrate Atg13 orthologues are tightly conserved (94% amino acid identity for mouse versus human), while the putative orthologues in *D. melanogaster* and *C. elegans* are clearly divergent.

To confirm the role of this putative Atg13 orthologue in autophagy, we obtained an siRNA pool targeting the human transcript NM_014741. In 293/GFP-LC3 cells, knockdown of Atg13 inhibited the formation of starvation-induced GFP-LC3 punctum formation to an extent similar to that of ULK1 knockdown (Fig. 8A). We identified two individual siRNA duplexes within this pool that could be confirmed to knock down Atg13 mRNA (data not shown) and inhibit starvation-induced lipidation of GFP-LC3 (Fig. 8B). We further confirmed that knockdown of Atg13 in parental HEK293 cells inhibited lipidation of endogenous LC3 during unstarved and starvation conditions, both without and with lysosomal protease inhibition by leupeptin (Fig. 8C).

As an independent means to confirm the function of Atg13 in autophagy, we investigated its role in mAtg9 trafficking under starvation conditions (Fig. 8D). mAtg9 is a multispanning membrane protein required for autophagy, and after amino acid starvation or rapamycin treatment, mAtg9 redistributes from a juxtanuclear clustered pool to a dispersed peripheral cytosolic pool (37). We have previously shown that siRNA knockdown of ULK1 inhibits the starvation-induced redistribution of mAtg9 (37). Using this assay, we find that knockdown of human Atg13 similarly prevented the starvation-induced dispersal of mAtg9, which supports the proposed identification of KIAA0652 as human Atg13 and demonstrates the function of Atg13 in a ULK1-dependent autophagic pathway.

We expressed the putative human Atg13 orthologue with a C-terminal FLAG tag in 293/GFP-LC3 cells (Fig. 9A). Ectopically expressed Atg13-FLAG existed primarily as a diffuse cytoplasmic pool in both unstarved (data not shown) and amino acid-starved conditions. In some cells, Atg13-FLAG could be observed on small cytoplasmic puncta that were often juxtaposed, but not substantially colocalized, with GFP-LC3-labeled structures. Consistently with this immunofluorescence analysis, approximately 5% of Atg13-FLAG (migrating at a 70-kDa apparent molecular mass by Laemmli SDS-PAGE) was membrane associated (Fig. 9B) in unstarved conditions. Amino acid starvation enhanced the membrane association of Atg13-FLAG. We generated polyclonal antisera toward Atg13 and confirmed the loss of the endogenous protein following knockdown (Fig. 9C). Endogenous Atg13 bound to membranes, although this association was sensitive to 1% TX-100 extraction (Fig. 9D), which contrasts with the TX-100-resistant membrane association of ULK1.

Overexpression of Atg13 is not sufficient to rescue inhibition of autophagy caused by ULK dominant-negative proteins. Data from yeast indicate that Atg13 binds Atg1 in a phosphorylation-dependent manner (10). We found that, in cotransfected HEK293 cells, Atg13-FLAG could readily coimmunoprecipitate both Myc-tagged ULK1 and ULK2 (Fig. 10A).

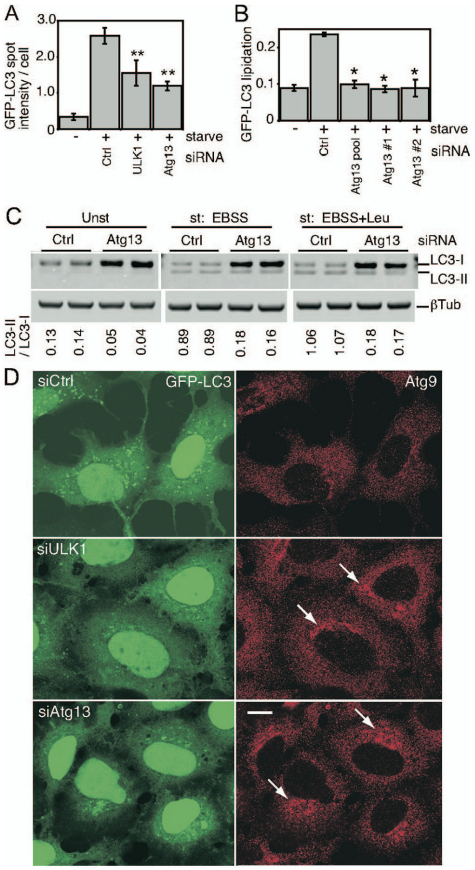

FIG. 8. A putative human Atg13 homologue is required for autophagy. (A) 293/GFP-LC3 cells were transfected with control siRNA (Ctrl) or siRNA targeting ULK1 or a SMARTpool targeting KIAA0652 (Atg13) for 72 h. Cells were then left unstarved or starved in EBSS-leupeptin for 2 h before fixation and morphological analysis. The quantification represents the total GFP-LC3 spot intensity per cell (arbitrary units), and each bar represents the average of 60 image fields (from six independent cell samples) ± the standard deviation. **, $P < 0.0007$ in pairwise comparisons with Ctrl knockdown starved cells. (B) 293/GFP-LC3 cells were transfected for 72 h with control siRNA, the Atg13 SMARTpool, or individual duplexes (#1 or #2) specific for Atg13. Cells were left unstarved or starved as described for panel A and then lysed for immunoblot analysis of GFP-LC3 lipidation, as described in the legend for Fig. 2. *, $P < 0.02$ in pairwise comparisons with siRNA Ctrl starved cells. (C) HEK293A cells were transfected with control siRNA or Atg13 duplex 2 for 72 h. Cells were then left unstarved (Unst) or starved (st) for 2 h in EBSS (with or without leupeptin [Leu]) before lysis for immunoblot analysis of endogenous LC3 lipidation. The quantified ratio of LC3-II/LC3-I is shown below each sample. βTub, β-tubulin. (D) 293/GFP-LC3 cells were transfected for 72 h with control siRNA (siCtrl) or siRNAs targeting ULK1 (siULK1) or Atg13 (duplex 2) (siAtg13), starved in EBSS-leupeptin for 2 h, and then fixed and immunostained to detect endogenous mAtg9 localization (red). After starvation in siCtrl-treated cells, mAtg9 becomes redistributed predominantly to a diffuse cytoplasmic pool. After knockdown of Atg13, mAtg9 redistribution is blocked and mAtg9-positive vesicles remain in juxtanuclear clusters (arrows) to an extent similar to that after knockdown of ULK1. Inhibition of starvation-induced GFP-LC3 autophagosome formation after knockdown of ULK1 and Atg13 is shown as a control. Bar = 10 μm.

With control immunoblots of the lysates, we consistently observed that Atg13-FLAG singly overexpressed migrated as a sharp band close to 70 kDa. Strikingly, coexpression with either ULK1 or ULK2 led to the reduced mobility of Atg13, suggesting that ULK1 and ULK2 were regulating the phosphorylation of human Atg13. In yeast, both Atg13 phosphorylation and Atg1-Atg13 binding could be regulated by rapamycin treatment (10). In contrast, amino acid starvation in our overexpression cell system did not robustly affect either the electrophoretic mobility of Atg13 or its ability to coimmunoprecipitate with ULK1 or ULK2 (data not shown). In contrast to wild-type ULK proteins, coexpressed ULK1-K46I or ULK2-K39I did not promote a hypershift of Atg13-FLAG. However, Atg13-FLAG still coimmunoprecipitated with both ULK1-K46I and ULK2-K39I, suggesting that binding was not regulated by Atg13 phosphorylation (Fig. 10B and C).

Since the last 20 residues of yeast Atg1 are critical for binding to yeast Atg13 (5), we predicted that the ULK CTD would be involved in the binding of human Atg13, and we tested this idea using coimmunoprecipitation experiments. While coexpression with ULK1ΔCTD resulted in the loss of the Atg13-FLAG protein, this effect was less pronounced when the ULK2ΔCTD mutant was used. As shown in Fig. 10D, when ULK2ΔCTD and Atg13 were coexpressed, Atg13 did not hypershift or coimmunoprecipitate with ULK2ΔCTD. Importantly, the CTDs of both ULK1 and ULK2 readily coimmunoprecipitated with Atg13-FLAG (Fig. 10E). Surprisingly, the ULK1 CTD lacking 50 residues from its C terminus [ULK1CTD(829–1001)] still coimmunoprecipitated with Atg13-FLAG with an efficiency similar to that of the full-length CTD (Fig. 10F). We similarly observed that the C-terminal 50 residues of ULK2 were dispensable for Atg13 binding (data not shown). Thus, the C-terminal portions of the ULK1 and -2 CTDs (including the dominant-negative IERRLSA motif) could be removed without affecting Atg13 binding.

Earlier, we hypothesized that the dominant-negative mechanism initiated by the CTDs and kinase-dead versions of ULK1 and -2 might involve the titration of an essential Atg13-dependent function, perhaps through Atg13 recruitment. However, our mapping data suggested that the region of the CTD binding Atg13 was separable from the residues that participated in dominant-negative interactions. In agreement with this conclusion, coexpression with Atg13-FLAG did not produce any rescuing effects toward the dominant-negative activities of the ULK1 and -2 CTDs on GFP-LC3 lipidation (Fig. 10G). Atg13-FLAG coexpression similarly could not rescue the inhibition of autophagy caused by ULK1-K46I or ULK2-K39I (data not shown). Thus, we conclude that the

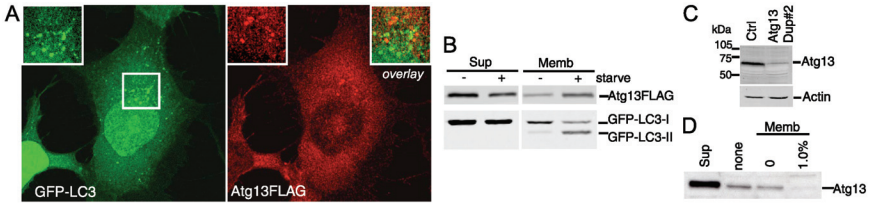

FIG. 9. Human Atg13 is membrane associated. (A) 293/GFP-LC3 cells expressing Atg13-FLAG were starved for 2 h in EBSS-leupeptin, fixed, and then immunostained using anti-FLAG antibody. Atg13-FLAG can be found both in a diffuse cytosolic pool and localized to punctate structures that do not colocalize with GFP-LC3. Bar = 10 μm. (B) Membrane association of Atg13-FLAG was analyzed as described in the legend for Fig. 6. (C) HEK293A cells were transfected with control or Atg13 duplex 2 (Dup#2) for 72 h. Cell lysates were then immunoblotted with a polyclonal antibody for endogenous Atg13 or actin as a loading control. (D) Membrane fractions analyzed as described for Fig. 6J from untransfected 293/GFP-LC3 cells were probed for endogenous Atg13. Sup, supernatant; Memb, membrane fraction; Ctrl, control.

dominant inhibitory mechanism involves an essential factor independent of Atg13.

Phosphorylation of Atg13 by ULK proteins. Last, because the kinase that phosphorylates Atg13 in yeast remains unclear, we investigated whether ULK1 and -2 could directly phosphorylate Atg13. We asked whether immunoprecipitated ULK proteins could phosphorylate immunoprecipitated Atg13-FLAG in a mixed-bead in vitro kinase reaction. Immunoprecipitated Atg13-FLAG incubated alone under reaction conditions did not undergo a mobility hypershift in SDS-PAGE, demonstrating that there was no associated kinase activity in the immunoprecipitate (Fig. 10H). However, incubation of Atg13 together with immunoprecipitated ULK1 or ULK2 did result in a decreased mobility of Atg13. This mobility change was not observed when Atg13 was incubated with kinase-dead ULK1 and -2 or ULK proteins lacking their CTDs. These data support the conclusion that Atg13 binds ULK1 and -2 via their CTDs, promoting phosphorylation of Atg13 via the catalytic kinase domain. Immunoblotting of lysates from cells under normal medium conditions revealed that endogenous Atg13 migrates as a doublet, suggestive of distinct species with different levels of phosphorylation (Fig. 10I). Expression of ULK1 or ULK2 promoted substantially more Atg13 with reduced mobility, further supporting the phosphorylation of Atg13 by ULK1 and -2 in vivo.

DISCUSSION

ULK proteins adopt a closed conformation to prevent the CTD from forming abnormal interactions. Our previous data showed unexpectedly that the ULK1-K46R kinase mutant (32) did not show a strong dominant inhibitory effect in our autophagy cell system (3). Here, we confirmed that while the K46R substitution significantly impaired catalytic function in vitro, the charge-disruptive K46I substitution fully ablated activity and produced a mutant protein that displayed less autophosphorylation and inhibited starvation-induced autophagy. These data agree with a recent report that showed a ULK1-K46N mutant to inhibit autophagy in NIH 3T3 fibroblasts (6). Our data also showed that the CTD was required for kinase-inactive ULK1 to inhibit autophagy. Similarly, in *D. discoideum*, deletion of CTD sequences rescued the dominant-negative effects of the Atg1-K36A kinase mutant on autophagy-dependent survival (30). Deletion of the CTD also stimulated in vitro autophosphorylation but decreased the ability of the kinase to phosphorylate exogenous substrates.

These findings and our other results led us to propose a working model in which the CTD is normally folded back onto the N-terminal region to keep the protein in a closed molecular conformation (Fig. 11). It is still unclear whether the interaction of the CTD with N-terminal regions is controlled by the kinase domain (perhaps via a protein-protein interaction) or via an interaction at the autophosphorylation sites. The K46I mutation triggers a robust conformational change leading to exposure of the CTD, potentially revealing a binding site in the CTD that interacts with essential autophagy regulatory factors.

Our deletion analysis has identified a 7-residue motif (IER RLSA) within the last 14 C-terminal amino acids of the CTD that was required for dominant-negative function, which we propose constitutes a binding site for a critical autophagy regulatory factor ("Y" in Fig. 11). Interestingly, the IERRLSA motif is well conserved in ULK1/2 proteins from mice, humans, and other vertebrates but not in Atg1 homologs of *S. cerevisiae*, *D. melanogaster*, and *C. elegans*. Based on this sequence information, we speculate that the factor binding to the IERRLSA motif might be specific to vertebrates.

Could conformational changes represent a physiological mechanism for the regulation of ULK proteins? The in vitro limited proteolysis assay that we employed could not detect significant changes after amino acid starvation (Chan and Tooze, unpublished), although this could represent a limitation of our system. However, our findings have established that an almost complete ablation of the kinase activity is required to produce readily detectable effects in protease cleavage and autophagy assays. It was recently demonstrated that the kinase activity of endogenous ULK1 in mouse embryonic fibroblasts was modestly activated following amino acid starvation (6), which suggests that subtle conformational alterations could possibly represent a normal means of ULK1 regulation.

Signals within the ULK1 CTD direct membrane binding and protein complex formation. We and others have seen that ULK1 localizes to GFP-LC3- or Atg16L1-positive autophagosomal structures (3, 6) and that this localization depends upon the CTD. In order to define the downstream effectors of the

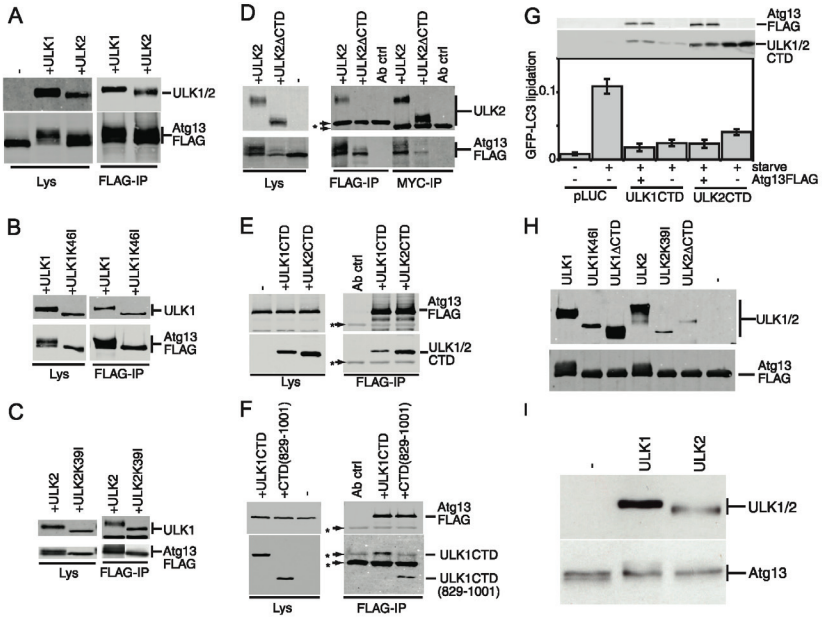

FIG. 10. Binding of Atg13 to the CTD is required for phosphorylation by ULK1 and ULK2. (A, B, and C) HEK293A cells were transfected with Atg13-FLAG alone (−) or in combination (+) with Myc-ULK1, Myc-ULK2, Myc-ULK1-K46I, or Myc-ULK2-K39I, as indicated. An aliquot of cell lysate was analyzed by SDS-PAGE and immunoblotting with Myc (top) and FLAG (bottom) antibodies. Lysates of doubly transfected cells were incubated with anti-FLAG beads to coimmunoprecipitate Atg13 and ULK proteins. (D) Myc-ULK2 and Myc-ULK2ΔCTD were coexpressed with FLAG-Atg13 in HEK293A cells. As a control, Atg13-FLAG was expressed alone (−). Cell lysates were immunoprecipitated with anti-Myc or anti-FLAG antibody and then immunoblotted as described above. (E) Coimmunoprecipitation of the Myc-tagged CTDs of ULK1 and ULK2 with Atg13-FLAG. Lysates and immunoprecipitates were analyzed as described above. (F) Coimmunoprecipitation of Myc-ULK1CTD(829–1001) with Atg13-FLAG. Lysates and immunoprecipitates were analyzed as described above. The asterisks in panels D, E, and F indicate nonspecific bands arising from the antibody used for immunoprecipitation, as demonstrated by the antibody-plus-beads-alone control (Ab ctrl). (G) 293/GFP-LC3 cells were cotransfected with Myc-ULK1 CTD or Myc-ULK2CTD with or without Atg13-FLAG for 24 h and then either left unstarved or starved in EBSS-leupeptin for 2 h before lysis for analysis of GFP-LC3 lipidation, as described in the legend for Fig. 2. Protein expression controls (top) using anti-FLAG and anti-Myc antibodies are shown. (H) Immunoprecipitated Atg13-FLAG protein was used as a substrate for immunoprecipitated Myc-ULK proteins in a mixed-bead in vitro kinase reaction. Phosphorylation of Atg13-FLAG is detected as a decrease in mobility. A control reaction without the addition of ULK proteins (−) shows no mobility shift. (I) HEK293A cells were either left untransfected (−) or transfected with Myc-ULK1 or Myc-ULK2 before cell lysates were immunoblotted to detect hypershifting on endogenous Atg13. Lys, lysates; IP, immunoprecipitate.

CTD (i.e., to identify factor "Y"), we used biochemical fractionation and imaging techniques to characterize the ULK CTD. The CTDs of both ULK1 and ULK2 contained signals that could direct membrane binding, and further deletion mapping identified N- and C-terminal sequences that were dispensable for membrane association. Importantly, CTD deletion mutants lacking the IERRLSA dominant-negative motif still retained normal membrane binding efficiencies, which suggests that the critical inhibitory interactions initiated by the CTD are not membrane associated (Fig. 11B). Our data on overexpressed and endogenous ULK1 also suggest that association to membranes was resistant to detergent extraction, unlike results for other autophagy proteins, such as the lipidated form of LC3, and Atg13. Our preliminary data using floatation in detergent-containing gradients suggest that ULK1 cofractionates with markers of lipid rafts (A. Longatti and S. A. Tooze, unpublished observations), although the molecular basis of these observations requires further investigation.

In *S. cerevisiae*, Atg1 enters into a number of protein complexes (9–12, 22). Using native gel electrophoresis, we observed ULK1 in two distinct populations suggestive of different subcomplexes. Inactivation of kinase function shifted the ULK1-K46I protein toward the higher-molecular-weight complex, with a corresponding loss of the low-molecular-weight species (Chan and Tooze, unpublished). Importantly, while entry of ULK1 into the higher-molecular-weight population required the entire CTD, up to 50 C-terminal residues, including the IERRLSA dominant-negative motif, could be removed from the CTD C terminus without affecting entry into either protein complex. Thus, the dominant-negative mo-

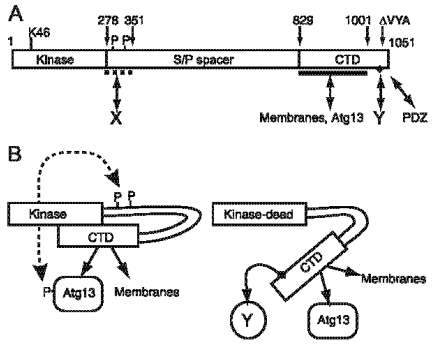

FIG. 11. Conformational changes of ULK proteins modulated by autophosphorylation status. (A) Domain structure of ULK1 showing the N-terminal kinase domain and the critical lysine 46 residue (K46) targeted in our mutant constructs. Our data are consistent with the existence of multiple, but so far unidentified, autophosphorylation (P) sites within residues 278 to 351 of the serine- and proline-rich spacer domain (S/P spacer). Our previous findings indicate a region spanning residues 278 to 351 that is critical for inhibition of autophagy, presumably via interaction with an unknown protein (X). Our previous data also indicated that the last three residues of ULK1 (VYA) are critical for regulatory function, possibly by binding a PDZ domain-containing protein. Our findings here indicate multiple functions directed by sequences within the conserved CTD. A region between residues 829 and 1001 contains signals for binding to membranes and interaction with human Atg13. Additional sequences between residues 1038 and 1044 (Fig. 2) contain a conserved motif (IERRLSA, black diamond) that is required for dominant inhibitory activity by interacting with another unknown factor (Y). (B) Proposed model showing phosphorylation-dependent conformational changes. In normal resting cells, ULK proteins are autophosphorylated, and these modifications help maintain a closed conformation that (i) brings Atg13 in closer proximity to the kinase domain for phosphorylation and (ii) keeps the dominant-negative motif hidden or inaccessible. Full ablation of kinase activity results in a low degree of autophosphorylation and a more open molecular conformation that exposes the dominant inhibitory CTD motif, allowing it to bind the unknown factor (Y) that is critical for autophagy.

tif proposed to bind the critical factor "Y" is separate from other CTD sequences that direct formation of higher-molecular-weight ULK1 protein complexes.

Our data further suggest the existence of two types of ULK1 complexes: a small one containing proteins that bind to ULK1 in a CTD-dependent manner, and a large complex containing proteins that can still bind kinase-inactive ULK1. It has been demonstrated that in *S. cerevisiae* Atg1 plays two roles in bulk nonselective autophagy: one being structural, facilitating recruitment of Atg proteins to the PAS, and the second being responsible for recycling proteins from the PAS during formation (4, 5). The former role requires the CTD, while the latter requires the kinase domain. While our data do not provide any support for a dual role of the mAtg1 orthologues, further analysis of the small and large complexes may shed light on whether ULK1 or ULK2 behaves similarly to yeast Atg1. Further investigation is also required to understand the differences between ULK1 and ULK2 complexes revealed by native gel analysis.

Human Atg13 binds to the CTD independently of the IER RLSA motif. Since binding of yeast Atg13 depends upon the C-terminal 20 residues of yeast Atg1 (5), we asked whether the ULK1 and ULK2 CTDs could bind the human homologue of Atg13 and whether this binding occurred via the IERRLSA motif. We identified and characterized a putative human Atg13 orthologue and showed that it was required for autophagy by using LC3 lipidation and the mAtg9 subcellular redistribution assays. Consistent with a role in autophagy, tagged versions of Atg13 became more enriched on membranes following the activation of autophagy. Alteration of mAtg9 trafficking caused by the loss of Atg13 could be due to either decreased Atg13 function or an indirect modulation of ULK1 function or stability. In yeast, Atg1 kinase activity is not required for Atg9 trafficking, so it is unlikely that the loss of ULK1 kinase activity underlies the aberrant mAtg9 trafficking. Rather, as we previously showed, siRNA-mediated depletion of ULK1 inhibits mAtg9 trafficking (37), and our preliminary data suggest that siRNA depletion of Atg13 causes a decrease in ULK1 levels (N. C. McKnight and S. A. Tooze, unpublished observations). Further work is required to clarify the role of human Atg13 in mAtg9 trafficking.

Despite their sequence differences, ULK1 and ULK2 both bound human Atg13 via their CTDs. The IERRLSA motif that we identified here, while not well conserved in yeast, includes an R residue (position 1041 in ULK1) which corresponds to the conserved R885 in yeast Atg1 that constitutes part of an Atg1-Atg13 interaction motif (5). Furthermore, within the C-terminal 20 amino acids of yeast Atg1 is a conserved Y residue at position 878, and substitution of both R885 and Y878 with alanine (Y878A/R885A) in Atg1 results in the loss of recruitment of Atg17 to the PAS (5). Interestingly, this Y residue is conserved in mouse and human ULK2 but not ULK1. However, our data using CTD deletions of ULK1 and ULK2 show that the IERRLSA motif (and also the last 20 amino acids) is not required for human Atg13 binding. We speculate either that another binding site has evolved in the ULKs for human Atg13 or possibly that the Y878A/R885A mutations, which were made in the context of the whole yeast Atg1 protein, altered the conformation or accessibility of the true Atg13 binding site.

In support of our model and binding data, coexpression with Atg13 did not rescue the inhibition of autophagy caused by ULK CTDs (or kinase-dead mutants [data not shown]), suggesting that Atg13 is not the protein being titrated out by the 7-residue CTD motif. A possible candidate for this binding protein (and perhaps factor "Y") is FIP200, which recently has been shown to bind ULK1 and ULK2 in a CTD-dependent manner and to regulate ULK1 kinase function and protein stability (6). Interestingly, Hara et al. suggest that FIP200 may be the human homologue of yeast Atg17 and that, although there is no sequence conservation between Atg17 and FIP200, both proteins have coiled-coil domains, suggesting a conservation of function as a scaffold protein (6).

Phosphorylation of Atg13 by ULK1 and ULK2. In the course of our studies, we observed that Atg13 displayed a decreased electrophoretic mobility when coexpressed with ULK1 or ULK2, suggestive of a modification by phosphorylation. Consistent with direct phosphorylation of Atg13 by ULK1 and ULK2, Atg13 did not show an altered migration

when coexpressed with ULK proteins lacking Atg13 binding sites (ΔCTD) or kinase-inactivated ULK proteins. Furthermore, both ULK1 and ULK2 could promote Atg13 phosphorylation in a kinase-dependent fashion following an in vitro kinase reaction. These data suggest that Atg13 binds to ULK1 and ULK2 via the CTDs and is phosphorylated by the kinase domain (Fig. 11). In contrast with findings for yeast, binding of Atg13 to ULK proteins in our HEK293 cell model was not modulated by starvation of cells or by the overall phosphorylation status of Atg13. The definition of Atg13 phosphorylation sites and their regulatory function requires further investigation.

Differences between ULK1 and ULK2. Several lines of evidence have shown that ULK1 and ULK2 behave similarly. Kinase mutants of both ULK1 and ULK2 have dominant-negative effects, and our findings suggest that this is via exposure of a conserved motif within their CTDs. In addition, both ULK1 and ULK2 localize to autophagosomal structures and both proteins bind Atg13 and FIP200.

However, multiple aspects of our findings also highlight that ULK1 and ULK2 may have independent functions or modes of regulation. Deletion of CTD sequences in overexpressed ULK1 and ULK2 appears to promote different downstream effects. ULK1 and ULK2 can enter into different molecular complexes, and the binding of ULK2 to membranes was increased following amino acid starvation, in contrast to results with ULK1. Finally, we previously observed that knockdown of ULK1 but not ULK2 in HEK293 cells inhibited starvation-induced autophagy and starvation-induced mAtg9 redistribution. We also previously observed that overexpression of ULK1 produced a mild dominant inhibitory effect on autophagy, while here we show that overexpression of ULK2 in the same cell system enhanced GFP-LC3 lipidation following starvation. We have not yet been able to confirm the ability of overexpressed ULK2 to modulate other measures of autophagic flux by use of assays such as degradation of long-lived proteins or p62/SQSTM-1 stability (Chan, Longatti, and Tooze, unpublished), possibly due to the limited capabilities of downstream pathways. While additional experiments are required to fully understand the functional differences between ULK1 and ULK2, our biochemical data presented here are in general agreement with recent knockout mouse data that suggest ULK1 and ULK2 could be performing distinct roles in specialized and general autophagy. In addition, to further understand the mammalian equivalent of the yeast Atg1 signaling complex, it will be important to dissect the binding site within the ULK CTD for FIP200 and Atg13 as well as to examine the relationship between FIP200 and Atg13 for regulating the kinase activity and function of ULK proteins.

ACKNOWLEDGMENTS

We thank Mike Howell (LRI High Throughput Screening Unit) for advice and assistance in the Cellomics array scan experiments and Mike Mitchell (CRUK Bioinformtics Unit) for help with Atg13 bioinformatics. We thank the Secretory Pathways Laboratory for advice and encouragement and Cancer Research UK for support.

REFERENCES

1. **Abeliovich, H., C. Zhang, W. A. Dunn, Jr., K. M. Shokat, and D. J. Klionsky.** 2003. Chemical genetic analysis of Apg1 reveals a non-kinase role in the induction of autophagy. Mol. Biol. Cell **14**:477–490.
2. **Budovskaya, Y. V., J. S. Stephan, S. J. Deminoff, and P. K. Herman.** 2005. An evolutionary proteomics approach identifies substrates of the cAMP-dependent protein kinase. Proc. Natl. Acad. Sci. USA **102**:13933–13938.
3. **Chan, E. Y., S. Kir, and S. A. Tooze.** 2007. siRNA screening of the kinome identifies ULK1 as a multidomain modulator of autophagy. J. Biol. Chem. **282**:25464–25474.
4. **Cheong, H., and D. J. Klionsky.** 2008. Dual role of Atg1 in regulation of autophagy-specific PAS assembly in Saccharomyces cerevisiae. Autophagy **4**:724–726.
5. **Cheong, H., U. Nair, J. Geng, and D. J. Klionsky.** 2008. The Atg1 kinase complex is involved in the regulation of protein recruitment to initiate sequestering vesicle formation for nonspecific autophagy in Saccharomyces cerevisiae. Mol. Biol. Cell **19**:668–681.
6. **Hara, T., A. Takamura, C. Kishi, S. Iemura, T. Natsume, J. L. Guan, and N. Mizushima.** 2008. FIP200, a ULK-interacting protein, is required for autophagosome formation in mammalian cells. J. Cell Biol. **181**:497–510.
7. **Iwata, A., B. E. Riley, J. A. Johnston, and R. R. Kopito.** 2005. HDAC6 and microtubules are required for autophagic degradation of aggregated huntingtin. J. Biol. Chem. **280**:40282–40292.
8. **Kabeya, Y., Y. Kamada, M. Baba, H. Takikawa, M. Sasaki, and Y. Ohsumi.** 2005. Atg17 functions in cooperation with Atg1 and Atg13 in yeast autophagy. Mol. Biol. Cell **16**:2544–2553.
9. **Kabeya, Y., T. Kawamata, K. Suzuki, and Y. Ohsumi.** 2007. Cis1/Atg31 is required for autophagosome formation in Saccharomyces cerevisiae. Biochem. Biophys. Res. Commun. **356**:405–410.
10. **Kamada, Y., T. Funakoshi, T. Shintani, K. Nagano, M. Ohsumi, and Y. Ohsumi.** 2000. Tor-mediated induction of autophagy via an Apg1 protein kinase complex. J. Cell Biol. **150**:1507–1513.
11. **Kawamata, T., Y. Kamada, Y. Kabeya, T. Sekito, and Y. Ohsumi.** 2008. Organization of the pre-autophagosomal structure responsible for autophagosome formation. Mol. Biol. Cell **19**:2039–2050.
12. **Kim, J., Y. Kamada, P. E. Stromhaug, J. Guan, A. Hefner-Gravink, M. Baba, S. V. Scott, Y. Ohsumi, W. A. Dunn, Jr., and D. J. Klionsky.** 2001. Cvt9/Gsa9 functions in sequestering selective cytosolic cargo destined for the vacuole. J. Cell Biol. **153**:381–396.
13. **Komatsu, M., S. Waguri, T. Ueno, J. Iwata, S. Murata, I. Tanida, J. Ezaki, N. Mizushima, Y. Ohsumi, Y. Uchiyama, E. Kominami, K. Tanaka, and T. Chiba.** 2005. Impairment of starvation-induced and constitutive autophagy in Atg7-deficient mice. J. Cell Biol. **169**:425–434.
14. **Kuma, A., M. Hatano, M. Matsui, A. Yamamoto, H. Nakaya, T. Yoshimori, Y. Ohsumi, T. Tokuhisa, and N. Mizushima.** 2004. The role of autophagy during the early neonatal starvation period. Nature **432**:1032–1036.
15. **Kundu, M., T. Lindsten, C. Y. Yang, J. Wu, F. Zhao, J. Zhang, M. A. Selak, P. A. Ney, and C. B. Thompson.** 2008. Ulk1 plays a critical role in the autophagic clearance of mitochondria and ribosomes during reticulocyte maturation. Blood. doi:10.1182/blood-2008-02-137398.
16. **Levine, B., and G. Kroemer.** 2008. Autophagy in the pathogenesis of disease. Cell **132**:27–42.
17. **Matsuura, A., M. Tsukada, Y. Wada, and Y. Ohsumi.** 1997. Apg1p, a novel protein kinase required for the autophagic process in Saccharomyces cerevisiae. Gene **192**:245–250.
18. **Meijer, W. H., I. J. van der Klei, M. Veenhuis, and J. A. Kiel.** 2007. ATG genes involved in non-selective autophagy are conserved from yeast to man, but the selective Cvt and pexophagy pathways also require organism-specific genes. Autophagy **3**:106–116.
19. **Melendez, A., and T. P. Neufeld.** 2008. The cell biology of autophagy in metazoans: a developing story. Development **135**:2347–2360.
20. **Melendez, A., Z. Talloczy, M. Seaman, E. L. Eskelinen, D. H. Hall, and B. Levine.** 2003. Autophagy genes are essential for dauer development and life-span extension in C. elegans. Science **301**:1387–1391.
21. **Mizushima, N., B. Levine, A. M. Cuervo, and D. J. Klionsky.** 2008. Autophagy fights disease through cellular self-digestion. Nature **451**:1069–1075.
22. **Nice, D. C., T. K. Sato, P. E. Stromhaug, S. D. Emr, and D. J. Klionsky.** 2002. Cooperative binding of the cytoplasm to vacuole targeting pathway proteins, Cvt13 and Cvt20, to phosphatidylinositol 3-phosphate at the pre-autophagosomal structure is required for selective autophagy. J. Biol. Chem. **277**:30198–30207.
23. **Otto, G. P., M. Y. Wu, N. Kazgan, O. R. Anderson, and R. H. Kessin.** 2004. Dictyostelium macroautophagy mutants vary in the severity of their developmental defects. J. Biol. Chem. **279**:15621–15629.
24. **Ravikumar, B., C. Vacher, Z. Berger, J. E. Davies, S. Luo, L. G. Oroz, F. Scaravilli, D. F. Easton, R. Duden, C. J. O'Kane, and D. C. Rubinsztein.** 2004. Inhibition of mTOR induces autophagy and reduces toxicity of polyglutamine expansions in fly and mouse models of Huntington disease. Nat. Genet. **36**:585–595.
25. **Reggiori, F., K. A. Tucker, P. E. Stromhaug, and D. J. Klionsky.** 2004. The Atg1-Atg13 complex regulates Atg9 and Atg23 retrieval transport from the pre-autophagosomal structure. Dev. Cell **6**:79–90.
26. **Rodriguez-Enriquez, S., L. He, and J. J. Lemasters.** 2004. Role of mitochondrial permeability transition pores in mitochondrial autophagy. Int. J. Biochem. Cell Biol. **36**:2463–2472.
27. **Scott, R. C., G. Juhasz, and T. P. Neufeld.** 2007. Direct induction of au-

tophagy by Atg1 inhibits cell growth and induces apoptotic cell death. Curr. Biol. **17**:1–11.
28. **Stanyon, C. A., G. Liu, B. A. Mangiola, N. Patel, L. Giot, B. Kuang, H. Zhang, J. Zhong, and R. L. Finley, Jr.** 2004. A Drosophila protein-interaction map centered on cell-cycle regulators. Genome Biol. **5**:R96.
29. **Straub, M., M. Bredschneider, and M. Thumm.** 1997. AUT3, a serine/threonine kinase gene, is essential for autophagocytosis in *Saccharomyces cerevisiae*. J. Bacteriol. **179**:3875–3883.
30. **Tekinay, T., M. Y. Wu, G. P. Otto, O. R. Anderson, and R. H. Kessin.** 2006. Function of the *Dictyostelium discoideum* Atg1 kinase during autophagy and development. Eukaryot. Cell **5**:1797–1806.
31. **Thumm, M., R. Egner, B. Koch, M. Schlumpberger, M. Straub, M. Veenhuis, and D. H. Wolf.** 1994. Isolation of autophagocytosis mutants of Saccharomyces cerevisiae. FEBS Lett. **349**:275–280.
32. **Tomoda, T., R. S. Bhatt, H. Kuroyanagi, T. Shirasawa, and M. E. Hatten.** 1999. A mouse serine/threonine kinase homologous to C. elegans UNC51 functions in parallel fiber formation of cerebellar granule neurons. Neuron **24**:833–846.
33. **Tomoda, T., J. H. Kim, C. Zhan, and M. E. Hatten.** 2004. Role of Unc51.1 and its binding partners in CNS axon outgrowth. Genes Dev. **18**:541–558.
34. **Tsukada, M., and Y. Ohsumi.** 1993. Isolation and characterization of autophagy-defective mutants of Saccharomyces cerevisiae. FEBS Lett. **333**:169–174.
35. **Yan, J., H. Kuroyanagi, A. Kuroiwa, Y. Matsuda, H. Tokumitsu, T. Tomoda, T. Shirasawa, and M. Muramatsu.** 1998. Identification of mouse ULK1, a novel protein kinase structurally related to C. elegans UNC-51. Biochem. Biophys. Res. Commun. **246**:222–227.
36. **Yan, J., H. Kuroyanagi, T. Tomemori, N. Okazaki, K. Asato, Y. Matsuda, Y. Suzuki, Y. Ohshima, S. Mitani, Y. Masuho, T. Shirasawa, and M. Muramatsu.** 1999. Mouse ULK2, a novel member of the UNC-51-like protein kinases: unique features of functional domains. Oncogene **18**:5850–5859.
37. **Young, A. R., E. Y. Chan, X. W. Hu, R. Kochl, S. G. Crawshaw, S. High, D. W. Hailey, J. Lippincott-Schwartz, and S. A. Tooze.** 2006. Starvation and ULK1-dependent cycling of mammalian Atg9 between the TGN and endosomes. J. Cell Sci. **119**:3888–3900.

Project Name/Mouse Line
ULK1 Genetrap KO

Genotype
Knockout

If 'Other', please give full details on the genotype

Mouse Number

Pair number

Litter number

Earclip

Colour

Sex of the mouse
Female

Date of Birth (DD/MM/YY format; if unknown, type in "Unknown")
April 07

Date of Death (DD/MM/YY format; if unknown, type in "Unknown")
24 July 08

Requesting Investigator
Andrea Longatti

Email address
andrea.longatti@cancer.org.uk

Requesting Lab
Secretory Pathways

Telephone/Ext Number
3145

Has it been in a fixative?
No fixative

If 'Other', please give details of the fixative used

Tissue/specimen
complete pathology report

Procedures required
Complete post-mortum after removal of part of spleen and thymus for FACS experiments

Project Background
ULK1 is serine/threonine kinase which is essential for autophagy. Autophagy is an intracellular lysosomal degrative pathway which is vital for cell homeostasis. A closely related gene ULK2 may also be involved in autophagy, however, ULK1 knockdown in HEK293 cell lines indicated that ULK1 was sufficient for autophagy. We generated the mice anticipating that they may exhibit the phenotype of other autophagy gene knockouts which is post-natal death within 24hs from lack of ATP and amino acids. However, to date the ULK1 mouse knock out has appeared to be normal. Recently however there has been some mortality in the knockouts which we would like to investigate.

EXPERIMENTAL PATHOLOGY LABORATORY

EPL PATHOLOGY REPORT

CANCER RESEARCH UK

Report Generated: 24/07/08

EPL NUMBER: 295
User: Andrea Longatti

LINE ULK1 Genetrap ACo566

SPECIMEN:Mice

GENOTYPE:ko

COLLECTED:

DISSECTED:

DOB: 31/02/07

DOD:21/05/08

SEX: Female

TISSUE WEIGHT: N/A

TOTAL No. OF BLOCKS:

TOTAL SLIDES (H&E):

TOTAL SLIDES (UNSTAINED):

TOTAL SLIDES (IHC):

TOTALSLIDES (ISH):

TOTAL SLIDES (SPECIALS):

TOTAL SLIDES (OTHER):

BACKGROUND

ULK1 is serine/threonine kinase which is essential for autophagy. Autophagy is an intracellular lysosomal degrative pathway which is vital for cell homeostasis. A closely related gene ULK2 may also be involved in autophagy, however, ULK1 knockdown in HEK293 cell lines indicated that ULK1 was sufficient for autophagy. We generated the mice anticipating that they may exhibit the phenotype of other autophagy gene knockouts which is post-natal death within 24hs from lack of ATP and amino acids. However, to date the ULK1 mouse knock out has appeared to be normal. Recently however there has been some mortality in the knockouts which we would like to investigate.

COMPLETE PM AFTER REMOVAL OF SPLEEN AND THYMUS FOR FACS/WB

ALSO REMOVED A BIT OF LIVER, LUNG, KIDNEY
A=ULK1 GENETRAP ~~KO~~ FEMALE HET !
B=ULK1 GENETRAP KO FEMALE
C=WT

SUMMARY

everything normal ?

B7, 9, 10 maybe
C2

Contact:
Experimental
Pathology Lab
Cancer Research
UK
44 Lincoln's Inn
Fields
London
WC2A 3BX

Tel: 0207 269 3621

PATHOLOGY REPORT

MACRO EXTERNAL/INTERNAL

A=ULK1 GENETRAP KO FEMALE
LUMP IN MESENTERY=BLOCK 7
B=ULK1 GENETRAP KO FEMALE
MASS IN STOMACH
C=WT

MACRO INTERNAL

HET

1. Normal skin. Subcutaneous lymph node contains pigment in macrophages with some granular grey histiocytes (probably not significant).
2. Normal uterus. Some scattered pigment-laden macrophages in endometrial stroma. Normal oviduct but no ovary present.
3. No spleen present.
4. Normal colonic mucosa.
5. Normal caecum and normal small intestine.
6. Normal pancreas. Mesenteric lymph node with possible early lymphoproliferative disease and some increased histiocyte population but no enhanced pigment.
7. Mesenteric lymph node with a few scattered pigment-laden macrophages in the peripheral sinusoids.
8. Normal kidneys. Normal adrenal gland.
9. Normal stomach.
10. Normal liver.
11. Normal thyroid gland normal respiratory epithelium in trachea. Normal lungs.
12. Parotid gland with some inflammation and granular cell metaplasia ?Significance.
13. Normal heart.
14. Normal submandibular gland.
15.
16. Normal eye structure normal Harderian glands.
17. Normal brain.
18. Normal pituitary gland.
19. Normal anterior head normal tooth development.
20. Normal spinal cord normal vertebral body normal haemopoietic marrow.

b KO

1. Normal skin and normal subcutaneous tissue no lymph node present normal mammary glands.
2. Normal urethra normal uterus with some endometrial glandular dilatation. Some pigment-laden macrophages in myometrium. Normal ovary.
3. No spleen present.
4. Colonic mucosa and adjacent lymph node within normal limits.
5. Normal caecum and normal small intestine.
6. Normal pancreas.
7. Mesenteric lymph node with reactive hyperplasia. A few pigment-laden cells are present.
8. Normal kidneys. Normal adrenal glands.
9. Gastric hyperplastic polyp with abundant crystalloids normal duodenum.
10. Liver with focal mild steatosis and some pigment deposition in Kupffer cells.
11. Normal lungs. Normal thyroid gland normal oesophagus.
12. Normal lachrymal gland.
13. NORMAL HEART.

EPL PATHOLOGY REPORT

SUPPLEMENTARY

14. NORMAL SALIVARY GLAND.
15. NORMAL EYE STRUCTURE. NORMAL HARDERIAN GLAND.
16. NORMAL BRAIN.
17. NORMAL PITUITARY GLAND.
18. NORMAL ANTERIOR HEAD.
19. NORMAL SPINAL CORD NORMAL VERTEBRAL BODY NORMAL HAEMOPOIETIC MARROW.

CWT

1. NORMAL SKIN.
2. NORMAL URETHRA. NORMAL URINARY BLADDER. FOCAL PELVIC FAT NECROSIS. NORMAL UTERUS OCCASIONAL PIGMENT-LADEN CELLS IN MYOMETRIUM.
3. NORMAL LARGE INTESTINE.
4. NORMAL CAECUM. NORMAL SMALL INTESTINE.
5. NORMAL CAECUM NORMAL SMALL INTESTINE.
6. NORMAL PANCREAS. NORMAL MESENTERIC LYMPH NODE.
7. NORMAL MESENTERIC NODE WITH A FEW PIGMENT-LADEN CELLS IN THE SINUSOIDS.
8. NORMAL KIDNEY SOME PERI-URETERIC LYMPHOID INFILTRATE. NORMAL ADRENAL GLAND.
9. NORMAL STOMACH.
10. NORMAL LIVER.
11. NORMAL LUNG. NORMAL THYROID GLAND.
12. NORMAL LACHRYMAL GLAND.
13. NORMAL HEART.
14. NORMAL SALIVARY GLAND.
15. NORMAL EYE STRUCTURE.
16. NORMAL BRAIN.
17. NORMAL ANTERIOR HEAD.
18. NORMAL SPINAL CORD NORMAL VERTEBRAL BODY

Special Techniques:

Future Experiments Required:

Comments:

User: Line: ANDREA LONGATTI
EPL No.: 295 Report completed: 01.09.08 Previous report :

References

1. Klionsky, D.J., et al., *A unified nomenclature for yeast autophagy-related genes.* Dev Cell, 2003. **5**(4): p. 539-45.
2. Hamasaki, M. and T. Yoshimori, *Where do they come from? Insights into autophagosome formation.* FEBS Lett, 2010. **584**(7): p. 1296-301.
3. Mizushima, N., et al., *Autophagy fights disease through cellular self-digestion.* Nature, 2008. **451**(7182): p. 1069-75.
4. Horst, M., E.C. Knecht, and P.V. Schu, *Import into and degradation of cytosolic proteins by isolated yeast vacuoles.* Mol Biol Cell, 1999. **10**(9): p. 2879-89.
5. Clark, S.L., Jr., *Cellular Differentiation in the kidneys of newborn mice studies with the electron microscope.* J. Cell Biol., 1957. **3**(3): p. 349-362.
6. Mortimore, G.E. and C.M. Schworer, *Induction of autophagy by amino-acid deprivation in perfused rat liver.* Nature, 1977. **270**(5633): p. 174-6.
7. Deter, R.L., P. Baudhuin, and C. De Duve, *Participation of lysosomes in cellular autophagy induced in rat liver by glucagon.* J Cell Biol, 1967. **35**(2): p. C11-6.
8. Komatsu, M., et al., *Impairment of starvation-induced and constitutive autophagy in Atg7-deficient mice.* J. Cell Biol., 2005. **169**(3): p. 425-434.
9. Kuma, A., et al., *The role of autophagy during the early neonatal starvation period.* Nature, 2004. **432**(7020): p. 1032-6.
10. Tsukada, M. and Y. Ohsumi, *Isolation and characterization of autophagy-defective mutants of Saccharomyces cerevisiae.* FEBS Lett, 1993. **333**(1-2): p. 169-74.
11. Barth, H., et al., *Autophagy and the cytoplasm to vacuole targeting pathway both require Aut10p.* FEBS Lett, 2001. **508**(1): p. 23-28.
12. Suriapranata, I., et al., *The breakdown of autophagic vesicles inside the vacuole depends on aut4p [In Process Citation]*. J Cell Sci, 2000. **113**(Pt 22): p. 4025-33.
13. Lang, T., et al., *Autophagy and the cvt pathway both depend on AUT9.* J Bacteriol, 2000. **182**(8): p. 2125-33.
14. Lang, T., et al., *Aut2p and Aut7p, two novel microtubule-associated proteins are essential for delivery of autophagic vesicles to the vacuole.* EMBO J., 1998. **17**(13): p. 3597-3607.
15. Straub, M., M. Bredschneider, and M. Thumm, *AUT3, a serine/threonine kinase gene, is essential for autophagocytosis in Saccharomyces cerevisiae.* J Bacteriol, 1997. **179**(12): p. 3875-83.
16. Schlumpberger, M., et al., *AUT1, a gene essential for autophagocytosis in the yeast Saccharomyces cerevisiae.* J Bacteriol, 1997. **179**(4): p. 1068-76.
17. Reggiori, F. and D.J. Klionsky, *Autophagy in the eukaryotic cell.* Eukaryot Cell, 2002. **1**(1): p. 11-21.
18. de Duve, C. and R. Wattiaux, *Functions of Lysosomes.* Ann Rev Physiol, 1966. **28**: p. 435 - 492.
19. Longatti, A. and S.A. Tooze, *Vesicular trafficking and autophagosome formation.* Cell Death Differ, 2009. **16**(7): p. 956-65.

20. Chan, E.Y., S. Kir, and S.A. Tooze, *siRNA screening of the kinome identifies ULK1 as a multidomain modulator of autophagy.* J Biol Chem, 2007. **282**(35): p. 25464-74.
21. Chan, E.Y., et al., *Kinase-inactivated ULK proteins inhibit autophagy via their conserved C-terminal domains using an Atg13-independent mechanism.* Mol Cell Biol, 2009. **29**(1): p. 157-71.
22. Chan, E.Y. and S.A. Tooze, *Evolution of Atg1 function and regulation.* Autophagy, 2009. **5**(6): p. 758-65.
23. Kamada, Y., et al., *Tor-mediated Induction of Autophagy Via an Apg1 Protein Kinase Complex.* J. Cell Biol., 2000. **150**(6): p. 1507-1513.
24. Melendez, A., et al., *Autophagy Genes Are Essential for Dauer Development and Life-Span Extension in C. elegans.* Science, 2003. **301**(5638): p. 1387-1391.
25. Scott, R.C., O. Schuldiner, and T.P. Neufeld, *Role and regulation of starvation-induced autophagy in the Drosophila fat body.* Dev Cell, 2004. **7**(2): p. 167-78.
26. Otto, G.P., et al., *Dictyostelium macroautophagy mutants vary in the severity of their developmental defects.* J Biol Chem, 2004. **279**(15): p. 15621-9.
27. Matsuura, A., et al., *Apg1p, a novel protein kinase required for the autophagic process in Saccharomyces cerevisiae.* Gene, 1997. **192**(2): p. 245-50.
28. Shintani, T., et al., *Apg2p Functions in Autophagosome Formation on the Perivacuolar Structure.* J. Biol. Chem., 2001. **276**(32): p. 30452-30460.
29. Wang, C.W., et al., *Apg2 is a novel protein required for the cytoplasm to vacuole targeting, autophagy, and pexophagy pathways.* J Biol Chem, 2001. **276**(32): p. 30442-51.
30. Ichimura, Y., et al., *A ubiquitin-like system mediates protein lipidation.* Nature, 2000. **408**(6811): p. 488-92.
31. Scherz-Shouval, R., et al., *The COOH Terminus of GATE-16, an Intra-Golgi Transport Modulator, Is Cleaved by the Human Cysteine Protease HsApg4A.* J. Biol. Chem., 2003. **278**(16): p. 14053-14058.
32. Marino, G., et al., *Human Autophagins, a Family of Cysteine Proteinases Potentially Implicated in Cell Degradation by Autophagy.* J. Biol. Chem., 2003. **278**(6): p. 3671-3678.
33. Kirisako, T., et al., *The reversible modification regulates the membrane-binding state of Apg8/Aut7 essential for autophagy and the cytoplasm to vacuole targeting pathway [In Process Citation].* J Cell Biol, 2000. **151**(2): p. 263-76.
34. Mizushima, N., et al., *A protein conjugation system essential for autophagy.* Nature, 1998. **395**(6700): p. 395-8.
35. Kametaka, S., et al., *Structural and functional analyses of APG5, a gene involved in autophagy in yeast.* Gene, 1996. **178**(1-2): p. 139-43.
36. Liang, X.H., et al., *Induction of autophagy and inhibition of tumorgenesis by beclin 1.* Nature, 1999. **402**: p. 672-676.
37. Kametaka, S., et al., *Apg14p and Apg6/Vps30p Form a Protein Complex Essential for Autophagy in the Yeast, Saccharomyces cerevisiae.* J. Biol. Chem., 1998. **273**(35): p. 22284-22291.
38. Tanida, I., et al., *Apg7p/Cvt2p: A novel protein-activating enzyme essential for autophagy.* Mol Biol Cell, 1999. **10**(5): p. 1367-79.
39. Kirisako, T., et al., *Formation Process of Autophagosome Is Traced with Apg8/Aut7p in Yeast.* J. Cell Biol., 1999. **147**(2): p. 435-446.

40. Weidberg, H., et al., *LC3 and GATE-16/GABARAP subfamilies are both essential yet act differently in autophagosome biogenesis.* Embo J, 2010. **29**(11): p. 1792-802.
41. Young, A.R.J., et al., *Starvation and ULK1-dependent cycling of Mammalian Atg9 between the TGN and endosomes.* J Cell Sci, 2006. **119**: p. 3888-3900.
42. Noda, T., et al., *Apg9p/Cvt7p is an integral membrane protein required for transport vesicle formation in the Cvt and autophagy pathways.* J Cell Biol, 2000. **148**(3): p. 465-80.
43. Yamada, T., et al., *Endothelial Nitric-oxide Synthase Antisense (NOS3AS) Gene Encodes an Autophagy-related Protein (APG9-like2) Highly Expressed in Trophoblast.* J Biol Chem, 2005. **280**(18): p. 18283-18290.
44. Shintani, T., et al., *Apg10p, a novel protein-conjugating enzyme essential for autophagy in yeast.* Embo J, 1999. **18**(19): p. 5234-41.
45. Ganley, I.G., et al., *ULK1.ATG13.FIP200 complex mediates mTOR signaling and is essential for autophagy.* J Biol Chem, 2009. **284**(18): p. 12297-305.
46. Jung, C.H., et al., *ULK-Atg13-FIP200 complexes mediate mTOR signaling to the autophagy machinery.* Mol Biol Cell, 2009. **20**(7): p. 1992-2003.
47. Hosokawa, N., et al., *Nutrient-dependent mTORC1 association with the ULK1-Atg13-FIP200 complex required for autophagy.* Mol Biol Cell, 2009. **20**(7): p. 1981-91.
48. Funakoshi, T., et al., *Analyses of APG13 gene involved in autophagy in yeast, Saccharomyces cerevisiae.* Gene, 1997. **192**(2): p. 207-13.
49. Sun, Q., et al., *Identification of Barkor as a mammalian autophagy-specific factor for Beclin 1 and class III phosphatidylinositol 3-kinase.* Proc Natl Acad Sci U S A, 2008. **105**(49): p. 19211-6.
50. Itakura, E., et al., *Beclin 1 forms two distinct phosphatidylinositol 3-kinase complexes with mammalian Atg14 and UVRAG.* Mol Biol Cell, 2008. **19**(12): p. 5360-72.
51. Mizushima, N., T. Noda, and Y. Ohsumi, *Apg16p is required for the function of the Apg12p-Apg5p conjugate in the yeast autophagy pathway.* Embo J, 1999. **18**(14): p. 3888-96.
52. Mizushima, N., et al., *Mouse Apg16L, a novel WD-repeat protein, targets to the autophagic isolation membrane with the Apg12-Apg5 conjugate.* J Cell Sci, 2003. **116**(9): p. 1679-1688.
53. Cheong, H., et al., *Atg17 Regulates the Magnitude of the Autophagic Response.* Mol. Biol. Cell, 2005: p. E04-10-0894.
54. Kabeya, Y., et al., *Atg17 Functions in Cooperation with Atg1 and Atg13 in Yeast Autophagy.* Mol Biol Cell, 2005.
55. Hara, T., et al., *FIP200, a ULK-interacting protein, is required for autophagosome formation in mammalian cells.* J Cell Biol, 2008. **181**(3): p. 497-510.
56. Nair, U., et al., *Roles of the lipid-binding motifs of Atg18 and Atg21 in the cytoplasm to vacuole targeting pathway and autophagy.* J Biol Chem, 2010. **285**(15): p. 11476-88.
57. Polson, H.E., et al., *Mammalian Atg18 (WIPI2) localizes to omegasome-anchored phagophores and positively regulates LC3 lipidation.* Autophagy, 2010. **6**(4).

58. Proikas-Cezanne, T., et al., *Human WIPI-1 puncta-formation: a novel assay to assess mammalian autophagy.* FEBS Lett, 2007. **581**(18): p. 3396-404.
59. Stromhaug, P.E., et al., *Atg21 is a Phosphoinositide Binding Protein Required for Efficient Lipidation and Localization of Atg8 during Uptake of Aminopeptidase I by Selective Autophagy.* Mol. Biol. Cell, 2004: p. E04-02-0147.
60. Traer, C.J., et al., *SNX4 coordinates endosomal sorting of TfnR with dynein-mediated transport into the endocytic recycling compartment.* Nat Cell Biol, 2007. **9**(12): p. 1370-80.
61. Nice, D.C., et al., *Cooperative binding of the cytoplasm to vacuole targeting pathway proteins, Cvt13 and Cvt20, to PtdIns(3)P at the pre-autophagosomal structure is required for selective autophagy.* J. Biol. Chem., 2002: p. M204736200.
62. Ano, Y., et al., *A sorting nexin PpAtg24 regulates vacuolar membrane dynamics during pexophagy via binding to phosphatidylinositol-3-phosphate.* Mol Biol Cell, 2005. **16**(2): p. 446-57.
63. Mercer, C.A., A. Kaliappan, and P.B. Dennis, *A novel, human Atg13 binding protein, Atg101, interacts with ULK1 and is essential for macroautophagy.* Autophagy, 2009. **5**(5): p. 649-62.
64. Hosokawa, N., et al., *Atg101, a novel mammalian autophagy protein interacting with Atg13.* Autophagy, 2009. **5**(7): p. 973-9.
65. Filimonenko, M., et al., *The selective macroautophagic degradation of aggregated proteins requires the PI3P-binding protein Alfy.* Mol Cell, 2010. **38**(2): p. 265-79.
66. Simonsen, A., et al., *Alfy, a novel FYVE-domain-containing protein associated with protein granules and autophagic membranes.* J Cell Sci, 2004: p. jcs.01287.
67. Fimia, G.M., et al., *Ambra1 regulates autophagy and development of the nervous system.* nature, 2007. **447**(7148): p. 1121-5.
68. Takahashi, Y., et al., *Bif-1 interacts with Beclin 1 through UVRAG and regulates autophagy and tumorigenesis.* Nat Cell Biol, 2007. **9**(10): p. 1142-51.
69. Axe, E.L., et al., *Autophagosome formation from membrane compartments enriched in phosphatidylinositol 3-phosphate and dynamically connected to the endoplasmic reticulum.* J Cell Biol, 2008. **182**(4): p. 685-701.
70. Pankiv, S., et al., *FYCO1 is a Rab7 effector that binds to LC3 and PI3P to mediate microtubule plus end-directed vesicle transport.* J Cell Biol, 2010. **188**(2): p. 253-69.
71. Jung, C.H., et al., *mTOR regulation of autophagy.* FEBS Lett, 2010. **584**(7): p. 1287-95.
72. Matsunaga, K., et al., *Two Beclin 1-binding proteins, Atg14L and Rubicon, reciprocally regulate autophagy at different stages.* Nat Cell Biol, 2009. **11**(4): p. 385-96.
73. Zhong, Y., et al., *Distinct regulation of autophagic activity by Atg14L and Rubicon associated with Beclin 1-phosphatidylinositol-3-kinase complex.* Nat Cell Biol, 2009. **11**(4): p. 468-76.
74. Lynch-Day, M.A., et al., *Trs85 directs a Ypt1 GEF, TRAPPIII, to the phagophore to promote autophagy.* Proc Natl Acad Sci U S A, 2010. **107**(17): p. 7811-6.

75. Nakashima, A., et al., *Identification of TBC7 having TBC domain as a novel binding protein to TSC1-TSC2 complex.* Biochem Biophys Res Commun, 2007. **361**(1): p. 218-23.
76. Liang, C., et al., *Autophagic and tumour suppressor activity of a novel Beclin1-binding protein UVRAG.* Nat Cell Biol, 2006. **8**(7): p. 688-99.
77. Simonsen, A. and S.A. Tooze, *Coordination of membrane events during autophagy by multiple class III PI3-kinase complexes.* J Cell Biol, 2009. **186**(6): p. 773-82.
78. Bjorkoy, G., et al., *p62/SQSTM1 forms protein aggregates degraded by autophagy and has a protective effect on huntingtin-induced cell death.* J. Cell Biol., 2005. **171**(4): p. 603-614.
79. Vergne, I., et al., *Control of autophagy initiation by phosphoinositide 3-phosphatase Jumpy.* Embo J, 2009. **28**(15): p. 2244-58.
80. Suzuki, K., et al., *Hierarchy of Atg proteins in pre-autophagosomal structure organization.* Genes Cells, 2007. **12**(2): p. 209-18.
81. Kundu, M., et al., *Ulk1 plays a critical role in the autophagic clearance of mitochondria and ribosomes during reticulocyte maturation.* Blood, 2008. **112**(4): p. 1493-502.
82. Young, A.R., et al., *Autophagy mediates the mitotic senescence transition.* Genes Dev, 2009. **23**(7): p. 798-803.
83. Mizushima, N., *The role of the Atg1/ULK1 complex in autophagy regulation.* Curr Opin Cell Biol, 2010. **22**(2): p. 132-9.
84. Tee, A.R., et al., *Tuberous sclerosis complex gene products, Tuberin and Hamartin, control mTOR signaling by acting as a GTPase-activating protein complex toward Rheb.* Curr Biol, 2003. **13**(15): p. 1259-68.
85. Inoki, K., et al., *Rheb GTPase is a direct target of TSC2 GAP activity and regulates mTOR signaling.* Genes Dev, 2003. **17**(15): p. 1829-34.
86. Zhang, Y., et al., *Rheb is a direct target of the tuberous sclerosis tumour suppressor proteins.* Nat Cell Biol, 2003. **5**(6): p. 578-81.
87. van Slegtenhorst, M., et al., *Identification of the tuberous sclerosis gene TSC1 on chromosome 9q34.* Science, 1997. **277**(5327): p. 805-8.
88. Kandt, R.S., et al., *Linkage of an important gene locus for tuberous sclerosis to a chromosome 16 marker for polycystic kidney disease.* Nat Genet, 1992. **2**(1): p. 37-41.
89. Huang, J. and B.D. Manning, *The TSC1-TSC2 complex: a molecular switchboard controlling cell growth.* Biochem J, 2008. **412**(2): p. 179-90.
90. Tomoda, T., et al., *Role of Unc51.1 and its binding partners in CNS axon outgrowth.* Genes Dev., 2004. **18**(5): p. 541-558.
91. Toda, H., et al., *UNC-51/ATG1 kinase regulates axonal transport by mediating motor-cargo assembly.* Genes Dev, 2008. **22**(23): p. 3292-307.
92. Klein, R., et al., *The trk proto-oncogene encodes a receptor for nerve growth factor.* Cell, 1991. **65**(1): p. 189-97.
93. Zhou, X., et al., *Unc-51-like kinase 1/2-mediated endocytic processes regulate filopodia extension and branching of sensory axons.* Proc Natl Acad Sci U S A, 2007. **104**(14): p. 5842-7.
94. Itoh, T. and P. De Camilli, *BAR, F-BAR (EFC) and ENTH/ANTH domains in the regulation of membrane-cytosol interfaces and membrane curvature.* Biochim Biophys Acta, 2006. **1761**(8): p. 897-912.

95. Obara, K., et al., *Transport of phosphatidylinositol 3-phosphate into the vacuole via autophagic membranes in Saccharomyces cerevisiae.* Genes Cells, 2008. **13**(6): p. 537-47.
96. Obara, K. and Y. Ohsumi, *Dynamics and function of PtdIns(3)P in autophagy.* Autophagy, 2008. **4**(7): p. 952-4.
97. Matsunaga, K., et al., *Autophagy requires endoplasmic reticulum targeting of the PI3-kinase complex via Atg14L.* J Cell Biol, 2010.
98. Itakura, E. and N. Mizushima, *Characterization of autophagosome formation site by a hierarchical analysis of mammalian Atg proteins.* Autophagy, 2010. **6**(6).
99. Tanida, I., et al., *The Human Homolog of Saccharomyces cerevisiae Apg7p Is a Protein-activating Enzyme for Multiple Substrates Including Human Apg12p, GATE-16, GABARAP, and MAP-LC3.* J. Biol. Chem., 2001. **276**(3): p. 1701-1706.
100. Fujita, N., et al., *The Atg16L complex specifies the site of LC3 lipidation for membrane biogenesis in autophagy.* Mol Biol Cell, 2008. **19**(5): p. 2092-100.
101. Mizushima, N., et al., *Dissection of autophagosome formation using Apg5-deficient mouse embryonic stem cells.* J Cell Biol, 2001. **152**(4): p. 657-68.
102. Tsukamoto, S., et al., *Autophagy is essential for preimplantation development of mouse embryos.* Science, 2008. **321**(5885): p. 117-20.
103. Fujita, N., et al., *An Atg4B mutant hampers the lipidation of LC3 paralogues and causes defects in autophagosome closure.* Mol Biol Cell, 2008. **19**(11): p. 4651-9.
104. Nakatogawa, H., Y. Ichimura, and Y. Ohsumi, *Atg8, a ubiquitin-like protein required for autophagosome formation, mediates membrane tethering and hemifusion.* Cell, 2007. **130**(1): p. 165-78.
105. Novak, I., et al., *Nix is a selective autophagy receptor for mitochondrial clearance.* EMBO Rep, 2010. **11**(1): p. 45-51.
106. Weidberg, H., et al., *Mammalian Atg8s: One is simply not enough.* Autophagy, 2010. **6**(6): p. 808-9.
107. Schwarten, M., et al., *Nix directly binds to GABARAP: a possible crosstalk between apoptosis and autophagy.* Autophagy, 2009. **5**(5): p. 690-8.
108. Klionsky, D.J., et al., *Guidelines for the use and interpretation of assays for monitoring autophagy in higher eukaryotes.* Autophagy, 2008. **4**(2): p. 151-75.
109. Kimura, S., T. Noda, and T. Yoshimori, *Dissection of the autophagosome maturation process by a novel reporter protein, tandem fluorescent-tagged LC3.* Autophagy, 2007. **3**(5): p. 452-60.
110. Nishida, Y., et al., *Discovery of Atg5/Atg7-independent alternative macroautophagy.* nature, 2009. **461**(7264): p. 654-8.
111. Mizushima, N., et al., *A new protein conjugation system in human. The counterpart of the yeast Apg12p conjugation system essential for autophagy.* J Biol Chem, 1998. **273**(51): p. 33889-92.
112. Robb, G.B., et al., *Post-transcriptional Regulation of Endothelial Nitric-oxide Synthase by an Overlapping Antisense mRNA Transcript.* J. Biol. Chem., 2004. **279**(36): p. 37982-37996.
113. Mari, M., et al., *Key role of a novel Atg9-containing compartment in the early steps of*
autophagosome biogenesis. J. Cell Biol., 2010.

114. Dusetti, N.J., et al., *Cloning and expression of the rat vacuole membrane protein 1 (VMP1), a new gene activated in pancreas with acute pancreatitis, which promotes vacuole formation.* Biochem Biophys Res Commun, 2002. **290**(2): p. 641-9.
115. Ropolo, A., et al., *The pancreatitis-induced vacuole membrane protein 1 triggers autophagy in mammalian cells.* J Biol Chem, 2007. **282**(51): p. 37124-33.
116. Calvo-Garrido, J., et al., *Vacuole membrane protein 1 is an endoplasmic reticulum protein required for organelle biogenesis, protein secretion, and development.* Mol Biol Cell, 2008. **19**(8): p. 3442-53.
117. Alberts, B., et al., *Molecular Biology of the Cell.* 4th Edition ed. 2002: Garland Science.
118. Baba, M., M. Osumi, and Y. Ohsumi, *Analysis of the membrane structures involved in autophagy in yeast by freeze-replica method.* Cell Struct Funct, 1995. **20**(6): p. 465-71.
119. Kovacs, A.L., et al., *Sequestration revisited: integrating traditional electron microscopy, de novo assembly and new results.* Autophagy, 2007. **3**(6): p. 655-62.
120. Novikoff, A.B. and E. Essner, *Cytolysomes and mitochondrial degeneration.* J Cell Biol, 1962. **15**: p. 140-6.
121. Dunn, W.A., Jr., *Studies on the mechanisms of autophagy: maturation of the autophagic vacuole.* J Cell Biol, 1990. **110**(6): p. 1935-45.
122. Hayashi-Nishino, M., et al., *A subdomain of the endoplasmic reticulum forms a cradle for autophagosome formation.* Nat Cell Biol, 2009. **11**(12): p. 1433-7.
123. Hayashi-Nishino, M., et al., *Electron tomography reveals the endoplasmic reticulum as a membrane source for autophagosome formation.* Autophagy, 2010. **6**(2): p. 301-3.
124. Yla-Anttila, P., et al., *3D tomography reveals connections between the phagophore and endoplasmic reticulum.* Autophagy, 2009. **5**(8): p. 1180-5.
125. Carlos Martin Zoppino, F., et al., *Autophagosome Formation Depends on the Small GTPase Rab1 and Functional ER Exit Sites.* Traffic, 2010.
126. Quatacker, J.R., *Formation of autophagic vacuoles during human corpus luteum involution.* Z Zellforsch Mikrosk Anat, 1971. **122**(4): p. 479-87.
127. Ravikumar, B., et al., *Plasma membrane contributes to the formation of pre-autophagosomal structures.* Nature Cell Biology, 2010.
128. Reggiori, F., et al., *Atg9 cycles between mitochondria and the pre-autophagosomal structure in yeast.* Autophagy, 2005. **1**(2): p. 101-109.
129. Mari, M. and F. Reggiori, *Atg9 trafficking in the yeast Saccharomyces cerevisiae.* Autophagy, 2007. **3**(2): p. 145-8.
130. Hailey, D.W., et al., *Mitochondria supply membranes for autophagosome biogenesis during starvation.* Cell, 2010. **141**(4): p. 656-67.
131. Locke, M. and A.K. Sykes, *The role of the Golgi complex in the isolation and digestion of organelles.* Tissue Cell, 1975. **7**(1): p. 143-58.
132. Geng, J., et al., *Post-golgi sec proteins are required for autophagy in Saccharomyces cerevisiae.* Mol Biol Cell, 2010. **21**(13): p. 2257-69.
133. Yen, W.L., et al., *The conserved oligomeric Golgi complex is involved in double-membrane vesicle formation during autophagy.* J Cell Biol, 2010. **188**(1): p. 101-14.

134. van der Vaart, A., J. Griffith, and F. Reggiori, *Exit from the golgi is required for the expansion of the autophagosomal phagophore in yeast Saccharomyces cerevisiae.* Mol Biol Cell, 2010. **21**(13): p. 2270-84.
135. Liang, X.H., et al., *Induction of autophagy and inhibition of tumorigenesis by beclin 1.* nature, 1999. **402**(6762): p. 672-6.
136. Aita, V.M., et al., *Cloning and genomic organization of beclin 1, a candidate tumor suppressor gene on chromosome 17q21.* Genomics, 1999. **59**(1): p. 59-65.
137. Yue, Z., et al., *Beclin 1, an autophagy gene essential for early embryonic development, is a haploinsufficient tumor suppressor.* PNAS, 2003. **100**(25): p. 15077-15082.
138. Qu, X., et al., *Promotion of tumorigenesis by heterozygous disruption of the beclin 1 autophagy gene.* J. Clin. Invest., 2003. **112**(12): p. 1809-1820.
139. Marino, G., et al., *Tissue-specific autophagy alterations and increased tumorigenesis in mice deficient in Atg4C/autophagin-3.* J Biol Chem, 2007. **282**(25): p. 18573-83.
140. Levine, B. and J. Yuan, *Autophagy in cell death: an innocent convict?* J. Clin. Invest., 2005. **115**(10): p. 2679-2688.
141. Hou, W., et al., *Autophagic degradation of active caspase-8: A crosstalk mechanism between autophagy and apoptosis.* Autophagy, 2010. **6**(7).
142. Carew, J.S., et al., *Targeting autophagy augments the anticancer activity of the histone deacetylase inhibitor SAHA to overcome Bcr-Abl-mediated drug resistance.* Blood, 2007. **110**(1): p. 313-22.
143. Abedin, M.J., et al., *Autophagy delays apoptotic death in breast cancer cells following DNA damage.* Cell Death Differ, 2007. **14**(3): p. 500-10.
144. Komatsu, M., et al., *Loss of autophagy in the central nervous system causes neurodegeneration in mice.* Nature, 2006. **441**
: p. 880-884.
145. Hara, T., et al., *Suppression of basal autophagy in neural cells causes neurodegenerative disease in mice.* Nature, 2006. **in press**.
146. Kegel, K.B., et al., *Huntingtin expression stimulates endosomal-lysosomal activity, endosome tubulation, and autophagy.* J Neurosci, 2000. **20**(19): p. 7268-78.
147. Ravikumar, B., R. Duden, and D.C. Rubinsztein, *Aggregate-prone proteins with polyglutamine and polyalanine expansions are degraded by autophagy.* Hum. Mol. Genet., 2002. **11**(9): p. 1107-1117.
148. Sarkar, S., et al., *Small molecules enhance autophagy and reduce toxicity in Huntington's disease models.* Nat Chem Biol, 2007. **3**(6): p. 331-8.
149. Arrasate, M., et al., *Inclusion body formation reduces levels of mutant huntingtin and the risk of neuronal death.* nature, 2004. **431**(7010): p. 805-10.
150. Yu, W.H., et al., *Macroautophagy--a novel Beta-amyloid peptide-generating pathway activated in Alzheimer's disease.* J Cell Biol, 2005. **171**(1): p. 87-98.
151. Cummings, J.R., et al., *Confirmation of the role of ATG16L1 as a Crohn's disease susceptibility gene.* Inflamm Bowel Dis, 2007. **13**(8): p. 941-6.
152. Fujita, N., et al., *Differential involvement of Atg16L1 in Crohn disease and canonical autophagy: analysis of the organization of the Atg16L1 complex in fibroblasts.* J Biol Chem, 2009. **284**(47): p. 32602-9.
153. Cadwell, K., et al., *A key role for autophagy and the autophagy gene Atg16l1 in mouse and human intestinal Paneth cells.* nature, 2008. **456**(7219): p. 259-63.

154. Taneike, M., et al., *Inhibition of autophagy in the heart induces age-related cardiomyopathy.* Autophagy, 2010. **6**(5).
155. Malicdan, M.C., et al., *Lysosomal myopathies: an excessive build-up in autophagosomes is too much to handle.* Neuromuscul Disord, 2008. **18**(7): p. 521-9.
156. Nishida, K., et al., *The role of autophagy in the heart.* Cell Death Differ, 2009. **16**(1): p. 31-8.
157. Hartley, T., J. Brumell, and A. Volchuk, *Emerging roles for the ubiquitin-proteasome system and autophagy in pancreatic beta-cells.* Am J Physiol Endocrinol Metab, 2009. **296**(1): p. E1-10.
158. Palade, G.E., *Intracellular aspects of the process of protein synthesis.* Science, 1975. **189**: p. 347-358.
159. Vitner, E.B., F.M. Platt, and A.H. Futerman, *Common and uncommon pathogenic cascades in lysosomal storage diseases.* J Biol Chem, 2010. **285**(27): p. 20423-7.
160. Beck, R., et al., *The COPI system: molecular mechanisms and function.* FEBS Lett, 2009. **583**(17): p. 2701-9.
161. Plutner, H., et al., *Rab1b regulates vesicular transport between the endoplasmic reticulum and successive Golgi compartments.* J Cell Biol, 1991. **115**(1): p. 31-43.
162. Antonny, B. and R. Schekman, *ER export: public transportation by the COPII coach.* Curr Opin Cell Biol, 2001. **13**(4): p. 438-43.
163. Appenzeller-Herzog, C. and H.P. Hauri, *The ER-Golgi intermediate compartment (ERGIC): in search of its identity and function.* J Cell Sci, 2006. **119**(Pt 11): p. 2173-83.
164. Razi, M., E.Y. Chan, and S.A. Tooze, *Early endosomes and endosomal coatomer are required for autophagy.* J Cell Biol, 2009. **185**(2): p. 305-21.
165. Hsu, V.W. and J.S. Yang, *Mechanisms of COPI vesicle formation.* FEBS Lett, 2009. **583**(23): p. 3758-63.
166. Gu, F., et al., *Functional Dissection of COP-I Subunits in the Biogenesis of Multivesicular Endosomes.* J. Cell Biol., 1997. **139**(5): p. 1183-1195.
167. Daro, E., et al., *Inhibition of Endosome Function in CHO Cells Bearing a Temperature-sensitive Defect in the Coatomer (COPI) Component epsilon - COP.* J. Cell Biol., 1997. **139**(7): p. 1747-1759.
168. Whitney, A.J., et al., *Cytoplasmic coat proteins involved in endosome function.* Cell, 1995. **83**(5): p. 703-713.
169. McNiven, M.A. and H.M. Thompson, *Vesicle formation at the plasma membrane and trans-Golgi network: the same but different.* Science, 2006. **313**(5793): p. 1591-4.
170. Robinson, M.S., *Adaptable adaptors for coated vesicles.* Trends Cell Biol, 2004. **14**(4): p. 167-74.
171. Burgos, P.V., et al., *Sorting of the Alzheimer's disease amyloid precursor protein mediated by the AP-4 complex.* Dev Cell, 2010. **18**(3): p. 425-36.
172. Mercer, J., M. Schelhaas, and A. Helenius, *Virus entry by endocytosis.* Annu Rev Biochem, 2010. **79**: p. 803-33.
173. Pearse, B.M., C.J. Smith, and D.J. Owen, *Clathrin coat construction in endocytosis.* Curr Opin Struct Biol, 2000. **10**(2): p. 220-8.

174. Roth, T.F. and K.R. Porter, *Yolk Protein Uptake in the Oocyte of the Mosquito Aedes Aegypti. L.* J Cell Biol, 1964. **20**: p. 313-32.
175. Heuser, J., *Three-dimensional visualization of coated vesicle formation in fibroblasts.* J Cell Biol, 1980. **84**(3): p. 560-83.
176. Ungewickell, E.J. and L. Hinrichsen, *Endocytosis: clathrin-mediated membrane budding.* Curr Opin Cell Biol, 2007. **19**(4): p. 417-25.
177. Bonifacino, J.S. and L.M. Traub, *Signals for sorting of transmembrane proteins to endosomes and lysosomes.* Annual Review of Biochemistry, 2003. **72**(1): p. 395-447.
178. Kornfeld, S. and I. Mellman, *The Biogenesis of lysosomes*, in *Annual Review of Cell Biology*, G.E. Palade, B.M. Alberts, and J.A. Spudich, Editors. 1989, Annual Reviews Inc.: Palo Alto, California. p. 483-526.
179. Raiborg, C. and H. Stenmark, *The ESCRT machinery in endosomal sorting of ubiquitylated membrane proteins.* nature, 2009. **458**(7237): p. 445-52.
180. Maxfield, F.R. and T.E. McGraw, *Endocytic recycling.* Nat Rev Mol Cell Biol, 2004. **5**(2): p. 121-32.
181. Rusten, T.E. and A. Simonsen, *ESCRT functions in autophagy and associated disease.* Cell Cycle, 2008. **7**(9): p. 1166-72.
182. Lee, J.A., et al., *ESCRT-III dysfunction causes autophagosome accumulation and neurodegeneration.* Curr Biol, 2007. **17**(18): p. 1561-7.
183. Jager, S., et al., *Role for Rab7 in maturation of late autophagic vacuoles.* J Cell Sci, 2004. **117**(20): p. 4837-4848.
184. Gutierrez, M.G., et al., *Rab7 is required for the normal progression of the autophagic pathway in mammalian cells.* J Cell Sci, 2004: p. jcs.01114.
185. Shen, F. and M.C. Seabra, *Mechanisms of digeranylgeranylation of rab proteins.* J. Biol. Chem., 1996. **271**: p. 3692-3698.
186. Pfeffer, S.R., *Structural clues to Rab GTPase functional diversity.* J Biol Chem, 2005. **280**(16): p. 15485-8.
187. Soldati, T., et al., *Membrane targeting of the small GTPase Rab9 is accompanied by nucleotide exchange.* nature, 1994. **369**(6475): p. 76-8.
188. Ullrich, O., et al., *Rab GDI as a general regulator for the membrane association of rab proteins.* J. Biol. Chem., 1993.
189. Ullrich, O., et al., *Membrane association of rab5 mediated by GDP-dissociation inhibitor and accompanied by GDP/GTP exchange.* Nature, 1994. **368**: p. 157-160.
190. Matsui, Y., et al., *Molecular cloning and characterization of a novel type of regulatory protein (GDI) for smg p25A, a ras p21-like GTP-binding protein.* Mol Cell Biol, 1990. **10**(8): p. 4116-22.
191. Chavrier, P., et al., *Localisation of low molecular weight GTP binding proteins to exocytic and endocytic compartments.* Cell, 1990. **62**: p. 317-329.
192. Sivars, U., D. Aivazian, and S.R. Pfeffer, *Yip3 catalyses the dissociation of endosomal Rab-GDI complexes.* nature, 2003. **425**(6960): p. 856-9.
193. Sonnichsen, B., et al., *Distinct Membrane Domains on Endosomes in the Recycling Pathway Visualized by Multicolor Imaging of Rab4, Rab5, and Rab11.* J. Cell Biol., 2000. **149**(4): p. 901-914.
194. Stenmark, H., *Rab GTPases as coordinators of vesicle traffic.* Nat Rev Mol Cell Biol, 2009. **10**(8): p. 513-25.

195. Pan, X., et al., *TBC-domain GAPs for Rab GTPases accelerate GTP hydrolysis by a dual-finger mechanism.* nature, 2006. **442**(7100): p. 303-6.
196. Itoh, T., et al., *Screening for target Rabs of TBC (Tre-2/Bub2/Cdc16) domain-containing proteins based on their Rab-binding activity.* Genes Cells, 2006. **11**(9): p. 1023-37.
197. Haas, A.K., et al., *A GTPase-activating protein controls Rab5 function in endocytic trafficking.* Nat Cell Biol, 2005. **7**(9): p. 887-93.
198. Tempel, W., et al., *First crystallographic models of human TBC domains in the context of a family-wide structural analysis.* Proteins, 2008. **71**(1): p. 497-502.
199. Fuchs, E., et al., *Specific Rab GTPase-activating proteins define the Shiga toxin and epidermal growth factor uptake pathways.* J Cell Biol, 2007. **177**(6): p. 1133-43.
200. Haas, A.K., et al., *Analysis of GTPase-activating proteins: Rab1 and Rab43 are key Rabs required to maintain a functional Golgi complex in human cells.* J Cell Sci, 2007. **120**(Pt 17): p. 2997-3010.
201. Yoshimura, S., et al., *Functional dissection of Rab GTPases involved in primary cilium formation.* J Cell Biol, 2007. **178**(3): p. 363-9.
202. Patino-Lopez, G., et al., *RAB35 and its GAP EPI64C in T-cells regulate receptor recycling and immunological synapse formation.* J Biol Chem, 2008.
203. Itoh, T. and M. Fukuda, *Identification of EPI64 as a GTPase-activating protein specific for Rab27A.* J Biol Chem, 2006. **281**(42): p. 31823-31.
204. Pfeffer, S., *Filling the Rab GAP.* Nat Cell Biol, 2005. **7**(9): p. 856-7.
205. Poteryaev, D., et al., *Identification of the switch in early-to-late endosome transition.* Cell, 2010. **141**(3): p. 497-508.
206. Rink, J., et al., *Rab conversion as a mechanism of progression from early to late endosomes.* Cell, 2005. **122**: p. 735-749.
207. Rivera-Molina, F.E. and P.J. Novick, *A Rab GAP cascade defines the boundary between two Rab GTPases on the secretory pathway.* Proc Natl Acad Sci U S A, 2009. **106**(34): p. 14408-13.
208. Shin, H.W., et al., *An enzymatic cascade of Rab5 effectors regulates phosphoinositide turnover in the endocytic pathway.* J Cell Biol, 2005. **170**(4): p. 607-18.
209. Christoforidis, S., et al., *Phosphatidylinositol-3-OH kinases are Rab5 effectors.* Nature Cell Biology, 1999. **1**(August): p. 249-252.
210. Hirota, Y. and Y. Tanaka, *A small GTPase, human Rab32, is required for the formation of autophagic vacuoles under basal conditions.* Cell Mol Life Sci, 2009. **66**(17): p. 2913-32.
211. Park, M., et al., *Rab32 regulates melanosome transport in Xenopus melanophores by protein kinase a recruitment.* Curr Biol, 2007. **17**(23): p. 2030-4.
212. Wasmeier, C., et al., *Rab38 and Rab32 control post-Golgi trafficking of melanogenic enzymes.* J Cell Biol, 2006. **175**(2): p. 271-81.
213. Erdman, R.A., et al., *Rab24 is an atypical member of the Rab GTPase family. Deficient GTPase activity, GDP dissociation inhibitor interaction, and prenylation of Rab24 expressed in cultured cells.* J Biol Chem, 2000. **275**(6): p. 3848-56.

214. Munafo, D.B. and M.I. Colombo, *Induction of Autophagy Causes Dramatic Changes in the Subcellular Distribution of GFP-Rab24.* Traffic, 2002. **3**(7): p. 472-82.
215. Atlashkin, V., et al., *Deletion of the SNARE vti1b in Mice Results in the Loss of a Single SNARE Partner, Syntaxin 8.* Mol. Cell. Biol., 2003. **23**(15): p. 5198-5207.
216. Fader, C.M., et al., *Induction of autophagy promotes fusion of multivesicular bodies with autophagic vacuoles in k562 cells.* Traffic, 2008. **9**(2): p. 230-50.
217. Ravikumar, B., et al., *Rab5 modulates aggregation and toxicity of mutant huntingtin through macroautophagy in cell and fly models of Huntington disease.* J Cell Sci, 2008.
218. Starr, T., et al., *Rab33b and Rab6 are functionally overlapping regulators of Golgi homeostasis and trafficking.* Traffic, 2010. **11**(5): p. 626-36.
219. Cheng, E., et al., *Rab33A: characterization, expression, and suppression by epigenetic modification.* J Invest Dermatol, 2006. **126**(10): p. 2257-71.
220. Zheng, J.Y., et al., *A novel Rab GTPase, Rab33B, is ubiquitously expressed and localized to the medial Golgi cisternae.* J Cell Sci, 1998. **111 (Pt 8)**: p. 1061-9.
221. Valsdottir, R., et al., *Identification of rabaptin-5, rabex-5, and GM130 as putative effectors of rab33b, a regulator of retrograde traffic between the Golgi apparatus and ER.* FEBS Lett, 2001. **508**(2): p. 201-9.
222. Itoh, T., et al., *Golgi-resident Small GTPase Rab33B Interacts with Atg16L and Modulates Autophagosome Formation.* Mol Biol Cell, 2008.
223. Klein, L., et al., *Antigen presentation in the thymus for positive selection and central tolerance induction.* Nat Rev Immunol, 2009. **9**(12): p. 833-44.
224. Virgin, H.W. and B. Levine, *Autophagy genes in immunity.* Nat Immunol, 2009. **10**(5): p. 461-70.
225. Saitoh, T. and S. Akira, *Regulation of innate immune responses by autophagy-related proteins.* J Cell Biol, 2010. **189**(6): p. 925-35.
226. Yano, T., et al., *Autophagic control of listeria through intracellular innate immune recognition in drosophila.* Nat Immunol, 2008. **9**(8): p. 908-16.
227. Nakagawa, I., et al., *Autophagy Defends Cells Against Invading Group A Streptococcus.* Science, 2004. **306**(5698): p. 1037-1040.
228. Yamaguchi, H., et al., *An initial step of GAS-containing autophagosome-like vacuoles formation requires Rab7.* PLoS Pathog, 2009. **5**(11): p. e1000670.
229. Romano, P.S., et al., *The autophagic pathway is actively modulated by phase II Coxiella burnetii to efficiently replicate in the host cell.* Cell Microbiol, 2007. **9**(4): p. 891-909.
230. Beron, W., et al., *Coxiella burnetii localizes in a Rab7-labeled compartment with autophagic characteristics.* Infect Immun, 2002. **70**(10): p. 5816-21.
231. Martens, S., et al., *Disruption of Toxoplasma gondii parasitophorous vacuoles by the mouse p47-resistance GTPases.* PLoS Pathog, 2005. **1**(3): p. e24.
232. Ling, Y.M., et al., *Vacuolar and plasma membrane stripping and autophagic elimination of Toxoplasma gondii in primed effector macrophages.* J Exp Med, 2006. **203**(9): p. 2063-71.
233. Sanjuan, M.A., et al., *Toll-like receptor signalling in macrophages links the autophagy pathway to phagocytosis.* nature, 2007. **450**(7173): p. 1253-7.
234. Shui, W., et al., *Membrane proteomics of phagosomes suggests a connection to autophagy.* Proc Natl Acad Sci U S A, 2008. **105**(44): p. 16952-7.

235. Ogawa, M., et al., *Escape of intracellular Shigella from autophagy.* Science, 2005. **307**(5710): p. 727-31.
236. Dreux, M., et al., *The autophagy machinery is required to initiate hepatitis C virus replication.* Proc Natl Acad Sci U S A, 2009. **106**(33): p. 14046-51.
237. Jackson, W.T., et al., *Subversion of cellular autophagosomal machinery by RNA viruses.* PLoS Biol, 2005. **3**(5): p. e156.
238. Lee, H.K., et al., *Autophagy-dependent viral recognition by plasmacytoid dendritic cells.* Science, 2007. **315**(5817): p. 1398-401.
239. Xu, Y., et al., *Toll-like receptor 4 is a sensor for autophagy associated with innate immunity.* Immunity, 2007. **27**(1): p. 135-44.
240. Delgado, M.A., et al., *Toll-like receptors control autophagy.* Embo J, 2008. **27**(7): p. 1110-21.
241. Saitoh, T., et al., *Loss of the autophagy protein Atg16L1 enhances endotoxin-induced IL-1beta production.* nature, 2008. **456**(7219): p. 264-8.
242. Tal, M.C., et al., *Absence of autophagy results in reactive oxygen species-dependent amplification of RLR signaling.* Proc Natl Acad Sci U S A, 2009. **106**(8): p. 2770-5.
243. Jounai, N., et al., *The Atg5 Atg12 conjugate associates with innate antiviral immune responses.* Proc Natl Acad Sci U S A, 2007. **104**(35): p. 14050-5.
244. Nedjic, J., et al., *Autophagy in thymic epithelium shapes the T-cell repertoire and is essential for tolerance.* nature, 2008. **455**(7211): p. 396-400.
245. Munz, C., *Enhancing immunity through autophagy.* Annu Rev Immunol, 2009. **27**: p. 423-49.
246. English, L., et al., *Autophagy enhances the presentation of endogenous viral antigens on MHC class I molecules during HSV-1 infection.* Nat Immunol, 2009. **10**(5): p. 480-7.
247. Vyas, J.M., A.G. Van der Veen, and H.L. Ploegh, *The known unknowns of antigen processing and presentation.* Nat Rev Immunol, 2008. **8**(8): p. 607-18.
248. Miller, B.C., et al., *The autophagy gene ATG5 plays an essential role in B lymphocyte development.* Autophagy, 2008. **4**(3): p. 309-14.
249. Stephenson, L.M., et al., *Identification of Atg5-dependent transcriptional changes and increases in mitochondrial mass in Atg5-deficient T lymphocytes.* Autophagy, 2009. **5**(5): p. 625-35.
250. Pua, H.H., et al., *Autophagy is essential for mitochondrial clearance in mature T lymphocytes.* J Immunol, 2009. **182**(7): p. 4046-55.
251. Yoshimura, S., A.K. Haas, and F.A. Barr, *Analysis of Rab GTPase and GTPase-Activating Protein Function at Primary Cilia.* Methods Enzymol, 2008. **439**: p. 353-64.
252. Hirbec, H., et al., *The PDZ proteins PICK1, GRIP, and syntenin bind multiple glutamate receptor subtypes. Analysis of PDZ binding motifs.* J Biol Chem, 2002. **277**(18): p. 15221-4.
253. Webber, J.L. and S.A. Tooze, *Coordinated regulation of autophagy by p38alpha MAPK through mAtg9 and p38IP.* Embo J, 2010. **29**(1): p. 27-40.
254. Dittié, A.S., J. Klumperman, and S.A. Tooze, *Differential distribution of mannose-6-phosphate receptors and furin in immature secretory granules.* J of Cell Sci, 1999. **112**: p. 3955 - 3966.
255. Harris, B.Z. and W.A. Lim, *Mechanism and role of PDZ domains in signaling complex assembly.* J Cell Sci, 2001. **114**(Pt 18): p. 3219-31.

256. Masuda, E.S., et al., *Rab37 is a novel mast cell specific GTPase localized to secretory granules [In Process Citation]*. FEBS Lett, 2000. **470**(1): p. 61-4.
257. Gao, Y., et al., *Recycling of the Ca2+-activated K+ channel, KCa2.3, is dependent upon RME-1, Rab35/EPI64C, and an N-terminal domain.* J Biol Chem, 2010. **285**(23): p. 17938-53.
258. Chen, L., et al., *Rab36 regulates the spatial distribution of late endosomes and lysosomes through a similar mechanism to Rab34.* Mol Membr Biol, 2010. **27**(1): p. 24-31.
259. Sato, N., et al., *Activation of an oncogenic TBC1D7 (TBC1 domain family, member 7) protein in pulmonary carcinogenesis.* Genes Chromosomes Cancer, 2010. **49**(4): p. 353-67.
260. Pan, F., et al., *Feedback inhibition of calcineurin and Ras by a dual inhibitory protein Carabin.* Nature, 2007. **445**(7126): p. 433-6.
261. Hsu, C., et al., *Regulation of exosome secretion by Rab35 and its GTPase-activating proteins TBC1D10A-C.* J Cell Biol, 2010. **189**(2): p. 223-32.
262. Georgakopoulos, T., et al., *Functional analysis of the Saccharomyces cerevisiae YFR021w/YGR223c/YPL100w ORF family suggests relations to mitochondrial/peroxisomal functions and amino acid signalling pathways.* Yeast, 2001. **18**(12): p. 1155-71.
263. Begley, M.J., et al., *Crystal structure of a phosphoinositide phosphatase, MTMR2: insights into myotubular myopathy and Charcot-Marie-Tooth syndrome.* Mol Cell, 2003. **12**(6): p. 1391-402.
264. Miinea, C.P., et al., *AS160, the Akt substrate regulating GLUT4 translocation, has a functional Rab GTPase-activating protein domain.* Biochem J, 2005. **391**(Pt 1): p. 87-93.
265. Huang, B., et al., *The Anaplasma phagocytophilum-occupied vacuole selectively recruits Rab-GTPases that are predominantly associated with recycling endosomes.* Cell Microbiol, 2010.
266. Brumell, J.H. and M.A. Scidmore, *Manipulation of rab GTPase function by intracellular bacterial pathogens.* Microbiol Mol Biol Rev, 2007. **71**(4): p. 636-52.
267. Yang, H., et al., *Identification of three novel proteins (SGSM1, 2, 3) which modulate small G protein (RAP and RAB)-mediated signaling pathway.* Genomics, 2007. **90**(2): p. 249-60.
268. Hanono, A., et al., *EPI64 regulates microvillar subdomains and structure.* J Cell Biol, 2006. **175**(5): p. 803-13.
269. Mizushima, N., *Methods for monitoring autophagy.* Internat J Biochem Cell Biol, 2004. **36**(12): p. 2491-2502.
270. Gronostajski, R.M. and A.B. Pardee, *Protein degradation in 3T3 cells and tumorigenic transformed 3T3 cells.* J Cell Physiol, 1984. **119**(1): p. 127-32.
271. Urbé, S., et al., *Rab11, a small GTPase associated with both constitutive and regulated secretory pathways in PC12 cells.* FEBS Letters, 1993. **334**(2): p. 175-182.
272. Ullrich, O., et al., *Rab11 regulates recycling through the pericentriolar recycling endosome.* J. Cell Biol., 1996. **135**: p. 913-924.
273. Graham, R.C., Jr. and M.J. Karnovsky, *The early stages of absorption of injected horseradish peroxidase in the proximal tubules of mouse kidney:*

ultrastructural cytochemistry by a new technique. J Histochem Cytochem, 1966. **14**(4): p. 291-302.
274. Graham, R.C., Jr. and M.J. Karnovsky, *Glomerular permeability. Ultrastructural cytochemical studies using peroxidases as protein tracers.* J Exp Med, 1966. **124**(6): p. 1123-34.
275. Hopkins, C.R. and I.S. Trowbridge, *Internalization and processing of transferrin and the transferrin receptor in human carcinoma A431 cells.* J Cell Biol, 1983. **97**(2): p. 508-21.
276. Yu, X., R. Prekeris, and G.W. Gould, *Role of endosomal Rab GTPases in cytokinesis.* Eur J Cell Biol, 2007. **86**(1): p. 25-35.
277. Bembenek, J.N., J.G. White, and Y. Zheng, *A role for separase in the regulation of RAB-11-positive vesicles at the cleavage furrow and midbody.* Curr Biol, 2010. **20**(3): p. 259-64.
278. Kyle, J.W., et al., *Expression of human cation-independent mannose 6-phosphate receptor cDNA in receptor-negative mouse P388D1 cells following gene transfer.* J Biol Chem, 1988. **263**(31): p. 16230-5.
279. Mu, F.T., et al., *EEA1, an early endosome-associated protein. EEA1 is a conserved alpha-helical peripheral membrane protein flanked by cysteine "fingers" and contains a calmodulin-binding IQ motif.* J Biol Chem, 1995. **270**(22): p. 13503-11.
280. Ponnambalam, S., et al., *Primate homologues of rat TGN38: primary structure, expression and functional implications.* J Cell Sci, 1996. **109 (Pt 3)**: p. 675-85.
281. Nakamura, N., et al., *Characterization of a cis-Golgi matrix protein, GM130.* J. Cell Bio., 1995. **131**: p. 1715-1726.
282. Lunemann, J.D. and C. Munz, *Autophagy in CD4+ T-cell immunity and tolerance.* Cell Death Differ, 2009. **16**(1): p. 79-86.
283. Pua, H.H., et al., *A critical role for the autophagy gene Atg5 in T cell survival and proliferation.* J Exp Med, 2007. **204**(1): p. 25-31.
284. Batista, F.D. and N.E. Harwood, *The who, how and where of antigen presentation to B cells.* Nat Rev Immunol, 2009. **9**(1): p. 15-27.
285. Kapsenberg, M.L., *Dendritic-cell control of pathogen-driven T-cell polarization.* Nat Rev Immunol, 2003. **3**(12): p. 984-93.
286. Wells, A.D., *New insights into the molecular basis of T cell anergy: anergy factors, avoidance sensors, and epigenetic imprinting.* J Immunol, 2009. **182**(12): p. 7331-41.
287. Parish, C.R., *Fluorescent dyes for lymphocyte migration and proliferation studies.* Immunol Cell Biol, 1999. **77**(6): p. 499-508.
288. Blott, E.J. and G.M. Griffiths, *Secretory lysosomes.* Nat Rev Mol Cell Biol, 2002. **3**(2): p. 122-31.
289. Lanzetti, L., et al., *The Eps8 protein coordinates EGF receptor signalling through Rac and trafficking through Rab5.* Nature, 2000. **408**(6810): p. 374-7.
290. Li, X., et al., *Mutant huntingtin impairs vesicle formation from recycling endosomes by interfering with Rab11 activity.* Mol Cell Biol, 2009. **29**(22): p. 6106-16.
291. Weigert, R., et al., *Rab22a regulates the recycling of membrane proteins internalized independently of clathrin.* Mol Biol Cell, 2004. **15**(8): p. 3758-70.
292. Proikas-Cezanne, T., et al., *Rab14 is part of the early endosomal clathrin-coated TGN microdomain.* FEBS Lett, 2006. **580**(22): p. 5241-6.

293. Chen, S., et al., *Complementary regulation of TBC1D1 and AS160 by growth factors, insulin and AMPK activators.* Biochem J, 2008. **409**(2): p. 449-59.
294. Chotard, L., et al., *TBC-2 Regulates RAB-5/RAB-7-mediated Endosomal Trafficking in C. elegans.* Mol Biol Cell, 2010.
295. Zhang, X.M., et al., *TBC domain family, member 15 is a novel mammalian Rab GTPase-activating protein with substrate preference for Rab7.* Biochem Biophys Res Commun, 2005. **335**(1): p. 154-61.
296. Seaman, M.N., et al., *Membrane recruitment of the cargo-selective retromer subcomplex is catalysed by the small GTPase Rab7 and inhibited by the Rab-GAP TBC1D5.* J Cell Sci, 2009. **122**(Pt 14): p. 2371-82.
297. Frasa, M.A., et al., *Armus is a Rac1 effector that inactivates Rab7 and regulates E-cadherin degradation.* Curr Biol, 2010. **20**(3): p. 198-208.
298. Hales, C.M., J.P. Vaerman, and J.R. Goldenring, *Rab11 family interacting protein 2 associates with Myosin Vb and regulates plasma membrane recycling.* J Biol Chem, 2002. **277**(52): p. 50415-21.
299. Zobiack, N., et al., *The annexin 2/S100A10 complex controls the distribution of transferrin receptor-containing recycling endosomes.* Mol Biol Cell, 2003. **14**(12): p. 4896-908.
300. Zhao, Y. and J.H. Keen, *Gyrating clathrin: highly dynamic clathrin structures involved in rapid receptor recycling.* Traffic, 2008. **9**(12): p. 2253-64.
301. Marie, M., et al., *The function of the intermediate compartment in pre-Golgi trafficking involves its stable connection with the centrosome.* Mol Biol Cell, 2009. **20**(20): p. 4458-70.